THE UNIVERSITY *of* LIVERPOOL

UHF PROPAGATION MEASUREMENTS FOR FUTURE CDMA SYSTEMS.

Thesis submitted in accordance with the requirements of the University of Liverpool for the Degree of Doctor in Philosophy

by

CHI NCHE

NOVEMBER 1995

Department of Electrical Engineering and Electronics,
The University of Liverpool, P.O. Box 147, Liverpool. L69 3BX.

ABSTRACT

The results of wideband propagation measurements in and around the City of Liverpool are presented in this thesis. The experimental investigations were carried out at a carrier frequency of 1.8 GHz using a purpose-built swept time-delay cross-correlator (STDCC) channel sounder. The system had a time resolution of 33.3 ns and provided an impulse response sounding rate of about 16 power delay profiles per second. By employing coherent demodulation at the receiver and using high quality signal sources, a phase change of 1 cycle in 360 s was achieved. This superior stability coupled with the inclusion of automatic gain control (AGC) circuitry in the RF stage of the receiver allowed continuous measurements over longer spatial distances.

The experimental system was used to undertake measurements in different locations, viz, urban and rural open areas, supermarkets and a train station. A substantial amount of wideband data was collected in the form of complex impulse responses of the propagation channel.

Due to the gross non-stationarity in the statistics of the propagation channel, the time dispersion results are presented in the form of cumulative distribution functions of the small-scale channel descriptors. The way in which these results may be used in assessing the performance of existing and future mobile radio systems is discussed. In addition, the overall pathloss was evaluated for data collected within the buildings surveyed and its variability examined. In general, the results indicate smaller estimates of delay spread when compared to some of those reported in the literature.

In a direct sequence CDMA system, the inherent path diversity can be exploited by employing a Rake type architecture in the receivers. To this end, the measured data was used to show the Rake gain which can be obtained through the use of a Rake-type receiver in a multipath environment. In these investigations, the signal-to-noise ratio (SNR) was used as a measure of performance. A Rake receiver that employs maximal ratio combining (MRC) and equal gain combining (EGC) was compared to a standard receiver that demodulates only the strongest path. The need for accurate power control in a direct sequence CDMA system was examined. By investigating the short-term variability of the SNRs at the output of the receiver, the required speed of the power control algorithm could be estimated.

The Rake receiver performance has been shown to vary with the percentage of arriving paths that are combined. It was observed that there is a diminishing return as the number of Rake branches is increased. This was shown to be largely due to the dominance of the first few multipath components. The probability of occurrence of echoes in the different locations was therefore evaluated to give an indication of the arrival times of the echoes. Their importance in using such probability of occurrence curves to aid in the design of an optimum Rake receiver was discussed.

ACKNOWLEDGEMENTS

I would like to express my profound gratitude to Professor J.D. Parsons, my supervisor and Dr. Adel Turkmani for their invaluable help, encouragement and guidance during the course of this project. I am also indebted to my colleague, Mr. J.G. Davies, who sacrificed numerous hours of his time to assist in many ways. The assistance of Paul Raouf was also greatly appreciated. I also wish to express my appreciation to Messrs Y.H. Chung and P.S.H. Leather for their invaluable discussions. My appreciations are also extended to Drs. A.A. Arowojolu, U. Goni, H. Vu, M. Chaaban, N. Natarajan, M.T. Khorami and A.F. Toledo. I would also like to acknowledge my appreciation to Mrs Brenda Lussey for her constant help and encouragement, and also to Mr. D.G. Lewis, Mr. R. Smith and Mr. G. King for their extensive assistance in the development of the experimental system.

I wish to thank the Cameroon Government for the financial support provided during the beginning of my studies.

Finally, my deepest appreciation goes to my loving parents, Mr. and Mrs. Nche, for their love, understanding, encouragement and support. To all my brothers and sisters and to my entire family which is too numerous to mention, I say 'thank you'.

Chi Nche

Liverpool
August 1995.

Dedicated to my loving parents,

my brothers and my sisters

TABLE OF CONTENTS

LIST OF SYMBOLS

The following list contains those symbols which have been used consistently throughout the text. Because of the large number of quantities to be represented and the undesirability of using symbols other than English and Greek, it has been found necessary to use some symbols to represent different quantities at different times. In every instance, the symbol has been defined where introduced to avoid misinterpretation of its meaning.

GSM	Global System for Mobile Communications
DECT	Digital European Cordless Telecommunications System
IS54	American Digital System (also ADC)
CDMA	Code Division Multiple Access
UMTS	Universal Mobile Telecommunications Systems
ISDN	Integrated Services Digital Network
DCS1800	Digital Cellular System 1.8 GHz
CT2	Cordless Telephone System - 2
COST	Cooperation in Science and Technology in Europe
AGC	Automatic Gain Control
LOS	Line-of-Sight
STDCC	Swept Time Delay Cross Correlation
IBER	Irreducible bit error rate
NLOS	Non-Line-of-Sight
CCIR	International Consultative Committee on Radio
NOT	Number of discernible echoes or taps in a power delay profile
SNR	Signal-to-noise ratio
$L(1m)$	Free space propagation pathloss at 1 m, (dB)
n	Propagation pathloss exponent
λ	Wavelength (m)
f	Frequency (MHz)
P_R	Received power (Watts)
P_T	Transmitter power (Watts)

N	Number of rays or taps
G_T, G_B	Base antenna power gain (dBi)
D	Average delay (μs)
S	Delay spread (μs)
Bc_{50}, Bc_{90}	Coherence bandwidths at 0.5 and 0.9 correlation respectively
I_{15}, I_{12}, I_9	15, 12 and 9 dB delay intervals respectively
W_{90}, W_{75}, W_{50}	90, 75 and 50 % delay windows respectively

Chapter One

INTRODUCTION

From its inception in the early 20's, the field of mobile radio communications has been expanding rapidly due to a very substantial growth in market demand for the services it provides. Nowadays, mobile radio communications play an unassailable role in business, public safety sectors and for private users. This rapid upsurge in demand, especially in the 80's has placed extra responsibilities not only on system designers and service providers, but also on the respective national radio regulatory administrators worldwide. In the first generation of public mobile radio systems, the cellular concept [1.1] together with frequency division multiple access (FDMA) was used to meet the growing demand for services. The application of the cellular concept implied that the capacity of these systems could be increased by cell splitting and sectorisation. Even with these features, the upsurge in demand continued and in 1987, the original analogue systems, such as the Nippon Telegraph and Telephone (NTT) system introduced in Japan in 1979, the Advanced Mobile Phone Service (AMPS) introduced in the U.S.A. in 1983, and the Total Access Communications System (TACS) introduced in the U.K. in 1985, were all beginning to face serious capacity problems [1.2-1.3]. Furthermore, the demand for services akin to those provided by the fixed telephone networks combined with the inherent capacity problems due to the limited availability of the frequency spectrum, have forced mobile communication engineers to look for alternative solutions.

In view of the above, there was a promotion of the developing digital cellular systems as a technology able to meet the increasing capacity demands and provide the flexibility of being able to offer similar services to those offered by the fixed telephone networks. The feasibility of digital transmission systems was further enhanced by the ongoing advancements in VLSI technology which made possible the introduction of small, low-powered and low cost components. By utilising digital

FDMA and TDMA schemes, the capacity of cellular radio systems can be increased by a factor between 3 and 4 [1.4] over what was provided by the corresponding first generation of analogue systems. This is merely by virtue of the fact that digital systems can tolerate a lower carrier-to-interference ratio (C/I) than the corresponding analogue systems.

The early 90's have witnessed the evolution of a number of second generation mobile radio systems, which are based almost entirely on digital technology. Such systems include the Global System for Mobile Communications (GSM), the American IS-54 (also known as D-AMPS), and the Qualcomm CDMA system (IS-95) all of which operate in the 900 MHz frequency band. The advent of personal communications networks (PCN) and the need for a new generation of cordless telephone systems has also led to the introduction of the Digital Communication Systems (DCS1800 in the U.K. and DCS1900 in the U.S.A.), the Digital European Cordless Telecommunications System (DECT) and the Second Generation Cordless Telephone (CT2) which operate in the 1800 MHz frequency band. With the exception of the CDMA system and CT2 which utilise spread spectrum multiple access and FDMA respectively, the other second generation systems utilise a TDMA structure as the multiple access technique.

The GSM system has been purposely designed as a high-capacity, wide-area coverage and multi-service cellular mobile radio system. The system must cope with high traffic densities in the major European cities and at the same time, provide continuous coverage in the rural areas. Ability to roam in Europe is one of its requirements. In this system 8 channels (full rate channels) are time multiplexed into each radio channel, the data rate of each radio channel being about 270 kb/s. Hence it is a wideband transmission system. DCS1800 is a close derivative of the GSM system which has most of its parameters, but operates at the 1800 MHz frequency band and utilises lower transmission power for smaller cells.

Although the above systems vary in complexity and their intended purpose, the data

transmission rates are of utmost importance since they set the operational bandwidth of the system. The decision to deploy wideband transmission techniques for the second generation of mobile radio systems, has taken in the knowledge that their performance would be affected by time dispersion due to delay spread [1.5-1.6], in addition to the effects of spatial fading which is normally observed in narrowband transmission systems. In digital transmission systems, the delay spread causes intersymbol interference, and will set the lower bound on the bit error rate for a specified data rate since increasing the signal-to-noise ratio will not effect a decrease in the effects of time dispersion [1.5]. The large time delays due to multipath propagation give rise to a phenomenon known as frequency selective fading [1.7]. In view of the time dispersion problems, it may appear that wideband systems have little or nothing to offer in the context of high capacity applications, but this is a simplistic view. Digital wideband transmission systems, such as the aforementioned, provide a much greater opportunity for the application of sophisticated modulation, coding and signal processing techniques which are essential for better noise and interference immunity in any system. A thorough knowledge of the wideband propagation characteristics of the mobile radio channel is therefore a major prerequisite to the specification, design and implementation of any future system. A knowledge of the propagation characteristics of the wideband propagation channel in different environments is important because the results can be used to formulate channel models and statistical parameters that could be used in the design of future very high capacity systems.

The concept of utilising digital wideband transmission techniques in mobile radio systems has its additional drawbacks. Specifically, the application of channel equalisation systems, error protective coding techniques, etc., increases the system complexity and hence cost. These considerations, among others and the restricted capacity of the first generation of narrowband mobile radio systems inspired the need to look for alternatives which had the potential to become the ultimate mobile radio system. Spread spectrum techniques were deemed to solve the capacity problems for the current and next generation systems because of their inherent ability to mitigate

the effects of multipath propagation and the possibility of coexistence with present systems. The latter is important, especially in certain countries (e.g the U.S.A.) where no additional spectrum will be allocated for digital cellular [1.2].

The interest in spread spectrum techniques in the field of mobile radio communications is increasing rapidly, with this topic representing one of the most interesting and challenging in this field. The use of special techniques, such as frequency hopping, direct sequence and time hopping, or hybrids, offers protection against detection, interception and intentional or unintentional interference [1.8]. These features coupled with its direction finding capabilities have been exploited exclusively in military communications in the past. To date, the impressive technical evolution over the past years in digital signal processing combined with VLSI has greatly reduced the cost of implementing spread spectrum systems. This has made possible the development of various civilian applications such as satellite communications, mobile radio communications, wireless indoor communications and power-line carrier transmission systems.

In a spread spectrum system, the assignment of a unique spread spectrum sequence to each of the users provides the multiple access capability which arises from the self-correlation of these unique sequences. This is termed code division multiple access (CDMA). For a CDMA system, each signal consists of a different pseudorandom binary sequence that modulates the carrier, thus, spreading the spectrum of the waveform. A large number of CDMA signals share the same frequency spectrum. If CDMA is viewed in either the time or frequency domains, the multiple access signals appear to be superimposed. In the receivers, the signals are separated out by using correlators which accept only signal energy from the selected binary sequence and despreads its spectrum. The signals from the other users, whose codes do not match are not despread in bandwidth and as a result, contribute only to the noise and hence represent self-interference generated by the system. There is therefore a resulting

increase in the signal-to-noise ratio, which is the processing gain[1] of the system. In addition to the inherent advantages of a digital system, a CDMA system offers capabilities for multiple forms of diversity, increased security, soft handoff, very high capacity, voice activity detection etc. [1.9-1.10].

It was for these reasons that Qualcomm Inc. in the U.S.A. developed a 'narrowband' CDMA system for cellular mobile radio, now known as IS-95 [1.9]. This is the only second generation system that is based on spread spectrum techniques. The IS-95 system overcomes the traditional difficulties of CDMA, namely, that of having to find millions of unique codes for millions of users, provision of accurate synchronisation and accurate implementation of power control strategies, factors that have inspired certain operators to opt for a CDMA system. In 1991, tests were successfully conducted using 70 mobile units with simulated other users and other base station interference over five cells. Similar tests were also conducted at 900 and 1700 MHz in GSM base sites around Europe. The results from the latter [1.11] indicated that in the large delay spread areas, the performance of the CDMA system greatly surpasses that of the GSM system.

Given the advantages of CDMA systems over the others, one may speculate that the third generation of mobile radio systems will utilise the CDMA concept. Another speculation which can be deduced from two of the properties of CDMA systems is that of readily coexisting with present systems. Specifically, spreading the message energy over a large bandwidth reduces interference to other users and the system's ability to withstand intentional and unintentional interference due to the correlation properties of the spreading codes provides a possibility of operating in hostile environments. This has already been demonstrated for fixed service microwave links [1.12]. The tests were conducted around 1850-1990 MHz, using a broadband CDMA system, by SCS Mobilecom of the U.S.A. The results from the tests demonstrated the feasibility of such coexistence with minimal interference to the fixed service

[1]The processing gain is the ratio of the spread bandwidth to the baseband data rate.

microwave users, a high quality of speech reproduction, and low bit error rates during data transmission. On the other hand, a very large investment of time and money has been used in the development of the present digital systems based on a TDMA strategy such as the GSM system and its derivatives. In addition, many countries around the world are opting for the GSM system as a national standard. It is therefore apparent that the GSM system and/or its derivatives are successful and may become the future global standard. The probable answer to this is that CDMA and TDMA systems may coexist in the future.

With the intuitive rationality that CDMA and other systems, in particular TDMA systems, will coexist in the future, the principal question is where to deploy these various systems with reference to either indoor or outdoor environments, macrocells or microcells, etc. The answer to this question is difficult to ascertain, especially because of the lack of experimental wideband data with regard to the performance of CDMA systems. This was one of the primary motivations of undertaking wideband channel sounding measurements in a variety of environments. It is expected that the results obtained from such a study can be used to aid the specification, design of receiver architectures and simulation of future high capacity systems.

1.1 AIMS OF THIS WORK

One of the primary objectives of this study was to undertake wideband propagation studies in a variety of scenarios in order to provide the data necessary for the specification, evaluation and implementation of future CDMA systems. Experimental field trials were therefore carried out in the following environments:

a) **Outdoors:** Field trials were conducted in urban and rural locations. The results from these locations were compared with published results from similar locations. In conducting the experiments, special attention was placed on the techniques and experimental designs in order to obtain data that provides a realistic representation of the wideband propagation channel in these environments. The results can then be used for the simulation of future CDMA systems, and the design and

implementation of optimum receiver architectures (e.g. Rake receivers).

b) **Indoors:** Supermarkets and train stations represent some of the places in which a large number of people congregate. Unfortunately, there is virtually no wideband data from such locations and therefore it was necessary to conduct some measurements in such locations. Areas such as these are likely contenders for wireless LANs and PCS.

A channel sounding system was required for this purpose. The purpose of the experimental system was to provide enough information in order to adequately characterise the wideband mobile radio propagation channel. Since there are virtually no commercial wideband channel sounders that provide the necessary flexibility, it was necessary to design a system to be used in this study. In order to design and implement an optimum experimental channel sounding system, it is important to consider some of the major issues which will be pertinent to CDMA systems in the future. One of the most important and delicate decisions is that of selecting the spread spectrum technique. In mobile radio systems, the most probable are direct sequence spread spectrum (DS/SS), frequency hopping spread spectrum (FS/SS) or a combination of both. In the design of a DS/SS system, the chip rate of the spreading code is important together with the receiver architecture. The latter refers to the multiple forms of diversity that a DS/SS system offers which can be exploited in the receiver. Since the chip rate determines the system bandwidth the experimental system should be able to measure the frequency selective behaviour of the propagation channel. This is also true for FS/SS systems in which the hop rate and minimum separation between hops should be determined. The requirements of the experimental system are presented in detail in Chapter 3.

In the ensuing section, the contents of this thesis is reviewed according to the respective chapters.

1.2 OVERVIEW OF THESIS

The work presented in this thesis may be divided into three main sections, namely design and implementation of an experimental wideband channel sounding system, data collection and analysis and finally presentation of the results. The thesis is divided into six chapters as below.

In Chapter 2, the mobile radio channel characteristics and characterisation techniques are reviewed, before embarking on a brief overview of the various practical channel sounding techniques. In the latter case, the advantages and disadvantages of the various techniques are highlighted with a view to selecting the optimum channel sounding technique for this study. A review of previous wideband experimental investigations is also presented in this chapter. The major problems encountered in these previous studies will be emphasised so as to devise methods of avoiding them. Finally, an overview of spread spectrum systems is given together with some of the benefits that a CDMA system can offer. This chapter ends with a brief discussion of the propagation aspects of a CDMA system.

One of the main requirements of any experimental study is a reliable measurement system. Chapter 3 is dedicated to the design and construction of the experimental system used in this study. It begins with a look at the requirements for an experimental wideband channel sounding system based from the observations from Chapters 1 and 2, before a detailed presentation of the implementation techniques that were used. The chapter concludes with a presentation of the results from the numerous performance tests that were used to validate the system.

Chapter 4 begins with a formulation of the experimental design, which is considered important, if a true picture of the mobile radio propagation channel is to be presented. The measurements techniques and experimental locations are also described in this chapter. Finally, the methods of data acquisition and storage are presented before definitions of the relevant channel parameters that were measured. Furthermore, the characterising techniques that were utilised in this study are presented together with the Rake receiver model that was used to show the Rake gain and the relevance of

an accurate power control mechanism.

The results from the entire measurement campaign are presented in Chapter 5. Emphasis is placed on the large-scale statistics of the propagation channel. Firstly, the large-scale distributions of the small-scale channel parameters which are defined in Chapter 4 are presented in the form of cumulative distribution functions and tables. Scatter plots of the coherence bandwidths at 0.5 and 0.9 correlation are also presented. Secondly, the results from the pathloss analysis for the within building environments are given mainly in the form of the pathloss exponent. Lastly, the results which are relevant to CDMA systems are presented. These were obtained by using the Rake receiver model presented in Chapter 4, with its parameters derived from the measurements in this study. The implications with reference to the relevance of power control in a CDMA system are discussed. In all cases, discussions with views to their relevance to systems design are presented together with relevant comparisons with the results from the literature.

In Chapter 6, conclusions are drawn from the work presented in this study. Finally proposals for future work are summarised.

REFERENCES

[1.1] MacDonald, V.H., 'Advanced Mobile Phone Service: The Cellular Concept', Bell Syst. Tech. Journal, Vol. 58, (1), Jan. 1979. pp15-41.

[1.2] Lee, W.C.Y., 'Overview of Cellular CDMA', IEEE Trans. on Veh. Technol., Vol. VT-40, No. 2, May 1991. pp291-302.

[1.3] Beddoes, E.W. and Germer, R.I., 'Traffic Growth in a Cellular Telephone Network', Journ. of IERE, Vol. 57, No. 1, Jan./Feb. 1987. pp22-26.

[1.4] Gilhousen, K.S., Jacobs, I.M., Padovani, R., Viterbi, A.J., Weaver Jnr, L.A. and Wheatly, C.E., 'On the Capacity of Cellular CDMA', IEEE Trans. on Veh. Technol., Vol. VT-40, No. 2, May 1991. pp303-312.

[1.5] Lee, W.C.Y., 'Mobile Communication Design Fundamentals', Sams, 1986.

[1.6] Jakes, W.C., 'Microwave Mobile Communications', John wiley, 1974.

[1.7] Parsons, J.D. and Gardiner J.G., 'Mobile Communication Systems', Blackie, 1989.

[1.8] Dixon, R.C., "Spread Spectrum Systems", Wiley, New York, 1982.

[1.9] Qualcomm Inc., 'An Overview of the Application of Code Division Multiple Access (CDMA) to Digital Cellular Systems and Personal cellular Networks', 1992.

[1.10] Milstein, L.B., Schilling, D.L., Erceg, V., Kullback, M., Kanterakis, E.G., Fishman, D.S., Biederman, W.H. and Salerno, D.C., 'On the Feasibility of a CDMA Overlay for Personal Communications Networks', IEEE Trans. on Veh. Technol., Vol. VT-40, No. 2, May 1991. pp313-321.

[1.11] Viterbi, A.J., Padovani, R., 'Implications of Mobile Cellular CDMA', IEEE Commun. Mag., Dec. 1992. pp38-41.

[1.12] Pickholtz, R.L., Milstein, L.B. and Schilling, D.L., 'Spread Spectrum for Mobile Communications', IEEE Journal Sel. Areas Commun., Vol. 10 (4), May 1992. pp655-668.

Chapter Two

REVIEW OF PREVIOUS WORK AND BACKGROUND THEORY

2.1 INTRODUCTION

In this chapter the characteristics of the mobile radio propagation channel are reviewed, together with the various techniques by which the channel can be characterised. A brief review of wideband propagation channel models is presented in section 2.3, before embarking on a comprehensive review of wideband channel sounding techniques. The advantages and disadvantages of these techniques are presented with a view of selecting the optimum method for implementing in this study.

In section 2.6, a review of previous wideband investigations in outdoor and indoor environments is presented. The limitations of the techniques used which cover the channel sounding technique employed, data acquisition and analysis and experimental design are also presented. In addition, a comparison of delay spreads from previous experiments is presented in section 2.6.3.

Finally, an overview of spread spectrum systems is given, together with the benefits that CDMA systems can offer. The chapter concludes with a brief discussion of the propagation aspects of a CDMA system.

2.2 MOBILE RADIO CHANNEL CHARACTERISATION TECHNIQUES

The nature of the mobile radio propagation channel greatly limits the performance of radio communication systems. When a radio signal is radiated from an antenna, the electromagnetic waves propagate in a direction perpendicular to the surface of

constant phase. The electromagnetic waves will travel in a straight line as long as the phase front is plane and infinite. In a mobile radio environment, there is often no line-of-sight path between the transmitter and the receiver, due to shadowing by natural and/or man-made obstacles along the radio path. Hence, the received signal is composed mainly of components scattered from these obstacles. There are two modes of radio wave scattering: reflection and diffraction. Reflection of radio waves occurs because of an abrupt change of direction of the phase front at the surface of the obstruction, while diffraction is an edge effect which occurs because the phase surface of the propagating wave is not infinite.

The impact of the multipath phenomenon which occurs in mobile radio channels is largely dependent on the data rate or operating bandwidth employed for the system, and determination of optimum methods of mitigating the impairments caused by multipath propagation necessitates the need for the transmission channel to be satisfactorily characterised. Characterisation is often expressed in terms of so-called narrowband or wideband channel parameters.

2.2.1 Narrowband Propagation Characteristics

A narrowband propagation channel is one in which the inverse of the transmitted signal bandwidth is much greater than the propagation path delays. In such circumstances, the arrival of multiple signals at the antenna causes rapid fading of the received signal envelope as the receiver is spatially displaced or as a result of the movement of the local scatterers. The variations in the received signal envelope are a consequence of the random phase additions of the radio waves arriving via multiple paths. This is termed fast fading and the envelope statistics can be adequately described by a Rayleigh distribution. In situations where there is a strong line-of-sight path, the envelope statistics are best described by a Rician distribution. However, it is sufficient to describe the envelope statistics as being Rayleigh distributed since areas which experience strong direct paths will most probably have higher signal levels than those with shadowed paths.

In addition to the Rayleigh distributed fast fading, there is a much slower variation

in mean signal level superimposed on the fast fading due to gross differences in the local terrain, range and/or number of scatterers. This is termed slow or shadow fading and a lognormal distribution with a distance-dependent mean is adequate for its description. A description of the narrowband propagation channel in terms of Rayleigh distributed fast fading and lognormally distributed shadow fading is usually adequate for the evaluation of narrowband systems [2.1].

2.2.2 Wideband Propagation Characteristics

The performance of wideband transmission systems is also limited by time dispersion due to multipath, in addition to the fast and slow fading which is encountered in narrowband systems [2.1]. For digital systems, the time delayed echoes cause signal smearing, which gives rise to intersymbol interference (ISI). In this case, increasing the signal to noise ratio will not effect a decrease in the error performance. The delay spread will therefore set the lower bound on error performance for a specified data rate. This is often referred to as the irreducible bit error rate (IBER) [2.2], and the error performance can only be improved by equalisation techniques.

Large excessively delayed paths gives rise to a phenomenon known as frequency-selective fading. This means that two sufficiently spaced frequencies fade in an uncorrelated manner. When a variation in the received signal strength as a function of frequency occurs, there is a lack of correlation between message-frequency components. In analogue frequency modulation systems, the frequency-selectivity limits the maximum usable frequency deviation. The implication of this phenomenon is that the characterising functions used to describe the wideband transmission channel should explicitly show its fading and dispersive properties.

2.2.3 Channel Characterisation

Signals that have suffered multipath propagation constitute a set of randomly attenuated and phased replicas of the transmitted RF signal. The resultant sensed at the receiver is therefore the superposition of contributions from various individual paths and, on this basis, it is reasonable to describe the mobile radio channel in terms

of a two-port filter with randomly time-varying transmission characteristics. The behaviour of the channel can then be described in terms of system functions which give an insight into the physical mechanisms which dominate the channel behaviour.

The first general analytical treatment of time variant linear filters was presented by Zadeh [2.3]. Kailath [2.4] subsequently produced further work, with special emphasis on channel characterisation. Bello [2.5] further developed the work of Zadeh and Kailath and presented a general characterisation of the channel, which he also applied to restricted classes of channels. The work of Bello was the basis of the studies of Bajwa [2.6] and Demery [2.7], where a characterisation of practical channels was presented. Kennedy [2.8] adopted an alternative approach to the time-variant filter description, using the point-scatterer method. The observed characteristics lead to the conclusion that strictly, mobile radio channels are non-stationary, but in practice, characterisation proves extremely difficult unless stationarity is assumed over short distances of travel[1] or short intervals of time.

A suitable statistical description of the mobile radio channel has been proposed in the form of a two-stage model [2.5]. A small-scale characterisation is first obtained over a period of time that is short in comparison to the period of the slow channel variations, so that the mean signal level appears reasonably constant. It is assumed that over this short period of time, the prominent features of the small-scale area remain the same, ie., the significant scattering centres do not change. A large-scale characterisation is subsequently obtained by averaging the small-scale statistics. This two-stage model was first used by Cox [2.9] and later by Bajwa [2.6] and the class of mobile radio channels for which it applies is termed quasi-wide-sense-stationary (QWSS). This approach has formed the backbone of mobile radio channel characterisation and has received extensive treatment by many researchers, [2.10,2.11]. It has therefore formed the basis of several experimental campaigns conducted to provide information on the channel in a variety of environments [2.12-

[1]This is usually a few tens of the wavelength of the RF carrier.

2.16]. A further simplification in the characterisation of mobile radio channels can be derived from the observation that contributions from scatterers with different time delays are uncorrelated. This class of channels has been termed quasi-wide-sense stationary uncorrelated scattering (QWSSUS) [2.3]. A description in terms of wide-sense stationary uncorrelated scattering statistics is therefore appropriate and the channel can be envisaged as a continuum of uncorrelated scatterers in both time delays and Doppler shifts.

The time-domain description of any linear system is completely specified by its complex impulse response. Since the channel is time-variant, the impulse response is also a time-varying function. The theory is well covered in the literature [2.5-2.7,2.17], but in brief, the complex envelope of the output of the channel equivalent filter, w(t), is given by

$$w(t) = \int_{-\infty}^{\infty} z(t-\tau)(h(t,\tau)d\tau \qquad (2.1)$$

where z(t) is the complex envelope of the real signal x(t), ie.

$$x(t) = Re[z(t)\exp(j2\pi f_c t)] \qquad (2.2)$$

In the above equations, f_c is the carrier frequency, $h(t,\tau)$ is the time-variant impulse response of the channel equivalent filter and τ is the time delay variable.

Equation (2.1) yields a physical representation of the channel as a continuum of non-moving, scintillating scatterers, with each elemental scatterer having a gain fluctuation $h(t,\tau)d\tau$ and providing delays in the range $(\tau,\tau+d\tau)$. Since any physical channel must be causal, the limits of integration in Equation (2.1) are strictly (0,T), where T is the observation time. The time-variant impulse response, $h(t,\tau)$, was termed the input delay-spread function by Bello [2.5].

A time domain description of the channel can be obtained by expressing the

autocorrelation function ,$R_w(t,t)$, of the channel output in terms of the autocorrelation function of the input delay-spread function. For WSSUS channels and when the time separation of the observation is zero, the relationship between the two autocorrelation functions can be simplified to [2.7]

$$R_w(t,t) = \int |z(t-\tau)|^2 P(\tau) d\tau \qquad (2.3)$$

Characterisation is also possible using other models, shown in the literature.

If $|z(t)|^2$ is an impulse function, then Equation (2.3) can be written as

$$R_w(t,t) = P(t) \qquad (2.4)$$

which shows that for WSSUS channels, the autocorrelation function of the channel output is described by the profile of the time distribution of received power, often termed the power delay profile (PDP). This description is valid provided $|z(t)|^2$ is impulsive with respect to P(t), this being satisfied if z(t) exists for a much smaller time than the spread of time delays within the channel. Provided the received signal has Gaussian statistics, then the channel behaviour will be completely described by P(t). Alternative channel descriptors can also be obtained from practical measurements performed in the frequency domain, for example, by estimating the frequency-selective behaviour of the channel. This is readily obtained by observing the correlation between two signals, at different frequencies, at the receiver [2.18]. The frequency domain description of the channel is often specified in terms of the frequency correlation function (FCF), $R_T(\Omega)$,where Ω is the frequency separation. It has been shown [2.5-2.7,2.17] that significant symmetrical interrelationships exist between the system functions in the different domains through Fourier transformations. Therefore, it is not necessary to perform a separate measurement of $R_T(\Omega)$, as this is equal to the Fourier transform of P(t), ie.,

$$R_T(\Omega) = \int P(t) \exp(-j2\pi\Omega t) dt \qquad (2.5)$$

It has been customary to measure the impulse response, $P(t,\tau)$, which describes the

complex amplitude of a multipath component arriving at the receiver at a certain time, t, with a delay, τ, either in its complex form with inphase and quadrature components or as an envelope. For convenience, $P(t,\tau)$ has its origin redefined so as to position the earliest received echo at t=0, and the function is then defined in terms of the excess time delay variable.

Many small-scale channel descriptors have been used to represent the statistics of the power delay profile, P(t). The average excess delay and delay spread have been widely utilised and were defined by Cox [2.9] as the first and second central moments respectively of the power delay profile. However, these two parameters are not sufficient to describe some of the important characteristics of the channel. Recognising this fact, the use of two further parameters has been recommended, COST207 [2.19], namely delay window and delay interval. The above parameters are defined in more detail in Chapter 4.

2.3 MODELLING THE WIDEBAND PROPAGATION CHANNEL

A variety of models to describe the wideband propagation channel have been presented in the literature. Initially, the propagation channel was modelled as follows:

$$h(t,\tau) = \sum_{k=0}^{\infty} \alpha_k(t) e^{-j\theta_k(t)} \delta(t-\tau_k) \qquad (2.6)$$

where $h(t,\tau)$ is the complex baseband impulse response of the channel, α_k, τ_k and Θ_k are respectively the amplitude, propagation time delay and phase shift of the k-th echo, and $\delta(\cdot)$ is the Dirac delta function. Hence the set of time varying path variables $\{\alpha_k, \tau_k, \Theta_k\}_{k=0,\infty}$ completely describes the propagation medium. The basis of some of the models has been to ascribe suitable global statistical descriptions to the amplitudes, α_k, time delay, τ_k and phase shifts, Θ_k, along with the spatial and temporal correlations between adjacent echoes in the same profile and between echoes in proceeding and succeeding profiles. The latter aspect accounts for the possibility of any correlated scattering in the channel. A large number of wideband channel impulse response measurements have therefore been carried out in an attempt to

formulate global statistical descriptions of these variables.

2.3.1 Statistical Modelling

A number of statistical models have been published in the studies of Turin *et al* [2.12], Bajwa [2.20], Suzuki [2.21], Hashemi [2.22], Saleh and Valenzuela [2.23] and Demery [2.7]. Typically, the amplitude variations, α_k, have been modelled by a lognormal distribution [2.12,2.22], a Nakagami or Suzuki distribution [2.21], a Rayleigh distribution [2.20,2.23] or by a Rayleigh and lognormal distribution [2.7]. In a similar manner, the excess propagation time delay of the multipath components, τ_k, are modelled by a Poisson distribution [2.20,2.23], a modified Poisson distribution [2.12,2.21,2.22] or are assumed to be fixed in time in general agreement with the concept of a tapped-delay line [2.7]. In most of these models, the carrier phases of the individual components, Θ_k, have been assumed *a priori* to be mutually independent random variables uniformly distributed from $-\pi$ to π, except in the case of Bajwa [2.20] who derived the relative phase changes for each power delay profile from the measured Doppler spectra and added to the assumed initial uniformly distributed random phases.

The above models have formed the basis of many software simulation studies. These models have been and will continue to be used for channel simulations. However, due to the fact that the channel characteristics are site specific, it is necessary to be able to relate the features of the environment in the areas surrounding the base station particularly for coverage estimation purposes. This is quite important as there is no standard method of categorising the various mobile radio environments.

2.3.2 Other Models for the Wideband Propagation Channel

Other deterministic models include the use of ray tracing or bistatic radar theory. The applicability of a possible ray tracing model for wideband studies has been demonstrated [2.24], but this is restricted to microcellular environments. The use of bistatic radar theory [2.25-2.27], in which the scattering function is associated with sources located on confocal ellipses with the transmitter and receiver at the foci,

proves difficult in its application and interpretation. This is mainly due to the assumption of single scattering in the medium.

2.4 PROPAGATION PATHLOSS

In all radio propagation channels, the transmission and subsequent receiving of radio signals results in a propagation pathloss or transmission loss. This is the single most important characteristic of any propagation channel and is equal to the ratio of the power transmitted to the power received. Propagation pathloss has been found to bear an inverse relationship to the distance between the transmitter and receiver. Free space propagation obeys an inverse square law with distance [2.17]. In general, propagation pathloss in the form of an n-th power law accounts for the decrease in signal strength as a function of distance between the transmitter and receiver.

In a typical multipath environment, where complex standing wave patterns results from the multiplicity of transmission paths, a slight change in the antenna position, orientation or position of the scattering objects can change the phase relationships of the different echo paths which may lead to large variations in the received signal level and hence the propagation pathloss. A basic problem, then, is to develop a measurement technique for measuring the propagation pathloss, which is not unduly sensitive to the interrelationships between the phases of the individual multipath components.

2.4.1 Propagation Pathloss Models

A fundamental requirement in the design of any land mobile radio system is a thorough knowledge of the mean signal and its variability at all locations surrounding the base station. With this information, systems designers can establish the coverage area and interference problems that may be associated with any base station. Whilst this information can be obtained by undertaking CW measurements, this is very expensive, especially in cellular systems comprising of a large number of base station sites. Measurements would need to be repeated for each base station location and this approach would be very expensive. It is therefore advantageous for systems designers

to have models which can easily be used to predict both the coverage and the likely effects of interference.

The propagation models described in the literature are either empirical or analytical or a combination of both. In general, the propagation pathloss L(d), can be modelled as

$$L(d) = 10 \cdot n \cdot \log d + L \qquad (2.7)$$

where d is the distance between the transmitter and receiver, L is a transmission loss parameter which depends on frequency and antenna heights, and n is the slope of the best-fit line, which can be regarded as the attenuation factor. A large number of propagation pathloss models have been formulated based on data obtained from CW measurements or from analytical techniques. These include the plane-earth equation, Allesbrook and Parsons model, Hata's model and Atefi and Parsons model [2.17] which predict a near-fourth power-distance dependence. Also the model of Okumura [2.28] gives a method for predicting the received signal level and service area for conventional macrocells.

Unfortunately, most of the propagation pathloss models have been derived with emphasis on outdoor macrocells, with very little on the indoor environments. Moreover the few indoor models that have been published have been based mostly from data obtained in multi-storey buildings [2.29-2.31]. Values of the pathloss exponent, n, from 1.4 to 5.7 have been reported from wideband and CW measurements within buildings [2.23,2.29,2.33-2.34]. It can therefore be inferred that the conventional pathloss models that apply to conventional macrocells cannot be applied to the within buildings environments, especially supermarkets, factories and train stations. Hence there is a necessity to investigate the distance dependence of the transmission loss in a variety of indoor environments, such as shopping malls, railway stations, supermarkets and the like.

2.5 CHANNEL SOUNDING TECHNIQUES: A REVIEW

The detailed nature of the multipath propagation characteristics can be observed by utilising various channel sounding techniques. These techniques provide a practical means of measuring the statistical functions required for characterising the time-dispersive mobile radio channel. The choice of the technique used depends, to some extent, on the parameters to be measured and the intended application. For example, measurement of the fading envelope of the received signal at a single transmitter frequency has been used to assess the performance of narrowband voice communication systems in multipath propagation environments. In this case, the multipath characteristics are specified in terms of parameters which relate to the statistics of the fading envelope of a carrier frequency [2.1]. Although this technique is sufficient for the characterisation of narrowband mobile radio channels, it is inadequate for wideband channels. The alternative, therefore, is wideband channel sounding, which has wider applications, for example, to speech or data in frequency division multiplexed schemes [2.1], wideband vehicle location systems or alternative signalling techniques like spread spectrum multiple access techniques (CDMA) and wideband time division multiple access techniques (TDMA).

It was mentioned in the previous section that significant symmetrical interrelationships exist between the characterising functions in the time-time delay, time-frequency, frequency-frequency shift and time delay-frequency shift domains [2.5-2.7,2.17]. Hence, the wideband transmission characteristics can be described in terms of the mean and correlations of the time varying transfer function T(f,t), the impulse response function, h(t,τ), the output frequency-Doppler spread function, H(f,v) and the delay-Doppler spread function S(τ,v). Consequently, a complete characterisation can be achieved in any domain using a suitable channel sounder. In cases where the Doppler shifts associated with the propagation channel are required, coherent detection of the inphase and quadrature components of the received signal allow the extraction of the angles of arrival of the multipath components which contain the Doppler shift information.

In the following sections, a brief assessment of narrow bandwidth sounding techniques is presented, prior to a more detailed review of the various methods of wideband channel sounding. These will be illustrated by way of examples from previous works. The limitations of methods used in previous experiments are discussed and the background to the method used in this study is presented. The various deficiencies in the measurement techniques which can lead to an under- or over-estimation of the channel parameters are also highlighted.

2.5.1 Narrow Bandwidth Channel Sounding Techniques (CW)

2.5.1.1 Single Tone Method

In this method, an unmodulated radio frequency carrier is used to excite the propagation medium. The received signal is a result of the combination of a large set of electromagnetic scattered waves. The phasor addition of these components, which are usually random phased, results in an amplitude fading of the envelope of the received RF signal. This essentially leads to a characterisation via the time varying transfer function, T(f,t).

This method has been greatly utilised in the study of land mobile radio propagation channels [2.1,2.29-2.31,2.35]. From these studies, descriptions of the propagation channel in terms of the statistical parameters relating to the fading envelope of the transmitted tone have been presented. It has been shown that, over spatial distances of a few tens of wavelengths, where the mean signal level is approximately constant, the variations in the envelope of the received signal are Rayleigh distributed. Departures from a Rayleigh distribution for areas with a strong specular component have been better described in terms of Rician statistics. The phase has been assumed to be uniformly distributed from $-\pi$ to π [2.1]. Therefore, the received signal constitutes a narrowband complex Gaussian process when the channel is excited by a single tone.

In addition to the small-scale variations, there is a perturbation in the mean received signal strength due to gross changes in the environment. These large-scale variations

are approximately lognormally distributed with a distance dependent mean. However, it is usually the small-scale statistics that are of utmost importance to systems designers.

Several small-scale models have been proposed [2.1,2.36-2.39] to describe the behaviour of the narrowband propagation channel, and all showed reasonable agreement with single tone measurements of the fading envelope. Hardware and software simulators based on these models have been developed [2.1,2.40-2.42] and have proved extremely useful in the assessment of various narrowband transmission systems.

Although Jakes [2.1], Clarke [2.38] and Gans [2.39] extended their models to include the correlation between two spaced frequencies in the presence of time delayed multipath, it is obvious that, in order to verify the models, the single tone measurements have to be repeated over the frequency band or an alternative sounding technique used. Hence, although the implementation of such a system is relatively easy, it does not explicitly illustrate the frequency selective behaviour of the channel. A direct extension of the single tone method to study the frequency coherence has been used in the form of spaced tone sounding.

2.5.1.2 Spaced Tone Method

In order to study the frequency selective fading of the envelope of the received signal, two tones adequately spaced in frequency are used as the sounding signal. This corresponds to the description of the channel using the frequency correlation function (FCF) which was defined in section 2.2.2. If the experiments are repeated with different spacings of the tones over the bandwidth of interest, an adequate description in the form of the two dimensional function of frequency shift and time is obtained.

This technique was used by Ossana and Hoffman at 836 MHz in suburban areas of USA. Their unpublished work was presented by Clarke [2.38], Gans [2.39] and Jakes [2.1] to support their theoretical scattering models in predicting the frequency

coherence of time delay multipath channels. The validity of these models was further substantiated by comparing the theoretical results with those obtained by Young and Lacy [2.43]. Comparisons of the measured frequency correlation functions have been generally made with multipath situations where the time delay spread is assumed to have a smooth distribution as a function of time delay. While this may be valid in some cases, it is possible that the multipath time delay distribution may be of a *spikey* nature with echoes having significant energy arriving at larger delays compared to the shortest path. This results in a frequency correlation function that is highly oscillatory and therefore constitutes a multivalued function [2.6,2.14,2.18,2.44-2.45]. As a result, ambiguities in determining the correlation bandwidth of the channel could arise depending on the separation of the transmitted tones. Similar observations have been noticed in the work presented in this study. An example of a measured power delay profile and its corresponding frequency correlation function is shown in Figures 2.1 and 2.2 respectively.

One obvious method of overcoming this ambiguity problem is to use a frequency hopping technique [2.18], which essentially measures the complex frequency response of the channel by sequentially stepping the tones across a band of frequencies. There is, however, a possibility of obtaining ambiguous results for the frequency correlation function, if the frequency separation is too large. Thus, the type of environment under surveyance should be considered.

Whilst the frequency hopping technique provides a wideband measurement with relatively simple and inexpensive narrowband equipment, it has two major drawbacks. Firstly, stepping a synthesizer over a large bandwidth is time consuming, even using modern fast switching designs. Secondly, it is impossible to make mobile measurements using such a system due to the stepping frequency technique. Therefore, no Doppler shift and hence, angle of arrival information can be obtained, which precludes identification of significant single scatterers.

An alternative approach which has been utilised in high resolution radars and HF

ionospheric links is a swept frequency continuous wave (chirp) technique [2.46-2.48]. A chirp signal is characterised by a linear frequency increase or decrease over a bandwidth, B, in a period of time, T. For measurements in the mobile radio environment, T should be small enough to ensure stationarity in the channel. If the chirp is repeated at a frequency, f_r, where f_r is the reciprocal of T, then the unambiguous Doppler coverage of the system is given by

$$F_d = \pm\frac{f_r}{2} \tag{2.8}$$

The time resolution is given by the reciprocal of the swept bandwidth, B.

Detection of the chirp signal may be achieved by either convolution or correlation. Convolution would involve the manufacture of a filter matched to the chirp signal and the output will consist of compressed pulses separated by the differential time delays between the different multipath components. On the other hand, correlation detection would require a locally generated dechirping signal which needs to be synchronised with the transmitted chirp. In this case, the output from the correlator would be made up of a series of beat notes with frequencies corresponding to the various multipath components. Although chirp sounders have been deemed to be more flexible in terms of conducting measurements over various bandwidths [2.49], a disadvantage is the reduction in the system resolution due to high sidelobes which result after the compression process.

Alternatively a network analyzer based receiver system can be employed [2.50]. A major limitation particular to this method is that, both the transmitter and receiver must be linked to the network analyzer by a coaxial cable. This therefore limits its application to relatively small indoor environments. However, the main practical difficulty is the calibration in order to remove the effects of the antennas, cables and power amplifiers which must be done in a clutter-free environment.

2.5.2 Wide Bandwidth Channel Sounding Techniques

2.5.2.1 Periodic Pulse Sounding Method

This technique is effected by probing the channel with a periodic wideband RF pulse. The received signal represents the convolution of the sounding pulse with the impulse response of the propagation channel, and hence provides a direct measure of the impulse response of the channel. The duration of the pulse determines the minimum echo path resolution of the system while the repetition frequency determines the maximum unambiguous propagation time delay that can be measured.

This method has been utilised by many researchers in this field [2.12,2.23,2.26,2.33,2.43] for outdoor as well as indoor environments. The simplistic nature of this technique is its main advantage. However, this apparent advantage is outweighed by the peak power requirement of the system that is necessary for the detection of weak echoes. For example, Turin *et al* [2.12] used peak transmitter powers ranging from 390 W to 3.24 kW. A further drawback of utilising this technique is the use of the video response of the received signal to trigger the collation of data [2.23,2.26,2.43]. This makes it impossible to distinguish between a line-of-sight or delayed obstructed path which appears as the first observable echo. This can, however, be remedied by the use of a common highly stable reference clock [2.12]. The use of photographic methods for data recording [2.12,2.43], made post processing of the data difficult. In general, pulse transmitters are peak power limited, prone to interference due to lack of processing gain, and therefore, a possible solution to this problem is to utilise a channel sounding technique which provides pulse compression at the receiver.

2.5.2.2 Pulse Compression Techniques

Inherent advantages of pulse compression include reduced interference to users sharing the same RF band, better immunity from certain types of interference and improved detectability within the peak power limitations of the transmitter. In systems which utilise this technique, deterministic waveforms which possess a noise-like character are used to angle modulate an RF carrier. At the receiver, pulse

compression can be obtained either by convolution using a matched filter, or by processing the signal using correlation. Evidently, there is a subtle difference between the two types of processing which will become clear in the next section. Since a pulse compression system is implemented at the receiver, the use of angle modulation will result in the necessary reduction in the required peak to mean power ratio at the transmitter.

The theory of linear systems provides the basis for pulse compression systems [2.51-2.52]. If white noise, n(t), is applied to the input of a linear system and the output, w(t), is cross-correlated with a delayed replica of the input, n(t-β), then the resulting cross-correlation coefficient is proportional to the impulse response of the system, h(β), evaluated at the delay time. This can be written as follows:

$$E[n(t)n^*(t-\beta)] = R_n(\beta) = N_o\delta(\beta) \qquad \textbf{(2.9)}$$

where $R_n(\beta)$ is the autocorrelation function of the noise and N_o is the single-sided noise power spectral density. The convolution relationship gives the output of the system as,

$$w(t) = \int h(\tau)n(t-\tau)d\tau \qquad \textbf{(2.10)}$$

Hence, the cross-correlation function of the output and the delayed input is given by,

$$\begin{aligned} E[w(t)n^*(t-\beta) &= E[\int h(\tau)n(t-\tau)n^*(t-\beta)d\tau] \\ &= \int h(\tau)R_n(\beta-\tau)d\tau \\ &= N_o h(\beta) \end{aligned} \qquad \textbf{(2.11)}$$

In experimental cross correlation type systems, deterministic waveforms which possess noise-like characteristics are generally employed, since white noise cannot be generated in practice. The most useful examples of such waveforms are the maximal length pseudo-random binary sequences (m-sequences or PRBS) [2.53]. These sequences are not strictly random, since their state transitions are determined by logic circuits and clock pulses. However, if the occurrences of the binary states are

observed with no prior knowledge of the runs of 1 s or 0 s in the sequence, they appear random. PRBSs are particularly useful because of their ease of generation from linear feedback shift registers and possession of excellent periodic autocorrelation properties.

The period, T, of a PRBS is determined by the number of stages in the shift register, N, and its chip rate, τ_o. The length of a PRBS is given by

$$m = 2^N - 1 \tag{2.12}$$

Hence, the period, T, can be expressed as

$$T = m\tau_0 = (2^N - 1)\tau_0 \tag{2.13}$$

The periodic autocorrelation function, $R_m(\beta)$, of a PRBS can then be expressed mathematically as,

$$R_m(\beta) = \begin{cases} m - \dfrac{(m+1)|\beta|}{\tau_0} & |\beta| \le \tau_0 \\ -1 & \tau_0 \le |\beta| \le (T - \tau_0) \end{cases} \tag{2.14}$$

The above equation shows that the autocorrelation function is a triangular function with a base width of $2\tau_o$ as illustrated in Figure 2.3. Figure 2.3 shows that, the maximum value of $R_m(\beta)$ equals m and occurs for a zero delay. Outside the interval $|\beta| \le \tau_o$, $R_m(\beta)$ has a residual bias value of -1. If $R_m(\beta)$ is normalised to the peak value m, then the peak value equals 1 and the residual bias value equals -1/m and therefore, $R_m(\beta)$ tends to a Dirac delta function, $\delta(\beta)$, as m tends to infinity and τ_o tends to zero. Hence, a PRBS will provide reasonable accuracy in the measurement of the impulse response of the channel depending on the values of m and τ_o.

The dynamic range (sensitivity to weak echoes) of such a system is limited by m due to the finite sidelobe levels, ie., it is the residual bias level of -1/m that limits the

dynamic range[2]. The value of m also determines the maximum unambiguous echo-path delay that can be measured by the system. The clock period of the PRBS determines the minimum detectable echo-path difference. They are two methods by which pulse compression can be achieved in practice, convolution matched filter technique and correlation technique. A discussion of these follows.

2.5.2.2.1 The Convolution Matched-Filter Technique

This method is usually effected by transmitting a CW signal, phase-reversal modulated by a PRBS. In the receiver, pulse compression is achieved by using a filter which is matched to the sounding waveform. If x(t) represents the PRBS waveform, then, for a physically realisable matched-filter, its impulse response must be x(T-t) [2.51]. It follows that, if x(t) is the input to a linear channel with an impulse response h(t), then, the output from the matched-filter, w(t), is given by the following convolution relationship,

$$w(t) = h(t) \otimes x(t) \otimes x(T-t) \qquad \textbf{(2.15)}$$

If the convolution of x(t) and x(T-t) is expressed as,

$$y(t) = \int x(\beta)x(T-t+\beta)d\beta \qquad \textbf{(2.16)}$$

then the convolution of h(t) and y(t) is given by

$$w(t) = \int h(\tau)y(t-\tau)d\tau \qquad \textbf{(2.17)}$$

This implies that w(t) can be written as

$$w(t) = \int h(\tau)\int x(\beta-\tau)x(T-t+\beta)d\beta d\tau \qquad \textbf{(2.18)}$$

The inner integral represents the autocorrelation function of the PRBS waveform within the period of observation, i.e.,

---

[2]It has been shown theoretically and analytically [2.54] that the dynamic range for an STDCC system is a function of the post multiplier filter if a bipolar and unipolar PRBS is employed in the transmitter and receiver respectively.

$$\int x(\beta-\tau)x(T-t+\beta)d\beta \propto AR_x(t-T-\tau) \tag{2.19}$$

where A is a proportionality constant. Hence,

$$\begin{aligned} w(t) &\propto A\int h(\tau)R_x(t-T-\tau)d\tau \\ &\propto Ah(\tau-T)\otimes R_x(t-T) \end{aligned} \tag{2.20}$$

If the autocorrelation function R_x(t-T) is a close approximation to the Dirac delta function, then the output of the matched-filter approximates to the impulse response of the propagation channel as a function of real time, i.e.,

$$w(t) \propto Ah(t-T) \tag{2.21}$$

This technique was utilised by Bajwa [2.6] in his study in the City of Birmingham, in which an experimental Surface Acoustic Wave (SAW) device was used to implement the matched-filter. In this study, accurate timing information at the receiver was provided by a timing circuit which was synchronised to the transmitter prior to each experimental run. Since the filter output was coherently demodulated using quadrature carriers, the phase information could be extracted from the measurements. Due to the large bandwidth of the quadrature baseband video responses, a suitable bandwidth reduction technique had to be employed to facilitate recording of data.

This technique has the advantage that it does not require local regeneration of the transmitted PRBS at the receiver in order to achieve pulse compression. However, the requirement for a suitable bandwidth reduction technique before recording of the impulse responses and the deficiencies associated with the manufacture of practical SAW devices greatly limits its appeal for mobile radio channel sounding. Specifically, the generation of spurious acoustic signals gives rise to phenomena such as multiple reflection, bidirectional re-radiation and scattering of the surface acoustic waves [2.6]. Also, since the devices are fabricated using standard photolithographic techniques, the placement accuracy in the mask-making process produces errors in the positioning of

the interdigitated transducers. As excitation of the transducers is dependent on the accurate spatial position of these interdigitated transducers, a degradation in performance arises. This manifests itself as time sidelobes in the output of the matched filter, and hence, causes a reduction to the sensitivity to weak echoes.

Alternatively, the convolution process can be implemented digitally off-line [2.56], since fast digital signal processors and analogue-to-digital converters are now widely available. This has been shown to possess enhanced overall performance due to the elimination of the limitations imposed by practical SAW devices. This technique, however, requires a very high sampling rate, resulting in a need to store large amounts of data. It also makes on-line viewing of the measured data impossible.

2.5.2.2.1 Swept Time-Delay Cross-Correlation (STDCC) Technique

Equation (2.11) clearly illustrates the principle of this technique, but highlights an obvious difference when compared to the convolution method as shown in Equation (2.20). Specifically, the output of the matched-filter is a series of snapshots, in real time, of the impulse response of the channel. The time delays therefore appear in time, and this amounts to a 1:1 mapping of time delays in the time domain. However, the output of the correlator is a sample of the impulse response at a single delay time. To make the two methods equivalent, a densely tapped delay line comprising of infinitesimal time delay lags and a bank of correlators would be needed, and in this case the time delays would be related to the correlation lags. Obviously, a practical system would be limited by the finite number of correlators and time delay elements which can feasibly be implemented. Price and Green [2.57] employed this technique in their famous RAKE receiver.

It is possible, however to design a receiver with only a single cross-correlator if the relative delay between the two PRBSs is allowed to vary linearly with time. This can be achieved by, either discretely stepping through each of the m phases of the PRBS or by slightly offsetting the clock frequencies of the two PRBSs and hence, causing the relative delay between them to vary linearly with time. The various correlation

peaks emerge as the received signal sweeps slowly across the reference. As a result, the parallel form of processing found in the RAKE system, is transformed into a serial form, with the penalty that instantaneous impulse responses can no longer be observed. Therefore, inherent in both techniques is time scaling, ie., bandwidth reduction of the correlator output. The swept time-delay cross-correlation technique which was first proposed by Bailey [2.58] for the characterisation of tropospheric scatter, has been widely used in the field for practical mobile radio channel sounders.

The first researcher to utilise the STDCC method in the field of mobile radio propagation was Cox [2.9], in which a scaling factor (bandwidth compression) of 5000 was used. Due to the inherent time scaling in the system, bandwidth reduction is not required. Since then, many researchers have utilised derivatives of Cox's sounder [2.7,2.14-2.16] for research in this field as will be seen in the next section.

An alternative approach which was developed by Levy *et al* [2.59] involves a process of off-line correlation and has been used by Street *et al* [2.60]. The main difference is in the receiver, where an identical frequency standard to that in the transmitter is used to clock a software generated modulated m-sequence and digital processing is then used to achieve the correlation process. This was shown to achieve a superior dynamic range over the hardware based STDCC method but with the penalty of extra computational complexity and eliminates the possibility of on-line viewing of the data in the field. It also requires very high sampling rates.

2.6 REVIEW OF PREVIOUS WIDEBAND EXPERIMENTS

Propagation studies in mobile radio environments have generally used qualitative descriptions to classify the different types of mobile radio scenarios. Often these environments have been described as dense-urban, urban or simply rural or residential. Although these measures are vague in the quantifying sense, there is no clear cut definitive way by which an area or a building can be categorised. Some methods have been used [2.6,2.61] which bring in factors such as storey index, land usage factor, building area density, building location with reference to the

surroundings, etc.

It is, however, easy to classify the mobile radio environment into two major categories: indoors and outdoors. The outdoor environments where mobile radio systems are expected to operate are relatively open and high power transceivers are usually deployed. The multipath power delay profile of such a channel often contains significant echoes arriving at long time delays. On the contrary, low power transceivers would be used in indoor environments. The consequence of this is that, as well as the additional building attenuation, echo contributions with significant time delays are improbable. The surroundings and the motion of scatterers in indoor environments will therefore have a relatively greater effect on the channel response due to the more shadowed transmitter and receiver antennas. This implies that the power delay profile will be more compact, but more susceptible to the surroundings. There has therefore, been a growing trend to obtain channel characterisations in all or most environments where a mobile radio system is expected to operate.

In the ensuing sections the previous work of other researchers is reviewed in these two categories. Special emphasis will be on the various measurement techniques that were utilised and their associated drawbacks. Furthermore, the methodology used and the results that were presented will be summarised for comparison with those obtained from this study.

2.6.1 Outdoor Experiments

The first wideband mobile radio propagation studies were carried out by Young and Lacy [2.43] in New York City in 1950. In their experiments, the periodic pulse sounding technique was employed in which a 0.5 μs pulse with a 10 kHz repetition period was used to modulate a 450 MHz carrier. This corresponds to a spatial resolution of 150 m and a maximum measurable excess time delay of 100 μs. The transmitted pulse had a peak power of 100 W, which was radiated from a vertically polarised antenna having a gain of 6 dB. At the mobile receiver, the pulsed RF carrier and the time delayed echoes due to multipath were received on a quarter-

wavelength antenna, before being fed to a conventional front end. The received signal was then translated to an IF frequency of 30 MHz and an envelope detector used to obtain the video response of the channel, which was subsequently displayed on an oscilloscope. An automatic gain control (AGC) was used in the IF stage so as to maintain the amplitude of the largest echo at a predefined level. The video response of the channel was also used to trigger the oscilloscope and therefore, in order to avoid missing the start of the first impulse response, the video response was passed through a 5 μs delay element before being fed to the oscilloscope.

A record of the impulse response of the channel was obtained by photographing the oscilloscope display with a 16 mm moving picture camera. To ensure that the measurements yielded unbiased results, photographs were taken at half mile intervals on an imaginary grid. At these locations, photographs were taken at a rate of 16 per second. With a vehicle speed of 10-15 m.p.h., this meant that successive pictures contained impulse responses corresponding to locations spaced approximately one foot of linear travel apart.

Clearly, the use of AGC removed the possibility of measuring the absolute signal level of the echoes, since this was not recorded. The use of photographic data recording also makes post data processing a difficult and time consuming task. Further, the use of an envelope detector implied that complex impulse response measurements could not be achieved.

A more comprehensive measurement programme was conducted by Turin et al [2.12] in 1972 using the same method as Young and Lacy. In these experiments, pulses with half power widths of 0.1 μs were used to probe the channel at carrier frequencies of 488, 1280 and 2920 MHz. The peak transmitted powers depended on the frequency and location of the experiment and ranged from 390 W to 3.24 KW. Receivers for the three frequencies were housed in the mobile and the video outputs were connected to a three trace oscilloscope with a camera attached for photographic recording. The use of IF logarithmic amplifiers with 60 dB dynamic range obviated the need for

automatic gain control.

Since the aim of the experiments was to use the measured impulse responses to obtain a statistical model of the urban multipath channel, it was necessary to obtain accurate timing measurements with respect to the line-of-sight time delay. This was achieved by using Rubidium atomic frequency standards at both the transmitter and receiver. These needed to be synchronised prior to the start of any experimental run. The transmitter clock was connected so as to pulse the transmitter once a second, while the receiver clock was connected so as to trigger the oscilloscope a short time, τ seconds later. τ was set less than the expected line-of-sight time delay and the traces were adjusted to provide 10 μs of video response of the multipath behaviour.

Van Rees [2.26,2.62] employed the periodic pulse method in his studies in the Netherlands. Impulse response measurements were obtained by transmitting a 10 W peak power pulse at 910 MHz, every 100 μs from a moving vehicle. Pulse durations of 50 ns, 100 ns [2.62] and 200 ns [2.26] were used. The receiving equipment was set up on the roof of a 50 m tall building. A directional antenna was used in the receiver, which was essentially of a similar design to that used by Turin et al [2.12], the only difference being in the method of data acquisition. In this case, the recording of the impulse responses was achieved by utilising a high speed digitiser capable of storing 512 data points at a sampling rate of 50 MHz. Although it was possible to detect echoes with excess time delays of up to 100 μs, only the first 10 μs of each impulse response was stored on a 10 MByte hard disk. The data transfer rate of between 20 to 50 ms depending on the pulse duration set the rate of data collection. The trigger level of the digitiser was set just above the noise floor of the receiving system, and therefore the video response was used to initiate triggering as in [2.43].

The earliest complex impulse response measurements of the mobile radio made using the STDCC technique were conducted by Cox [2.9] in New York City at 910 MHz. In his experiments a 511-bit PRBS at a chip rate of 10 MHz was used to phase-reversal modulate a 70 MHz carrier. This modulated signal was then translated to the

sounding frequency by mixing with an 840 MHz carrier and the resulting 910 MHz modulated signal was amplified (10 W) and radiated from an omnidirectional antenna, fixed on a 20 m tower. All frequencies were derived from a stable 5 MHz frequency standard.

The signal was received on a quarter wavelength monopole and applied to a receiver with a conventional front end. The resulting signal was subsequently translated to an IF frequency of 70 MHz. The 70 MHz IF signal was then split in a wideband quadrature hybrid before application to two correlators. Again, all frequencies were derived from a similar 5 MHz standard.

In each correlator, an identical PRBS to that in the transmitter, but clocked at the slightly slower rate of 9.998 MHz was used to phase-reversal modulate a 70 MHz carrier. This signal was then multiplied with the IF signal from the quadrature hybrid and a low-pass filter on each arm completed the correlation process.

The complete system offered a 0.1 μs time resolution and a maximum excess delay of 51.1 μs. The difference in clock rates between the two PRBSs, which was 2 kHz, determines the bandwidth of the correlation function. This corresponds to a time scaling factor of 5000. This implies that the features of 5000 individual impulse responses are contained within each power delay profile obtained at the output of the cross-correlator. Since it was anticipated that echo path delays would not exceed 15 μs, the receiver PRBS was reset every 75 ms (5000 x 15 μs). All measurements were made at a constant speed of 1.4 m/s, and thus the spatial distance traversed by the mobile in 75 ms was approximately one third of the carrier wavelength. As a result, the 5000 individual complex responses are unlikely to have appreciably altered in their multipath structure. The validity of this argument was later confirmed by Bajwa [2.6] in his real time observation of the output of his matched filter receiver. The inherent bandwidth reduction therefore, allowed for easy data recording using a conventional analogue tape recorder.

Although there was a phase change of about 360° in 10 s, the relative phases of each path were more important. This therefore permitted the measurement of the Doppler shifts associated with various paths to be evaluated. Hence, for the first time, it was possible to simultaneously measure the time delays and the Doppler shifts in mobile radio channels.

The convolution matched filter sounding method was used by Bajwa [2.6] in Birmingham, in which an experimental surface acoustic wave (SAW) device was used to realise the matched filtering. In these experiments, a 76.5 MHz carrier was phase-reversal modulated with a 127-bit PRBS which was clocked at 12.75 MHz. The resulting signal was then translated to 436.5 MHz and subsequently amplified. This signal, with a mean power of 1 W was then radiated using a collinear array of folded dipoles. All frequencies were derived from a highly stable 5 MHz crystal oscillator.

In the receiver, an identical 5 MHz crystal oscillator was used to derive all the required frequencies. After suitable front end amplification and filtering, the received signal was translated to an IF frequency of 76.5 MHz, which was then applied to the input of the SAW device. This constituted a matched filter for the 76.5 MHz carrier, phase-reversal modulated by the 127-bit PRBS. Hence, pulse compression was achieved as successive bursts of the 76.5 MHz carrier were obtained at the filter output for each multipath time-delayed component of the received signal. The output of the SAW device was split into two cophasal components before demodulation to baseband using quadrature carriers. The bandwidth of the quadrature baseband video responses was 12.75 MHz and thus, necessitated the need for a suitable bandwidth reduction technique before data acquisition. A bandwidth reduction to 6.375 kHz (scaling factor of 2000) was effected using a sample-and-hold arrangement. The resulting output was then recorded on a conventional tape recorder.

Accurate timing information, at the receiver, was provided by a timing circuit which was synchronised to the transmitter clock prior to each experimental run. It was therefore possible to distinguish between line-of-sight and obstructed paths arriving

as the first discernible echo. Following suitable data processing, all information concerning echo time-delays, Doppler shifts, etc., could be obtained.

The frequency hopping technique was employed by Matthews and Molkdar [2.63] to measure the complex frequency response of the UHF mobile radio channel. Their experiments in Leeds were undertaken in three frequency bands, viz 852-888 MHz, 917-923 MHz and 952-958 MHz in areas ranging from open suburban to dense urban. At the transmitter modulation frequencies of 25, 50 and 100 kHz were generated and used to modulate the carrier frequency. The separation of the sidebands could therefore be set to 50, 100 or 200 kHz. For each band of frequencies, measurement of the complex frequency response was effected by transmitting pairs of frequencies. All frequency sources in the transmitter and receiver were locked to highly stable Rubidium frequency standards in order to maintain phase synchronism.

The stepping operation at both the transmitter and receiver were controlled by microcomputers. In the receiver, the group delay was measured by comparing the phase of the difference frequency between the two carriers with a locally generated reference frequency. The amplitude of one of the carriers was also measured. From the measurement of the complex frequency response of the channel, the frequency correlation function was determined. This was then inverse Fourier transformed to obtain the power delay profile.

One of the main disadvantages in these experiments was the time necessary to conduct the measurements, due to the requirement of having to wait for the frequencies and phase to settle before measurements are made. This results in a low stepping rate. Furthermore, only static measurements could be achieved, hence no Doppler shift information.

The complex impulse response of urban mobile radio channels at a carrier frequency of 900 MHz in Liverpool was measured by Demery [2.7] using an improved version the STDCC sounder, to that used by Cox [2.9]. Both the transmitter and receiver

complexities were greatly reduced by removing the IF stage and directly modulating the RF carrier with a 127-bit PRBS. The chip rate of the PRBS was 10 MHz, which provided a time resolution of 0.1 μs and a maximum excess time delay capability of 12.7 μs. In the transmitter, this modification eliminated the need for any RF filter after up-conversion of the signal. In the receiver, the modification implied that, the multiplicative part of the cross-correlation process had to be carried out at the same time as down-conversion to an IF of 69.93 MHz. This resulted in an IF bandwidth reduction from 20 MHz to twice the slip rate between the transmitter and receiver clocks. In this case, a slip rate of 2 kHz resulted in an IF bandwidth of 4 kHz and hence a bandwidth compression factor of 5000.

The 69.93 MHz IF signal was then split in a wideband quadrature hybrid and demodulated in two correlators in a similar manner to that of Cox [2.9]. The low-pass filtered quadrature outputs were then recorded on an analogue instrumentation tape. The reduced IF bandwidth therefore provided improved performance in the system and the accuracy of the outputs from the quadrature demodulator.

Recently, Natarajan [2.14] used the STDCC method, essentially similar to that employed by Demery, to measure the impulse response of the channel in a variety of environments at 1.8 GHz. The major difference is the use of envelope detection to achieve demodulation. This was effected using a logarithmic amplifier with an 80 dB dynamic range. As in Demery's case, the video output was recorded using an analogue instrumentation tape.

2.6.2 Indoor Experiments

In the mid-80s, the first generation of cellular mobile radio systems became operational and the concept of universal portable communications was well established. A knowledge of the propagation characteristics was necessary before these concepts could be fully realised. Hence, attention was being directed towards into and within building environments.

The first delay spread measurements within buildings were reported by Devasirvatham [2.64]. These measurements were conducted within a large office building at a carrier frequency of 850 MHz using a channel sounder based on that used by Cox. In these measurements, a 1023-bit PRBS at a chip rate of 40 MHz was used in the transmitter. In the receiver an identical PRBS clocked at a slower rate of 39.996 MHz provided a bandwidth compression factor of 10000. In the transmitter and receiver, vertically polarised sleeved dipole antennas were used. These were mounted about 2 m above the ground. The measurements were conducted by moving the transmitter or receiver through 8 equally spaced points along the perimeter of a 1.2 m square. These 8 measurements were averaged to obtain the average power delay profile.

A more comprehensive measurement campaign was also undertaken by Devasirvatham [2.34,2.65] at a carrier frequency of 850 MHz. The measurements were conducted using the same experimental system as that used in reference [2.64]. The transmitter and receiver antenna height was about 1.8 m. Measurements were conducted in two large dissimilar office buildings [2.65], office buildings and residences [2.34].

Generally, wideband propagation studies have been reported in factory buildings [2.33], office buildings and residences [2.34,2.65]. There has been, however, no published work on wideband propagation results in areas like supermarkets or train stations.

2.6.3 Comparison of Delay Spreads in Outdoor Macrocellular and Indoor Environments

In Tables 2.1 and 2.2, a summary of results from previous time dispersion measurements in a variety of outdoor environments at different carrier frequencies are listed. It is evident that, since comparable results have been obtained in similar locations at different carrier frequencies, the frequency independence of delay spread is almost confirmed. From these tables, it is clear that the radio channel in

mountainous and hilly regions is the most dispersive, with delay spreads ranging from 10-35 μs [2.67,2.75]. Delay spread values in dense-urban and urban areas are typically less than 4 μs although higher values (8-13 μs [2.66-2.67]) have been reported. In rural areas delay spread values are typically less than 1 μs [2.26], though larger values in areas with neighbouring hills have also been reported.

In indoor environments, only a small amount of delay spread results have been published, a summary of which is presented in Table 2.3. These results show that delay spread is less than 420 ns [2.34]. Overall median delay spread values ranging from 15.29-126 ns have been reported. It is interesting to note that the higher values of delay spread have been obtained from large buildings with cluttered surroundings.

It is worthwhile pointing out that some of these results have been based on data obtained from mostly worst case locations. The implication of this is that some of time dispersion descriptors may be over-estimated.

2.7 OVERVIEW OF SPREAD SPECTRUM SYSTEMS

It is well known that the frequency bands allocated for mobile radio communications are highly congested. With the ever increasing demand for mobile radio services, there is, therefore, a need to use communication techniques which offer efficient spectrum utilisation with enhanced system performance. In the past, the use of spread spectrum techniques has been confined to military defence systems for anti-jamming tactical transmission and aircraft guidance handling. Recently, there has been an overwhelming interest in deploying spread spectrum techniques for civilian purposes. A few of such applications include mobile radio communications, indoor wireless communications, satellite communications and power line carrier transmission systems. The first two applications are relevant in the field of mobile radio communications, especially because of the advent of PCS.

The code division multiple access (CDMA) capability of spread spectrum systems arises from the auto-correlation and cross-correlation properties of the pseudo-random

sequences used in the signal spreading process [2.53]. Basically, spread spectrum techniques can be classified in three categories:

i. Direct sequence spread spectrum (DS/SS), where the data bits are modulated by a pseudo-random code sequence to generate the spreading function.

ii. Frequency hopping spread spectrum (FH/SS), where the carrier frequency is changed in a pseudo-random manner over the spread bandwidth.

iii. Time hopping (TH/SS) modulation where rapid bursts of the data-modulated carrier are transmitted, with each burst having a pseudo-random duration and start instant.

The amount of improvement that is achieved through the use of spread spectrum techniques is termed the processing gain, and can be defined as the ratio of the spread bandwidth to the information rate. The above techniques have their advantages and disadvantages[2.53]. However, deploying a hybrid system is a possibility which can be used to exploit only the advantages of each technique.

Spread spectrum techniques for mobile radio communications appear to be suitable because of their multiple access capability and the prospect for the evolution of very high capacity systems [2.76]. Other characteristics like protection against interference and\or multipath fading and inherent privacy of the modulated signal also appear very valuable in the field of mobile radio communications. Wireless communications in an indoor environment are characterised by a Rayleigh fading multipath channel. The robustness of a direct sequence (DS) spread spectrum system to the path delay distribution seems promising.

2.7.1 CDMA System Benefits

The inherent existence of multiple paths in a mobile radio environment causes severe fading in the received signal level in narrowband FDMA cellular systems. With CDMA, the different paths may be independently received, thus greatly reducing the severity of multipath fading. Although some fading behaviour still exists due to the

inability of the demodulator to independently process certain paths[3], the received signal level is very much enhanced.

A favoured approach for mitigating the fading phenomenon is diversity, of which there are three major types, viz, time, frequency and space diversity [2.1]. Time diversity can be obtained by the use of interleaving and error correction coding. A wideband system, like CDMA, offers a form of frequency diversity by spreading the signal energy over a wide bandwidth. Space or path diversity can be exploited in three main ways. Firstly, the possibility of using soft handoff allows the mobile unit to receive multiple paths from simultaneous links from two or more base stations. There is therefore a possibility of enhanced signal reception in the fringe areas. Secondly, the multipath environment can be exploited by deploying a Rake receiver architecture. This allows signals arriving with different propagation time delays to be received separately and combined. Lastly, antenna diversity, which has already been greatly utilised in mobile radio communication systems, can also be employed.

Antenna diversity can be deployed in FDMA and TDMA systems. Time diversity can be used for any digital mobile radio system that can tolerate the required higher transmitted symbol rate needed to make the required error correction process effective. However, the other methods can only be easily realised in a CDMA system. In fact, the provision of extensive path diversity is a unique feature of direct sequence CDMA and the greater the order of diversity in a system, the better the performance. Qualcomm [2.76] has proposed a 3- and 4-path Rake receiver for the uplink and downlink respectively in their proposed CDMA system.

Other CDMA system benefits include high capacity, low transmit power, voice activity detection, soft capacity and its ability to coexist with existing narrowband systems.

---

[3] All paths that arrive at the receiver antenna with time delays less that the time resolution of the receiver will combined vectorially to give the signal at that time. Hence, these unresolved paths may cause fading. This has been observed in some wideband studies [2.6-2.7, 2.12].

2.7.2 Propagation Aspects of Spread Spectrum Systems

Unlike other multiple access techniques, the performance of a CDMA system can only be realistically evaluated in the presence of the majority of the other system users. It will therefore be very expensive to undertake a hardware-based system evaluation, even though it is desirable. However, a lot of work based on simulation has been conducted to evaluate the performance of CDMA systems [2.66-2.77]. In order to fully exploit the benefits of a CDMA system, a large amount of propagation data is required, to evaluate its performance so as to fully exploit its advantages.

Inherent in a direct sequence CDMA system is the near-far [2.53] problem since all mobile stations utilise the same frequency band. This can be alleviated by an efficient power control algorithm, which can only be implemented by having a thorough knowledge of the wideband propagation channel. An efficient power control algorithm will also enhance the capacity of the system and will result in a reduction of the average transmitted power. Furthermore, the Rake gain can only be achieved by proper designing of the Rake receiver. The main features of a Rake receiver include the number of taps, time span, echo cancellation or diversity combining, which have to be carefully selected to provide optimum performance at low cost. Also the system bandwidth has to be chosen and or whether direct sequence or frequency hopping should be used or even a hybrid system.

Most of the solutions can be obtained by providing wideband propagation data which can be analysed to provide information about the time and frequency response of the radio channel, hence a major requirement to provide the relevant data that shows the variations in time and frequency of the radio channel and the transmission loss associated with it.

In Chapter 4, a BPSK Rake receiver model is presented. Parameters for this receiver model are taken from the experimental data. The Rake receiver is then used to show the Rake gain and the necessity of power control in a CDMA system. In this analysis, the signal-to-noise ratio (SNR) is used as a measure of performance. Furthermore,

by analysing the short term variability of the received SNR, speed of the power control algorithm can be investigated.

2.8 SUMMARY

The channel characterisation techniques and previous experimental investigations into wideband channel characterisation have been presented. The purpose of conducting the experiments in this study is to expand on the amount of knowledge concerning wideband propagation in different locations. Most importantly, these experiments should be conducted in a manner that will provide a realistic picture of the channel.

In the next chapter, the requirements of an experimental channel sounding system are discussed before a presentation of how the system was implemented and evaluated.

REFERENCES

[2.1] Jakes, W. C., 'Microwave Communications', John Wiley, 1974.

[2.2] Lee, W.C.Y., 'Mobile Communication Design Fundamentals', Sams, 1986.

[2.3] Zadeh, L.A., 'Frequency Analysis of Variable Networks', Proc. IRE, 38, 1950, pp291-299.

[2.4] Kailath, T., 'Sampling Models for Linear Time-variant Filters', M.I.T. Research Lab. of Electronics, Cambridge, Mass., Rep. No. 352, 1959.

[2.5] Bello, P. A., 'Characterisation of Randomly Time-variant Linear Channels', IEEE Transactions on Communication Systems, Vol. CS-11, Dec. 1963, pp360-393.

[2.6] Bajwa, A. S., 'Wideband Characterisation of UHF Mobile Radio Propagation in Urban and Suburban Areas', PhD. Thesis, Department of Electronic and Electrical Engineering, University of Birmingham, 1979.

[2.7] Demery, D. A., 'Wideband Characterisation of UHF Mobile Radio Channels in Urban Areas', PhD. Thesis, Department of Electrical Eng. and Electronics, University of Liverpool, 1989.

[2.8] Kennedy, R.S., 'Fading Dispersive Communication Channels', Wiley-Interscience, 1969.

[2.9] Cox, D. C., 'Delay Doppler Characteristics of Multipath Propagation at 910 MHz in a Suburban Mobile Radio Environment', IEEE Transactions on Antennas and Propagation, Vol. AP-20, No. 5, Sept. 1972, pp625-635.

[2.10] Cox, D.C., '910 MHz Urban Mobile Radio Propagation: Multipath Characteristics in New York City', IEEE Trans. Comm., Vol. COM-21, No. 11, Nov. 1973, pp1188-1194.

[2.11] Parsons, J.D., and Bajwa, A.S., 'Wideband characterisation of fading mobile radio channels', IEE Proc. Pt. F, Vol. 129, No. 2, April 1982, pp95-101.

[2.12] Turin, G. L., Clapp, F. D., Johnston, T. L., Fine, S. B. and Lavry, D., 'A Statistical Model of Urban Multipath Propagation', IEEE Transactions on Vehicular Technology, Vol. VT-21, No. 1, Feb. 1972, pp1-9.

[2.13] Turkmani, A.M.D., Demery, D.A. and Parsons, J.D., 'Measurement and Modelling of Wideband Mobile Radio Channels at 900 MHz', IEE Proc. Pt. I, Vol. 138, No.5, Oct. 1991, pp447-457.

[2.14] Natarajan, N., 'Wideband Characterisation of Mobile Radio Channels at 1.8 GHz', PhD. Thesis, Department of Electrical Eng. and Electronics, University of Liverpool, 1992.

[2.15] Huish, P. W. and Gurdenli, E., Radio Channel Measurement and Predictions for Future Mobile Radio Systems', BR. Telecom. Technol. J., Vol. 6, No. 1, Jan 1988, pp43-53.

[2.16] Sousa, E.S., Jovanovic, V.M. and Daigneault, C., 'Delay Spread Measurements for the Digital Cellular Channel in Toronto', IEEE Trans. on Veh. Tech., Vol. 43, No. 4, Nov. 1994, pp837-847.

[2.17] Parsons, J. D., 'The Mobile Radio Propagation Channel', Pentech Press, London 1992.

[2.18] Molkdar, D. and Matthews, P.A., 'Measurements and characterization of the UHF mobile radio channel. Part 1: Measurements over the band 853-885 MHz', Journal IERE, Vol. 58, No. 6 (supplement), Sept. - Dec. 1988, ppS145-S156.

[2.19] CCIR Report 567-3 (MOD F), 'Propagation Data and Prediction Methods for the Terrestrial Land Mobile Service Using the Frequency Range 30 MHz to 3 GHz', CCIR XVIIth Plenary Assembly, Dusseldorf, 1990.

[2.20] Bajwa, A.S., 'UHF Wideband statistical model and simulation of mobile radio multipath propagation effects', IEE Proc. Pt. F, Vol. 132, No. 5, Aug. 1985, pp327-33.

[2.21] Suzuki, H., 'A statistical model for urban radio propagation', IEEE Trans. on Communs., Vol. COM-25, No. 7, July 1977, pp203-210.

[2.22] Hashemi, H., Tholl, D., and Morrison, G., 'Statistical modelling of the indoor radio propagation channel - Part I', IEEE 42nd Veh. Tech. Conf., Denver, May 1992, pp338-342.

[2.23] Saleh, A.A.M. and Valenzuela, R.A., 'A statistical model for indoor multipath propagation', IEEE J. Selected Area Comms., Vol. 5, No. 3, Feb. 1987, pp128-137.

[2.24] Parsons, J.D., Turkmani, A.M.D., and Khorami, M., 'Microcellular radio modelling', IEE 6th Int'l. Conf. on Mobile Radio and Personal Communications, Publ. No. 351, Dec. 1991, pp182-190.

[2.25] Seidel, S.Y., Rappaport, T.S., Jain, S., Lord, M.L. and Singh, R., 'Pathloss, scattering and multipath delay statistics in four European cities for digital cellular and microcellular radiotelephone', IEEE Trans. on Veh. Tech., Vol.

40, No. 4, Nov. 1991, pp721-730.

[2.26] Van Rees, J., 'Measurements of the wideband radio characteristics for rural, residential and sub-urban areas', IEEE Trans. on Veh. Tech. Vol. 36, No. 1, Feb. 1987, pp2-6.

[2.27] Bajwa, A.S. and Kafaru, O.O., 'A simple environment-dependent approach to wideband multipath propagation modelling', IEE Colloquium on Propagation in an Urban Environment, Savoy Place, London, 3rd April 1986, pp5/1-5/5.

[2.28] Okumura, Y., Ohmori, E., Kawano, T. and Fukuda, K., 'Field Strength and its Variability in VHF and UHF Land-Mobile Radio Service', Rev. Elect. Commun. Lab., Vol. 16, Sept. 1968. pp825-873.

[2.29] Alexander, S.E., 'Radio Propagation within buildings at 900 MHz', Electronics Letters, Vol. 18, No. 21, 1982. pp913-914.

[2.30] Motley, A.J. and Keenan, J.M.P., 'Personal Communication Radio Coverage in Buildings at 900 MHz', IEEE Electronics Letters, Vol. 24, No. 12, 1988. pp763-764.

[2.31] Toledo, A.F., 'Narrowband Characterisation of Radio Transmissions into and Within Buildings at 900, 1800 and 2300 MHz', Ph.D. Thesis, Department of Electrical Eng. and Electronics, University of Liverpool, 1992.

[2.32] Pahlavan, K., Ganesh, R. and Hotaling, T., 'Multipath Propagation Measurements on Manufacturing Floors at 910 MHz', Electronics Letters, Vol. 25, No. 3, Feb. 1989. pp225-227.

[2.33] Rappaport, T. S., 'Characterisation of UHF Multipath Radio Channels in Factory Buildings', IEEE Transactions on Antennas and Propagation', Vol. 37, No. 8, Aug. 1989, pp1058-1069.

[2.34] Devasirvatham, D. M. J., 'Time Delay Spread and Signal Level Measurements of 850 MHz Radio Waves in Building Environments', IEEE Communications Magazine, Vol. 25, No. 6, June 1987, pp13-21.

[2.35] Atefi, A., 'An Investigation of Radio Wave Propagation in Mobile Frequency Bands', Ph.D. Thesis, Department of Electrical Eng. and Electronics, University of Liverpool, 1985.

[2.36] Ossanna, J.F., 'A Model for Mobile Radio Fading due to Building Reflections: Theoretical and Experimental Fading Waveform Power Spectra', Bell System Tech. Journ., Vol. 43, Nov. 19964, pp2935-2971.

[2.37] Gilbert, E.N., 'Energy Reception for Mobile Radio', Bell System Tech. Journ., Vol. 44, No. 8, Oct. 19965, pp1779-1803.

[2.38] Clarke, R.H., 'A Statistical Theory of Mobile Radio Reception', Bell System Tech. Journ., Vol. 47, July-Aug. 19968, pp951-1000.

[2.39] Gans, M. J., 'A Power-spectral Theory of Propagation in the Mobile-radio Environment', IEEE Transactions on Vehicular Technology, Vol. VT-21, No. 1, Feb. 1972, pp27-38.

[2.40] Arredondo, G.A., Chriss, W.H. and Walker, E.H., 'A Multipath Fading Simulator for Mobile Radio', IEEE Transactions on Vehicular Technology, Vol. VT-22, No. 4, Nov. 1973, pp241-246.

[2.41] Ball, J.R., 'A Real-time Fading Simulator for Mobile Radio', The Radio and Electronic Engineer, Vol. 52, No. 10, Oct. 1982, pp475-478.

[2.42] An, J.F., 'The Implementation of Mobile Radio Channel Simulators', Ph.D. Thesis, Department of Electrical Eng. and Electronics, University of Liverpool, 1991.

[2.43] Young, W. R. and Lacy, L. Y., 'Echoes in Transmission at 450 Megacycles from Land-to-Car Radio Units', Proc. IRE, Vol. 38, March 1950, pp255-258.

[2.44] Cox, D. C., 'correlation Bandwidth and Delay Spread Multipath Propagation Statistics for 910 MHz Urban Mobile Radio Channels', IEEE Trans. Comm. Vol. COM-23, No. 11, Nov. 1975, pp1271-1280.

[2.45] Nche, C., Parsons, J.D. and Turkmani, A.M.D., 'Indoor and Outdoor Time Dispersion Measurements at 1.8 GHz', IEE 9th Intl. Conf. on Antennas Propagation, ICAP95, IEE Conf. Publication No. 407, Vol. 2, April 1995, pp13-17.

[2.46] Salous, S., 'FMCW Channel Sounder with Digital Processing for Measuring the Coherence Bandwidth of Wideband HF Radio Links', IEE Proc. Pt. F, Vol. 133, No. 5, Aug. 1986, pp456-462.

[2.47] Bailey, R. and Summers, G.,'Radio Channel Characterisation for the Digital European Cordless Telecommunication Systems', BR. Telecom Tech., 8(1), 1990. pp25-30.

[2.48] Raekken, R.H., Langass, H., Lovnes, G. and Paulsen, S.E., 'Wideband Impulse Response Measurements at 900 MHz and 1.7 GHz', Globecom 1991, pp1303-1305.

[2.49] Salous, S., Pantzaris, P. and Green, P., 'FMCW Waveforms for UHF/SHF

Wideband Channel Sounders', IEE Colloquium on High Bit Rate UHF/SHF Channel Sounders - Technology and Measurement., Digest No. 1993/233, London, 3rd Dec. 1993, pp2/1-2/5.

[2.50] Street, A.M., Moss, J.G.O, Jenkins, A.P., Edwards, D.J. and Mehler, M.J., 'Indoor Propagation Measurements at Millimetric Frequencies', IEE 9th Intl. Conf. on Antennas Propagation, ICAP95, IEE Conf. Publication No. 407, Vol. 2, April 1995, pp9-12.

[2.51] Strembler, F.G., 'Introduction to Communication Systems', Addison-Wesley, 3rd Edition, 1990.

[4.52] Papoulis, A., 'Probability, Random Variables and Stochastic Processes', McGraw-Hill, 1965.

[2.53] Dixon, R. C., 'Spread Spectrum Systems', Wiley, New York, 1982.

[2.54] Street, A.M. and Edwards, D.J., 'A High Dynamic Range Swept Time Delay Cross Correlator, IEEE Electronic Letters Vol. 30, No. 21, Feb. 1994, pp1742-1744.

[2.55] Urkowitz, H., 'Signal Theory and Random Processes', Arteh House, Inc., 1983.

[2.56] Cullen, P.J., Fannin, P.C., and Molina, A., 'Wide-Band Measurement and Analysis Techniques for the Mobile Radio Channel', IEEE Transactions on Vehicular Technology, Vol. 42, No. 4, Nov. 1993, pp589-603.

[2.57] Price, R. and Green, P. E., 'A Communication Technique for Multipath Channels', IRE, Vol. 46, March 1958, pp555-570.

[2.58] Baily, C.C., 'Characterisation of Tropospheric Scatter Channels by Impulse Response Measurements', 16 th Symposium AGARD electromagnetic wave propagation panel (NATO), Dusseldorf, Germany, Aug. 31 - Sept. 4 1970, Part II, pp1-11.

[2.59] Levy, A.J., Rossi, J.P., Barbot, J.P. and Martin, J., 'An improved Channel Sounding Technique Applied to Wideband Mobile 900 MHz Propagation Measurements', 40th IEEE Vehicular Techn. Conf., Florida, May 6-9, 1990, pp513-519.

[2.60] Street, A.M., Jenkins, A.P. and Edwards, D.J., 'Time Delay Spread Profile Measurement Using a Spread Spectrum Off-line Correlation Technique', IEE Colloquium on High Bit Rate UHF/SHF Channel Sounders - Technology and Measurement., Digest No. 1993/233, London, 3rd Dec. 1993, pp1/1-1/5.

[2.61] Molkdar, D., 'A Reiview on Radio Propagation into and Within Buildings'.

[2.62] Van Rees, J., 'Measurements of Impulse Response of a Wideband Radio Channel at 910 MHz from a moving Vehicle', IEEE Electronic Letters Vol. 22, No. 5, Feb. 1986, pp246-247.

[2.63] Molkdar, D. and Matthews, P.A., 'Measurements and Characterisation of the UHF Mobile Radio Channel. Part 2: Characterisation over the Band 869-877 MHz',. Journal of IERE, Vol. 58, No. 6, Sept 1988, pp157-168.

[2.64] Devasirvatham, D. M. J., 'Time Delay Spread Measurements of Wideband Radio Signals Within a Building', Electronics Letters, Vol. 20, No. 23, Nov. 1984, pp950-951.

[2.65] Devasirvatham, D. M. J., 'A Comparison of Time Delay Spread and Signal Level Measurements Within Two Dissimilar Office Buildings', IEEE Transactions on Antennas and Propagation, Vol. AP-35, No. 3, March. 1987, pp319-324.

[2.66] Rappaport, T. S., Seidel, S. Y. and Singh, R., '900-MHz Multipath Propagation Measurements for U.S. Digital Cellular Radiotelephone', IEEE Transactions on Vehicular Technology, Vol. 39, No. 2, May. 1990, pp132-139.

[2.67] Seidel, S.Y., Rappaport, T.S., Jain, S., Lord, M.L. and Singh, R., 'Pathloss, scattering and multipath delay statistics in four European cities for digital cellular and microcellular radiotelephone', IEEE Trans. on Veh. Tech., Vol. 40, No. 4, Nov. 1991, pp721-730.

[2.68] Bajwa, A.S. and Parsons, J.D., 'Large area characterisation of urban UHF multipath propagation and its relevance to the performance bounds of mobile radio systems', IEE Proc. Pt. F, Vol. 132, No. 2, April 1985.

[2.69] Bajwa, A.S. and Parsons, J.D., 'Small-area characterisation of UHF urban and suburban mobile radio propagation', IEE Proc. Pt. F., Vol. 129, No. 2, April 1982, pp102-109.

[2.70] Parsons, J.D. and Bajwa, A.S., 'Wideband characterisation of fading mobile radio channels', IEE Proc., Pt. F, Vol. 129, No. 2, April 1982, pp95-101.

[2.71] Bultitude, R.J.C., and Bedal, G.K., 'Propagation characteristics on microcellular urban mobile radio channels at 910 MHz', IEEE Journal on Selected Area in Comms. Vol. 7, No. 1, Jan. 1989, pp31-39.

[2.72] Cox., D., '910 MHz urban mobile radio propagation multipath characteristics in New York City', IEEE Trans. on Communications, Vol. 21, Nov. 1973,

pp1188-1194.

[2.73] Cox, D.C., 'Time- and frequency-domain characterizations of multipath propagation at 910 MHz in a sub-urban mobile radio environment', Radio Science, Vol. 7, No. 12, Dec. 1972, pp1069-1077.

[2.74] Cox, D.C. and Leck, R.P., 'Distribution of multipath delay spread and average excess delay for 910 MHz urban mobile radio paths', IEEE Trans. on Ant. and Prop., Vol. 23, No. 2, 1975, pp206-213.

[2.75] Zogg, A., 'Multipath delay spread in a hilly region at 210 MHz', IEEE Trans. on Veh. Tech., Vol. 36, No. 4, Nov. 1987., pp184-187.

[2.76] Qualcomm Inc., 'An Overview of the Application of Code Division Multiple Access (CDMA) to Digital Cellular Systems and Personal cellular Networks', 1992.

[2.77] Goni, U. S., 'Performance Evaluation of a Direct Sequence CDMA System for Future Mobile Radio Networks', PhD. Thesis, Department of Electrical Eng. and Electronics, University of Liverpool, 1994.

[2.78] Devasirvatham, D. M. J. and Murray, R.R., 'Time Delay Spread Measurements at 850 MHz and 1.7 GHz Inside a Metropolitan Office Building', Electronics Letters, Vol. 25, No. 3, Feb. 1989, pp194-196.

Table 2.1 - Summary of Delay Spread Results for Outdoor Macrocells I

Reference	Frequency (MHz)	Locations	Environment Type	Base Antenna Heights (m)	Typical/ Median RMS Delay Spreads (μs)	Worst-case rms delay spread (μs)
Rappaport et al [2.66]	892 MHz	a. Washington D.C. b. Greenbelt, M.D. c. Oakland d. San Francisco (USA)	a. Urban, buildings in area lower than antenna b. Sub-urban/residential, small hills, apartment buildings c. Elevated urban area, LOS to mountains, hills, large building facades. d. Mountainous region	a. 35 m b. 21 m c. 43 m d. 10 m	a. 1.69 μs b. (not quoted) c. 1 μs (generally < 2-3 μs) d. (not quoted)	a. 7-8 μs b. 7-8 μs c. 13.5 μs d. 10-25 μs
Van Rees [2.26]	910 MHz	Leidschendam, (The Netherlands)	a. Sub-urban with local clusters of high buildings b. Rural with few houses c. Residential	50 m	(not quoted)	a. < 2 μs b. < 1 μs c. < 1 μs
Seidel et al [2.67]	942 MHz	a. Hamburg b. Dusseldorf c. Frankfurt d. Kronberg (Germany)	a. urban area, 4- and 8-storey buildings. b. Urban, high rise buildings., business district close by. c. Dense urban, adjacent buildings. of comparable height to base d. Base has LOS to mountains, rolling hills, urban skyline	a. 40 m b. 88 m c. 93 m d. 50 m	(not quoted)	a. 2.7 μs b. 4.0 μs c. 8.3 μs d. 19.6 μs
Bajwa, Parsons and Bajwa [2.6,2.64,2.69-2.70]	436 MHz	Birmingham (UK)	a. Sub-urban area, residential streets, high rise developments, wide roads. b. Urban area, dense high-rise shopping centre, commercial and industrial.	a. 28 m b. 36 m	a. 1.04 μs std. 0.57 μs b. 1.44 μs std. 0.5 μs	a. 2.2 μs b. 3.0 μs
Turkmani et al [2.13]	880 MHz	Liverpool (UK)	A mixture of urban and sub-urban areas, residential	35 m	0.7 μs (range is 0.1-6 μs)	6 μs
Bultitude and Bedal [2.71]	910 MHz	Ottawa (Canada)	Urban area	78 m	0.46 μs	1.26 μs
Molkdar and Matthews [2.18,2.63]	869-877 MHz, 917-923 MHz, 952-958 MHz	Leeds (UK)	a. BT category 5 (open suburban area) b. BT category 6 (dense suburban area) c. BT category 7 (urban area)	35 m	(not quoted)	90% CDFs: a. 0.57 μs b. 1.2 μs c. 1.4 μs

Table 2.2 - Summary of Delay Spread Results for Outdoor Macrocells - II

Reference	Frequency (MHz)	Locations	Environment Type	Base Antenna Heights (m)	Typical/ Median RMS Delay Spreads (μs)	Worst-case rms delay spread (μs)
Cox, Cox and Leck [2.72-2.74]	910 MHz	a. New Jersey [2.68] b. New York [2.69] c. New York [2.70] (USA)	a. Sub-urban, b. Dense-urban area, heavily built-up financial district, surrounding buildings are considerably taller, 2-20 storey buildings, 11-32 m wide streets. c. Same location as (b), more streets	a. 90-120 m b. 120 m c. 120 m	a. 0.25 μs b. (not quoted) c. (not quoted)	a. 2.05 μs b. 2.5 μs c. 3.5 μs
Natarajan [2.14]	1800 MHz	Liverpool and London (UK)	a. Dense urban, high rise buildings, at least 4-storeys high (Liverpool) b. Dense urban, 6-storey buildings, factories, residential houses (Liverpool) c. Residential, woodland, large detached houses (Kent) d. Urban, high rise buildings, base located near bridges, overpasses, train stations (London) e. Dense urban, similar to (a) (London) f. Dense Urban, similar to (a) (London)	a. 10-storey bldg. b. 6-storey bldg. c. 10 m d. 8-storey bldg. e. 6-storey bldg. f. 16-storey bldg.	Median values a. 0.70 μs b. 1.10 μs c. 0.06 μs d. 0.44 μs e. 0.52 μs f. 0.71 μs	90% cum a. 1.29 μs b. 2.90 μs c. 0.16 μs d. 1.36 μs e. 1.55 μs f. 1.36 μs
Sousa *et al* [2.16]	910	Toronto (Canada)	a. urban - comprises 2 existing cell sites, with high rise buildings in downtown Toronto b. suburban areas - comprises 2 existing cell sites c. Combined - typical rural area (north) and suburban (south)	(not quoted)	a. mean = 0.73 μs median =0.713 μs b. mean = 0.59 μs median = 0.31 μs c. mean = 0.66 μs median = 0.48 μs	a. < 3 μs b. < 7 μs c. --
Zogg [2.75]	210 MHz	Bern (Switzerland)	Hilly region, 25 km away from mountains, 5-10 km from hills.	947 m	(not quoted)	generally < 10 μs in town and > 35 μs in hilly area

Table 2.3 - Summary of Delay Spread Results for Indoor Environments

Reference	Frequency (MHz)	Locations	Environment Type	Base Antenna Heights (m)	Typical/ Median RMS Delay Spreads	Worst-case rms delay spread (μs)
Devasirva-tham [2.34]	850	New Jersey (USA)	i. office buildings a. Large 6-storey office building b. medium-sized 2-level structure by a hill c. Large complex of 3 buildings each 14 m high ii. Residences d. apartment on level 2 of a large building e. 2-storey house	(not quoted)	(not quoted)	a. 250 ns b. 322 ns c. 420 ns d. 420 ns e. 311 ns
Rappaport [2.33]	1300	Indiana (USA)	a. Office building b. Food processing plant - multifloor structure with thick concrete walls, metal ceiling c. Engine manufacturing plant - single floor d. Aluminum manufacturing facility - 1 floor e. Casting foundry - 1 floor f. Engine machine and assembly shop - 1 floor	2 m	a. LOS:median=98 ns,OBS:112 ns b. 49 ns and 56 ns c. 120 ns and 119 ns f. 123 ns and 126 ns overall 96 ns (LOS), 105 ns (OBS)	Maximum b. 129 ns (OBS) 131 ns (LOS) c. 300 ns generally < 140 ns
Saleh and Valenzuela [2.23]	1500	Holmdel (USA)	Medium-sized 2-storey building with external walls made of steel beams and glass, internal walls made of wood studs/plasterboard, rooms full of furniture.	2 m	median = 25 ns	50 ns
Pahlavan et al [2.32]	910	Worcester (USA)	a. Electronics shop floor - containing PCB design equipment, soldering and chip mounting stations b. Equipment storage area - partitioned by metal screens c. Floor containing grinding machines, large ovens, transformers, etc. d. Car assembly floor e. Vast open area for final inspection of new cars	1.5 m	Median values: a. 15.29 ns b. 31.62 ns c. 48.9 ns d. 52.57 ns e. 19.37 ns	Worst case values: a. 40 ns b. 60 ns c. 152 ns d. 150 ns e. 146 ns
Devasirva-tham,Murray [2.64,2.78]	850 [2.64] 850 & 1700 [2.78]	Holmdel (USA) New York (USA)	a. Large complex consisting of 4 to 6-floor buildings, outer wall made of metallised glass. b. large mid-block 8-floor building, each floor partitioned into 2 parts by sheet rock walls.	2 m	median: a. 125 ns b. (not quoted)	Worst case: a. 250 ns b. < 100 ns

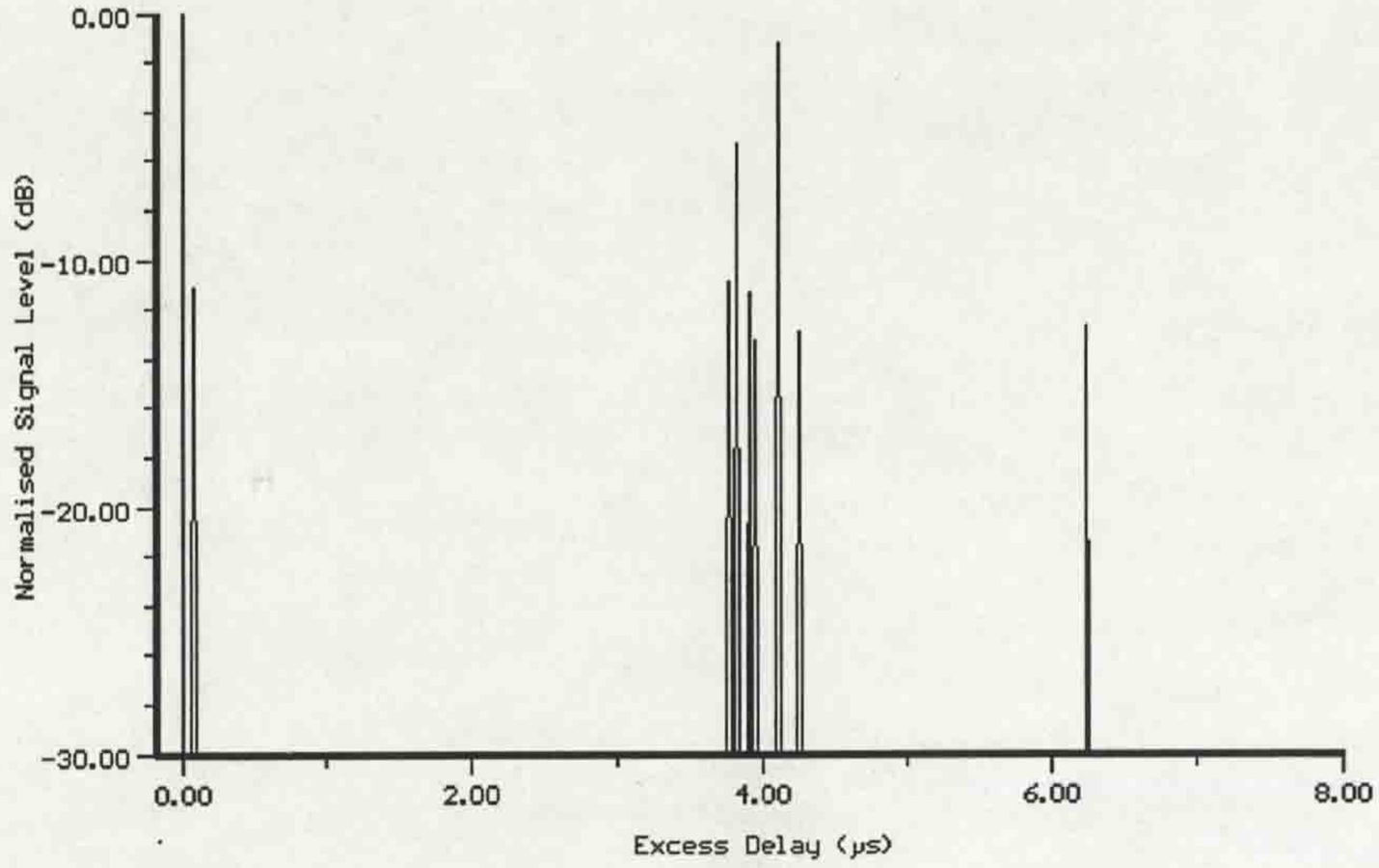

Figure 2.1 Normalised power delay profile.

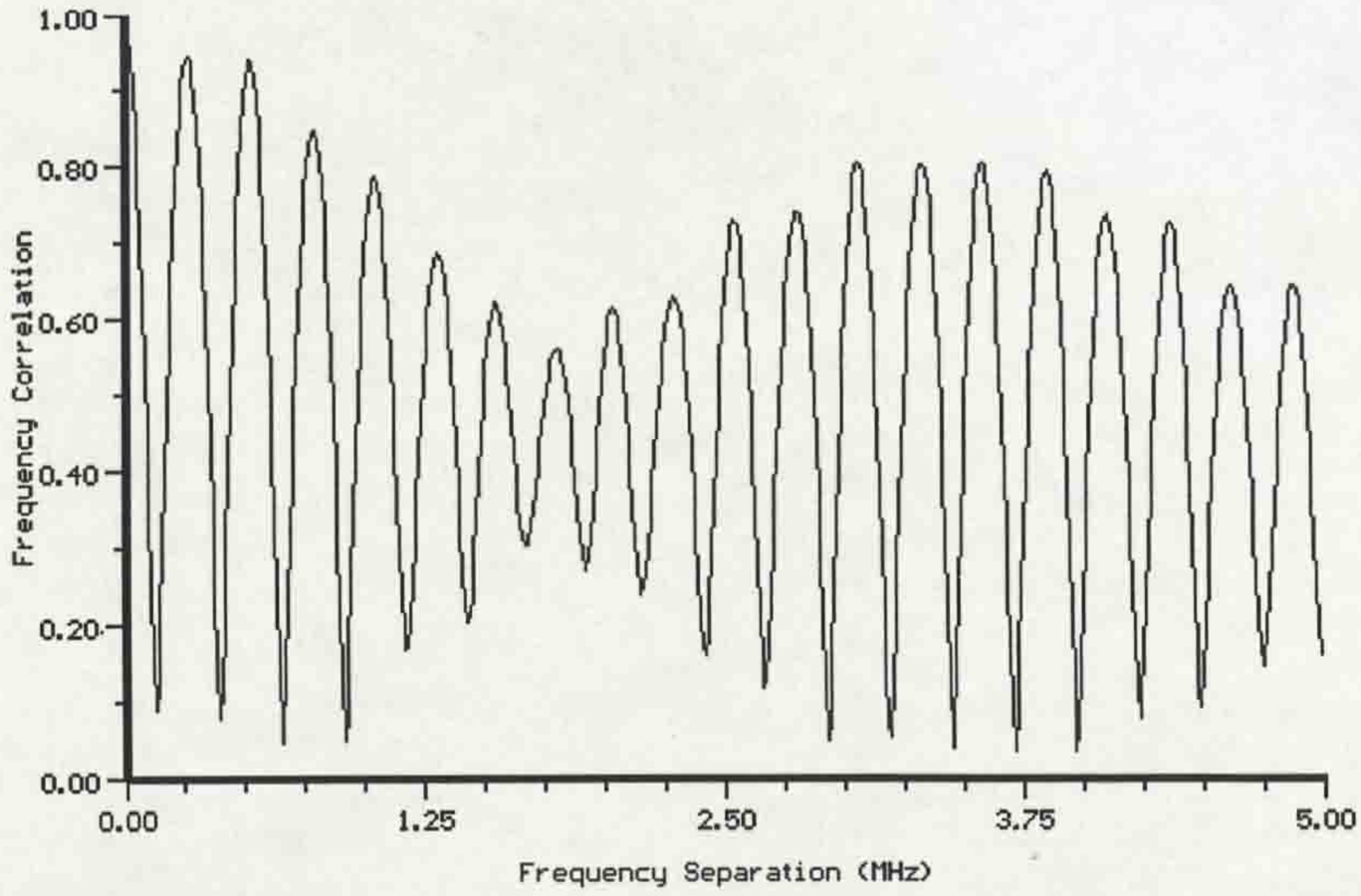

Figure 2.2 Frequency correlation function of the profile in shown Figure 2.1.

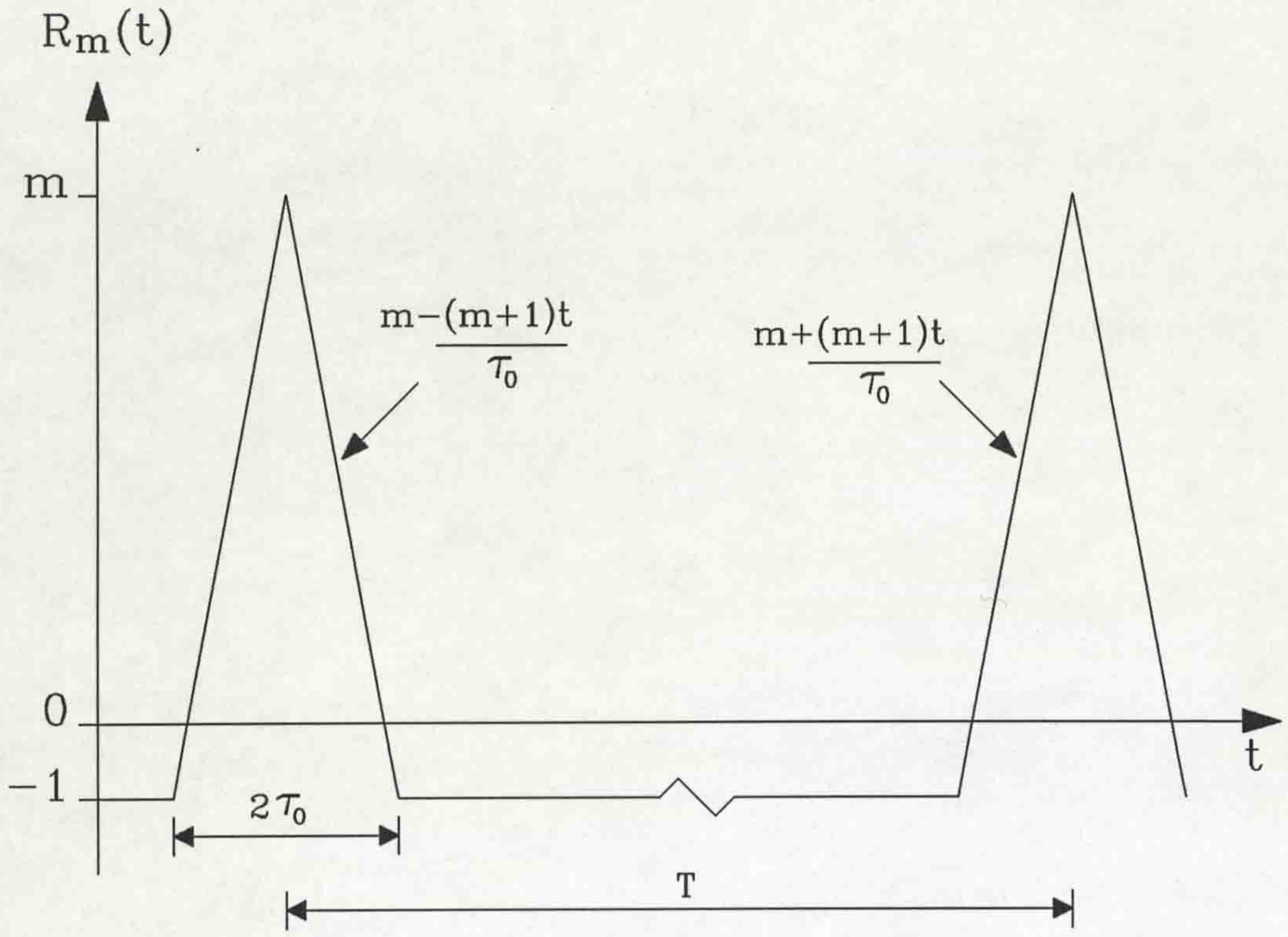

Figure 2.3 Periodic autocorrelation function of an m-sequence.

Chapter Three

THE EXPERIMENTAL WIDEBAND CHANNEL SOUNDING SYSTEM

3.1 INTRODUCTION

The relative merits of the various wideband sounding techniques have been discussed in chapter 2. It is evident that the Swept Time-Delay Cross-Correlation (STDCC) technique is the optimum. In this method, the time delay separation of the multipath echoes is determined by transmitting a coded signal (PRBS in this study). In the receiver a sliding correlator identifies the coded signal and hence the output shows the multipath nature of the propagation channel in the form of pulse compression spikes with time varying amplitudes and phases.

In the ensuing sections, the general requirements of the experimental system are discussed together with a detailed description of how it was implemented. The method used and the results obtained from evaluating the performance of the complete system are also presented.

3.2 MAIN REQUIREMENTS OF THE SYSTEM

Due to the rapid growth in wideband transmission systems, there is a need for accurate methods of predicting and/or assessing the system performance quickly and without incurring huge costs. Radio System Engineers require propagation information which allows the evaluation of modulation, diversity, coding and equalisation schemes. Radio propagation modelling requires information that relates the multipath phenomenon to the local environment, in order to predict coverage and assess the effects of cochannel and adjacent channel interference. Furthermore, with the advent of Personal Communication Systems (PCS) and high bit rate wireless local area networks (WLANs), there is an increasing demand for wideband channel sounders for in-building channel characterisation. In theory, a system is required to

provide all the necessary information to system designers. However, in practice, the various channel sounding techniques have some fundamental limitations to the amount of information they can provide. In addition, commercial wideband channel sounders are rare and not very flexible. It was therefore necessary to design and construct a system for use in this study.

For an STDCC system, interrelationships exist between the parameters that the system is able to measure, for example, delay spread, coherence bandwidth[1], etc. A consequence of this is that, to effect an improvement in one may result in a degradation in another. In the design of the system, nine main requirements had to be considered in order to obtain a suitable compromise. These are:

i. Dynamic range of the system,
ii. Capability of absolute received power measurement,
iii. The need for automatic gain control (AGC),
iv. Time resolution,
v. Maximum measurable excess time delay,
vi. The need for phase measurement,
vii. Doppler shift resolution,
viii. Quality and accuracy of frequency sources,
ix. Fast and efficient data acquisition system.

3.2.1 Dynamic Range of the System

The dynamic range of a system is the range between the maximum and minimum signal levels that the system can measure, i.e., the range within which the input/output characteristics are linear. For channel sounding techniques that employ pulse compression, this dynamic range is dependent on the length of the m-sequence used and is equal to $20 \log_{10} m$, where m is the length of the m-sequence. In practice the effects of noise and filtering in the system can result in a substantial reduction in the dynamic range. Hence, for an STDCC channel sounder, the dynamic range

[1]These parameters will be defined in chapter 4.

window will set the limit on the difference between the strongest and the weakest echoes within one repetition period of the m-sequence that the system can measure. Since there is a need to assess the spatial and distance dependence of the power delay profiles a method of positioning this dynamic range window was required. Furthermore, there is a need to conduct measurements over longer spatial distances; and so the movement of this limited dynamic range window will ensure that the received signal strength is always within the dynamic range of the receiving system as it traverses the measurement route.

Lastly the importance of a high enough dynamic range in the system is further emphasised by the CCIR [3.1]. The recommendations are that only recorded power delay profiles which have a peak-to-noise level of 15 dB with a 3 dB error margin should be used for analysis[2]. In this study, a 511-bit m-sequence was considered to be adequate and this gave a theoretical dynamic range of 54 dB.

3.2.2 Capability of Measuring the Average Received Power

One of the most important characteristics of any propagation medium is the transmission loss or propagation pathloss, which is usually calculated from the ratio of the transmitted power to the received power. Knowledge of the variability of the transmission loss allows the formulation of pathloss models which are required for coverage predictions. Most importantly, the near-far[3] problem which is inherent in a direct-sequence CDMA system, by virtue of the fact that it is a 'one-cell repeat' system, can only be alleviated by using accurate power control algorithms. These algorithms can only be reliably implemented by knowing the extent of the variability of the propagation pathloss or from accurate pathloss prediction models. This is 7further emphasised in the proposed CDMA system by Qualcomm [3.2], which intends to employ both open and closed loop power control algorithms. The channel

---

[2]These recommendations were adhered to in this study.

[3]The near-far problem in a spread spectrum system relates to the problem of very strong signals originating closer to the base station swamping out the effects of weaker signals. A frequency hopping CDMA system is less susceptible to this problem because it is an avoidance system.

sounding system should therefore be designed in such a way that the average power received can be calculated.

3.2.3 The Need for Automatic Gain Control (AGC)

The dynamic signal range a particular receiver system must handle largely depends on the type of environment in which it is expected to operate; for example, a satellite-to-ground link is much more stable than a land-to-land mobile radio link. In the latter case the nature of wave propagation mechanisms makes the link highly variable and generally unpredictable due to man-made and/or natural obstacles along the radio path. In a land mobile radio environment, the received signal level can vary by up to 100 dB over a few tens of wavelengths. This means that any receiver system whose demodulation process is sensitive to input level must, for optimum reception, incorporate some method of compensating for the changes in the RF signal level as seen at its antenna. Because of the limited dynamic range inherent in channel sounding systems, there is a need to suitably move this dynamic range window as the signal level changes. There are two possible methods of achieving this:

i. the use of a manual attenuator and
ii. the use of automatic gain control (AGC).

The use of a manual attenuator is easy to implement, though, it imposes restrictions on how data is collected. This requires previewing the measurement route in order to manually set the attenuation value and hence, makes data collection a difficult task. It also excludes the possibility of continuous measurements over longer spatial distances, thereby precluding the assessment of distance and spatial dependence of the power delay profiles. Previous studies by Bajwa [3.3], Demery [3.4] and Natarajan [3.5] utilised this method. This limited the continuous collection of data to only 10-20 m stretches.

In view of the drawbacks associated with the use of manual attenuators, an AGC circuit was developed for this study. The AGC system is expected to provide good linearity over the full range of the desired input levels and to provide close control

of the demodulator input signal level[4]. A possible block diagram of an AGC configuration for a correlation-type receiver is shown in Figure 3.1. This configuration was implemented by generating a control voltage from the envelope detector output of the receiver and manipulating it to switch a programmable attenuator in the RF stages. Since a knowledge of the absolute signal level of the received echoes was required, the AGC voltage was also recorded. In so doing, the AGC compensated for the signal strength variations thereby providing a suitable method of conducting measurements over longer spatial distances without the need to preview the measurement route. The inclusion of the AGC consequently made data collection relatively easy and facilitated the collection of a substantial database of power delay profiles.

3.2.4 Time Resolution of the System

The time resolution of the STDCC system, which is a direct function of the clock rate of the PRBS, is a measure of the minimum time delay between two successive echo paths that the system can measure. This can also be regarded as the spatial resolution of the system. The clock rate of the PRBS has to be high enough to enable the observation of the multipath echoes. This is important since the system will also be used in indoor situations in which the distance between scatterers is always small.

Although Young and Lacy [3.6] used a 0.5 μs time resolution system while Cox [3.7], Turin et al [3.8] and Demery [3.4], used a 0.1 μs time resolution system, they all reported rapid fading of the signal level in the time delay bins due to unresolved echoes. In this study a chip rate of 30 MHz was chosen as it is suited to outdoor as well as indoor measurements. This provided a time resolution of 33.3 ns which corresponds to a spatial resolution of 10 m.

---

[4]This is necessary since data processing was based on the peaks. A saturated front end would limit the received signal and hence the peaks cannot be accurately identified.

3.2.5 Maximum Measurable Excess Delay

This parameter determines the maximum unambiguous excess time delay that can be measured by the system. For an STDCC system, the maximum measurable excess delay is the product of the PRBS length and the clock period. A maximum excess delay of 20 μs has been recommended for the GSM system [3.9]. Since the system is expected to operate in areas where the maximum excess time delay was not anticipated to exceed 16 μs, the 511-bit PRBS which offers a 17.03 μs capability is considered to be adequate.

3.2.6 Bandwidth Compression Factor

The STDCC system operates by cross-correlating two identical m-sequences that are clocked at slightly different rates as explained in Chapter 2. The small difference in clock rates results in a time-scaling or bandwidth compression of the cross-correlation function. This implies that the measured channel impulse response from the output of the receiver is equivalent to the average of 3750[5] individual instantaneous impulse responses. The drawback in this approach is a limitation in the speed of the mobile vehicle as will be shown in section 3.2.8. The time-scaling factor, k, is given by the ratio of the highest clock frequency to the frequency difference between the clocks in the transmitter and receiver.

Although the bandwidth compression factor[6], k, may initially be regarded as arbitrary, previous work by Cox [3.6] and Parsons *et al* [3.10] has shown that severe distortion of the measured impulse response is produced if k is set too low. This is caused by the significant difference in the periods of the transmitter and receiver chip lengths. In this study, a slip rate of 8 kHz was chosen giving a bandwidth compression factor of 3750. Cox and Demery used a bandwidth compression factor of 5000 in their studies with 10 MHz clock rates.

---

[5]This is the value of the bandwidth compression factor utilised in this study.

[6] The time-scaling factor and the bandwidth compression factor are interchangeable.

3.2.7 The Need for Phase Measurement

Radio propagation modelling requires information which assesses the effects of the natural and/or man-made environment on the propagation mechanisms of radio waves. In an attempt to model the mobile radio channel when it is excited by a wideband radio signal, most researchers [3.7, 3.11-3.12] have assumed *a priori* that the phases of the received echoes are a set of mutually independent random variables which are uniformly distributed from 0 to 2π. This assumption has been based solely on a theoretical understanding of radio wave propagation. It was therefore deemed necessary to measure the phase and verify this widely used assumption, especially for the late echoes. Measurement of the phase also permits the study of the frequency selective behaviour of the channel.

3.2.8 Doppler Shift Resolution

A channel sounder can also provide the necessary information for identifying the location of the scatterers. This information is the angles-of-arrival of the echo paths which are in the form of Doppler-shifts associated with the received echoes. The limits to which an STDCC system can resolve Doppler shifts depends on five factors, namely the vehicle speed (v), the carrier frequency (f_c), the PRBS length (m) and chip rate (τ), the scaling factor (k) and the number of samples (N) used for spectral estimates.

The bandwidth compression factor defines the length of a single impulse response measurement[7], T_{IR}, and as a consequence, there is an upper bound on the velocity at which the vehicle bearing the receiver can travel if the measurements are to be realistic. The measurement interval is defined as,

$$T_{IR} = \frac{m}{f_{slip}} \qquad (3.1)$$

where f_{slip} is the difference between the transmitter and receiver clock rates. It is

[7]The channel is assumed to remained stationary over the measurement interval.

sufficient to assume that the channel will remain stationary over the measurement interval provided that the distance traversed during T_{IR} is less than half a wavelength. Thus, the maximum velocity, V_{max}, can be written as :

$$V_{\max} = \frac{c}{2f_c T_{IR}} \tag{3.2}$$

where c is the velocity of light. In terms of k, V_{max} becomes [3.4]:

$$V_{\max} = \frac{c}{2km\tau f_c} \tag{3.3}$$

The above equation shows that, for k, τ and f_c constant, V_{max} is inversely proportional to m. For this study with k=3750, τ=33.33 ns, m=511 and fc=1.8 GHz the maximum vehicle velocity is 1.3 m/s. This value is small for a vehicle borne receiver system. A method of determining and monitoring the vehicle speed was therefore required.

From equation 3.3, the maximum Doppler shift frequency that the STDCC system can measure is,

$$F_D = \frac{1}{2km\tau} \tag{3.4}$$

The minimum Doppler shift that can be measured by the system is given by

$$F_{\min} = \frac{1}{Nkm\tau} \tag{3.5}$$

where N equals the number of samples in each power delay profile used for spectral analysis. The overall frequency resolution will depend on the stability of the frequency sources and the ability to maintain a constant vehicle speed. Above all, it can be observed that a trade-off can be obtained by altering one of the parameters of the system.

3.2.9 Quality and Accuracy of Frequency Sources

The quality and stability of the frequency sources in the system become very important issues when the measurements are to be conducted for longer spatial distances and when the phases of the received echoes are required. These aspects of the frequency sources will affect the performance of the system in two ways: the accuracy with which time delay measurements are obtained and the validity of the phase data.

In the first case, relative drift between the sources in the transmitter and receiver results in ambiguities in the exact timing of the time delays of the echoes. This implies that echoes with the same time delay will no longer occupy the same time resolution cell. In order to identify accurately contributions from echoes within the same time delay bin over the duration of the experiments, the clocks are expected to have a steady drift less than 33 ns[8] over the period of the measurement campaign. This will therefore set the upper limit for the period of measurements in the field if the recorded data is to be reliable. The stability of frequency sources, [3.13], is usually expressed in terms of drift measured relative to a primary master source, generally a Caesium atomic standard. This was not necessary in this study, since it was the performance of the sources in relation to each other that was of interest. The problem of stability also determines the lowest Doppler shift frequency that can be unambiguously resolved by the system. Specifically, this refers to how accurately the system can measure echoes arriving with angles close to 90° relative to the direction of motion.

Although the long-term stability of the frequency sources is vital for systems that employ coherent detection, the short-term stability also affects system performance. For perfect coherent detection, the injected carrier must be identical in both phase and frequency to that of the received signal. This is often impossible in the mobile radio environment where the mobile is always randomly located. However, if identical

[8]33 ns is the time delay resolution of the system and represents one time delay bin.

frequency multipliers are used in the transmitter and receiver then, the degree to which frequency synchronism can be achieved is dependent on the magnitude of any frequency offset between the frequency references and their stability.

If perfect frequency synchronism was to exist between the transmitter and receiver, the I and Q outputs of the receiver would define a received vector with a constant amplitude and arbitrary phase angle. In practice, all signal sources exhibit random perturbations in both amplitude and phase. The spurious amplitude modulation is much smaller than the random phase modulation (also known as phase noise) and is often ignored [3.14]. In an STDCC system, the effect of phase noise is to induce random amplitude fluctuations in the I and Q outputs. This will result in inaccuracies in the measurement of the phase, and therefore defines the accuracy of the phase measurements in the system.

3.2.10 Fast and Efficient Data Acquisition System

Since the outputs from the receiver are analogue signals, a method of recording and storing the data for post-processing was required. Early experimental investigations by researchers [3.6-3.7] utilised photographic methods in which snapshots of the impulse responses were taken using a 16 mm picture camera. This technique places practical limitations on the amount of data that can be collected. It is also very inefficient and makes data reduction and analysis a tedious and time-consuming process. Others studies [3.3-3.5] have employed a data acquisition process which involves recording data in analogue form using an FM instrumentation tape recorder. Consequently, this has to be digitised off-line before analysis can be performed. Again this technique requires a lot of time and makes it difficult to identify errors in the field.

In this study, there was therefore a need to eliminate these intermediate processes. This has been made possible by the introduction of high speed computers with fast processor and hard disk capabilities. It was therefore possible to design a data acquisition system around a personal computer (PC) and a commercial analogue-to-

digital (ADC) card. This method provided a direct digitisation and storage facility. Using this approach, it was possible to preview and analyse the data on-line while still in the field. Hence, the system could allow the immediate identification of errors in the field so that experiments could be repeated, if required.

3.3 THE TRANSMITTER

A block diagram of the transmitter is shown in Figure 3.2. A 511-bit PRBS at 30 MHz chip rate which had been low-pass filtered, was used to phase-reversal modulate a 1.8 GHz RF carrier. The local oscillator, LO, was locked to a highly stable Rubidium frequency standard. The resulting signal had a constant RF envelope with 180° phase changes at the ± 1 transitions of the PRBS. If the low-pass filtering was excluded prior to the modulation process (see Figure 3.3) the transmitted spectrum had a sin(x)/x form with spectral lines separated by the PRBS repetition rate. The RF spread spectrum-type signal was then amplified and radiated from a wideband discone antenna. The five main modules which made up the transmitter are described below.

3.3.1 The PRBS and Clock Generator

Pseudo random binary sequences (PRBS) or maximal length sequences (m-sequences) are the longest codes that can be generated by a given shift register or a delay element of a given length. In hardware, these can easily be generated from linear shift registers and modulo-2 adders. A PRBS can be generated by modulo-2 addition of two or more of the intermediate stages of the shift register sequence and feeding the resulting output into the input of the shift register. This method gives a maximal sequence of length 2^N-1, where N is the number of stages in the shift register. Different combinations of the outputs provide sequences with different lengths and are well documented in Dixon [3.15].

For every rising edge of the clock, the contents of the shift registers are shifted by one bit to the right. The output of the last stage is the appropriate bit of the PRBS. For a complete code cycle, all possible states of the code must occur, with the

exception that the all zeros condition should not be allowed to occur, because this will force the shift register into a cleared state. This situation was prevented by using an N-input NAND gate, which forced a one into the serial input if the all zeros condition was detected. In this study a 511-bit PRBS was required and was therefore generated by using stages five and nine of the shift registers. This necessitated the use of two 8-bit shift registers. Implementation was accomplished with TTL integrated logic devices.

The PRBS clock frequency of 30 MHz was obtained from a commercial low-noise crystal oscillator. This had a stability of better than ± 1 part in 10^7 within a temperature range of 5 to 40° C (manufacturer's figure). The 30 MHz clock rate gave a repetition period of 17.03 μs for the 511-bit PRBS.

3.3.2 The PSK Driver, Low-pass Filter and Double Balanced Mixer

Binary phase-shift keying (BPSK) or phase-reversal keying was the modulation scheme employed in this study. This was due to the relative ease of implementing the scheme using a double balanced modulator as shown in Figure 3.2. The phase of the carrier was changed by $\pm\pi$ radians depending on the polarity of the current drive at the IF port of the double balanced mixer. BPSK will produce an RF spectrum whose frequency span from null to null (main lobe) is twice the clock frequency of the PRBS clock rate, a first side lobe with a maximum 13 dB below the peak of the main lobe and a roll-off of 6 dB per octave (see Figure 3.3).

The PRBS generator hardware used TTL integrated circuits which therefore had unipolar outputs. Since the double balanced mixer required a bipolar current drive at its IF port, a unipolar to bipolar transform was required. This was accomplished by the use of a diode-steered current source. This circuit is based on a design by Turner [3.16], which was later adapted and used by Bajwa [3.3] and Demery [3.5]. For a high TTL level (logic 1), the PSK driver acted as a 15 mA current source to the double balanced mixer while acting as a 15 mA current sink for a low TTL level (logic 0).

The output of the PSK driver was low-pass filtered before application to the IF port of the double balanced mixer. The inclusion of the low pass filter prior to the modulation process dispensed with the need for any RF filtering before transmission. Figures 3.3 and 3.4 show the transmitted RF spectrum, the former without low pass filtering of the PRBS. A closer look at Figure 3.4 reveals that the energy outside the main lobe was greatly reduced and most of the transmitted power was within the main lobe. This ensured that no significant interference was caused to other users of the radio frequency spectrum.

3.3.4 The Local Oscillator (LO) and Frequency Standard

One of the requirements of the system was to provide the phase information associated with individual echo paths. Therefore, the quality and stability of the LOs in both the transmitter and the receiver was of utmost importance if realistic complex impulse data were to be obtained. The quality of a frequency source is always described in terms of its single sideband phase noise spectral density. However, there is no readily available information that directly links the quality of signal sources to the performance of the STDCC system. In his study, Demery [3.4] concluded after carrying out a comparative survey on a number of sources, that the criterion for satisfactory performance in a frequency source was a low value of phase noise power spectral density close-in to the carrier. Hence, a comparison between the various available sources was performed.

In this study, a commercial signal generator at a carrier frequency of 1.8 GHz was utilised. This was selected because of its superior performance compared to the available frequency synthesizers. The generator had a single sideband phase noise power spectral density of -101 dBc/Hz at a carrier offset of 1 kHz (manufacturer's figure) compared to -70 and -80 dBc/Hz at a carrier offset of 10 kHz for two other available frequency synthesizers[9].

[9]These were the values measured using a spectrum analyzer.

The issue of stability was remedied by locking this generator to a highly stable Rubidium frequency standard at 10 MHz. This had a stability of better than 5 parts in 10^{11} and a single sideband phase noise power spectral density of at least -110 dBc/Hz at a carrier offset of 100 Hz.

3.3.5 RF Amplification

The RF output of the mixer provided an average power of -25 dBm. In order to provide sufficient power for coverage of large areas, a power amplifier was required to raise the spread spectrum-type signal to the required level before coupling to an antenna. In this case, the characteristics of the power amplifier were of primary concern, since an antenna that was broadband enough to pass the signal satisfactorily was easily obtained. It was therefore necessary to use a power amplifier with sufficient bandwidth to pass the signal.

The amplifier used was a commercial broadband class A linear amplifier capable of handling a maximum output of 10 W. This had a measured gain of 31 dB and an amplitude response that was flat within ± 1 dB in the 1700-1900 MHz frequency band. The VSWR at the input and the output was 2:1 and the output power at the 1 dB compression point was 40 dBm. The maximum output of the transmitter was set to 7 W.

3.3.6 The Antennas and VSWR

Wideband antennas were used in both the transmitter and the receiver. These were laboratory-constructed wideband vertically polarised discones, which had an omnidirectional azimuthal radiation pattern and voltage standing wave ratio (VSWR) of 1:1.25 over the 1700-1900 MHz band. Coupling between the transmitter and antenna was achieved using a low-loss coaxial cable.

The broadband nature of the signal and the acute frequency dependency of VSWR when termination is improper combine to work against the effective performance of

the system as a whole [3.15]. Hence extra care had to be taken in both the transmitter and receiver to ensure that terminations were correct. This included not only impedance matching but also connector mating and cable shield terminations.

3.4 THE RECEIVING SYSTEM

The receiving system essentially acted as a pulse compression type sweeping cross-correlator to the transmitted PRBS. A block diagram of this system is shown in Figure 3.5. It can be seen from this diagram that the receiver consists of four main sections: the RF front end, the locally generated 'offset' modulated PRBS[10], the IF stage and the demodulation stage. The front end comprises of three wideband low-noise amplifiers, a 60 MHz RF bandpass filter, a programmable attenuator and a mixer. The programmable attenuator was configured to switch automatically as the received signal level changes, thus acting as an AGC. To reduce errors due to up or down conversion of the reference clock for coherent detection, the IF frequency was made the same as that of the reference frequency of 10 MHz. The translation to an IF of 10 MHz was achieved by mixing with a 1.79 GHz carrier which had been phase-reversal modulated by a 511-bit PRBS, identical to that in the transmitter, but running at a slightly slower clock rate (29.992 MHz). The IF output was passed through a bandpass filter centred on 10 MHz and with a bandwidth of 19 KHz. The resulting output was split into two cophasal components, one of which was used to obtain the envelope of the received signal. The other component was suitably amplified before being presented to a quadrature demodulator. The resulting outputs from the envelope detector and quadrature demodulator were suitably conditioned for recording. Also, the value of the programmable attenuator was recorded so that absolute received signal levels could be determined. A more detailed description of the various sections follows.

3.4.1 The RF Front End

After reception from a wideband discone antenna, the received signal was presented

---

[10]The implementation of this section was identical to that employed in the transmitter.

envelope of the received signal. This was used to provide the AGC control voltage and was also used for visual inspection. The logarithmic amplifier used was a high performance commercial discrete component design. This had an 80 dB dynamic range and a bandwidth of 2 MHz centred on 10 MHz.

Coherent detection of the other output from the power splitter was employed using a commercial I and Q demodulator. The LO signal of 10 MHz was obtained from the Rubidium frequency standard. This was amplified and filtered in order to obtain a level of 10 dBm as required by the I and Q demodulator. The IF signal was also further amplified in order to eliminate splitter losses before being applied to this device. The inphase (I) and quadrature (Q) outputs were then low-pass filtered before suitably conditioning them for recording.

3.4.3 The AGC System

The heart of this process was a programmable RF attenuator. This had an insertion loss of 4 dB and could be switched digitally from 0 dB to 127 dB in steps of 1 dB, although 4 dB steps were used for this study. The video output of the logarithmic amplifier was made up of a series of pulses depending on the number of resolvable multipath components. This was passed through an envelope detector with a long time constant in order to give a constant level indication of the received signal level. The resulting output was then presented to a 'window circuit' which was made up of two comparators and a 'directional indicator circuit' which was made up of a single comparator (see Figure 3.6). An up/down counter, which was clocked by a 64 ms clock signal derived from a 555 timer, was used to control the programmable attenuator. The control of the counter was derived from the 'window circuit' and 'directional indicator' circuit. The former, when suitably adjusted, prevented the counter and hence the attenuator from continuously switching, i.e. sets the limits within which the programmable attenuator should not switch. The latter sensed whether the signal was above or below a certain threshold, in which case the counter counts up or down respectively. There was also a circuit which monitors the outputs of the counter in order to avoid it toggling from 0 dB to 127 dB and/or vice versa.

to a wideband low-noise amplifier. This had the effect of amplifying the signal and effectively determining the noise figure of the receiver. The next component was a pre-selector RF bandpass filter with a 60 MHz bandwidth centred on 1.8 GHz. This filter removes strong out-of-band interference which may cause saturation of the other front end amplifiers. The output of this filter was passed through the programmable attenuator before being further amplified by a wideband low-noise amplifier. The resulting output was presented to a mixer for translation to IF. The programmable attenuator could be switched in steps of 1 dB and has a maximum attenuation of 127 dB. The control voltage of the programmable attenuator was derived from the output level of the envelope of the received signal.

A 1.79 GHz LO frequency is generated by another high quality commercial frequency generator. This was locked to a highly stable Rubidium frequency standard identical to that used in the transmitter. The LO was phase reversal modulated by a PRBS that is identical to that in the transmitter, but operating at the slower clock rate of 29.992 MHz. This coded signal was used to down convert the received signal to an IF of 10 MHz. The importance of applying the PRBS at this stage was that the multiplicative part of the cross-correlation process was carried out [3.4]. This permitted the use of a narrowband IF stage. This gave an IF bandwidth of 16 kHz compared to Cox [3.7] and Bajwa [3.3] who used IF bandwidths of 20 MHz. This resulted in the use of narrowband components which were easily available.

3.4.2 The IF Stage and Demodulation

After bandpass filtering of the IF signal, the output was split into two cophasal components using a hybrid power splitter. The bandpass filter used in this case was a commercial four-pole monolithic crystal with a centre frequency of 10 MHz, a 3 dB bandwidth of 19 kHz and an insertion loss of 4 dB. The importance of such a filter is its possession of good intermodulation characteristics.

One of the outputs from the splitter was presented to the input of a logarithmic amplifier which performed an envelope detection process and hence provided the

If this condition was detected the counter was inhibited. Since a step size of 4 dB was used only five outputs were used to control the attenuator. These were then converted to analogue signals, and suitably conditioned for recording and visual display. A simplified block diagram of the AGC circuitry is shown in Figure 3.6.

3.5 SPEED MONITOR AND DISTANCE MEASUREMENT

As stated in section 3.2.8, the maximum allowable vehicle speed was 1.3 m/s. To overcome the problem of trying to control a vehicle at this very low speed using its speedometer, a slotted-disk was fitted to the propeller shaft of the vehicle. The distance marker pulses generated by a photo-detector straddling the slotted-disk were fed into an LED and audio circuitry. This circuitry was suitably adjusted to provide audible and visible warnings to the driver when the speed was outside $\pm 10\%$ of the required speed.

The distance traversed during the course of each experiment was also required for pathloss analysis and to evaluate the distance variations of the impulse responses of the channel. Distance was measured by recording the distance marker pulses as the vehicle traversed the measurement site. The recording was done by combining the speed marker pulses with the AGC outputs before conversion to analogue form for recording. This necessitated separation before data storage.

3.6 THE DATA ACQUISITION SYSTEM

Four outputs from the receiver needed to be recorded for post-processing. These were: the video output, the AGC signal and the inphase and quadrature outputs. It should be noted that the AGC signal also contained distance information as mentioned in section 3.5 and should be separated out before storage. Since a Personal Computer was to be used, an analogue-to-digital interface was required. This was achieved using a commercial 12-bit, 16 channel I/O ADC card that occupied one of the full expansion slots of the PC. The operation of the card was controlled by a purpose written interactive menu-driven software package.

The software package allowed the sampling rate to be changed if required. For a typical experimental run, the file name was entered and sampling was initiated. During this period the samples were stored in the extended memory of the PC, making use of direct memory access (DMA) techniques for speed enhancement. When the extended memory was full the software automatically transferred the samples on to the PC hard disk. Five files were created for each experimental run; the phase, amplitude, AGC level, distance and information files. A brief summary of the features of the data acquisition package all of which were under user control are:

- initiation of sampling
- stores data on the hard disk
- allows plotting of all or parts of the recorded data
- on-line analysis[11] and viewing of the results
- creates an archival information file containing pertinent details such as date, time, location of experimental sites and comments during each measurement.

Even though the throughput of the overall system was 200 kHz, the sampling rate used in this study was 20 kHz which was equivalent to 75 MHz in real time due to the inherent time scaling. This was adequate since it satisfied the Nyquist criterion of at least two impulse response samples per period. This gave approximately 5 samples per echo. The four outputs were sampled simultaneously.

3.7 SYSTEM EVALUATION AND PERFORMANCE

In order to assess the overall performance and evaluate the system, the transmitter and receiver were connected back-to-back in the laboratory. To prevent saturation of the front end amplifiers in the receiver a manually adjustable RF attenuator was placed between the transmitter and receiver. The attenuator thus accounted for the path loss encountered in the mobile radio channel. Plate 3.1 shows a photograph obtained showing the period of the power delay profiles to be approximately 64 ms.

---

[11]The analysis in this case refers to the calculation of the time domain channel descriptors such as average delay, delay spread, etc. These will be defined in Chapter 4.

In the following sections the techniques and the results of the relevant performance measures are presented.

3.7.1 Dynamic Range and Calibration

Although the theoretical dynamic range of an STDCC system with a 511-bit PRBS is 54 dB, the presence of noise generated by the system and filtering reduces this value. The data acquisition unit was configured to digitise signals in the range 0-10 V, hence the signals to be recorded were scaled accordingly by using d.c. amplifiers and level shifters. To determine the linearity and dynamic range of the system, the AGC system was disabled in such a way that the programmable attenuator could still be manually switched. Initially the value was set to 0 dB. Having set the value of the external manual attenuator to a suitable value to have the maximum signal level as shown in Plate 3.1, the external attenuator was reduced in steps of 5 dB until the signal level at the output reduced to a minimum. The output voltages with the corresponding values of external attenuation values were recorded and the value of the programmable attenuator increased by 4 dB before the process is repeated. This procedure continued until the value of the programmable attenuator was 64 dB. A table was thus generated showing the external attenuation values and the corresponding voltage levels for different values of receiver attenuation (programmable attenuator). This technique is similar to that given in [3.5]. Figure 3.7 shows a family of curves for the video output voltage as a function of external attenuation for different receiver attenuations.

The graph in Figure 3.7 shows that the system dynamic range was 30 dB and the system maintained linearity as the AGC operated. The minimum input to the receiver for which a dynamic range of 30 dB still existed was found to be about -90 dBm.

3.7.1.1 Calibration of AGC Output

The five outputs that controlled the programmable attenuator were connected to an 8-bit analogue-to-digital converter (see Figure 3.5). Since the 1 and 2 dB cells were not utilised, the two least significant bits of the ADC were grounded. The output of

the optical detector, which generated distance marker pulses, was a TTL logic signal. This was connected to the most significant bit of the ADC. The output of the ADC was suitably scaled to provide an output range from 0 to 10 V. This arrangement implied that, if the distance marker pulse was at logic 0, then the maximum output from the ADC was 127, due to operation of the AGC circuit alone. On the other hand, if this was at logic 1, the maximum was 255. Hence, it is clear that these two signals can easily be separated out by simply checking the recorded integer value and appropriately subtracting 127.

The calibration curve was obtained by disabling the operation of the AGC circuit and directly applying digital signals ranging from 0-255 to the ADC. The corresponding values for the input and output were recorded. Figure 3.8 shows the calibration curve, which as expected is a straight line.

3.7.1.2 Calibration for Transmission Loss (Pathloss)

Unlike a narrowband receiver, calibration of the STDCC system for measuring the average received power is not a straight forward task. The average received power from a wideband receiver is equivalent to CW received power averaged over the band of frequencies occupied by the wideband probing signal (30 MHz in this study). Therefore, the output from the channel sounder is as a result of the average power over this frequency band that is sensed at its antenna. The average received power is therefore the area under the power delay profile.

To perform the calibration, the system was connected back-to-back in the laboratory, with a suitable attenuation between the transmitter and receiver. The AGC system was disabled so that the output was at the maximum (see Plate 3.1). The average power at the input of the receiver was then measured using a power meter. The AGC system was enabled and 200 power delay profiles were recorded at the sampling rate of 20 kHz. Subsequent data files containing 200 power delay profiles were recorded after the input to the receiver was increased or decreased in steps of 5 dB.

Since this was a back-to-back measurement, only one echo was present at the output. The absolute values of the peak values[12] are extracted and used to calculate the average power in each power delay profile. The power average of the 200 power delay profiles was then evaluated. Hence, a table containing the input power to the corresponding output power was obtained. Figure 3.9 shows the calibration curve for output power as a function of input power, which is a straight line as expected.

3.7.2 Time Delay Resolution

Bandlimiting of the signal with filters is expected to result in a slight loss of bandwidth in the system. This can be regarded as the correlation loss due to RF filtering and has been investigated by Holmes [3.17]. According to Holmes, for a 3 dB filter bandwidth-chip rate product ($B\tau$) of 5.0, the correlation loss is less than 0.5 dB, while the loss in time delay resolution is less than 0.1 of a chip for a $B\tau$ product of 2.0. In this study $B\tau$ was 2.0 and hence the error in time delay resolution was $\pm$3.3 ns.

Ideally, a time delay resolution of 33.3 ns and a triangular shaped autocorrelation function should be achieved. Because of the bandwidth compression inherent in this system, the theoretical base width of the autocorrelation function should be 0.25 ms. In practice, Plate 3.2 was obtained. Clearly the autocorrelation function was slightly broadened at the base and was not perfectly triangular due to filtering and the use of the logarithmic amplifier. A convenient measurement point was chosen to be the middle of the peak to noise level of the autocorrelation function. As shown in Plate 3.2, the value of 0.25 ms was achieved.

3.7.3 Stability of Frequency Sources

As mention in section 3.2.9 the stability of the frequency sources in the system will set the maximum period for reliable field trials. The relative frequency drift between

---

[12]In Chapter 4, the peak identification algorithm is presented together with noise thresholding for each power delay profile.

the Rubidium standards was minimised by fine-tuning in the laboratory. Also since commercial signal generators were employed with a frequency resolution of 0.01 Hz, it was possible to minimise errors in the up-conversion of the 10 MHz reference signal to 1.8 GHz, by slightly offsetting the frequency by 0.1 Hz.

After fine-tuning and frequency offsetting, the frequency difference, Δf, works out to be 1.54×10^{-12}. This provided a maximum period of field trials of about 6 hours.

3.7.4 Accuracy of Phase Measurement and Phase Noise

Generally frequency sources exhibit a combination of a steady frequency drift and random phase fluctuations, which will affect the integrity of the phase measurements. In theory, if perfect frequency synchronism was possible between the transmitter and receiver, the quadrature outputs would map out a vector with a fixed and arbitrary phase angle when displayed on an oscilloscope which is set in the X-Y mode. However, due to the frequency difference, Δf, between the standards, the vector rotates in the IQ-plane at a rate proportional to Δf. This is further magnified by the inaccuracies in the multiplication process inherent in the signal generators which took the 10 MHz reference to 1.8 GHz. It was therefore possible to reduce Δf by fine-tuning the frequency standards and slightly offsetting the LO in the receiver by a tenth of a Hertz.

After extended periods of fine-tuning in the laboratory a phase change of 360° in 360 seconds was consistently obtained. This is far superior to that of Cox and Demery who had similar changes in 10 and 30 seconds respectively. This resulted in Δf of approximately 1.54×10^{-12}.

Phase noise from the frequency sources in the system will cause phase jitter and consequently the IQ vector fluctuates. This will result in errors in measurement of the phase. Since the phase noise of the Rubidium frequency standards was superior to that of the signal generators, the random phase fluctuations could safely be attributed to the signal generators.

Plate 3.3 shows the quadrature components for the case when all the energy was in the inphase channel. It can be noticed that the fluctuation induced in the quadrature channel was extremely small. This gave a measured phase accuracy of $\pm 5°$.

3.7.5 Phase Offsets due to Programmable Attenuator

It was observed that the phase changes exhibited by the programmable attenuator in the RF stage of the receiver was not constant when different attenuation cells were activated. Using a network analyzer the values of the phase offsets when the individual attenuation cells are active were measured. Table 3.1 below shows the phase offsets for the programmable attenuator cells when active.

Table 3.1 Phase offsets for the programmable attenuator cells.

Programable Attenuator Cell	Phase Offset
0	0.0°
4	13.0°
8	10.0°
16	-7.0°
32	-58.0°
64	-121.0°

As will be explained in Chapter 4, these values were added to the phase values before storage. This was done by checking the AGC value for each power delay profile and adding the phase offset to each of the echo phases in the power delay profile. For example, if the AGC value is 52 dB, this is made up of the 4, 16 and 32 dB cells in the programmable attenuator. Hence the phase offset is -52° (13-7-58°).

3.8 SUMMARY

In this chapter, the requirements for the experimental channel sounding system have been presented. The design and implementation of the experimental channel sounding system which satisfies these requirements was presented in sections 3.3 and 3.4. The

PC-based data acquisition system, techniques and results from the performance evaluation of the system in the laboratory have also been presented. Below in Table 3.2 is a summary of the main features of the experimental system.

Table 3.2 Main features of the experimental wideband channel sounding system.

Characteristic	Typical value
Carrier Frequency	1.8 GHz
Clock Rate	30 MHz
Maximum measurable excess delay	17.03 μs
Slip rate	8 kHz
Impulse response sounding rate	$\approx$ 16 power delay profiles per second
Dynamic range	30 dB
Frequency stability	5 parts in 10^{11}
Single sideband phase noise spectral density of signal sources	-101 dBc/Hz at a carrier offset of 1 kHz.
Phase stability	1° per second
Phase accuracy	$\pm$5°
AGC switching range	0 to 124 dB

In the next chapter, the measurement techniques that were utilised during the measurement campaign are presented. A description of the salient features of the locations surveyed together with the various methods of data reduction and analysis are presented.

REFERENCES

[3.1] CCIR Report 567-3 (MOD F), 'Propagation Data and Prediction Methods for the Terrestrial Land Mobile Service Using the Frequency Range 30 MHz to 3 GHz', CCIR XVIIth Plenary Assembly, Düsseldorf, 1990.

[3.2] Qualcomm Inc., 'An Overview of the Application of Code Division Multiple Access (CDMA) to Digital Cellular Systems and Personal cellular Networks', 1992.

[3.3] Bajwa, A.S., 'Wideband Characterisation of UHF Mobile Radio Propagation in Urban and Suburban Areas', Ph.D Thesis, Department of Electronic and Electric Engineering, The University of Birmingham, 1979.

[3.4] Demery, D.A., 'Wideband Characterisation of UHF Mobile Radio Channels in Urban Areas', Ph.D Thesis, Department of Electric Engineering and Electronics, The University of Liverpool, 1989.

[3.5] Natarajan, N., 'Wideband Characterisation of Mobile Radio Channels at 1.8 GHz', Ph.D Thesis, Department of Electric Engineering and Electronics, The University of Liverpool, 1992.

[3.6] Young, W.R., and Lacy, L.Y., 'Echoes in Transmission at 450 Megacycles from Land-to-Car Radio Units', Proc. IRE, 1950, Vol. 38, pp255-258.

[3.7] Cox, D.C., 'Delay Doppler Characteristics of Multipath Propagation at 910 MHz in a Suburban Mobile Radio Environment', IEEE Trans. on Antennas and Prop., Vol. 20, No. 5, Sept. 1972, pp625-635.

[3.8] Turin, G.L., Clapp, F.D., Johnston, T.L., Fine, S.B. and Lavry, D., 'A Statistical Model of Urban Multipath Propagation', IEEE Trans. on Veh. Tech., Vol. 21, No. 1, Feb. 1972, pp1-9.

[3.9] G.S.M. Recommendations 5.0X Series.

[3.10] Parsons, J.D., Demery, D.A. and Turkmani, A.M.D., 'Sounding Techniques for Wideband Mobile Radio Channels: A Review', IEE Proc-I, Vol. 138, No. 5. Oct 1991. pp437-446.

[3.11] Hashemi, H., 'Simulation of the Urban Radio Propagation Channel', IEEE Trans. on Veh. Tech., Vol. VT-28, No. 3, Aug. 1979. pp213-225.

[3.12] Saleh, A.A.M. and Valenzuela, R.A., 'A Statistical Model for Indoor Multipath Propagation', IEEE Journal on Sel. Areas in Comms., Vol. SAC-5, No. 2, Feb. 1987 pp128-137.

[3.13] Kartaschoff, P., 'Frequency and Time', Academic Press, 1978.

[3.14] Robins, W.P., 'Phase Noise in Signal Sources', IEE Telecommunications Series 9, Peter Periginus Ltd., London, 1982.

[3.15] Dixon, R.C., 'Spread Spectrum Systems', Wiley, New York, 1982.

[3.16] Turner, R.J., 'Binary Biphase Modulation Switches in 3 nanoseconds', Electronics, 26th April, 1973, p104.

[3.17] Holmes, J.K., 'Coherent Spread Spectrum Systems', Wiley, New York, 1982.

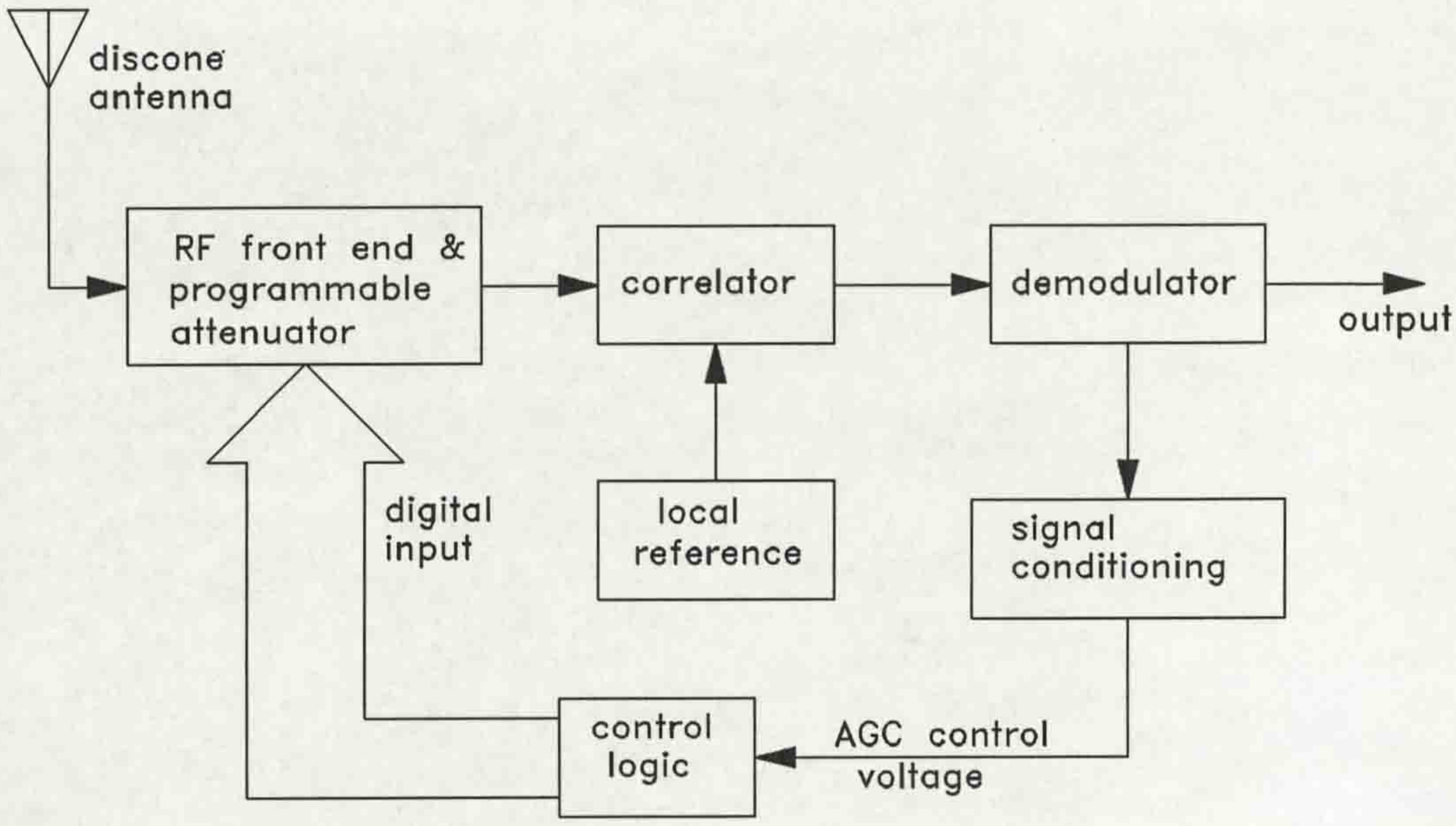

Figure 3.1 Schematic diagram of an STDCC receiver system with AGC configuration.

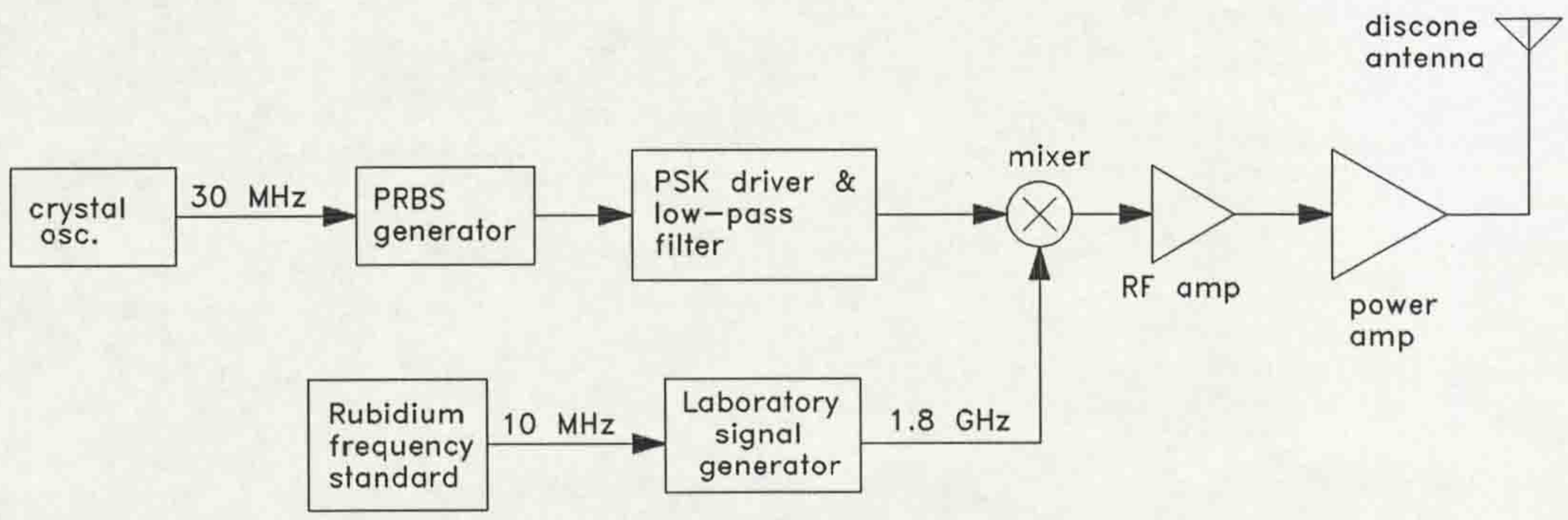

Figure 3.2 Simplified block diagram of the transmitter.

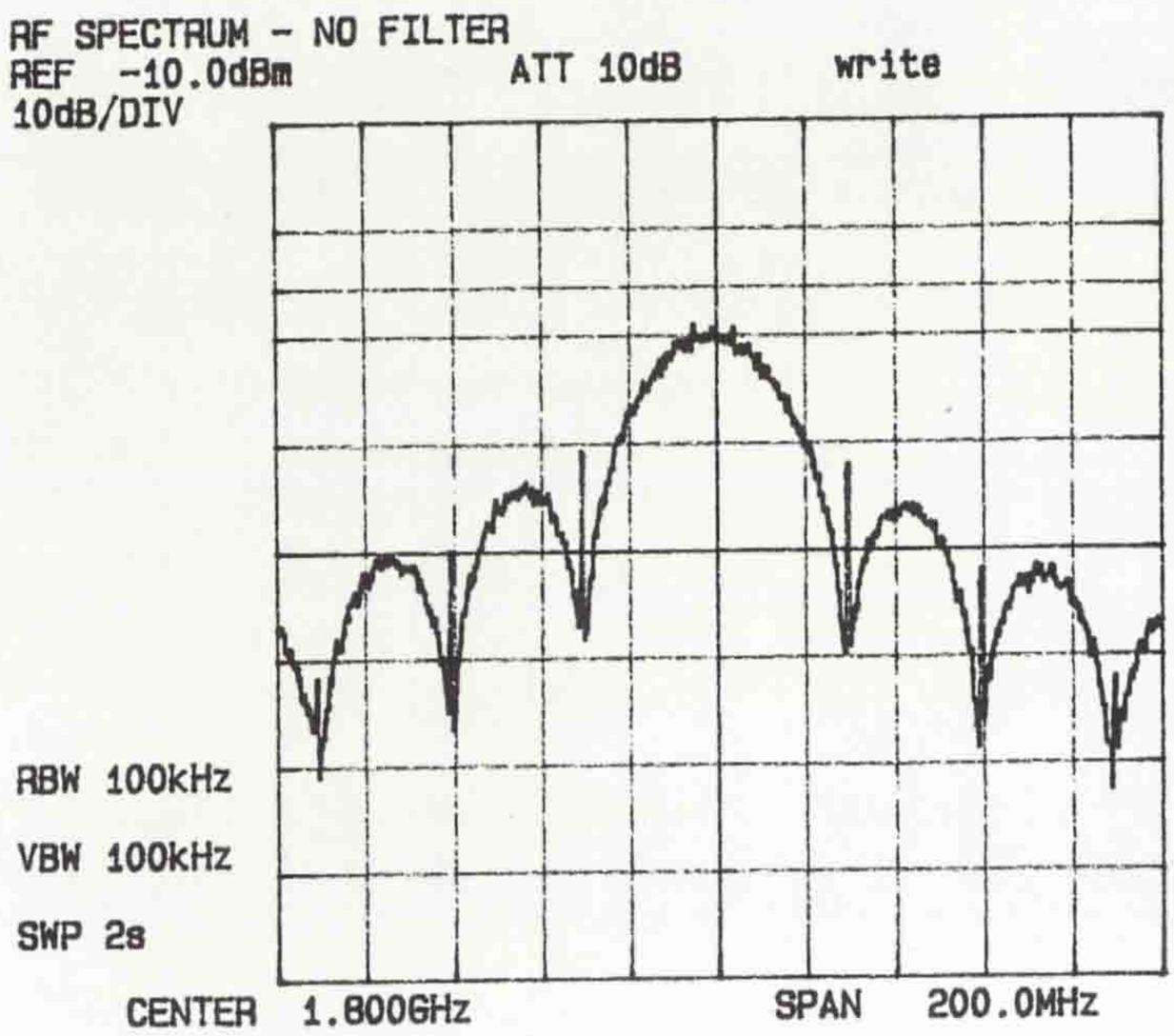

Figure 3.3 RF Spectrum of the transmitted signal without low-pass filtering of the PRBS.

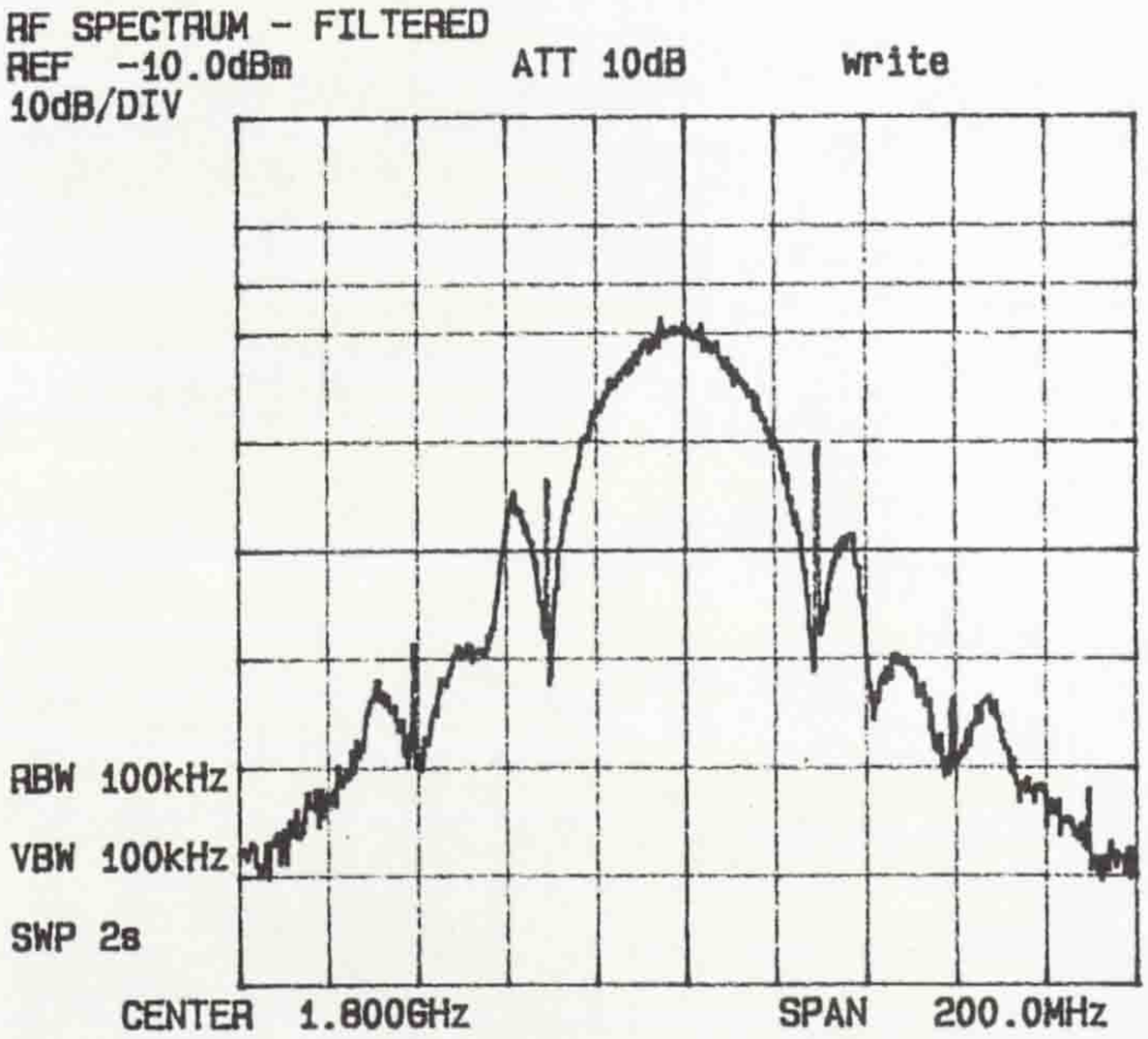

Figure 3.4 RF spectrum of the transmitted signal with low-pass filtering of the PRBS.

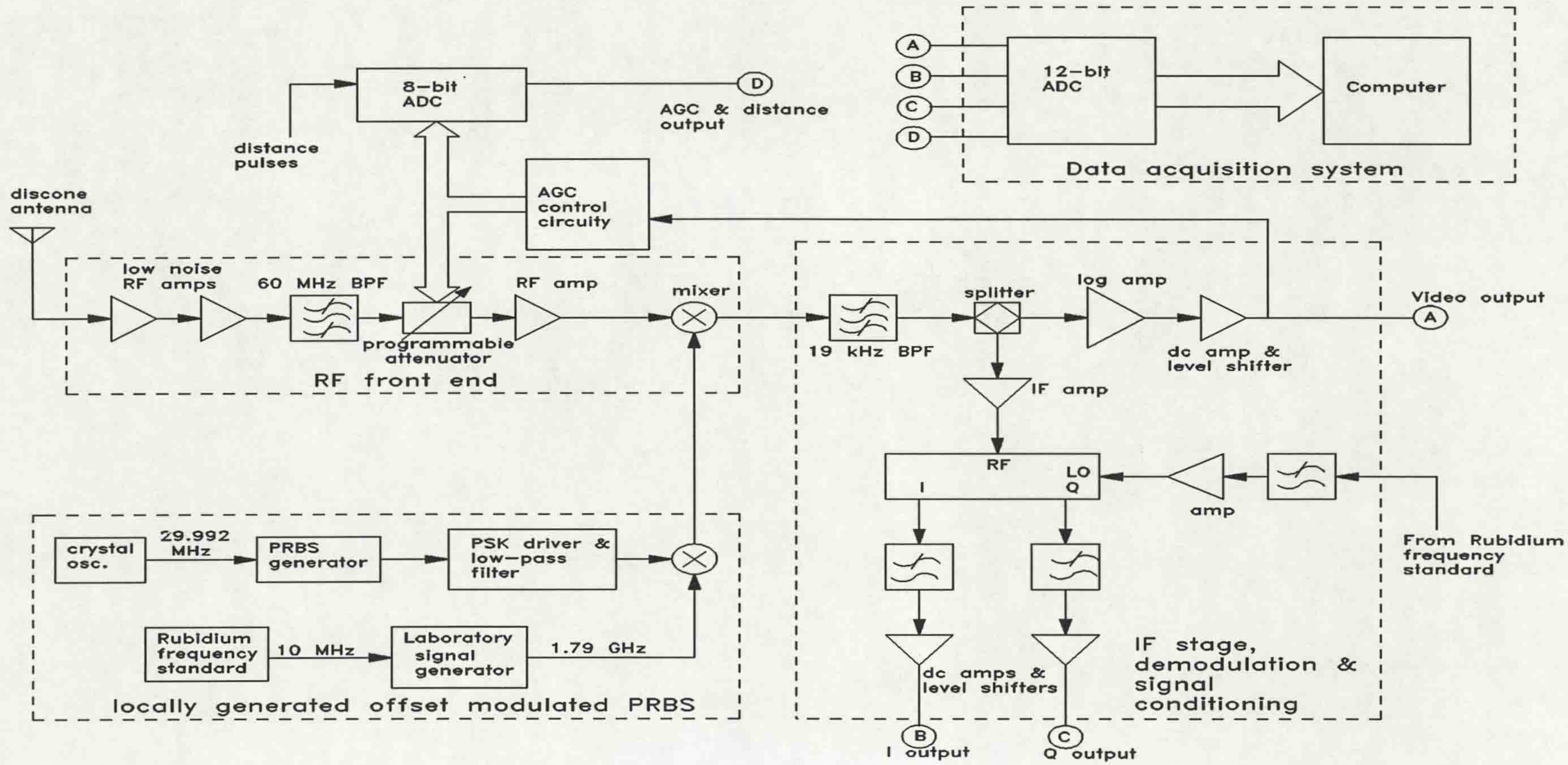

Figure 3.5 Block diagram of the receiver system.

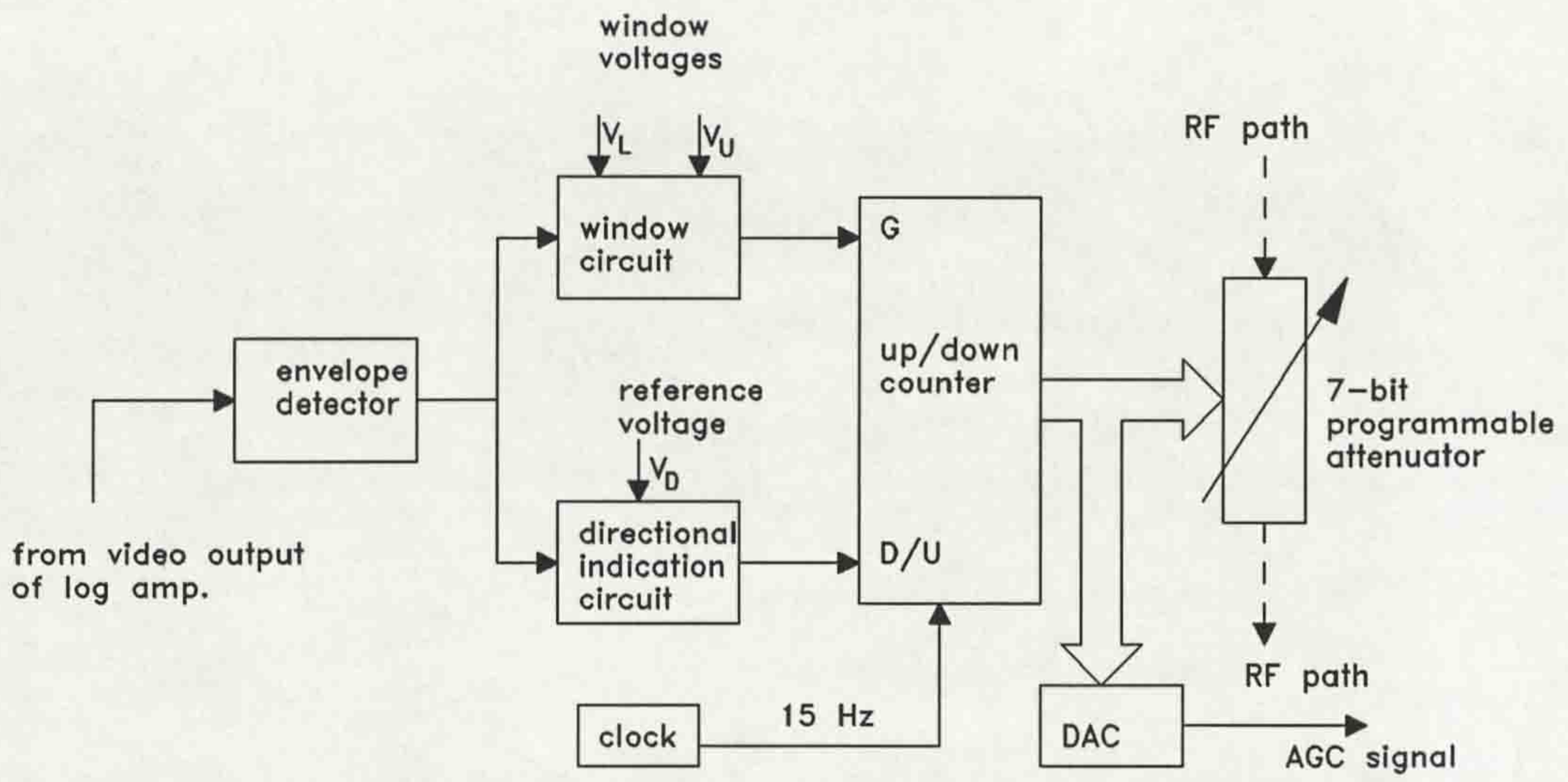

Figure 3.6 Block diagram of the AGC system.

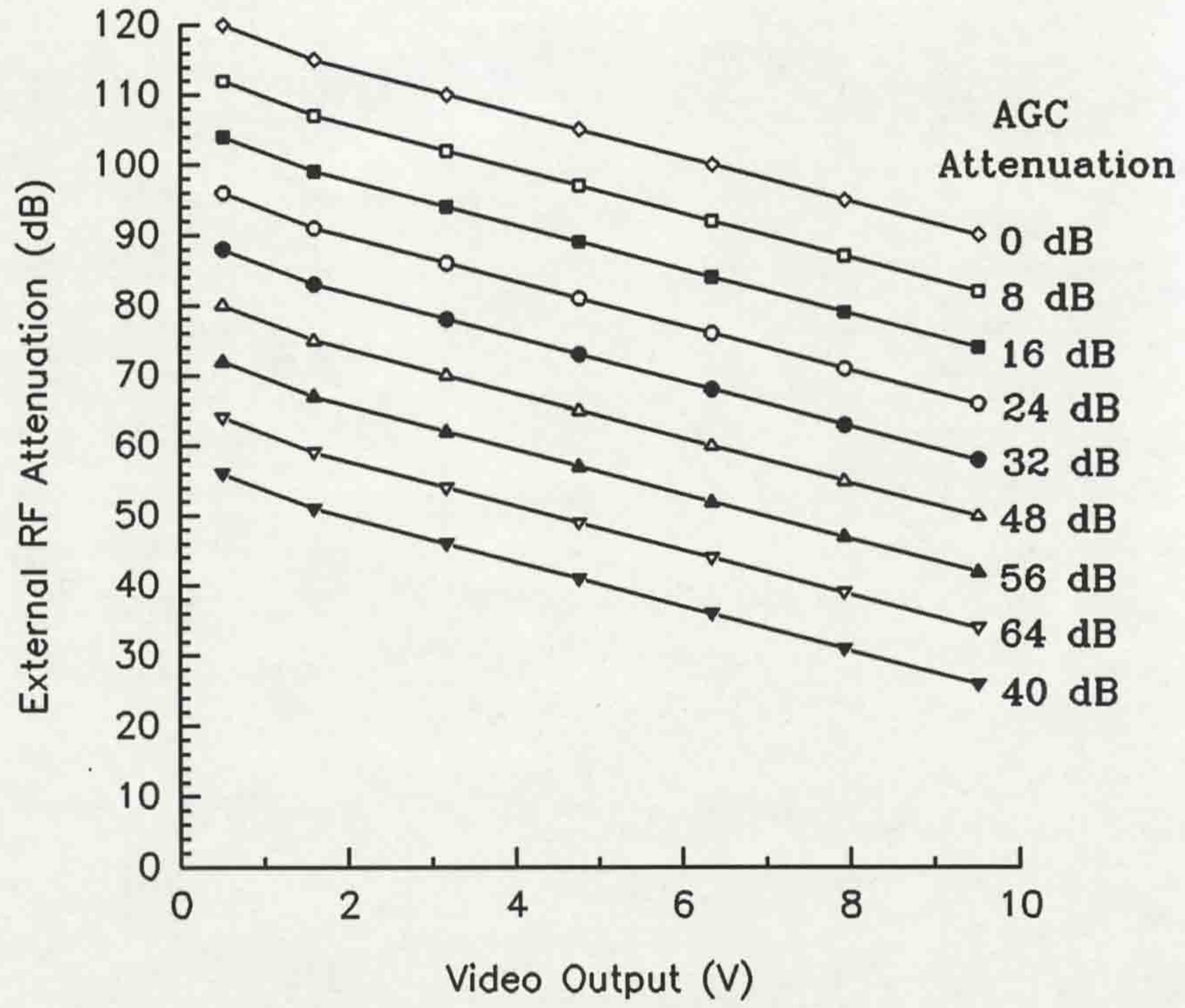

Figure 3.7 Receiver calibration curves for the video output.

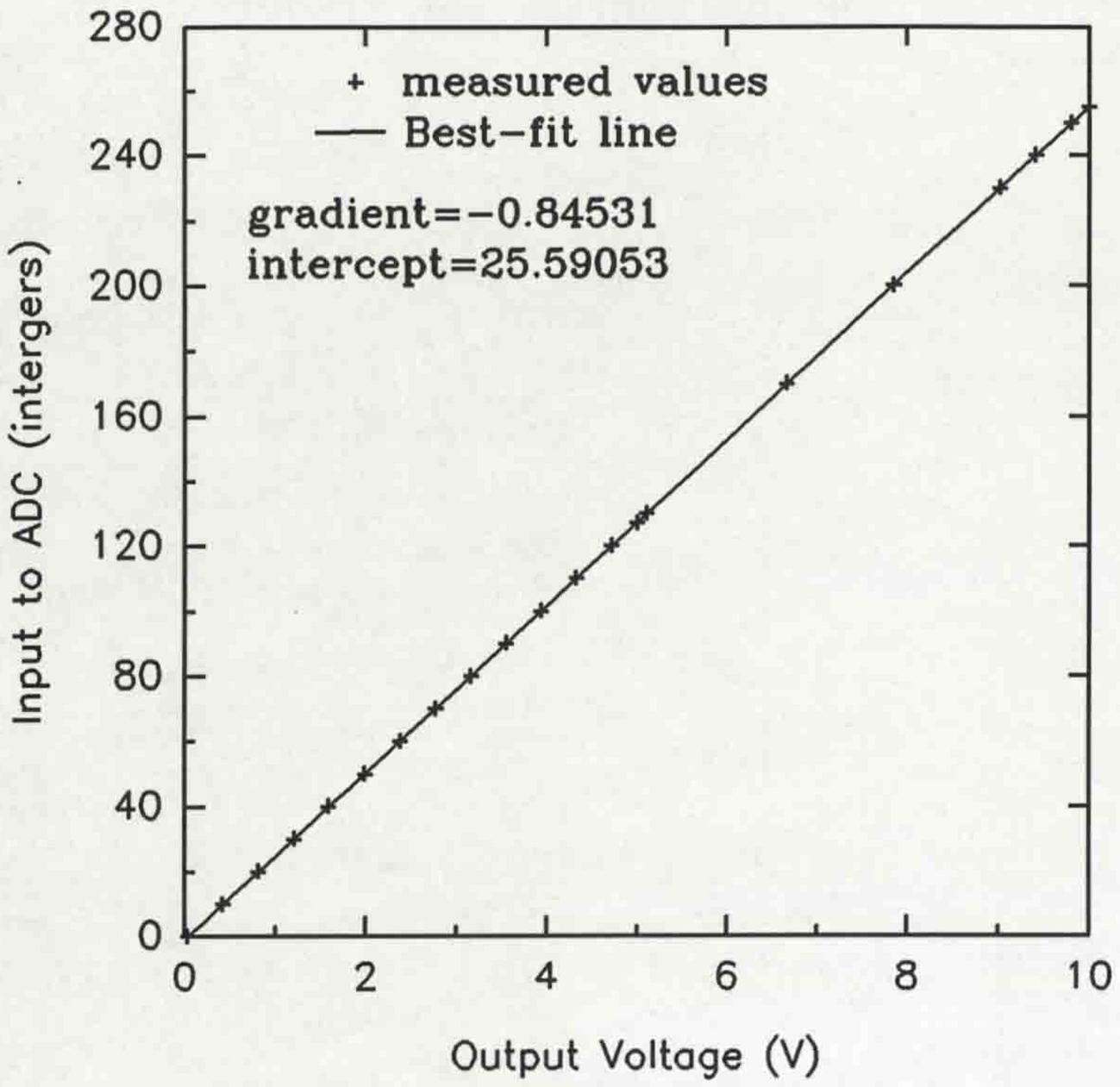

Figure 3.8 Calibration curve for the AGC system.

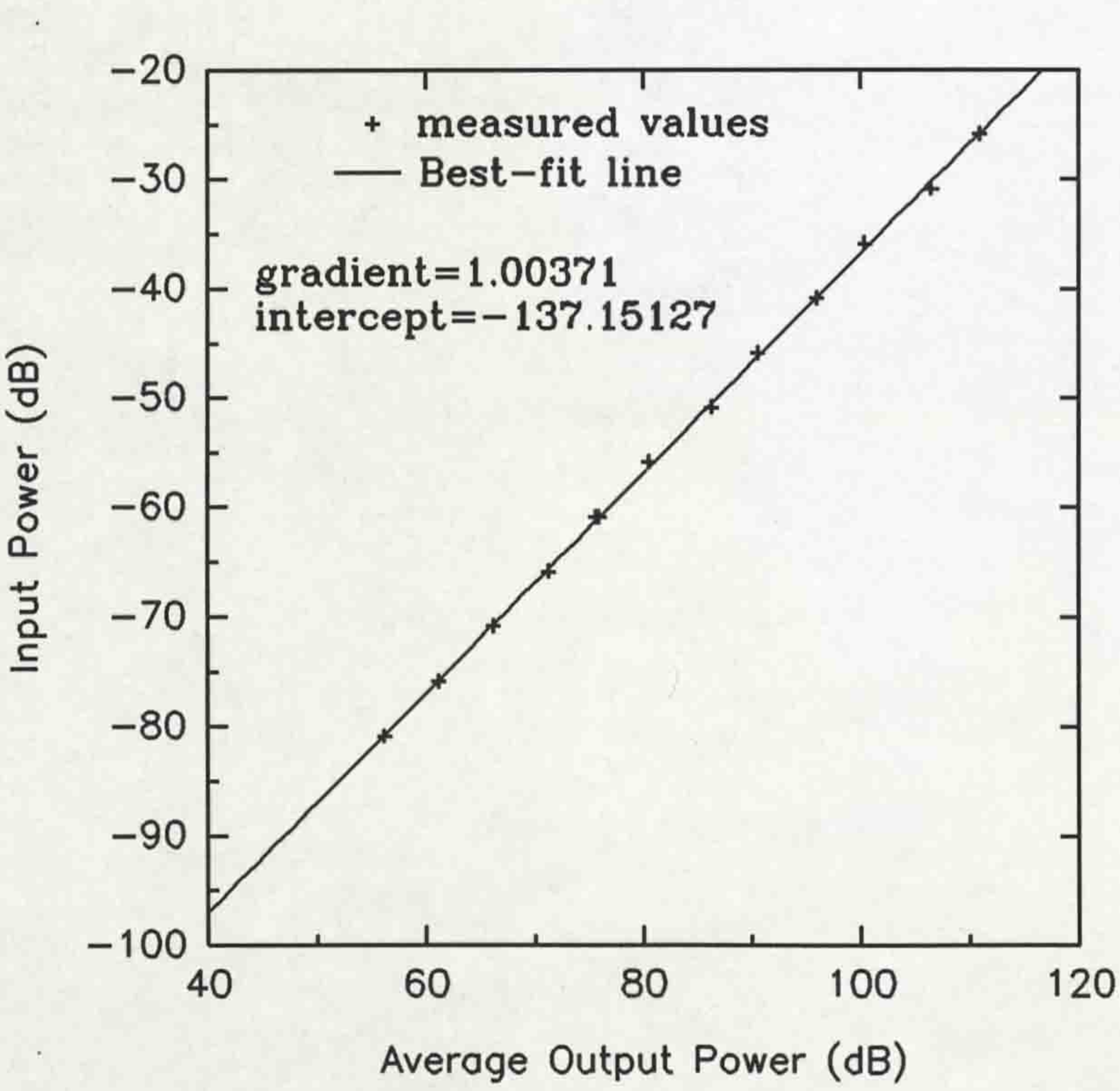

Figure 3.9 Calibration curve for calculating received average power.

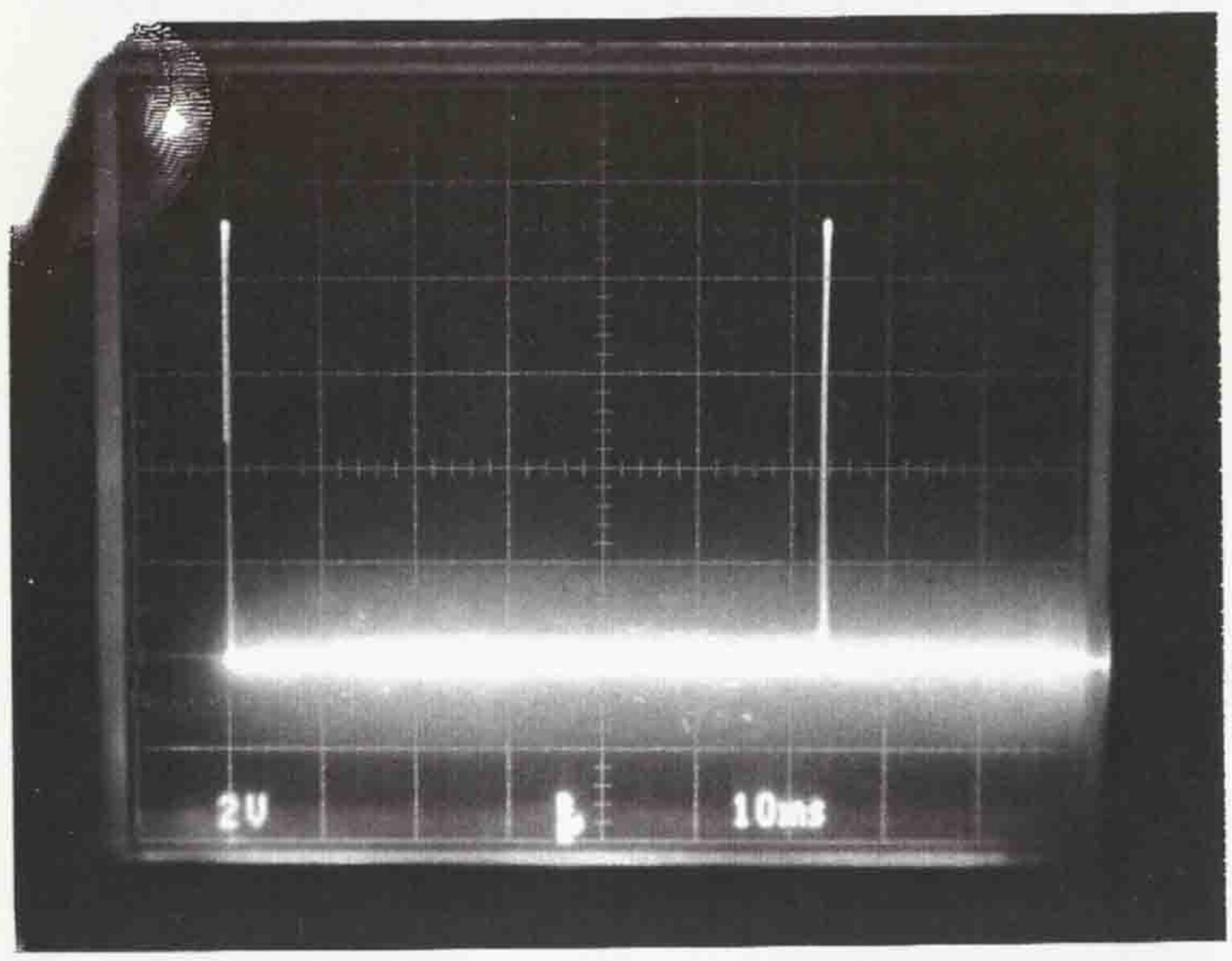

Plate 3.1 Video Output of the system, showing a 64 ms period for the power delay profiles and a maximum echo strength of 10 V.

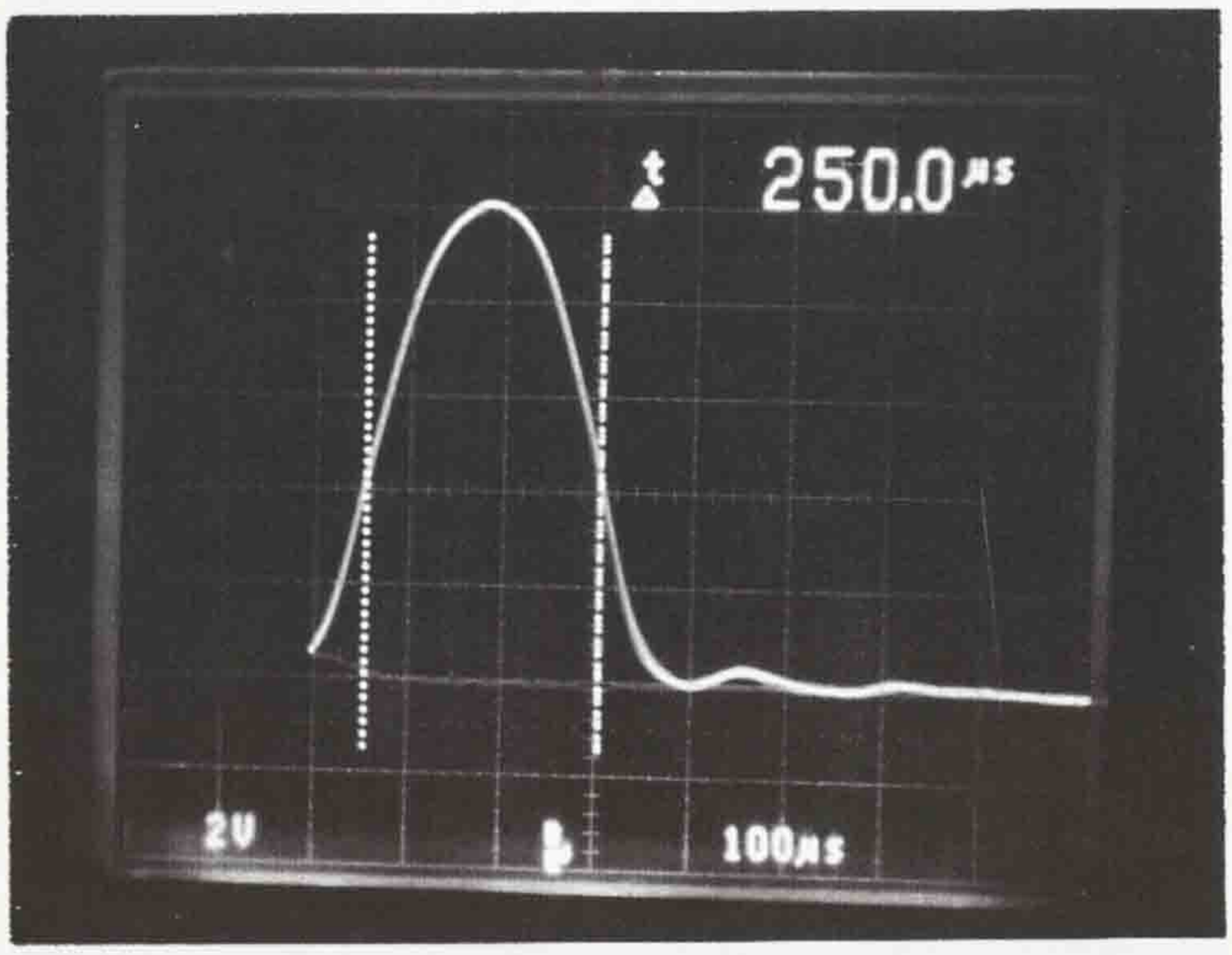

Plate 3.2 Video output of the system showing an echo with a base width of 0.25 ms.

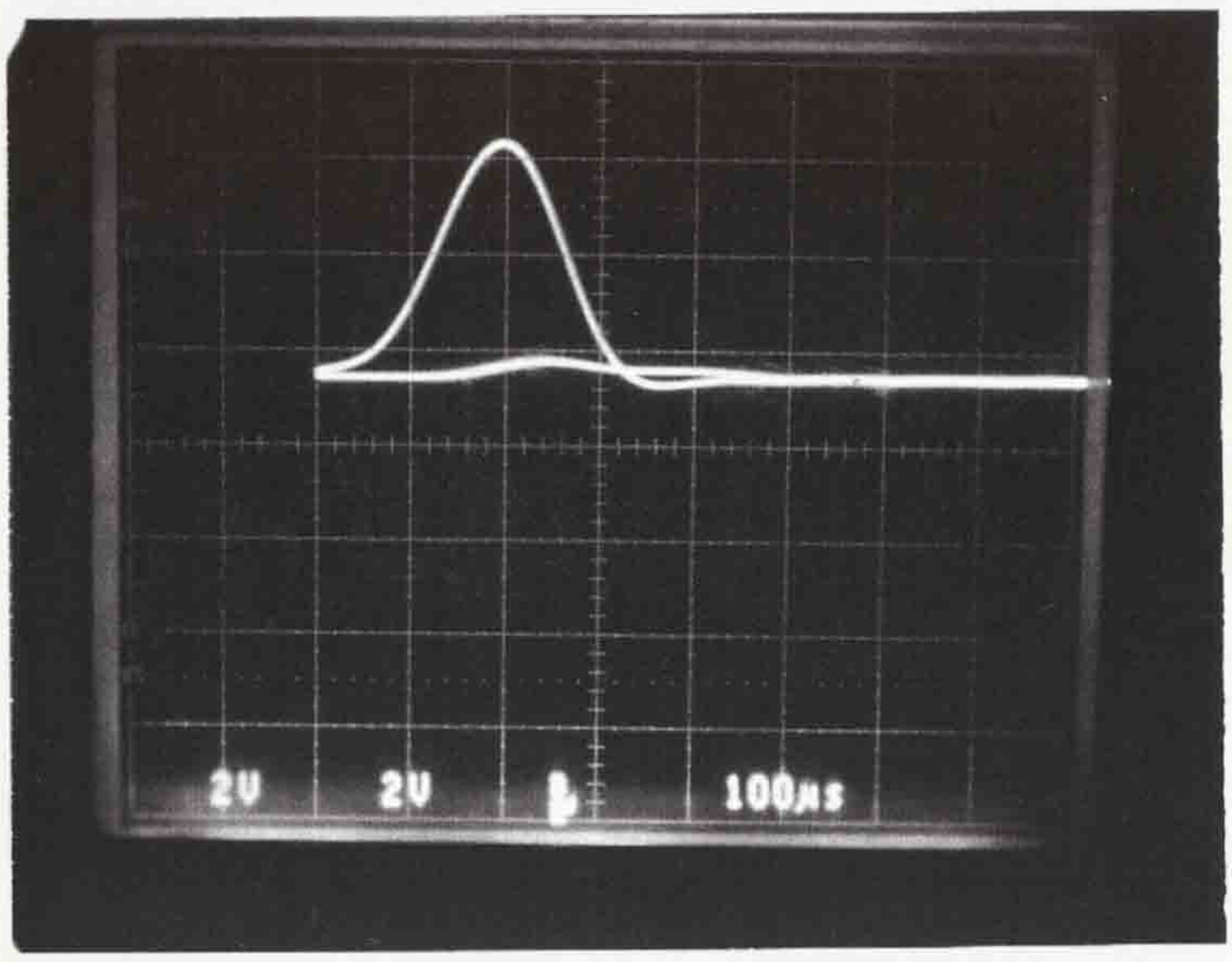

Plate 3.3 Autocorrelation function of the I and Q components from the system.

Chapter Four

MEASUREMENT TECHNIQUES, EXPERIMENTAL LOCATIONS AND DATA PROCESSING

4.1 INTRODUCTION

A series of wideband complex impulse response measurements was conducted in and around the City of Liverpool at a carrier frequency of 1.8 GHz using the channel sounder system described in Chapter 3. Due to the nature of the environments used, the experimental techniques can be divided into two main parts relating to the outdoor and indoor measurements. In this chapter, the techniques used for these measurements are presented, together with a description of the salient features of the experimental locations. Finally, the various methods of off-line data reduction and analysis are presented.

4.2 EXPERIMENTAL DESIGN

A limited number of results from time dispersion measurements in outdoor as well as indoor environments have been published in the literature as reviewed in Chapter 2. Most of the outdoor measurements were performed on selected short portions of main streets around the experimental base site, hence, the data was too sparse to derive reliable echo statistics. Furthermore, the sparsity of the experimental data results in the small-scale descriptors being over-estimated in both cases, as worst case power delay profiles were often sought. It was therefore necessary to design outdoor experiments which would cover all possible streets irrespective of their widths or orientations. We also sought to perform measurements in a random manner rather than search for what is deemed to be the worse case power delay profiles and to perform the measurements in longer stretches of streets.

Microcell structures are under consideration for coverage and capacity enhancement

into areas such as shopping malls, railway stations, etc., where large numbers of people congregate and as a design aid it is appropriate to conduct wideband studies in these locations. Measurements were therefore conducted in a train station and two modern superstores. Again, it was deemed necessary to cover most of the floor area in these buildings.

4.3 EXPERIMENTAL MEASUREMENT TECHNIQUES

The techniques used for the measurements depended on the type of environment to be surveyed. Since wideband propagation measurements were required in outdoor as well as within buildings, there were fundamental differences in the way the transmitter and receiving system were mounted and adapted to traverse the measurement sites. For example, a trolley-based receiving system was required for the indoor measurements whereas, a vehicle-borne receiving system was preferred for the outdoor measurements. These fundamental differences will be clarified in the next section.

4.3.1 Outdoor Experiments

For these sets of experiments, the transmitter was mounted on the roof of an appropriate building so as to illuminate the measurement area. This was achieved by mounting the power amplifier on a tripod and coupling the transmitting discone antenna directly onto it. The receiving system was mounted in a vehicle which contained the necessary power supplies to drive the system. In addition, a tachometer in the form of a slotted-disk was installed on the propeller shaft of the vehicle. This provided the distance marker pulses which were recorded to indicate the distance traversed during each experimental run and to indicate the speed of the vehicle as explained in Chapter 3 (section 3.5).

The receiving discone antenna was mounted on the roof of the vehicle about 2 m above ground level. This discone antenna was coupled to the receiver system, which was mounted in the back of the vehicle, using a low-loss coaxial cable. The video

output of the receiver was also displayed on an oscilloscope to allow the examination of field data and to ensure that most of the recorded profiles had a peak-to-spurious level of 20-30 dB. This is in accordance with the CCIR recommendations [4.1] which were adhered to in this study.

Three base station locations were selected: two urban (URBAN1 and URBAN2) and one rural open locations. For each of these outdoor base station locations, a number of streets around the base site were chosen at random, prior to the measurement campaign. These streets were chosen so as to cover all possible street orientations (circumferential, tangential, radial, etc.) as well as main and side streets relative to the base station. This *a priori* selection of the streets was necessary to avoid the inclination towards the selection of worst case locations and other possible operator-induced biases. Two people were required for these sets of measurements: one to drive the vehicle and the other to monitor and perform recording of the data. For each experimental run, the mobile station traversed the chosen streets around the selected base station[1]. Due to the inclusion of the AGC system, the run length was limited only by the amount of extended memory in the PC and distances of 100 m could be accommodated. Table 4.1 shows the number of experimental runs together with the average run length and total distance covered for each of these locations.

Table 4.1 Experimental details for the outdoor experiments.

Base Station location	Total Number of Runs	Average Run Length (m)	Total Distance covered (km)
URBAN1	43	90	3.9
URBAN2	39	80	3.4
rural open area	21	80	1.8

Experiments in the urban locations were conducted from 7.00 pm onwards as dictated by the local police while those in the rural areas were carried out on Sunday

[1]A preselected street was only replaced if the signal levels were visibly below 15 dB, ie., 5 V on the oscilloscope display.

afternoons. This meant that very few cars and buses were present on the streets. Thus, there were virtually no intervening obstacles other than features of the environment itself.

4.3.2 Indoor Experiments

Experiments were conducted in two different indoor environments; supermarkets and a train station. Even though the environments are different in terms of contents, shape and building construction, the experimental technique adopted was the same in both cases. The transmitting discone antenna was coupled to the power amplifier by a 4 m low-loss coaxial cable and mounted about 2-4 m above ground level depending on the height of the building under surveyance. In the case of the supermarkets, the antenna was mounted in the centre of the building to be surveyed, while it was mounted in one corner in the train station for convenience.

The receiving system was mounted on a trolley. The power supply was obtained from a mains[2] supply using a 50 m trailing power cable. A fifth wheel was installed on the trolley so as to generate the distance marker pulses. The receiving discone antenna was mounted about 1.8 m above ground level and was coupled to the receiver by another low-loss coaxial cable.

Three base sites were chosen for this set of experiments: two supermarkets (SMARKET1 and SMARKET2) and one train station. For each indoor base station, a number of aisles were chosen prior to the experimental field trials. These were chosen at random and in such a way as to cover most of the building. Again, this ensured that any possible inclination towards the selection of worst case locations was avoided. For each experimental run, the trolley traversed the selected aisles at a normal but constant walking speed. The average run length was determined by the lengths of the aisles. Table 4.2 shows the number of experimental runs, the average

[2]In the train station, mains sockets were not evenly distributed around the building, hence, a 1.5 kVA petrol generator mounted on a trolley, was used to supply power to the receiving system.

run length and the total distance covered for these sites.

Table 4.2 Experimental details for the indoor experiments.

Base Station location	Total Number of Runs	Average Run Length (m)	Total Distance covered (km)
SMARKET1	26	15	0.32
SMARKET2	24	15	0.32
Train Station	16	45	0.74

The experiments in these locations were conducted during the early hours of the morning. During this period, these buildings are relatively quiet. This ensured that fewer obstructions were encountered during the experiments and more importantly, the trailing cable was not a danger to the public.

4.4 DATA ACQUISITION AND STORAGE

For each experimental run four outputs from the receiving system were time-sampled at a rate of 20 kHz. These were:

i. The envelope of the power delay profiles

ii. The inphase output

iii. The quadrature output

iv. The analogue voltage corresponding to the attenuation setting of the AGC system, superimposed with the distance-marker pulses.

During the process of sampling, the samples are temporarily stored in the extended memory of the PC. When this is full or the experimental run is completed, the data is transferred to the hard disk of the PC for permanent storage. It should be noted that (iv) above contains two pieces of information that required separating prior to storage[3].

[3]Since the tachometer output was connected to the most significant bit of the DAC in the AGC system, the maximum integer value of the AGC signal alone is 127. The software checks these values and generates the resulting distance pulses as explained in Chapter 3.

Five files were generated for each experimental run: the power delay profile (PDP), AGC signal, phase, distance and information files. The phase file was generated by applying the equation below to the quadrature samples sequentially.

$$\phi_i = \tan^{-1}\frac{Q_i}{I_i} \qquad (4.1)$$

where ϕ_i is the phase of the i^{th} sample, Q_i and I_i are the i^{th} samples from the quadrature and inphase channels respectively.

For the PDP files, the following information was stored sequentially in binary format:

i. The number of samples in the file, stored as a 4-byte long integer .

ii. The sampling frequency in Hertz, stored as a 4-byte floating point number.

iii. The slope of the receiver calibration curve, stored as a 4-byte floating point number.

iv. The intercept of the receiver calibration curve, stored as a 4-byte floating point number.

v. Recorded data, with each sample stored as a 2-byte integer.

The AGC data file was stored using the same format with the slope and intercept values obtained from the calibration curve of the digital-to-analogue converter (DAC) used in the AGC system. The distance file contained the integer values zero or one and the phase file was contained floating point numbers.

For the PDP file, the actual voltage from each sample is given by:

$$\textit{Actual Voltage(PDP)} = \textit{stored integer value} \cdot \frac{10.0}{4095.0} \qquad (4.2)$$

The corresponding voltage from the AGC file is given by:

$$\textit{Actual voltage(AGC)} = \textit{stored integer value} \cdot \frac{10.0}{255.0} \qquad (4.3)$$

The signal levels in dBm for the PDP and AGC samples are given by:

$$dBm(PDP) = PDP_{slope} \cdot actual\ voltage(PDP) + PDP_{intercept}$$
$$dBm(AGC) = AGC_{slope} \cdot actual\ voltage(AGC) + AGC_{intercept} \quad \textbf{(4.4)}$$

The absolute signal level in dBm is obtained from the equation below:

$$Absolute\ level(dBm) = dBm(PDP) + dBm(AGC) \quad \textbf{(4.5)}$$

It should be noted that profiles in which there is a transition in the AGC signal level equal to or greater than 4 dB are discarded, i.e., not included in the analysis. This is essential since the attenuation setting for any of the power delay profiles should be constant.

It was shown in Chapter 3 (section 3.7.5) that the phase of the input signal to the programmable attenuator in the RF stage was not the same when different attenuator cells were activated. The phase offsets for the various attenuator cells were shown in Table 3.1. Therefore, before storing the computed phase values for each profile, the programmable attenuator value was checked and the appropriate phase offset was added. Figures 4.1 and 4.2 are typical plots obtained from two of the locations showing the AGC signal in blue, the power delay profile (PDP) in red and the echo phases in green.

4.5 DESCRIPTION OF MEASUREMENT SITES

Extensive wideband propagation measurements were undertaken in urban and rural areas, as well as within buildings, to amass a database of complex power delay profiles for each of the locations. The description of the salient features of each of the areas surveyed follows.

4.5.1 Urban Areas

Two base station sites were selected in the City of Liverpool which are typical of urban environments in the U.K. These will subsequently be referred to as URBAN1 and URBAN2.

For URBAN1, the transmitter was coupled to a linear power amplifier and adjusted to give an average output power of 7 W. This was set up on the roof of Silkhouse Court, Tithebarn Street, in the city centre of Liverpool. The building is 10 storeys high and is significantly taller than the adjacent buildings. The streets in the city centre are flanked on both sides by buildings which are at least 4 storeys high, with the occasional building having a height in excess of 7 floors. South east of the transmitter location, about 800 m away is the River Mersey. There are buildings across the river which can significantly affect the propagation characteristics in this area. There are also some high-rise council dwellings located westwards from the transmitter location. Experiments were conducted on streets up to 4 km away. Figure 4.3 is a map showing the transmitter location and the approximate locations of the experimental runs. Plate 4.1 shows the transmitter on the roof of the building looking north into the city centre. Plate 4.2 shows a photograph taken from the roof of the building looking south and across the River Mersey, plate 4.3 is looking eastward. Plate 4.4 shows a photograph from the roof of the building looking into the city centre.

For URBAN2, the transmitter which was adjusted to provide an average output power of 7 W, was set up on the roof of the Mechanical Engineering building in the precinct of the University of Liverpool. The building is 8 storeys high and is one of several high-rise buildings within the precinct. The experiments were conducted around the base station up to 4 km away. The area surveyed comprised a combination of low level factory units, residential premises with typical high-rise council flats and the city centre with high-rise office and shop buildings. A map of the area indicating the position of the transmitter and the various positions of the receiver is shown in Figure 4.4. Plate 4.5 shows an ariel photograph of Liverpool city centre, depicting the transmitter locations for URBAN1 and URBAN2 .

4.5.2 Rural Open Area

The transmitter was set up on the roof of a three storey building in Halewood, which is located in the outskirts of Liverpool. The average output power of the transmitter

was 7 W. In the immediate vicinity of the transmitter, there were mainly open fields and woodlands with relatively narrow winding roads. Farm houses were dotted around the area. Some residential houses were located south east of the transmitter location, about 750 m away. The majority of these houses were typical 2-storey high residential houses with the occasional high-rise council block of flats. The experiments were conducted into the residential area and around the base station up to 2.5 km away. Figure 4.5 shows a map of the area indicating the position of the transmitter and the approximate positions of the receiver.

4.5.3 Supermarkets

Experiments were undertaken in two large modern supermarkets. These will subsequently be referred to as SMARKET1 and SMARKET2. One of the fundamental differences between these two locations is the nature of goods sold in these stores. SMARKET1 is a typical general purpose food superstore, while SMARKET2 is a typical hardware "Do it Yourself" (DIY) superstore. They are therefore differences in the type and nature of the contents together with the general layout of these stores.

In SMARKET1, the transmitter was coupled to a linear power amplifier and adjusted to provide an average output power of 0.6 W. The transmitting discone antenna was placed in the centre of the store, 2 m above ground level. This was located such that the antenna cleared all visible obstructions which were mainly metal display shelves. This superstore is a typical modern design with three main aisles running its length. Minor aisles flanked on both sides by metal display shelves, about 1.8 m high run across these main aisles. The main aisle on the left is wider as it contains the checkout desks. The building is steel-framed with the walls constructed of brick. Concrete metal truss works support a corrugated steel roof. There are no glass sections except the entry and exit doors. Figure 4.6 shows the floor plan of this supermarket. Plates 4.6 and 4.7 are photographs showing one of the main aisles (M2) in this superstore. Plate 4.8 shows one of the minor aisles and Plate 4.9 shows the outside of the building.

In SMARKET2, the average output power of the transmitter was also set to 0.6 W. The transmitting discone antenna was placed 2.9 m above ground level. It was not possible to clear all visible obstructions since some of the display units were mounted from the roof of the store. The store is a typical hardware DIY superstore with sections for kitchen, bathrooms and toilets, paints, wood, lighting, etc,. Most of the shelves in this store were on average, 2.5 m high. The walls of the building are made of brick and the roof, which was supported by concrete metal truss works, was constructed of corrugated steel. The only glass sections to this building are the entry and exit doors; set in the front and another in the rear. Figure 4.7 shows the floor plan of this superstore. Plate 4.10 is a photograph showing a typical aisle and part of the lighting section. Plate 4.11 shows one of the minor aisles and Plate 4.12 shows the bathrooms section. Plate 4.14 shows the outside of the supermarket.

4.5.4 Train Station

Experiments were also conducted in Lime Street Station, Liverpool (see Plate 4.5). The average power of the transmitter was again set to 0.6 W. The transmitting discone antenna was mounted about 3.3 m above ground level, close to the main pedestrian entrance to the building. The building is constructed of mainly steel and glass. A crisscross pattern of metal, supported by large metal concrete pillars, supports the roof which is made of hard glass. There are three main sections: the concourse section surrounded by shops and time table display units, the inner section containing three railway terminals with six platforms and the outer section containing two railway terminals with three platforms and a car park. All five railway terminals lead into a tunnel which takes the trains out of the city centre. The floor plan is shown in Figure 4.8. Plates 4.14 and 4.15 show platform 6 and platforms 7 and 8 respectively. Plate 4.16 shows one of the columns of supporting metal pillars and Plate 4.17 shows the car park entrance to the building.

4.6 DATA REDUCTION AND ANALYSIS

In order to analyse the data collected, some techniques of data reduction had to be

implemented. These data reduction techniques consists of four main parts. Firstly, the points in the data stream which denote the start of the power delay profile had to be determined. Secondly, the peaks in each power delay profile were extracted. The small-scale descriptors associated with individual power delay profiles were calculated and lastly large-scale characterisation techniques were used. A detailed description of these processes is outlined below.

4.6.1 Locating the Start of the Power Delay Profile

When sampling is initiated during the course of any experimental run, the recorded data can start anywhere within a power delay profile. There are two reasons for this. Firstly the channel sounding system employs two PRBS sequences with different clock rates, making synchronization between them impossible. Secondly, the channel sounding system does not provide any synchronization signals to the data acquisition system.

The software package therefore includes a feature which allows the user to locate, manually, the position in the data stream corresponding to the start of the first power delay profile. The user is requested to move a blinking cursor to the start of the first profile as shown in Figure 4.9. Once the appropriate position has been located, its corresponding sample number is recorded for use during further processing of the data file. The beginning of all other profiles are assumed to be integral multiples of the profile duration, with the selected starting position as the reference. It should be noted that the software has additional features which check and appropriately adjust the start of subsequent profiles if the profile duration drifts from the theoretical value of 17.03 μs.

4.6.2 Detection of Peaks in the Power Delay Profiles.

To ensure that the finite bandwidth of the measurement system does not influence the computation of the small-scale descriptors, it was necessary to determine the number of distinct paths within a power delay profile and to extract the peak values. This

technique is different to that which has been employed by other researchers, [4.2-4.4], who used the entire over-sampled data in their computations of the small-scale descriptors[4]. Figure 4.10 shows how the number of peaks in a power delay profile are determined. A peak identification algorithm was incorporated in the software. In this algorithm, the magnitudes, time delays and phases of the peaks in the power delay profile above a certain noise threshold are extracted. The noise threshold used was 3 dB. All recorded power delay profiles had to satisfy two constraints: compliance with the CCIR recommendations of at least 15 dB peak-to-spurii [4.1], and containing no AGC system transition. If these two conditions were met, the power delay profile was deemed as 'good', else it was discarded.

After the peak detection process, the power delay profile is made up of a series of impulses at specific time delays and phase values. Figure 4.11 shows a portion of a typical power delay profile as recorded for an experimental run. Figure 4.12 shows the same portion after the peak identification process. The latter is normalised with respect to the maximum echo within the power delay profile.

4.6.3 Channel Parameters Relevant to System Design and Simulations

When the mobile radio propagation channel is excited by a wideband signal, the channel has been found to possess statistics that are wide-sense stationary over small time and spatial intervals, whilst being highly non-stationary over much larger intervals. In this case, the channel is described as Quasi-Wide-Sense Stationary (QWSS) [4.5-4.6]. This has resulted in a two-stage characterisation process in which the small-scale channel descriptors are evaluated first, followed by cumulative distributions of these small-scale descriptors to estimate the large-scale channel statistics. In the ensuing sections, the small-scale channel descriptors evaluated in this study are presented together with the various large-scale characterisation techniques that were used.

---

[4]Calculations of delay windows and delay intervals were performed using the entire over-sampled data for increased accuracy.

Since the channel sounding system employed in this study was designed from the outset to provide the average received power, it was deemed necessary to evaluate the transmission loss, especially in the indoor environments. Analysis was therefore performed to determine the propagation pathloss exponent in the indoor locations.

4.6.3.1 Small-scale Characterisation

The wideband channel sounder employed in this study provides a measure of the complex impulse response of the channel in the time domain. It was shown in Chapter 2 that interrelationships exist between the time domain and frequency domain descriptors through Fourier transformations. It is therefore possible to separate the small-scale descriptors into time and frequency domains.

4.6.3.1.1 Time Domain Description

Figure 4.13 shows a typical power delay profile. Two statistical moments of interest to system design are the average excess delay and the delay spread [4.7], which were first defined by Cox [4.8].

The average excess delay, D, is the first moment of the power delay profile. This is equal to the power weighted average value of the multipath delays. In terms of the recorded data, D is given by:

$$D = \frac{\sum_{i=1}^{N} \tau_i P(\tau_i)}{\sum_{i=1}^{N} P(\tau_i)} \qquad (4.6)$$

where $P(\tau_i)$ is the power in Watts of the echo at a time delay of τ_i and N is equal to the number of discernible echoes (taps) in the power delay profile.

The delay spread[5], S, is defined as the second central moment of the power delay profile, ie., it provides a measure of the variability of the mean delay. This is equal to the power weighted rms value of the multipath component delays. In terms of the recorded data, S can be expressed as:

$$S = \sqrt{\frac{\sum_{i=1}^{N} (\tau_i - D)^2 P(\tau_i)}{\sum_{i=1}^{N} P(\tau_i)}} \qquad (4.7)$$

The average excess delay is a measure of the errors that are likely to occur in phase ranging systems and the delay spread places limits on the performance of wideband transmissions over non-equalised channels [4.2,4.10-4.11].

It has been recognised by COST207 [4.12] that these two parameters are not sufficient to describe all the important characteristics of the channel. Hence, two further parameters have been recommended. These are the delay intervals and delay windows [4.13-4.14]. These two parameters essentially describe the effective length of the impulse response and the distribution of energy within it, ie., the shape of the power delay profile. This has been shown to be important in determining the performance of wideband transmission systems [4.11].

The delay interval, I_P, is the difference in time delay between the points where the power delay profile first crosses a point X dB below its maximum value and the point where it falls below that threshold for the last time. This is illustrated in Figure 4.13 and can be expressed as:

$$I_P = (\tau_4 - \tau_1)_P \qquad (4.8)$$

In this study, delay interval values were computed for three different thresholds, viz:

---

[5]An alternative parameter that is equal to twice S has also been used [4.9] and is termed the total multipath spread.

15, 12 and 9 dB, which are similar to those used by Natarajan [4.3]. Huish and Gürdenli [4.15] used values of 5, 7 and 12 dB.

The delay window, W_q, is the duration of the middle portion of the power delay profile that contains q% of the energy in that power delay profile. Again, this is illustrated in Figure 4.13 and can be expressed as:

$$W_q = (\tau_3 - \tau_2)_q \tag{4.9}$$

where the boundaries τ_3 and τ_2 are defined by

$$\int_{\tau_2}^{\tau_3} P_h(\tau)d\tau = q\int_{\tau_1}^{\tau_4} P_h(\tau)d\tau = qP_{tot} \tag{4.10}$$

P_{pot} is the total power contained within the power delay profile and the energy outside the window is split into two equal parts, each being equal to:

$$(\frac{1 - q}{2})P_{tot} \tag{4.11}$$

The delay window was evaluated for three different values of q. These were 90, 75 and 50 %.

4.6.3.1.2 Frequency Domain Description

The frequency selective behaviour of the mobile radio channel is readily obtained by observing the correlation between two signals, at different frequencies, at the receiver. It was shown in Chapter 2 that this can be described in terms of the autocorrelation function, $R_T(\Omega)$, where Ω is the frequency separation, for a Wide-Sense Stationary Uncorrelated Scattering (WSSUS) channel. This was shown to be related to the power delay profile, $P(\tau)$, by Fourier transformation. This can be written as:

$$R_T(\Omega) = \int_{-\infty}^{\infty} P(\tau)\exp[-j2\pi\Omega\tau]d\tau \qquad (4.12)$$

$R_T(\Omega)$ is known as the frequency correlation function (FCF). This provides a measure of the degree of correlation between two spaced carrier frequencies and can be evaluated from $P(\tau)$ using Fast Fourier Transform (FFT) algorithms [4.16,4.17].

The coherence bandwidth, B_c, is the smallest value of Ω for which $R_T(\Omega)$ equals some specified correlation coefficient. This is a frequency-domain parameter which is useful not only for system evaluation but also provides data for the design of systems which employ frequency diversity to improve performance [4.10]. Apparently, no definitive value of correlation has emerged for the specification of coherence bandwidth. This may be due to the fact that, a dispersive channel may either be under- or over-estimated for different values of correlation used. However, values of correlation equal to 0.5 and 0.9 have been adopted widely [4.2,4.3,4.18]. Molkdar [4.19] used values of 0.37, 0.5 and 0.8 while Bajwa [4.20] used a value of 0.5 only. Two values, B_{c90} and B_{c50}, were therefore evaluated from each frequency correlation function.

The resolution in the time-domain is directly related to the clock period of the PRBS which was 33.33 ns for this study. However, the resolution in the frequency domain is related to the pulse repetition frequency (PRF) of the spread spectrum probing signal, which is defined as:

$$PRF = \frac{1}{mT} \qquad (4.13)$$

where m is the PRBS length and T is the chip period. For m = 511 and T = 33.33 ns, the PRF is 58.7 kHz. In his study at 910 MHz, Cox [4.21] reported minimum values of B_{c90} and B_{c50} of 20 kHz and 55 kHz respectively. Clearly, the degree of confidence in these small values of the coherence bandwidths, which are the most critical in terms of error performance must be low.

One obvious method of counteracting this problem is to increase the length of the PRBS by adding zero-valued samples at the end of the power delay profile. This was originally used in this field by Demery [4.18] and later by Natarajan [4.3]. This is possible since it can be safely assumed that all discernible echoes are contained within the 17.03 μs time delay window and so the zero-padding does not affect the shape of the frequency correlation function. There is no restriction on the number of zero-valued samples that can be added, the only penalty being the increase in computational time. The main advantage of undergoing this process is the increased accuracy of the interpolation process which is used to evaluate the values of the coherence bandwidths.

In this study, the power delay profiles were extended to 8192 samples prior to the FFT process. Each power delay profile was therefore lengthened from its nominal length of 17.03 μs to 273 μs. This improved the frequency resolution from 58.7 kHz to 3.7 kHz.

4.6.3.1.3 Propagation Pathloss

The propagation pathloss was evaluated using the equation below[6].

$$L_m = 10 \cdot \log_{10}\left[\frac{P_t}{P_m}\right] - L(1m) \qquad (4.14)$$

where P_t is the average transmitted power and P_m is the average received power and L(1m) is the loss when the two discone antennas are separated by a distance of 1 m. These values were averaged over 3.2 m long route segments. This is equivalent to averaging over approximately 20 wavelengths. The local mean pathloss was plotted against the distance from the transmitter. The data from the scatter plots of pathloss versus distance were fitted to a regression line of the form:

---

[6]The gains of the receiving and transmitting antennas were removed from the pathloss data so that it could be applied to other similar cases using equivalent base station antennas with different gains.

$$L = 10 \cdot n \cdot \log_{10} d + F \qquad (4.15)$$

The reference distance of 1 m was used because of the environment, which is small and allows only the use of low antenna heights[7]. The measured loss between a back-to-back connection and with the two discone antennas separated by 1 m was 33.82 dB, which agrees with the free space inverse square law relationship

$$P_r = \frac{P_t G_T G_R \lambda^2}{(4\pi)^2 R^2} \qquad (4.16)$$

between power and distance, where $G_t = G_r = 1.6$ for discone antennas and the theoretical free space loss is 33.46 dB at 1800 MHz.

4.6.3.2 Large-Scale Characterisation

Most researchers in the field have utilised one of two different techniques for large-scale characterisation of wideband mobile radio channels. The first technique provides a description of the channel in terms of the small-scale descriptors. The second technique uses a number of individual power delay profiles obtained over a topographically similar area to obtain statistics of the echo strengths, excess time delays, phases, etc.

The first approach is essentially the second stage of the 2-stage description of the channel based on direct data reduction techniques [4.5,4.22]. This has been widely utilised in the field of mobile radio communications for large-area characterisation of the channel [4.3,4.5,4.15,4.23]. The results from such an approach are important for system engineers, who must design communication systems which will operate satisfactorily in a large variety of geographical locations. Specifically, they need to know the percentage of locations and/or time that allow a specific level of performance to be maintained. For example, the percentage of locations that the delay

[7]Pathloss calculations were performed on the data collected from the indoor environments only.

spread exceeds a certain threshold may be required. In theory, cumulative distribution functions [4.24] of the small-scale descriptors are required. Regression analysis techniques can then be used to determine the dependence of the small-scale descriptors in a large-scale area.

In the second approach, statistics of echo strengths, excess time delay delays, phases, etc., are evaluated from the recorded data. These statistics are important for modelling and/or simulation of various systems. For example, previous studies [4.25,4.26] have used a channel model based on knowledge and/or assumptions of the probability distributions of echo strengths, phases and time delays as shown in Chapter 2. The results will also aid in the design of systems which utilise CDMA or TDMA techniques. They will also be useful for performance evaluation of these systems and for implementing other aspects such as Rake receivers, equalisation, diversity and coding schemes.

4.6.3.2.1 Cumulative Distributions

The large-scale characteristics of the channel were obtained by evaluating the cumulative distribution functions of the following parameters for each base station location:

i. Average delay
ii. Delay spread
iii. Delay intervals at 15, 12 and 9 dB
iv. Delay windows at 90, 75 and 50 %
v. Coherence bandwidths at 0.5 and 0.9 correlation
vi. Number of echoes per power delay profile

Knowledge of the distribution of the number of multipath echoes or taps will aid in the development of wideband simulators and designing of systems which employ path diversity such as CDMA systems through the use of Rake receivers.

4.6.3.2.2 Regression Relationships

Several studies, [4.10-4.11,4.27-4.29], have been undertaken in order to relate the

bit error rate for transmission over a non-equalised multipath channel, to the small-scale descriptors. These studies have all been undertaken for different systems. The work of Ladki [4.11] and Chaaban [4.29], have specifically shown that the irreducible bit error rate (IBER) bears an exponential relationship with the ratio of the delay spread to the bit duration in a digital communication system. Arnold and Bodtmann [4.31] reported the existence of a fourth power relationship between the IBER and the normalised delay spread. Performance evaluation of the GSM system by Chaaban [4.29] has established the following relationship;

$$IBER = 0.1945 \cdot \left(\frac{S_{mean}}{T}\right)^{1.8878} \qquad (4.17)$$

where T is the bit duration which is 3.7 μs for the GSM system and S_{mean} is the mean of the delay spread. Work by Lorenz [4.31], has even suggested that the delay spread is not the only contributor to the error mechanisms and proposed the use of parameters such as coherence bandwidth.

In addition, there may be occasions where the distribution of one of the small-scale descriptors is available along with an equation connecting an alternative parameter, say the coherence bandwidth, to the error rate. It is therefore necessary to formulate expressions which interrelates the two parameters, so that a simple substitution can be made. This is particularly important since most wideband channel sounders will provide channel information directly in either time or frequency domains.

With regards to these facts, scatter plots of the coherence bandwidths at 0.5 and 0.9 correlations versus delay spread were obtained. A least-squares linear regression analysis provided their mathematical interrelationships. This approached has been utilised previously [4.3,4.17,4.18,4.22]. In this study, delay spread, which has been shown to have an inverse relationship to the coherence bandwidths, has been preferred since it is the most widely used small-scale descriptor.

Generally, the data from the scatter plots of the coherence bandwidths at 0.5 or 0.9

gain combining (EGC). Consideration is given to an optimum Rake receiver that combines all received paths and that which combines only the first few strongest paths.

In the analysis, the signal-to-noise ratio (SNR) is used as a measure of performance. In a direct sequence CDMA system, the variation in the SNR is desired to be low and this can be accomplished through power control. We also consider the short term variability of the SNR at the output of the Rake receiver. This will give an insight into the required speed of the power control algorithm. In the next section, the Rake receiver model that was used in this study is presented.

4.7.1 Received Signal and Rake Receiver Model

In a multipath propagation channel, the received BPSK signal for a single user can be written as

$$r(t) = \sum_{i=0}^{n} a_i d(t-\tau_i)c(t-\tau_i)\cos(w_c t+\theta_i)+n(t) \qquad (4.19)$$

where n+1 is the number of received taps, a_i, τ_i and Θ_i are the amplitude, time delay and phase respectively of the i-th tap, c(t) is the spreading code, d(t) is the binary data, w_c is the carrier frequency and n(t) is additive white Gaussian noise (AWGN).

Figure 4.14 is a model of a coherent BPSK Rake receiver that can be used to demodulate the received signal of Equation 4.19. The weights, w_i, are set depending on the type of combining that is used. It is also assumed that the time delay and phase estimates are perfect, so the cophasing process which is required for a predetection diversity scheme is not required.

The SNR at the output of the Rake receiver can then be written as

correlation against delay spread have been fitted to regression lines of the form:

$$B_c = \frac{1}{A_c S^{i_c}} \tag{4.18}$$

where B_c is the coherence bandwidth at 0.5 or 0.9 correlation and S is the delay spread.

Although the regression analysis between delay spread and the coherence bandwidths gives a good approximation of estimating the coherence bandwidth, it will be shown in Chapter 5 that there is an equation which can be used to determine the minimum coherence bandwidth for a given delay spread. This is particularly important since most of the previous experimental investigations have focused on worst case locations, hence some of the small-scale parameters have been over-estimated.

4.7 CDMA-BASED RESULTS

All the above mentioned channel parameters can be utilised in the design of any future spread spectrum system. In addition, a spread spectrum CDMA system can offer path diversity through the use of a Rake-type receiver as mentioned in Chapter 2. The Rake gain will be examined by using a BPSK Rake receiver model.

The Rake receiver, which was originally proposed by Price and Green [4.32], is a spread spectrum receiver which can be used to track and demodulate the resolvable multipath components. Therefore, provided the system bandwidth is large enough to isolate a number of independently fading echoes, the effects of multipath propagation can be alleviated through the Rake approach. In this study, a BPSK direct sequence modulation scheme with coherent detection is assumed. At the base station, the signal from each user is demodulated by employing a coherent BPSK Rake receiver. Furthermore, we consider a Rake receiver which is provided with time delay estimates of the arriving multipath components. The signal is despread only at these time delays before combining using either maximal ratio combining (MRC) or equal

$$SNR = \frac{\left(\sum_{i=0}^{n} w_i s_i\right)^2}{\sum_{i=0}^{n} w_i^2 E(n_i^2)} \qquad (4.20)$$

where s_i is the signal level and n_i is the noise component of the output of the i-th branch. E(·)denotes expectation. For MRC, Equation 4.20 can be rewritten as [4.33]

$$SNR = \sum_{i=0}^{n} \frac{s_i^2}{E(n_i^2)} \qquad (4.21)$$

which is the sum of the individual SNRs of each branch of the Rake receiver.

In practice, only a small proportion of the resolvable multipath components will be demodulated due to the fact that only a finite number of correlators can be implemented in the receiver. Moreover, the Rake gain in changing from an L-path receiver to an L+1-path receiver may be very small, hence the added cost and complexity may be too high [4.10]. Therefore, the practical optimum Rake receiver will possess only a small number of branches. Hence, its design is based on the channel characteristics. Knowledge of the probability of occurrence of the various received echoes is therefore required.

4.7.2 Probability of Occurrence of Echoes

For any Rake receiver design, two important considerations are its time span and the number of branches. In addition, and for optimum performance, the location of these branches with respect to the estimated time delays is also required. To this end two probability of occurrence curves were produced, namely,

i. Probability of occurrence (%) versus the time-delay bins and

ii. probability of occurrence (%) versus the number of echoes (taps).

In order to eliminate the distance dependence, the AGC values were not included in the evaluation of these probability curves.

i. Probability of occurrence (%) versus the time-delay bins

Each power delay profile is made up of 511 time delay bins. Firstly, the power delay profiles are normalised with respect to the highest echo within the PDP and all received echo is placed into one of the 511 time delay bins[8]. Five different echo levels, A_l, were selected (-5, -10, -15, -20 and -25 dB) and the object was to determine the probability that the echoes arriving in a certain time delay bin will have an amplitude greater than or equal to A_l. For example, if A_l is -25 dB, then a count of all echoes greater than -25 dB in each time delay been was obtained. The total count in each time delay bin was then divided by the total number of power delay profiles that were analysed.

ii. Probability of occurrence (%) versus the number of echoes

This was evaluated in a similar way as the above, except that the time of arrival of the echoes is ignored and only the sequential arrival of these echoes is considered.

It is expected that the above two plots can aid in the design of an optimum Rake receiver. Specifically, (i) above can be used to give an indication of the time span of the Rake receiver and a combination of (i) and (ii) can be utilised to give the number of paths to be used and the time delays between these paths.

4.8 SUMMARY

In this chapter, the experimental design and measuring techniques that were used during the measurement campaign have been presented. In particular, the experimental design was devised such that the results from this experimental investigations provides a realistic picture of the radio channel in the environments surveyed. The technique used for data acquisition, storage and validation were presented in section 4.4. In section 4.5, the salient features of the experimental locations were presented. The chapter concludes with a presentation of the various

---

[8]It should be noted that the first resolvable echo has a time delay of zero, and the subsequent echoes in the power delay profile are with referenced to this first echo.

off-line data reduction and analysis techniques that were utilised, and definitions of the parameters that were evaluated. The Rake receiver model that was used to show the Rake is also presented. In Chapter 5 the results obtained from this experimental investigation are presented.

References

[4.1] CCIR Report 567-3 (MOD F), 'Propagation Data and Prediction Methods for the Terrestrial Land Mobile Service Using the Frequency Range 30 MHz to 3 GHz', CCIR XVIIth Plenary Assembly, Düsseldorf, 1990.

[4.2] Cox, D.C., 'Delay Doppler Characteristics of Multipath Propagation at 910 MHz in a Suburban Mobile Radio Environment', IEEE Trans. on Antennas and Prop., Vol. 20, No. 5, Sept. 1972, pp625-635.

[4.3] Natarajan, N., 'Wideband Characterisation of Mobile Radio Channels at 1.8 GHz', Ph.D Thesis, Department of Electric Engineering and Electronics, The University of Liverpool, 1992.

[4.4] Sousa, E.S., Jovanovic, V.M. and Daigneault, C., 'Delay Spread Measurements for the Digital Cellular Channel in Toronto', IEEE Trans. on Veh. Tech., Vol. 43, No. 4, Nov. 1994, pp837-847.

[4.5] Bello, P.A., 'Characterisation Randomly Time-Variant Linear Channels', IEEE Trans. Com. on Syst., Vol. CS-11, Dec. 1963. pp360-393.

[4.6] Cox, D.C., '910 MHz Urban Mobile Radio Propagation: Multipath Characteristics in New York City', IEEE Trans. Comm., Vol. COM-21, No. 11, Nov. 1973, pp1188-1194.

[4.7] Parsons, J.D., 'The Mobile Radio Propagation Channel', Pentech Press, 1992.

[4.8] Cox, D.C., 'Time and Frequency Domain Characterisation of Multipath Propagation at 910 MHz in a Suburban Mobile Radio Environment', Radio Science 7, No. 12, Dec. 1972, pp109-1077.

[4.9] Lorenz, R.W., 'Impact of Frequency-Selective Fading on Binary and Quadrature Phase Modulation in Mobile Radio Communication Demonstrated by Computer Simulations Using the WSSUS Channel Model', COST207 Technical Document, TD(86), No. 1, 1986.

[4.10] Jakes, W.C., 'Microwave Mobile Communications', John Wiley, 1974.

[4.11] Ladki, M., 'The Determination of the Figure of Merit for the Wideband Mobile Radio Channel', Ph.D Thesis, Department of Electric Engineering and Electronics, The University of Liverpool, Sept. 1991.

[4.12] 'Digital Land Mobile Radio Communications', Final Report of COST Project 207, Commission of the European Communities, Brussels, 1989.

[4.13] Lorenz, R.W. et al, 'Evaluation of Delay Profiles in Mountainous Terrain',

COST207 Technical Document, TD(87), No. 16, May 1987.

[4.14] Lorenz, R.W., '12th Report of the Work Group on Propagation', COST207 Technical Document, TD(87), No. 30, May 1987.

[4.15] Huish, P. W. and Gurdenli, E., Radio Channel Measurement and Predictions for Future Mobile Radio Systems', BR. Telecom. Technol. J., Vol. 6, No. 1, Jan 1988, pp43-53.

[4.16] Elliot, D. F. and Rao, K. R., 'Fast Fourier Transforms: Algorithms, Analyses, Applications', Academic Press, 1982.

[4.17] Press, W. H., Teukolsky, A. A., Flannery, B. P. and Vetterling W. T., 'Numerical Recipes in C', Cambridge University Press, 1990.

[4.18] Demery, D.A., 'Wideband Characterisation of UHF Mobile Radio Channels in Urban Areas', Ph.D Thesis, Department of Electric Engineering and Electronics, The University of Liverpool, 1989.

[4.19] Molkdar, D. and Mathews, P.A., 'Measurements and Characterisation of the UHF Mobile Radio Channel. Part 2: Characterisation over the Band 869-877 MHz', Journal of IERE, Vol. 58, No. 6, Sept 1988, pp157-168.

[4.20] Bajwa, A.S. and Parsons, J.D., 'Large Area Characterisation of Urban UHF Multipath Propagation and its Relevance to the Performance Bounds of Mobile Radio Systems', IEE Proc., Vol. 132, Pt. F, No. 2 April 1985. pp99-106.

[4.21] Cox, D.C., '910 MHz Urban Mobile Radio Propagation: Multipath Characteristics in New York City', IEEE Trans. Comm., Vol. COM-21, No. 11, Nov. 1973, pp1188-1194.

[4.22] Cox, D. C., 'correlation Bandwidth and Delay Spread Multipath Propagation Statistics for 910 MHz Urban Mobile Radio Channels', IEEE Trans. Comm. Vol. COM-23, No. 11, Nov. 1975, pp1271-1280.

[4.23] Bajwa, A.S., 'Wideband Characterisation of UHF Mobile Radio Propagation in Urban and Suburban Areas', Ph.D Thesis, Department of Electronic and Electric Engineering, The University of Birmingham, 1979.

[4.24] Papoulis, A., 'Probability, Random Variables and Stochastic Processes', McGraw-Hill, 1965.

[4.25] Turin, G. L., Clapp, F. D., Johnston, T. L., Fine, S. B. and Lavry, D., 'A Statistical Model of Urban Multipath Propagation', IEEE Transactions on Vehicular Technology, Vol. VT-21, No. 1, Feb. 1972, pp1-9.

[4.26] Bajwa, A.S., 'UHF Wideband Statistical Model and Simulation of Mobile Radio Multipath Propagation Effects', IEE Proc., Pt. F, Vol. 132, No. 5. Aug. 1985. pp327-333.

[4.27] Bello, P. A. and Nelin, B. D., 'The effects of Frequency Selective Fading on the Binary Error Probabilities of incoherent and Differentially Coherent Matched Filter Receivers', IEEE Transactions on Communication Systems, Vol. CS-11, June 1963, pp170-186.

[4.28] Gans, M. J., 'A Power-spectral Theory of Propagation in the Mobile-radio Environment', IEEE Transactions on Vehicular Technology, Vol. VT-21, No. 1, Feb. 1972, pp27-38.

[4.29] Chaaban, R.S., Private Communication.

[4.30] Arnold, H.W. and Bodtmann, W.F., 'The Performance of FSK in Frequency-Selective Rayleigh Fading', IEEE Trans. on Comms., Vol. 31, No. 4, April 1983, pp568-572.

[4.31] Lorenz, R., 'Impact of Frequency-Selective Fading on Digital Land-Mobile Radio Communications at Transmission Rates of Several Kbits/sec', IEEE Trans. on Veh. Tech., Vol. 35, No. 3, Aug. 1987, pp122-128.

[4.32] Price, R. and Green, P. E., 'A Communication Technique for Multipath Channels', IRE, Vol. 46, March 1958, pp555-570.

[4.33] Chan, N.L.B, 'Multipath Propagation Effects on a CDMA Cellular System', IEEE Transactions on Vehicular Technology, Vol. 43, No. 4, Nov. 1994, pp848-855.

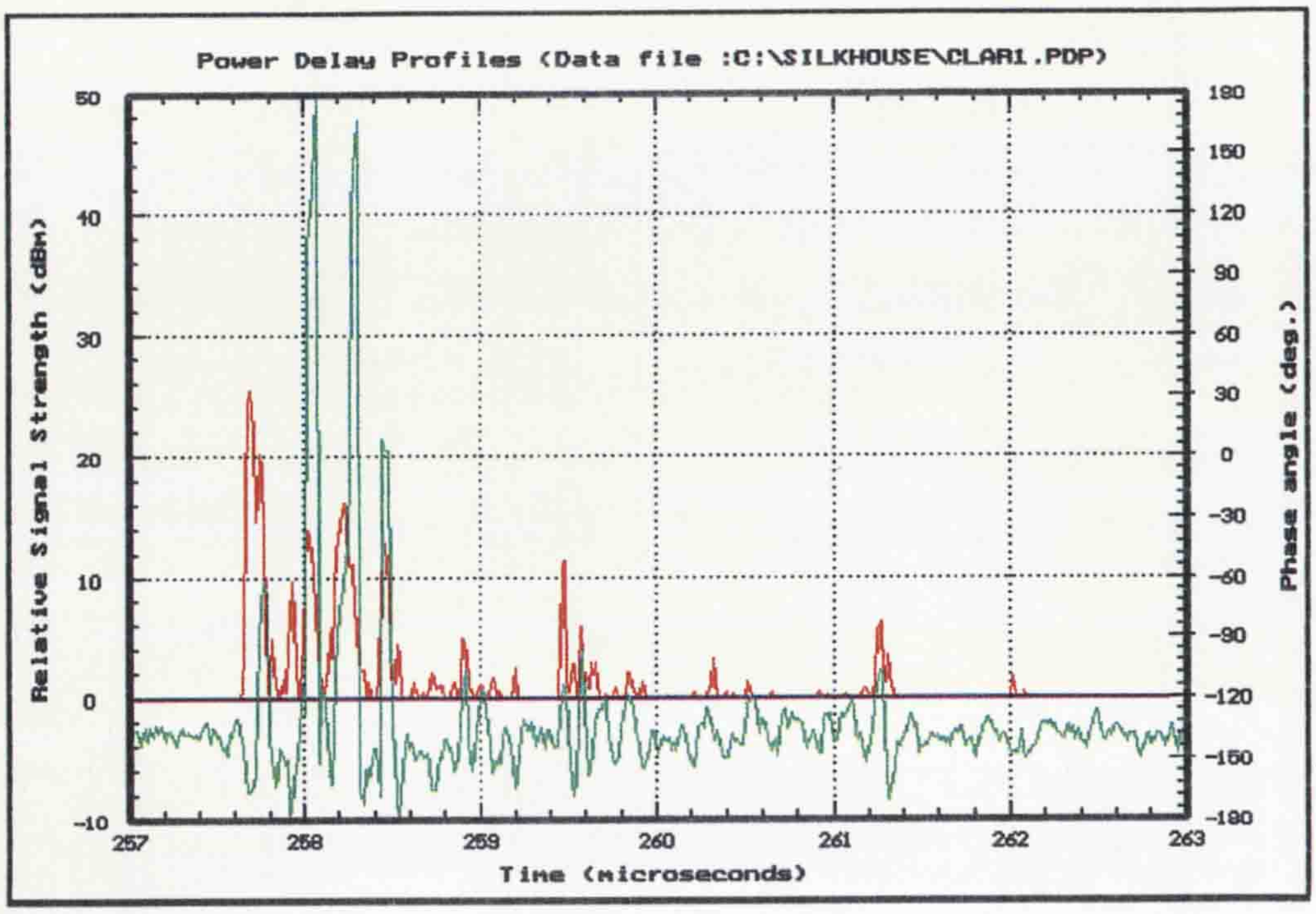

Figure 4.1 Typical plot of a power delay profile from the data acquisition system showing the PDP in red, AGC in blue and the phase in green. This was ontained from URBAN1.

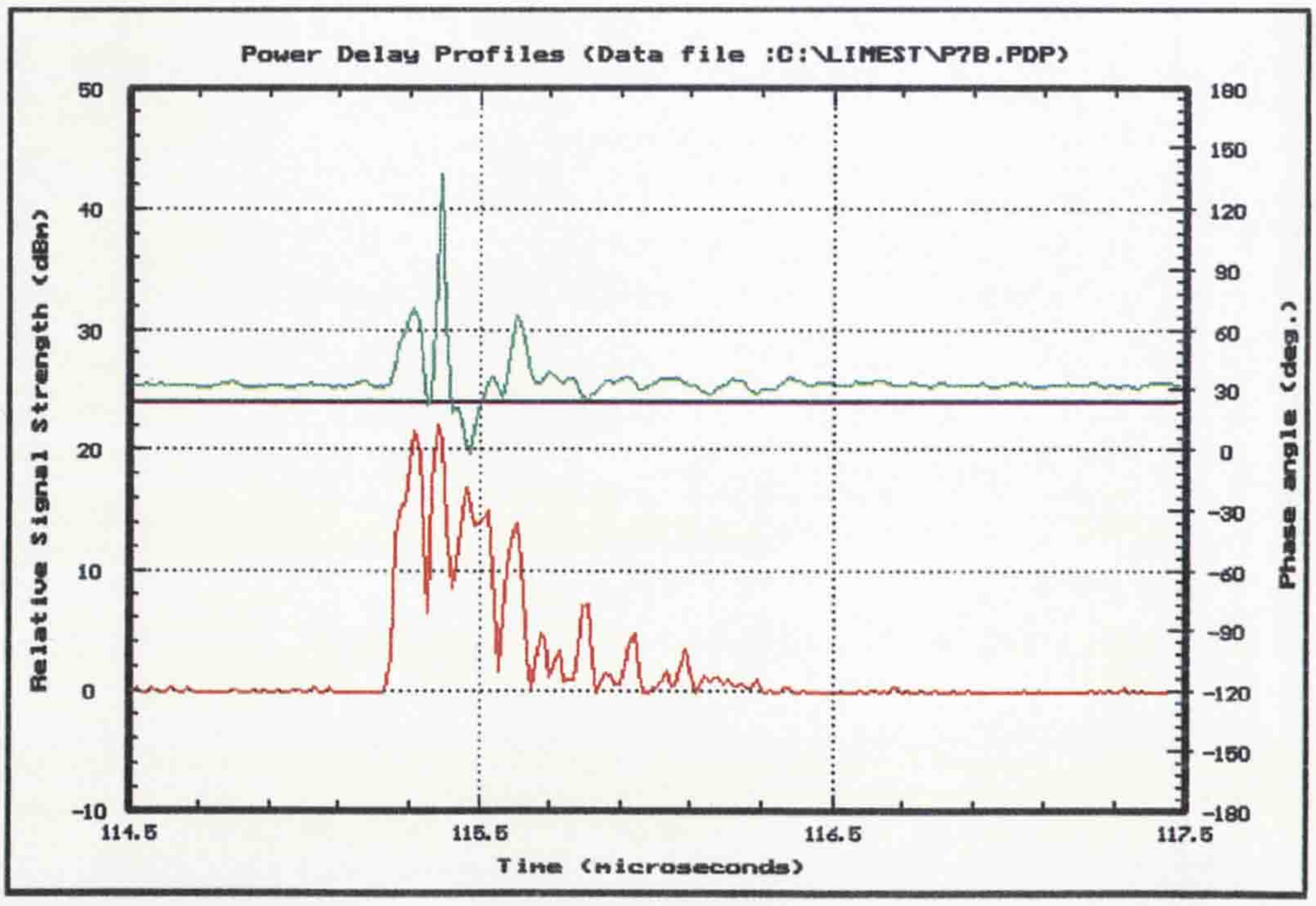

Figure 4.2 Typical plot of a power delay profile from the data acquisition system showing the PDP in red, AGC in blue and the phase in green. This was obtained from Lime Street Station.

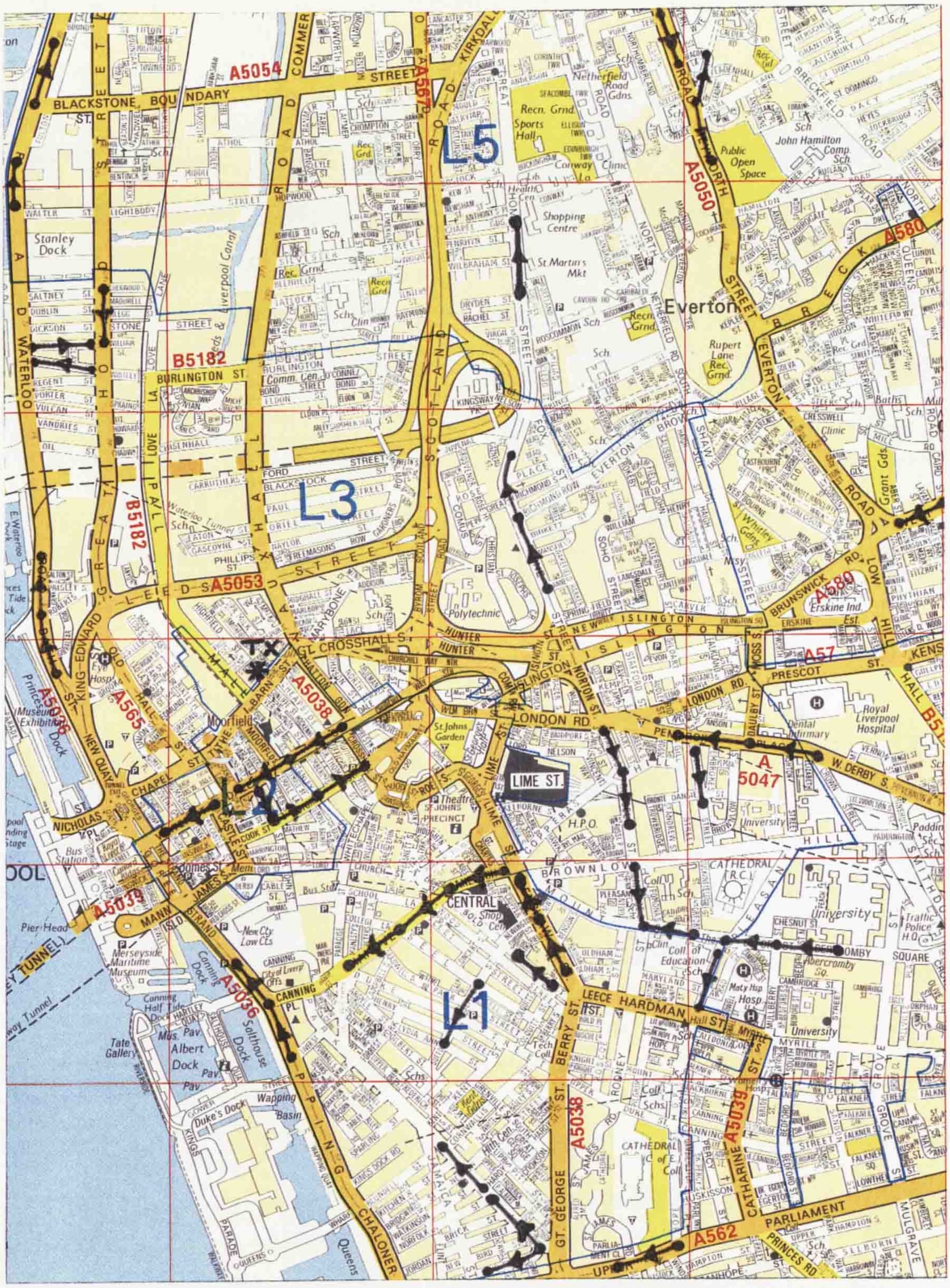

Figure 4.3 Map of URBAN1 showing the position of the transmitter and the approximate experimental routes.

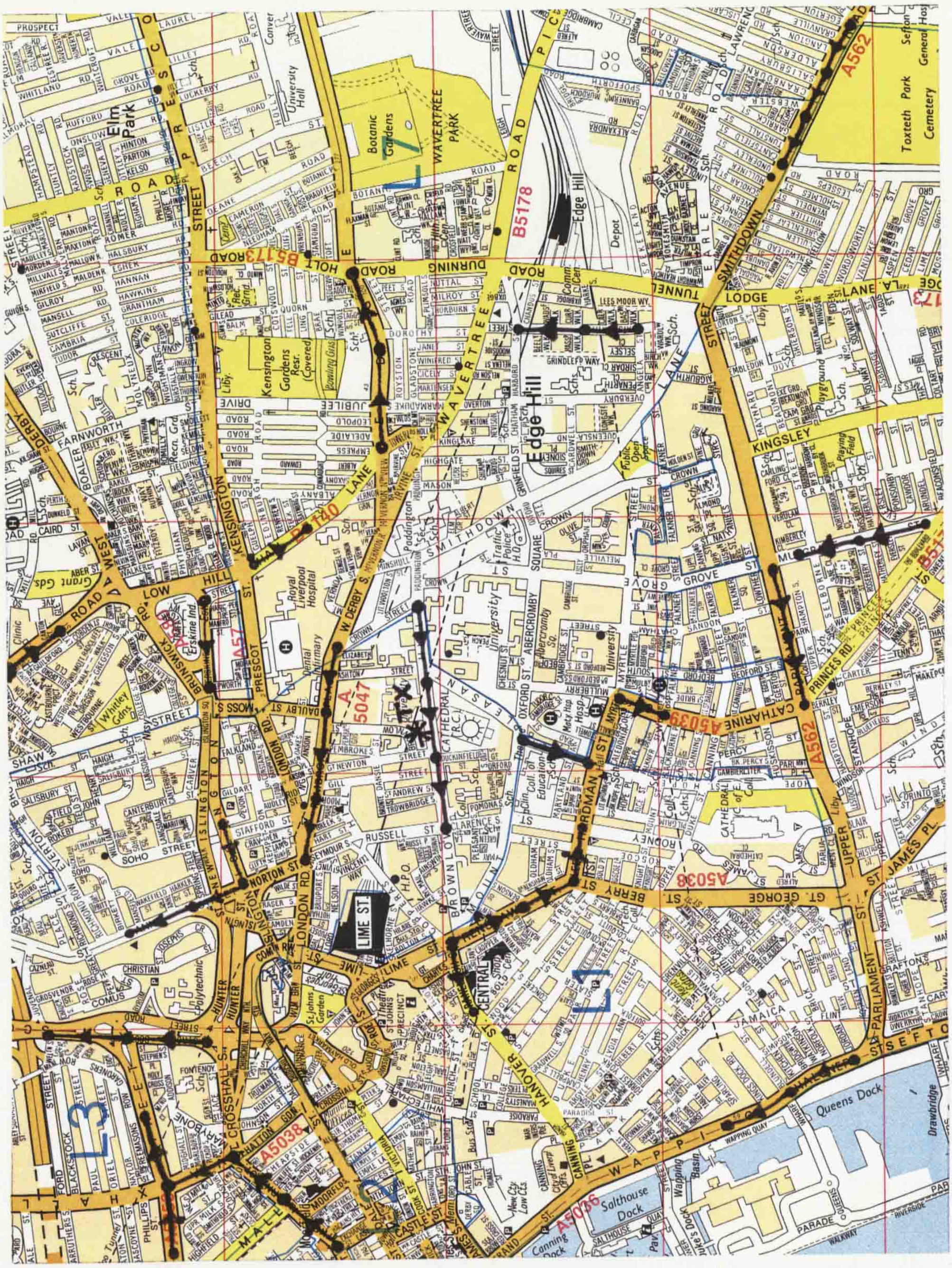

Figure 4.4 Map of URBAN2 showing the position of the transmitter and the approximate experimental routes.

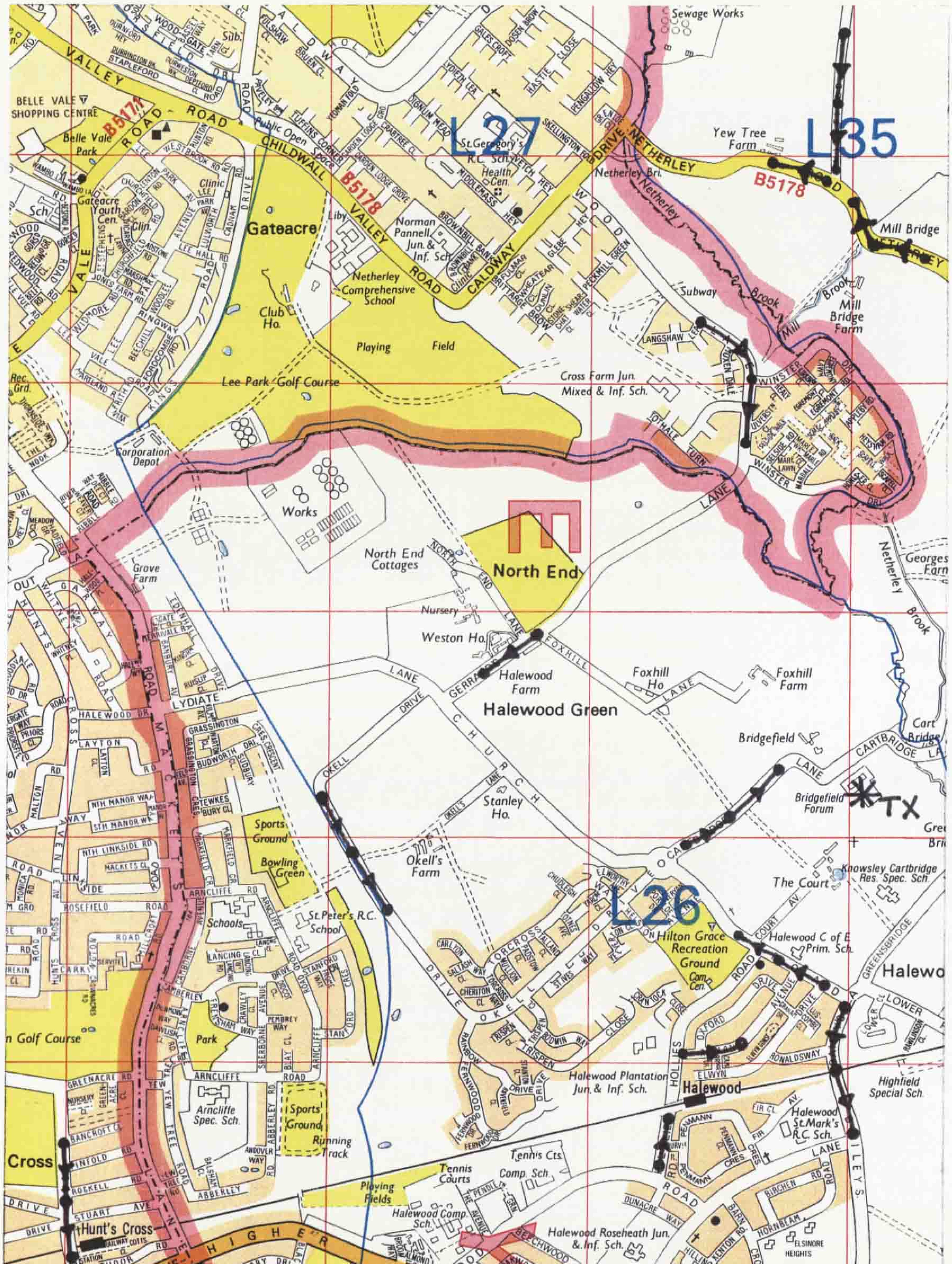

Figure 4.5 Map of the rural open area showing the position of the transmitter and the approximate experimental routes.

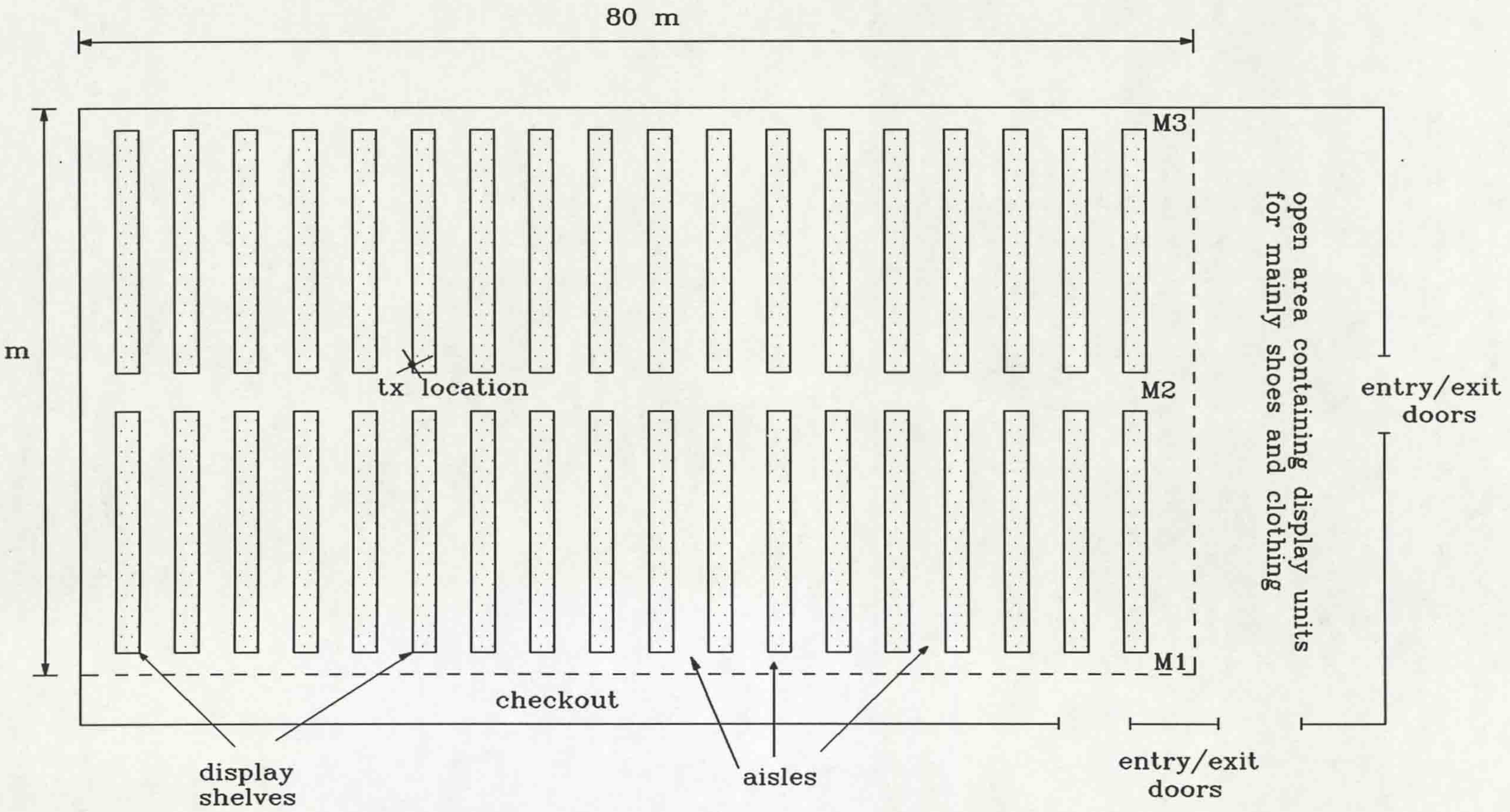

Figure 4.6 Floor plan of SMARKET1.

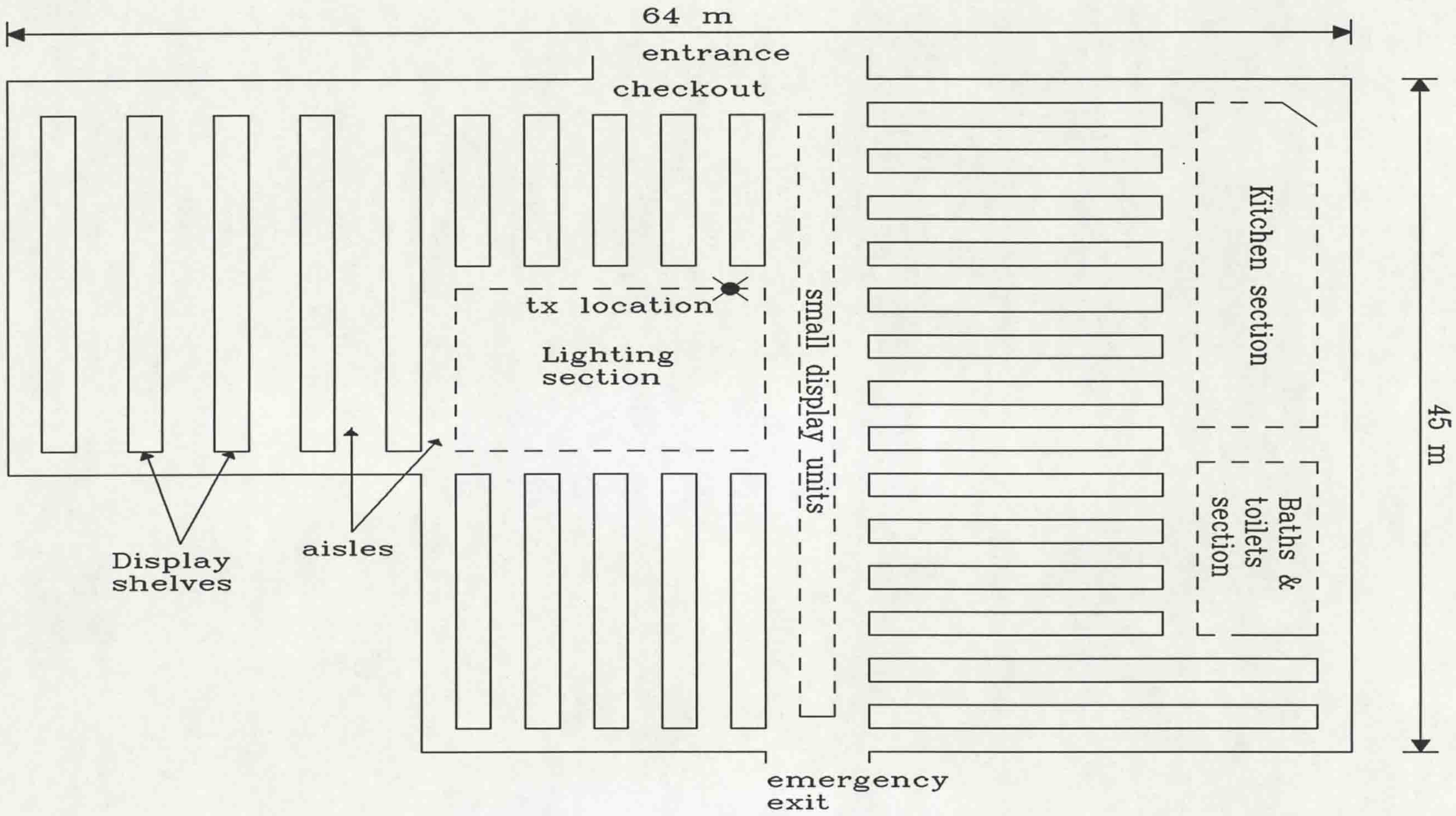

Figure 4.7 Floor plan of SMARKET2.

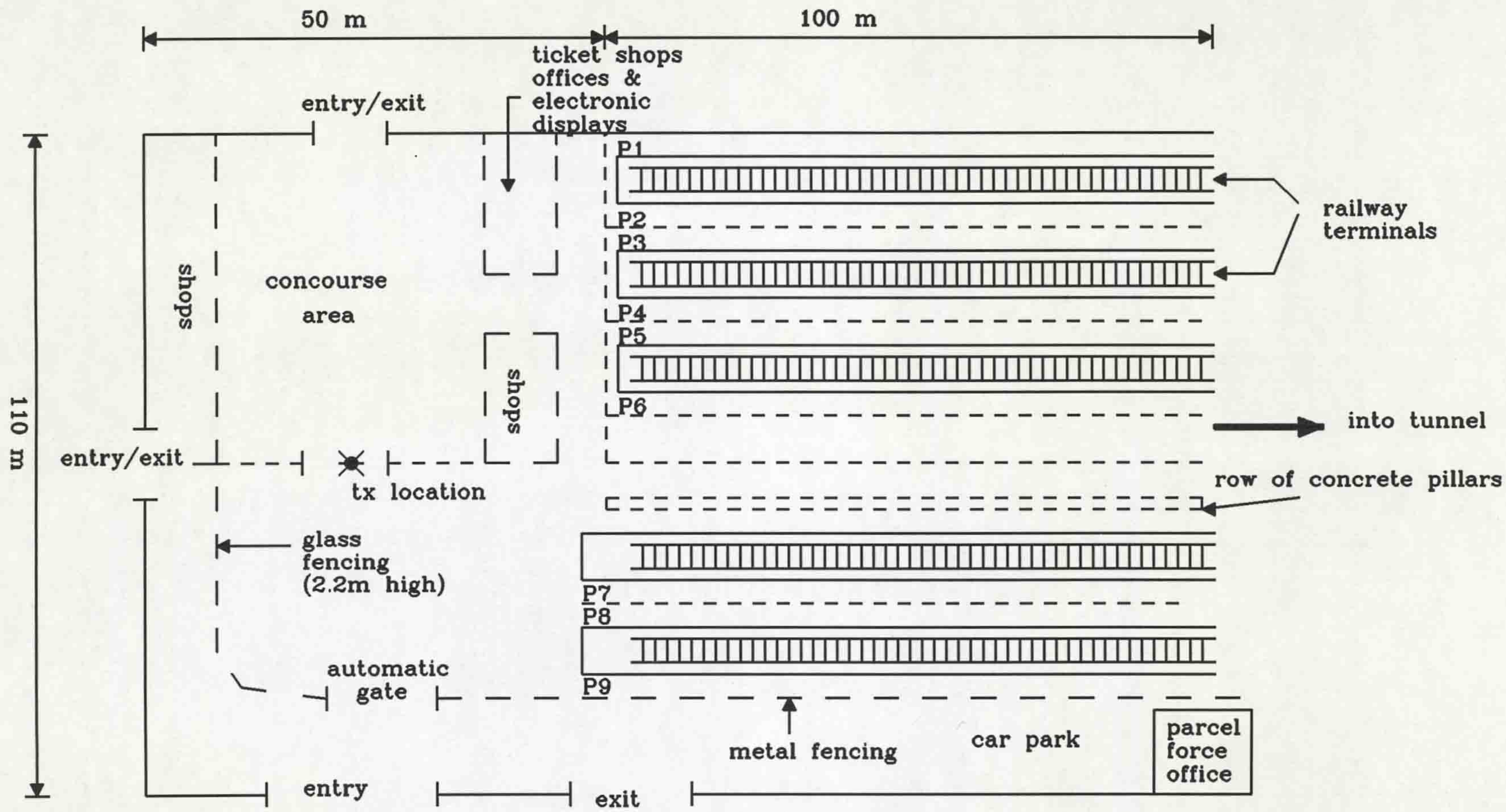

Figure 4.8 Layout of Lime Street Station.

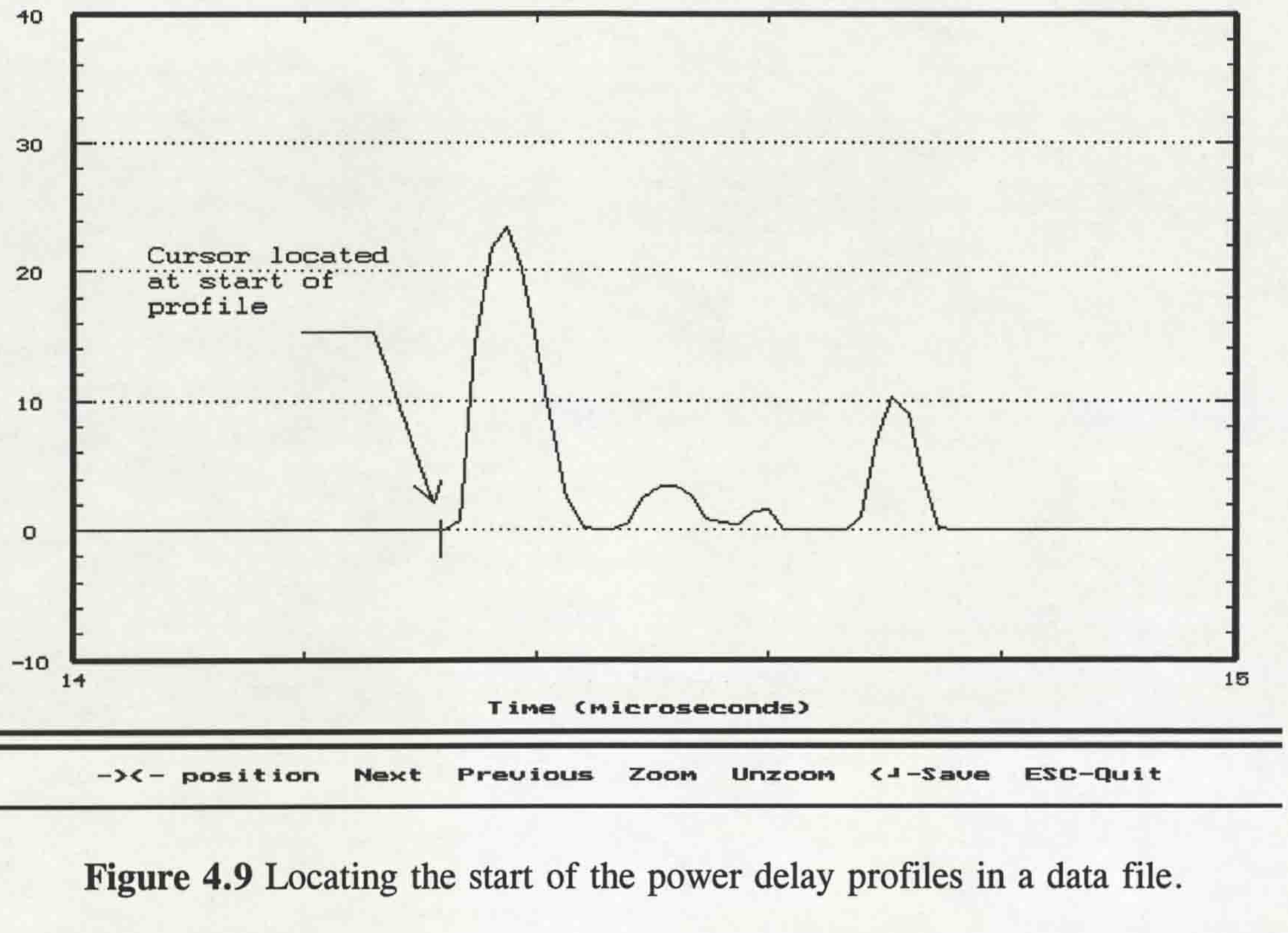

Figure 4.9 Locating the start of the power delay profiles in a data file.

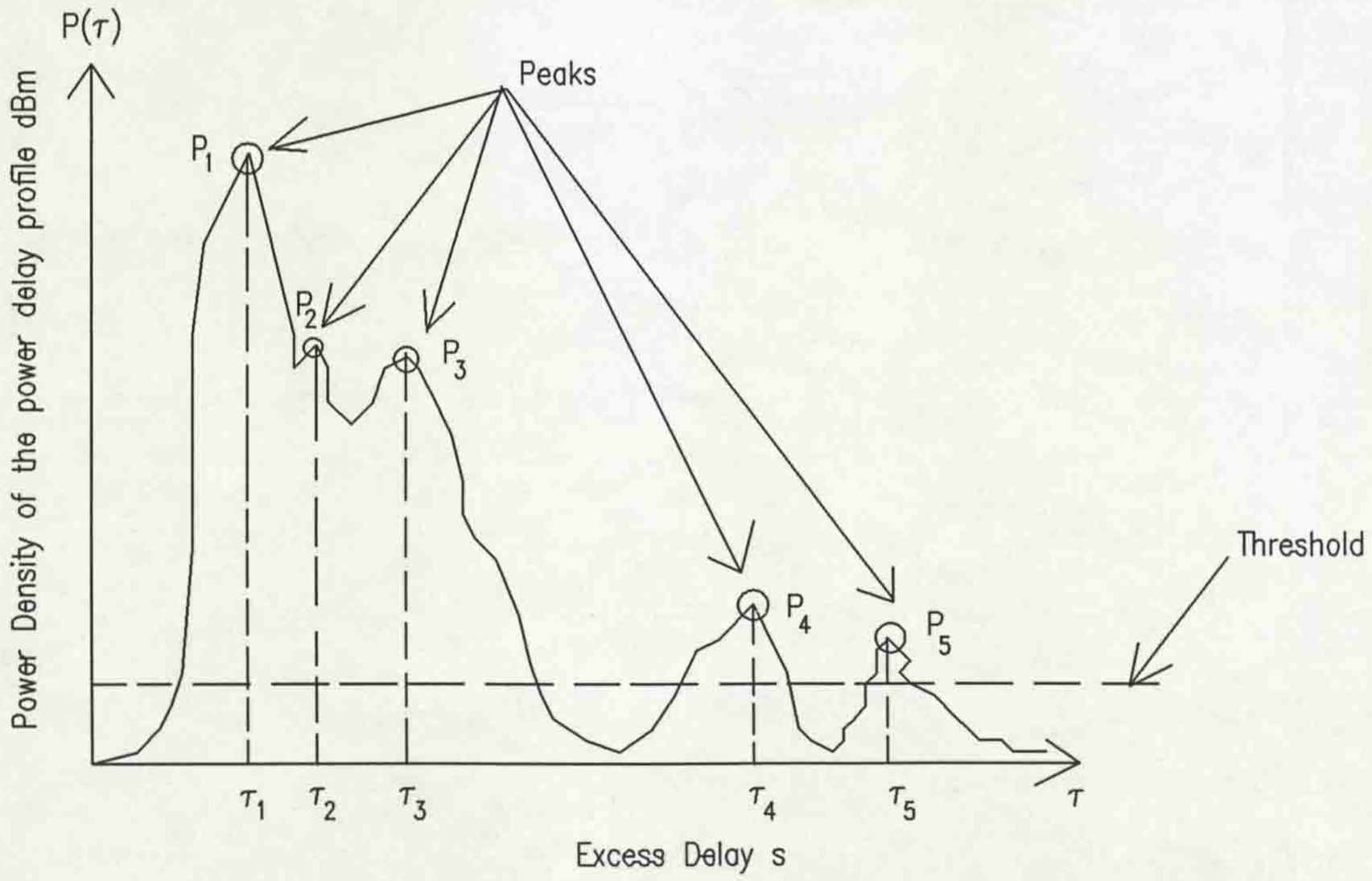

Figure 4.10 Determining the peaks in a power delay profile.

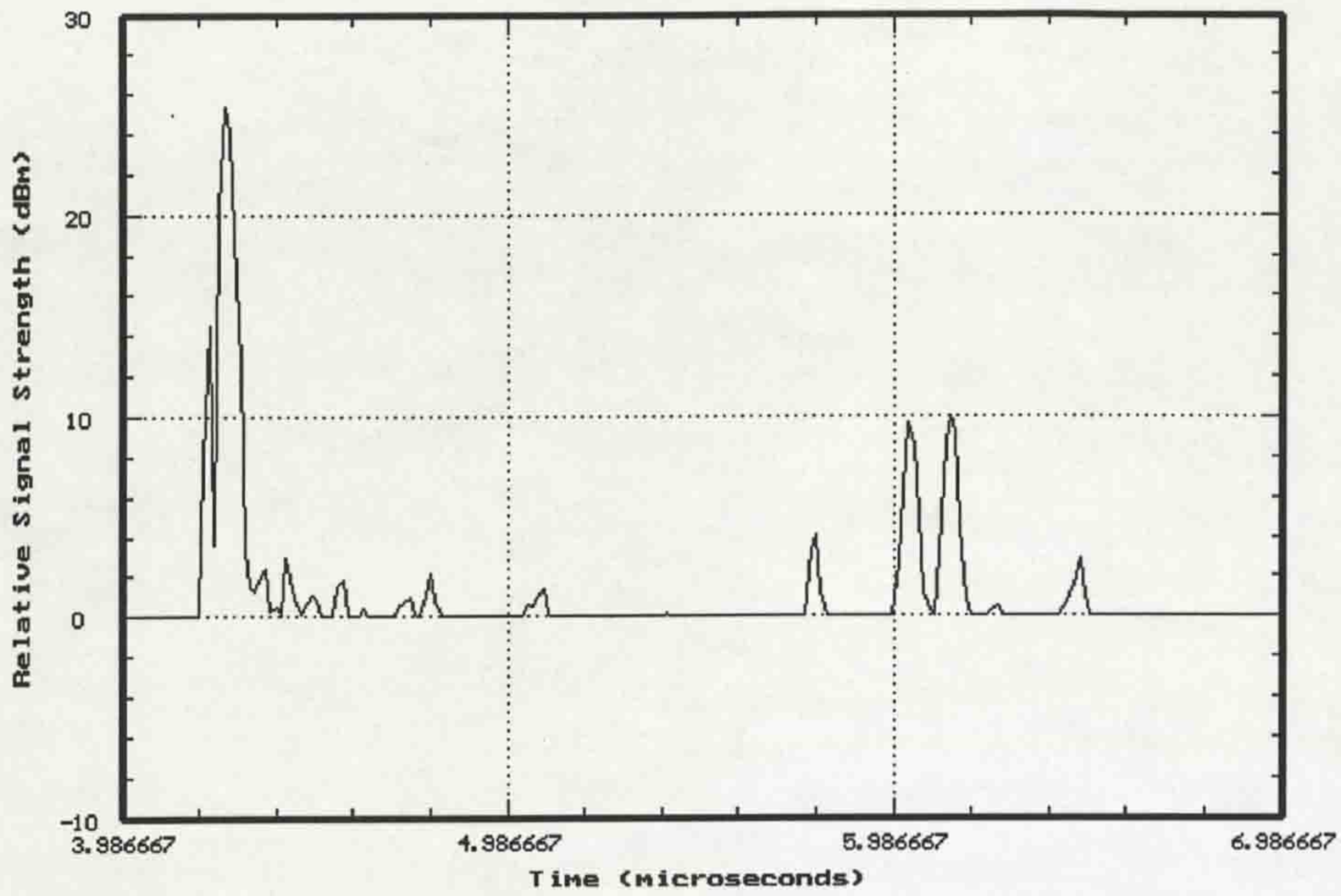

Figure 4.11. Typical power delay profile as recorded by the system from the rural open area.

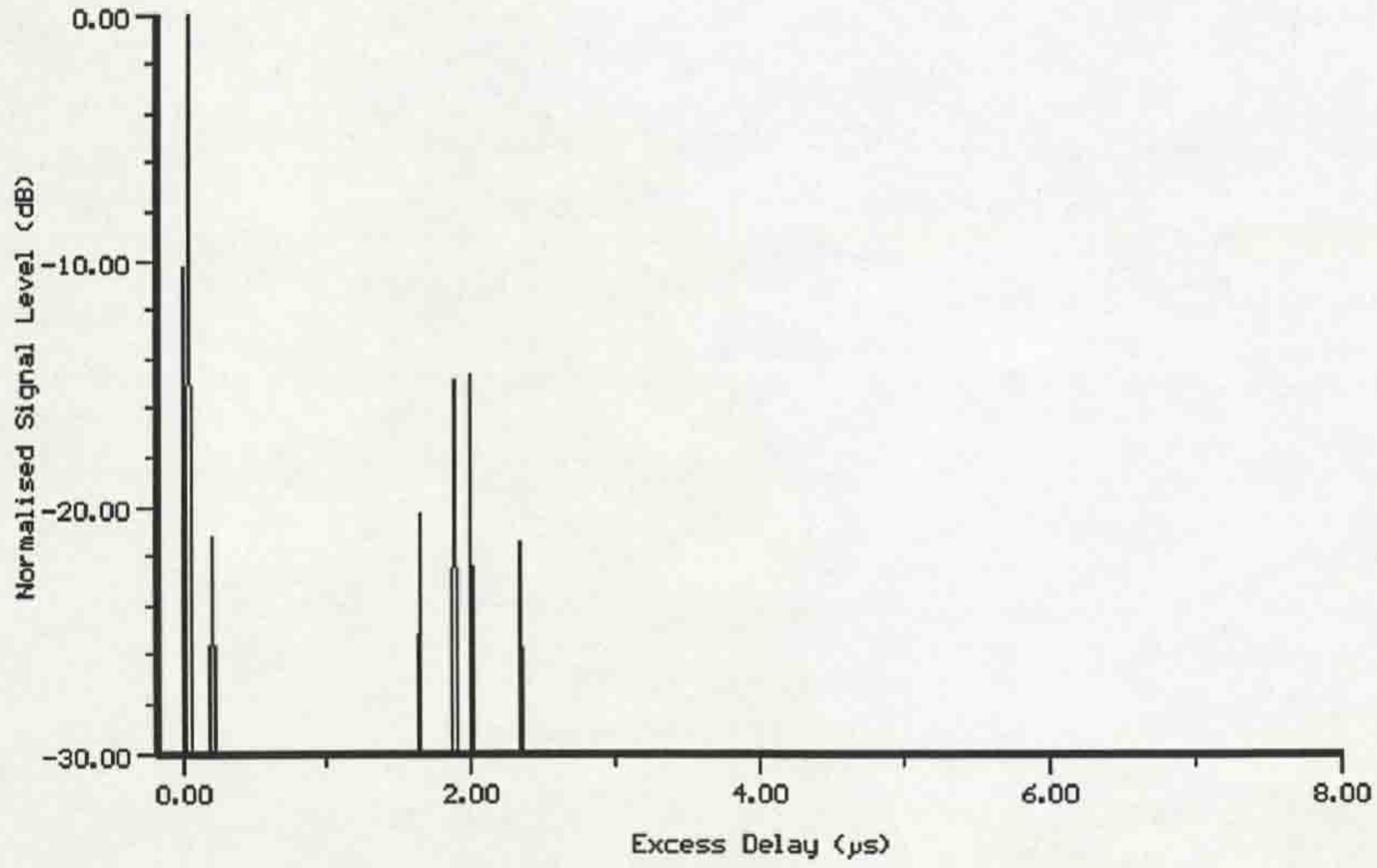

Figure 4.12. Normalised power delay profile of Figure 4.11, after the peak identification process.

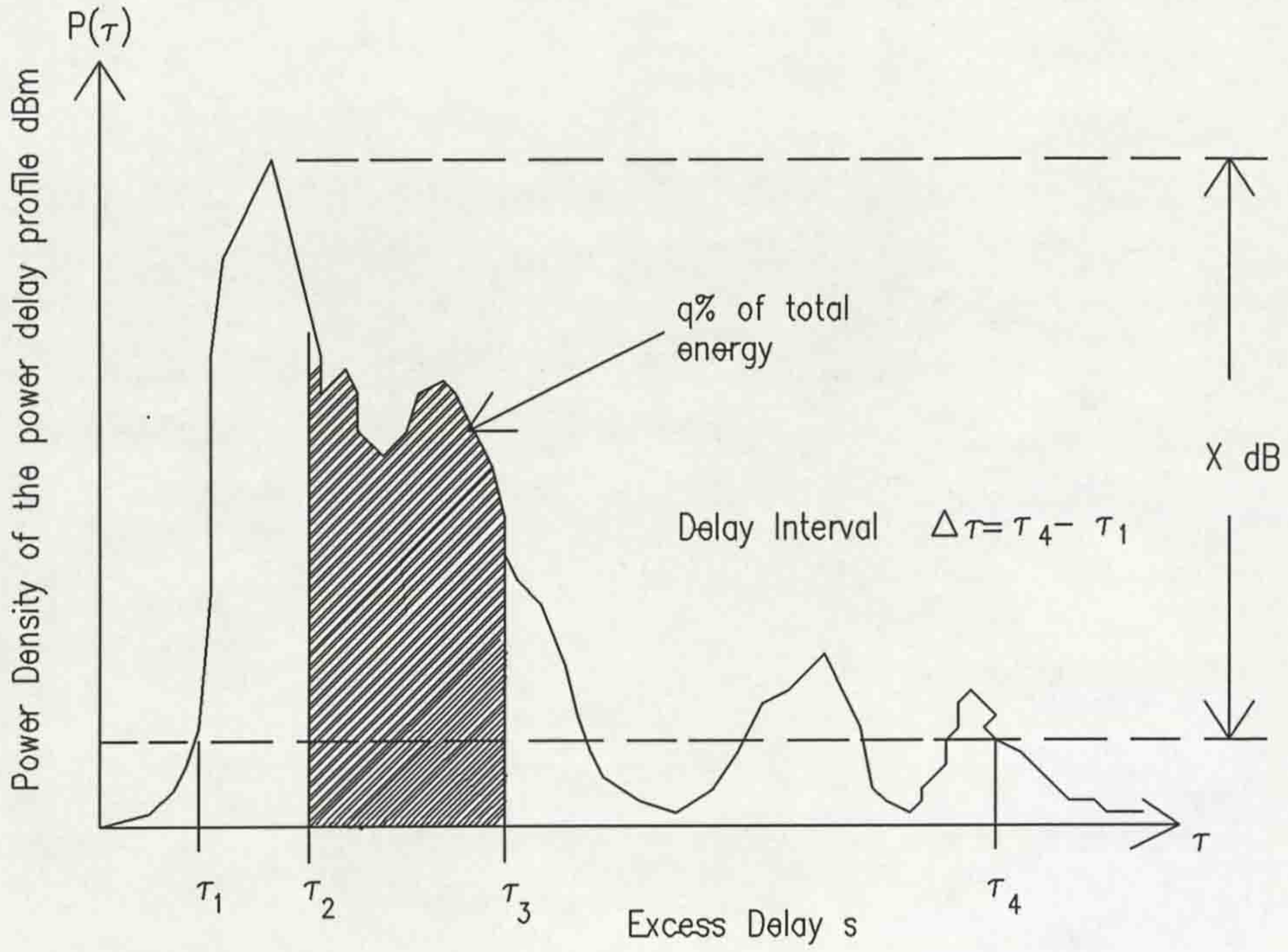

Figure 4.13 Determining the small-scale time domain descriptors in a power delay profile.

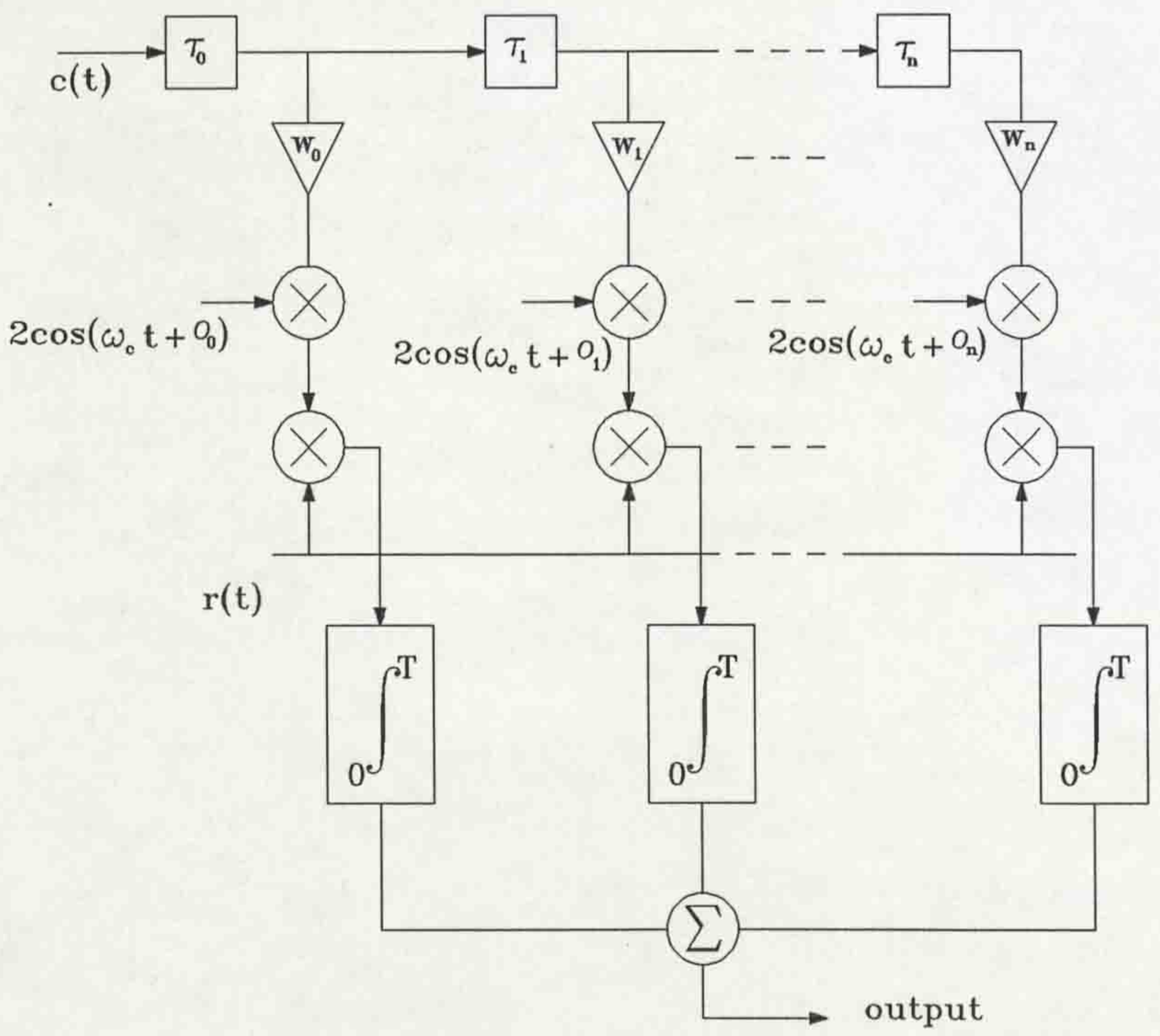

Figure 4.14 BPSK Rake Receiever.

Plate 4.1 Photograph taken from the roof of the building showing the transmitter setup and looking north into the city centre.

Plate 4.2 Photograph taken from the roof of the building looking southwards and across the River Mersey.

Plate 4.3 Photograph looking eastwards from the transmitter location.

Plate 4.4 Photograph showing the western part of the city centre from the transmitter location.

Plate 4.5 Aerial photograph of Liverpool city centre and the surroundings.

Plate 4.6 Photograph showing part of one of the main aisles in SMARKET1 (M2).

Plate 4.7 Photograph showing the part of one of the main aisles in SMARKET1 (M2) looking torwards the entrance.

Plate 4.8 Photograph showing a typical minor aisle in SMARKET1.

Plate 4.9 Photograph showing an exterior view of SMARKET1.

Plate 4.10 Photograph showing part of the lighting section in SMARKET2.

Plate 4.11 Photograph showing a typical aisle in SMARKET2 looking towards the entrance.

Plate 4.12 Photograph showing part of the bathrooms section and some aisles in SMARKET2.

Plate 4.13 Photograph showing an exterior view of SMARKET2.

Plate 4.14 Photograph looking down into one of the platforms (P6) in Lime Street Station.

Plate 4.15 Photograph showing platforms 7, 8 and 9 and looking towards the car park.

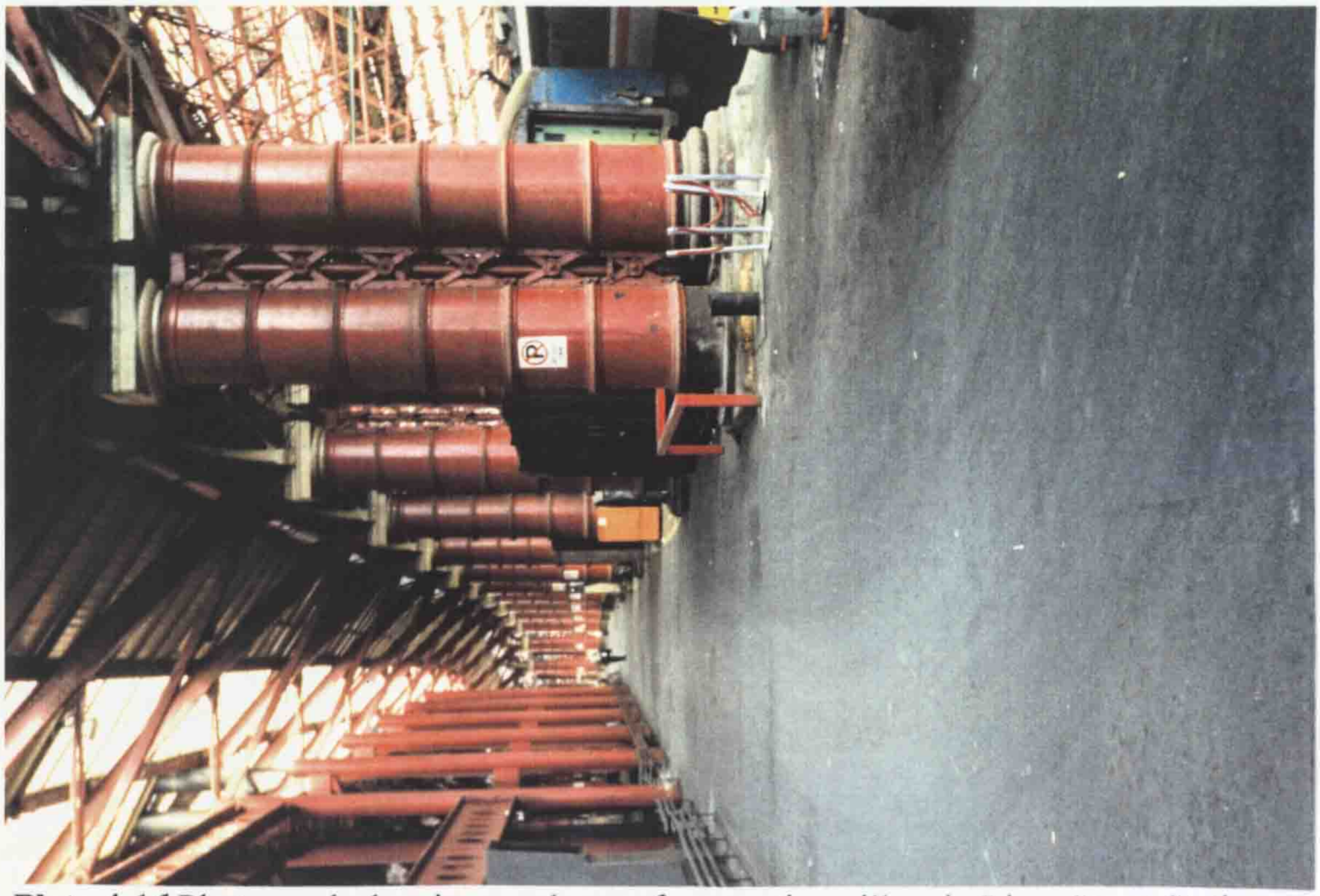

Plate 4.16 Photograph showing a column of supporting pillars in Lime Street Station.

Plate 4.17 Photograph showing an exterior view of Lime Street Station looking towards the car park entrance.

Chapter Five

EXPERIMENTAL RESULTS

5.1 INTRODUCTION

The results obtained from the entire measurement campaign are presented in this chapter. The time dispersion results are presented in the form of cumulative distribution functions of the small-scale parameters described in Chapter 4, in order to show the large-scale behaviour of the propagation channel. For the within buildings propagation studies, pathloss was calculated. Scatter plots of the measured pathloss versus distance from the transmitter were then plotted and a linear regression analysis provided the pathloss exponent.

Although all the results can be utilised in any wideband transmission system, further results are presented which are relevant only for CDMA systems. Specifically, this refers to the exploitation of the multipath nature of the channel through the use of a Rake-type receiver.

5.2 TIME DISPERSION RESULTS

A total of 152,834 'good' power delay profiles were amassed during the entire measurement campaign. For each of these power delay profiles nine small-scale time domain and two frequency domain parameters were evaluated as described in Chapter 4. The CDFs of each of these parameters were plotted to show their large-scale variabilities. In the following sections the time dispersion results obtained in the different locations surveyed are presented in the form of CDFs and tables.

5.2.1 Propagation in Urban Area (URBAN1)

A total of 48,834 'good' power delay profiles were obtained from this location. The CDFs of the eleven parameters, which were evaluated for the entire base site, are shown in Figures 5.1 through to 5.6. The 50 % and 90 % CDF values were obtained

from the graphs and these are presented in Table 4.1. This table also includes the mean, standard deviation and maximum values for each of the eleven parameters. In the case of the coherence bandwidths at 0.5 and 0.9 correlation, the minimum values, which are more critical for system design, are presented.

Table 5.1. Summary of time dispersion results from URBAN1.

Parameter	50% cdf value	90% cdf value	Mean	Standard Deviation	Maximum value
D (μs)	0.29	1.51	0.80	1.88	15.32
S (μs)	0.43	1.79	0.72	0.83	6.84
I_{15} (μs)	1.65	6.76	2.60	3.28	16.31
I_{12} (μs)	0.92	4.90	1.87	2.72	14.30
I_9 (μs)	0.47	3.34	1.29	2.16	9.25
W_{90} (μs)	1.01	3.93	1.79	2.51	16.21
W_{75} (μs)	0.50	2.24	1.08	1.78	14.61
W_{50} (μs)	0.16	1.34	0.57	1.21	8.31
NOT[1]	14.83	29.95	17.56	10.34	69.0
B_{c50} (kHz)	1008.1	7006.2	1497.8	3240.5	***59.5***
B_{c90} (kHz)	202.2	1183.0	461.6	1448.9	***32.0***[2]

Scatter plots of the coherence bandwidths at 0.5 and 0.9 correlation versus delay spread were plotted and are shown in Figures 5.7 and 5.8 respectively. For this base station, it was found that 36,657 power delay profiles featured a coherence bandwidth corresponding to a 0.5 correlation in the frequency correlation function (FCF). The corresponding number of profiles for 0.9 correlation was 45,683. In these figures the solid line is the least squares regression fit to the empirical data for this base station.

The significance of the thick broken line in Figures 5.7 and 5.8 and the ensuing

[1]NOT refers to the number of discernible taps or echoes in each power delay profile.

[2] In the following tables, the values in bold italics are minimum values.

scatter plots of the coherence bandwidths at 0.5 and 0.9 correlation versus delay spread will be explained in section 5.3.2.

The above table reveals that the range of values for the large-scale time domain descriptors is generally lower than that obtained from previous experimental investigations. For say, delay spread, the values range from 0.0[3] to 6.84 μs and a mean and standard deviation of 0.72 and 0.83 μs respectively were obtained from this study. These values are slightly lower than some of those reported in the literature, which can be observed from Tables 2.1 and 2.2 in Chapter 2. For example, for delay spread, Bajwa [5.1] reported a mean and standard deviation of 1.44 and 0.52 μs respectively compared to values of 0.72 and 0.83 μs which were obtained from this location. Lee [5.2] indicates a typical delay spread value of 1.3 μs. However, the results are similar to those published by Sousa *et al* [5.3] who reported a mean delay spread of 0.73 μs in an urban environment. Natarajan [5.4], who undertook measurements around the same base station location, reported 50 and 90 % CDF values of 0.99 and 1.86 μs respectively for delay spread which are about a factor of 2 higher than those listed in Table 5.1. Furthermore, some of the worst case locations around this base site were recorded along a street close to the River Mersey. This suggests that some multipath echoes were received from across the river.

It can also be observed from Table 5.1 that the maximum number of received multipath components is 69. This was recorded on a street close to the base station. In general, a large number of multipath components were detected in this location as can be seen from the mean value of 17.6.

The calculations of the coherence bandwidth at 0.9 and 0.5 correlation reveal minimum values of 32.2 kHz and 59.5 kHz respectively. Cox [5.5] reported minimum values of 20 kHz and 55 kHz respectively. Therefore, wideband systems will be affected by frequency selective fading in some areas around this base station

[3]In some locations, only one resolvable path was received, hence delay spread is 0.0.

location. If the coherence bandwidth at 0.9 correlation is to be taken as a figure of merit to predict system performance, then the 50% CDF value of 202.2 kHz suggests that, for eample, the performance of Qualcomm's proposed CDMA system will be degraded in 50% of the locations in this area. The large values of standard deviation indicates a high variability in the FCFs of the power delay profiles.

5.2.2 Propagation in Urban Area (URBAN2)

A total of 43,074 'good' power delay profiles were obtained in this location. The CDFs of the eleven parameters, which were evaluated for the entire base site, are shown in Figures 5.9 through to 5.14. Table 5.2 below, which has a similar format to Table 5.1, was generated for this base site.

Table 5.2. Summary of time dispersion results from URBAN2.

Parameter	50% cdf value	90% cdf value	Mean	Standard Deviation	Maximum value
D (μs)	0.09	0.57	0.26	0.38	13.71
S (μs)	0.17	0.74	0.37	0.53	7.87
I_{15} (μs)	0.63	3.81	1.68	2.94	16.23
I_{12} (μs)	0.32	1.60	0.91	1.85	14.83
I_{9} (μs)	0.12	1.12	0.57	1.36	11.92
W_{90} (μs)	0.37	1.39	0.85	1.70	16.07
W_{75} (μs)	0.15	0.91	0.44	0.90	14.21
W_{50} (μs)	---	0.52	0.22	0.46	10.12
NOT	8.62	17.82	10.21	6.58	44.0
B_{c50} (kHz)	1782.3	9996.7	1746.6	3829.6	***77.8***
B_{c90} (kHz)	198.4	2177.3	719.5	1873.8	***32.0***

For this location, it was found that 24,819 power delay profiles featured a coherence bandwidth corresponding to a 0.5 correlation in the FCF. The corresponding number of profiles for a 0.9 correlation was 36,387. Scatter plots of the coherence bandwidths at 0.5 and 0.9 correlation versus delay spread were plotted and are shown in Figures

5.15 and 5.16 respectively. In these figures the solid line is the least squares regression fit to the empirical data for this base station.

Comparison of the CDFs from URBAN1 and URBAN2 reveals that, although the maximum value of delay spread of 7.87 μs was recorded in the latter case, the overall nature of the channel is worst in URBAN1. However, the values obtained from URBAN2 are also slightly lower than those that have been reported in the literature.

5.2.3 Propagation in Rural Open Area

A total of 21974 'good' power delay profiles were obtained in this location. The CDFs of the eleven parameters, which were evaluated for the entire base site, are shown in Figures 5.17 through to 5.22. Table 5.3 summarises the time dispersion results obtained from this location.

Table 5.3 Summary of the time dispersion results from the Rural Open Area.

Parameter	50% cdf value	90% cdf value	Mean	Standard Deviation	Maximum value
D (μs)	0.03	0.21	0.10	0.14	4.35
S (μs)	0.08	0.47	0.20	0.29	3.94
I_{15} (μs)	0.26	1.75	0.90	1.85	16.37
I_{12} (μs)	0.11	0.86	0.41	0.72	10.76
I_{9} (μs)	---	0.53	0.24	0.41	8.12
W_{90} (μs)	0.14	0.80	0.40	0.60	11.40
W_{75} (μs)	---	0.39	0.20	0.32	8.08
W_{50} (μs)	---	0.09	0.07	0.17	3.67
NOT	4.91	9.94	5.88	3.35	20.0
B_{c50} (kHz)	3465.5	12282.5	1890.0	4256.7	***114.4***
B_{c90} (kHz)	830.1	3592.1	995.6	2197.1	***32.0***

In this location, it was found that 8,651 power delay profiles featured a coherence bandwidth corresponding to a 0.5 correlation in the FCF. The corresponding number

of profiles for a 0.9 correlation was 16,658. Scatter plots of the coherence bandwidths at 0.5 and 0.9 correlation versus delay spread were plotted and are shown in Figures 5.23 and 5.24 respectively. In these figures the solid line is the least squares regression fit to the empirical data for this base station.

Table 5.3 above, indicates that this location is the least dispersive of the outdoor environments surveyed. For delay spread, a maximum value of 3.94 μs was recorded, together with a mean and standard deviation of 0.2 and 0.29 μs respectively. This maximum value could have been due to distant reflectors in the small neighbouring town near the base site. Again the values obtained from this study are lower than those from previous studies. For example, Bajwa [5.1] reported a mean value of 1.04 μs in suburban Birmingham. In general, the number of resolvable multipath components are smaller, with a recorded maximum of 20, compared to the other outdoor locations.

5.2.4 Propagation within a Supermarket (SMARKET1)

A total of 10,654 'good' power delay profiles were obtained in this location. The CDFs of the eleven parameters, which were evaluated for the entire base site, are shown in Figures 5.25 through to 5.30. A summary of the time dispersion results obtained from this location are shown below in Table 5.4

Scatter plots of the coherence bandwidths at 0.5 and 0.9 correlation versus delay spread were plotted and are shown in Figures 5.31 and 5.32. The plots were generated using 5,531 and 10,010 power delay profiles for the coherence bandwidth at 0.5 and 0.9 correlation respectively. In these figures the solid line is the least squares regression fit to the empirical data for this base station.

The range of values obtained from this location are generally lower than some of those from previous within building experimental investigations (see Table 2.3). However, to the authors knowledge, no propagation studies within a modern supermarket have been reported in the literature.

Table 5.4 Summary of the time dispersion results from SMARKET1.

Parameter	50% cdf value	90% cdf value	Mean	Standard Deviation	Maximum value
D (μs)	0.28	0.83	0.04	0.03	0.84
S (μs)	0.06	0.08	0.06	0.02	0.6
I_{15} (μs)	0.18	0.34	0.29	0.58	1.98
I_{12} (μs)	0.19	0.31	0.20	0.09	1.55
I_{9} (μs)	0.12	0.24	0.15	0.06	1.53
W_{90} (μs)	0.18	0.26	0.19	0.07	1.49
W_{75} (μs)	0.1	0.18	0.12	0.06	1.37
W_{50} (μs)	0.04	0.1	0.06	0.04	1.25
NOT	5.68	7.84	5.78	1.64	20.0
B_{c50} (kHz)	4802.1	12322.7	3324.0	5293.7	***297.5***
B_{c90} (kHz)	1092.1	2336.7	1576.3	2180.8	***132.8***

5.2.5 Propagation within a supermarket (SMARKET2)

A total of 9,274 'good' power delay profiles were obtained in this location. The CDFs of the eleven parameters, which were evaluated for the entire base site, are shown in Figures 5.33 through to 5.38. Table 5.5 below shows a summary of the time dispersion results obtained from this location.

Scatter plots of the coherence bandwidths at 0.5 and 0.9 correlation versus delay spread were plotted and are shown in Figures 5.39 and 5.40. In this location, it was found that 6,677 power delay profiles featured a coherence bandwidth corresponding to a 0.5 correlation in the FCF. The corresponding number of profiles for a 0.9 correlation was 9,080. In these figures the solid line is the least squares regression fit to the empirical data for this base station.

Table 5.5 below reveals that the time dispersion results are similar to those obtained from SMARKET1, although a maximum value of delay spread of 0.6 μs was obtained

in SMARKET1 compared to a value of 0.37 μs from SMARKET2. However, the 50 and 90 % CDF values of the coherence bandwidths at 0.5 and 0.9 correlation indicate that SMARKET2 is slightly more dispersive than SMARKET1.

Table 5.5 Summary of the time dispersion results from SMARKET2.

Parameter	50% cdf value	90% cdf value	Mean	Standard Deviation	Maximum value
D (μs)	0.046	0.096	0.056	0.033	0.64
S (μs)	0.061	0.084	0.066	0.018	0.367
I_{15} (μs)	0.204	0.377	0.348	0.872	1.32
I_{12} (μs)	0.228	0.337	0.241	0.08	0.92
I_{9} (μs)	0.169	0.27	0.184	0.073	0.45
W_{90} (μs)	0.19	0.27	0.204	0.06	0.907
W_{75} (μs)	0.11	0.187	0.132	0.05	0.827
W_{50} (μs)	0.057	0.11	0.073	0.037	0.227
NOT	5.8	7.9	6.2	1.55	12.0
B_{c50} (kHz)	3925.0	9214.0	3937.2	4860.5	***517.3***
B_{c90} (kHz)	971.5	1780.0	1403.3	1677.1	***206.0***

5.2.6 Propagation Within a Train Station

A total of 19,204 'good' power delay profiles were obtained in this location. The CDFs of the eleven parameters, which were evaluated for the entire base site, are shown in Figures 5.41 through to 5.46. A summary of the time dispersion results obtained from this location are presented in Table 5.6 below.

Scatter plots of the coherence bandwidths at 0.5 and 0.9 correlation versus delay spread were plotted and are shown in Figures 5.47 and 5.48. In this location, it was found that 17,564 power delay profiles featured a coherence bandwidth corresponding to a 0.5 correlation in the FCF. The corresponding number of profiles for a 0.9 correlation was 19,152. In these figures the solid line is the least squares regression to the empirical data for this base station.

Table 5.6 Summary of the time dispersion results from the Train Station.

Parameter	50% cdf value	90% cdf value	Mean	Standard Deviation	Maximum value
D (μs)	0.119	0.196	0.124	0.058	0.92
S (μs)	0.121	0.157	0.123	0.032	0.508
I_{15} (μs)	0.437	0.663	0.542	0.668	2.19
I_{12} (μs)	0.402	0.587	0.406	0.147	1.147
I_9 (μs)	0.298	0.47	0.306	0.132	1.08
W_{90} (μs)	0.366	0.493	0.367	0.108	1.053
W_{75} (μs)	0.228	0.339	0.237	0.086	0.813
W_{50} (μs)	0.11	0.203	0.131	0.062	0.64
NOT	10.8	14.02	10.6	2.85	20.0
B_{c50} (kHz)	2109.5	5614.9	2930.2	3292.7	***471.5***
B_{c90} (kHz)	454.1	899.3	726.2	709.7	***206.0***

Table 5.6 shows that the results obtained from this location are the worst compared to the other indoor environments. In addition, the number of resolvable multipath components in this location is greater than those obtained in the other buildings. This may be as a result of multiple reflections or scattering from the crisscross pattern of metal that dominates the structural contents of the building.

5.3 BRIEF DISCUSSION OF TIME DISPERSION RESULTS

In general, the above tables show that the channel is more dispersive in the outdoor environments than in the indoor scenarios, as expected. Furthermore URBAN1 is the most dispersive of the outdoor environments with a mean delay spread of 0.72 μs compared to a corresponding value of 0.20 μs for the rural open area. For the indoor locations, the train station is the most dispersive, with a mean delay spread of 0.123 μs.

5.3.1 Time Domain

Having obtained the above typical estimates of the small-scale channel descriptors in the locations surveyed, it is possible to use equation 4.17 to predict the performance of a GSM system. In URBAN1, the mean value of delay spread of 0.72 μs gives a predicted IBER of 8.8 x 10^{-3}. However, with a maximum recorded delay spread of 6.84 μs in this location, the predicted IBER increases to 620 x 10^{-3} which necessitates the use of equalisers. In the other locations, the channel is less dispersive and so the performance of the GSM system in these locations is expected to be better.

A general observation from the time dispersion measurements in the outdoor locations is that the measured values are lower than those that have been reported in the literature. This apparent difference can be attributed to the measurement environment, the total number of power delay profiles used for analysis and the nature of collecting experimental data. In this study, a substantial number of power delay profiles were acquired from random locations around the base sites, with no preferences given to the nature of the power delay profiles. It is expected that utilisation of such techniques will provide reliable estimates of the nature of the propagation channel. This was also observed by Sousa *et al* [5.3].

It is interesting to note that delay spread results from the supermarkets are in the same order of magnitude as those reported by Arowojolu [5.6] from his microcellular measurements. In his study, a discone antenna at height of 10 m gave a mean delay spread of 62.1 ns in the main street and 41 ns in the side streets. This compares favourably with the results obtained from the supermarkets in which mean delay spreads of 60 and 66 ns were recorded. Arowojolu also obtained similar values when a Yagi antenna was used at heights of 5 and 10 m.

Time dispersion results presented by Rappaport [5.7] show median delay spreads of up to 120 ns. This value is about a factor of 2 higher than those obtained from the supermarkets. A possible reason for the higher values reported by Rappaport and Devasirvatham [5.8] is that, in the supermarkets surveyed, there were virtually no

windows or large glass sections, whereas, the buildings surveyed by the above researchers contained large glass windows. Hence, virtually all the signal is contained within the supermarkets and there is very little probability of receiving multipath components originating from outside the building.

5.3.2 Frequency Domain

As mentioned in Chapter 4, the data from the scatter plots of the coherence bandwidths at 0.5 and 0.9 correlation were fitted to regression lines of the form

$$B_c = \frac{1}{A_c S^{i_c}} \qquad \textbf{(5.1)}$$

In the work presented by Bajwa [5.1], Cox and Leck [5.9], Demery [5.10], and Natarajan [5.4], the values of the coefficients showed a high degree of correlation, especially for the coherence bandwidth at 0.9 correlation. In contrast, inspection of the scatter plots of the coherence bandwidths against delay spread reveal a very small degree of correlation. Hence, the values of the coefficients do not agree with those from the literature.

The reason for this apparent anomaly is simple. In the experimental campaigns of previous researchers, worst case power delay profiles were often sought, whereas, in this study the power delay profiles were collected at random. However, a closer examination of the scatter plots reveals that the points on the graphs trace a line which shows the minimum value of the coherence bandwidths for any value of delay spread. The equations which represent these two lines were determined. These equations were the same for all the base station locations that were surveyed. The two equations are given below.

$$B_{c0.5} = \frac{1}{5.62 \cdot S^{1.0}} \qquad \textbf{(5.2)}$$

$$B_{c0.9} = \frac{1}{13.80 \cdot S^{1.0}} \qquad (5.3)$$

The thick broken line in the scatter plots were obtained by using these equations and these are more consistent with similar equations from previous studies. These equations define the minimum coherence bandwidths at 0.5 or 0.9 correlation that are possible in any location for any value of delay spread.

The 50 % CDF values for the coherence bandwidth at 0.5 correlation indicate that, the CDMA system proposed by Qualcomm will be affected by frequency selective fading in URBAN1 only, and data rates higher than that of the GSM system could be accommodated in all the buildings surveyed.

5.4 PATHLOSS CHARACTERISTICS

The local mean signal has been estimated by averaging the power delay profiles over a spatial distance of approximately 20λ, ie., over a spatial distance of about 3.3 m at 1.8 GHz. The median pathloss for the 20λ segments were extracted and scatter plots of median pathloss with respect to 1 m separation versus distance from the transmitter were plotted. A linear regression analysis was performed to determine the best-fit line to the empirical data.

5.4.1 Pathloss Characteristics in SMARKET1

It was found necessary to analyse the data obtained from this location into five sections, namely, line-of-sight (LOS), main aisles (M1 and M3), all minor aisles and the entire superstore. A combined scatter plot of all the main aisles was also produced. It should be noted that M2 is the only line-of-sight section of the store that was surveyed (see Figure 4.7). Figures 5.49 to 5.54 show the scatter plots of pathloss versus distance in the various categories as outlined above. Table 5.7 below summaries the results obtained from this location.

Table 5.7 Summary of pathloss results obtained from SMARKET1.

Location	Slope (n)	Intercept	Correlation
Main aisle 2 (M2, LOS)	1.67	5.4	0.97
Main aisle 1 (M1, NLOS)	4.4	-32.6	0.81
main aisle 3 (M3, NLOS)	1.8	8.96	0.93
All three main aisles (M1, M2, M3)	1.97	3.6	0.88
All minor aisles	2.02	4.67	0.93
Entire superstore	1.97	4.5	0.89

5.4.2 Pathloss Characteristics in SMARKET2

Since the shelves in this location were arranged in an irregular manner compared to the layout of SMARKET1, the data was analysed in two sections, viz, LOS and NLOS. The LOS section was mainly the main aisle where the transmitter was located (see Figure 4.7). Figures 5.55 and 5.56 show the scatter plots that were obtained in this location and a summary of the results is presented in Table 5.8 below.

Table 5.8 Summary of pathloss results obtained from SMARKET2.

Location	Slope (n)	Intercept	Correlation
LOS	2.01	-6.2	0.98
NLOS	2.3	0.91	0.84
Entire Superstore	2.4	0.2	0.84

5.4.3 Pathloss Characteristics in the Train Station

The data from this location was analysed in three main categories. These were the concourse area, the inner section with 6 platforms and the outer section (see Figure 4.8). The data obtained from each of the platforms was further analysed. Figures 5.57 to 5.60 show some of the scatter plots obtained from this location and the summary of the pathloss results is shown in Table 5.9 below.

Table 5.9 Summary of pathloss results obtained from the Train Station.

Location	Slope (n)	Intercept	Correlation
Platform 1 (P1)	2.0	-5.2	0.95
Platform 3 (P3)	1.9	-2.1	0.92
Platform 4 (P4)	1.9	-3.5	0.95
Platform 6 (P6)	1.7	1.0	0.97
Total (P1, P3, P4, P6)	1.8	-1.5	0.93
Platform 7 (P7)	2.4	-1.7	0.96
Platform 9 (P9)	2.5	-16.3	0.92
Total (P7, P9)	2.4	-16.8	0.93
LOS area	1.9	-8.8	0.83
Concourse area	1.7	-10.1	0.97
Entire Building	2.4	-13.2	0.89

5.4.4 Brief Discussion of Pathloss Results

In general, the correlation between pathloss and distance in the buildings surveyed is very high, as can be seen from the clustering of data points along the regression lines. This is further substantiated by the correlation values listed in Tables 5.7 to 5.9.

A closer inspection of the values listed in Table 5.7, which was generated for SMARKET1, reveals that the pathloss exponent, n, varies between 1.67 and 4.4. In some parts of this superstore, the received signal level falls off at a rate less than the square of the distance due to a wave guiding effect [5.11] by the metal display shelves. This phenomenon, which has also been observed in some other buildings [5.12-5.16], was observed in two of the three main aisles (M2 and M3). In main aisle M1, n is 4.4. The high value of n along this aisle is probably due to the fact that this aisle is more open and contains a row of checkout desks.

In SMARKET2, the value of n for the entire building is 2.4 compared to 1.97 for SMARKET1. This shows that, the former is more lossy. This is probably due to the

general layout and contents of these superstores. In SMARKET1, the display shelves are arranged in a regular manner, while in SMARKET2, the display shelves are not arrange in such a regular pattern. In addition, these display shelves are higher in SMARKET2, with some extending from the roof. This may therefore, result in a heavily cluttered environment.

The results from the supermarkets also indicate patterns which have been observed in microcellular environments. Specifically, there is a drop in signal level when the receiver moves from a main aisle into a minor aisle. This is analogous to the microcell case when the receiver moves from the main street into the side street [5.6].

In Lime Street Station, the value of n for the whole building is 2.4. However, in certain locations (P1, P3, P4 and P6), n is equal to or less than 2. This is the wave guiding phenomenon which was observed in certain locations in SMARKET1. This was probably due to the crisscross pattern of metal that makes up most of the building structure. In addition, these platforms lead straight into the tunnel. For platforms 7 and 9 (P7 and P9), the values of n are 2.4 and 2.5 respectively. These higher values may be due partly to the fact, that these two platforms curve into the tunnel. Furthermore, the car park entrance is situated close to platform 9, and the wall on this side of the building contains large glass sections, hence, some of the transmitted energy propagates through these glass sections rather than being contained within the building.

5.5 AMPLITUDE AND PHASE DISTRIBUTIONS

CDFs of the normalised amplitudes of some of the received multipath echoes were generated and plotted on Rayleigh graph paper. Least square fits were then made to the data. Although this was not examined in detail, the indications were that, the amplitudes of the echoes in the various time delay bins do not fit either the Rayleigh or the Rician Distribution. This attests the fact that, as the resolution of the measuring system increases, many paths are resolved and hence, there is less probability for the echoes in the different time delay bins to exhibit Rayleigh fading.

The phase distributions for the first two taps was briefly examined. A typical plot is shown in Figure 5.61, which shows that the phases of the echoes in first two time delay bins are uniformly distributed between $-\pi$ and π. The slight deviations might have been due to imperfections in the I and Q demodulator that was employed in the receiver.

5.6 CDMA-BASED RESULTS

All the above time dispersion and pathloss results can be utilised in the design and implementation of any CDMA system. In addition, the data can also be used to show the Rake gain if a Rake-type receiver is employed at the receiver. This was illustrated by using the Rake receiver model that was presented in Chapter 4.

5.6.1 Large-Scale variability of Received Signal

Using Equation 4.21, the relative SNRs were evaluated for each power delay profile in the respective street sections. The average relative SNR was evaluated for each experimental run and plotted against the distance from the transmitter site (base station). This was performed for a Rake receiver which combines all paths using maximal ratio combining (MRC), equal gain combing (EGC) and a standard receiver which demodulates only the strongest path. Figures 5.62 to 5.67 show the average relative SNR versus distance for the various base stations. In each case, the SNR values are normalised to the highest received SNR on the respective streets.

These plots can be interpreted as the received SNR in the base stations without power control. In all the base stations examined, it can be observed that maximal ratio combining provides the best performance. The standard 1-path receiver performs better than a Rake receiver with equal gain combining if most of the received signal power is contained in one path and the rest of the paths contain very little energy. This is because, with equal gain combining, the paths with small power contribute more noise, thereby lowering the received SNR. This was more predominant in the supermarkets.

CDFs of the relative SNR for the various base stations were also plotted, in order to show their variability over a large-scale area. Figures 5.68 to 5.73 show the plots from the different locations. These figures reveal a variation in relative SNR of up to 40 dB. This signifies the need for power control in a CDMA system, in which case the variation in SNR can be reduced.

The above plots have been computed from all the resolvable echo paths from the measurements. In some cases, as many as 69 received paths were recorded. In practice, it is not beneficial to combine all received paths because of the number of correlators that may be required. In addition, some of these paths may contain very little signal power.

With respect to the above facts, results are presented for a Rake receiver with a reduced number of paths. Using maximal ratio combining, relative SNRs of different receiver systems were evaluated. Cumulative distribution functions of the relative SNR for the various base stations were then obtained. This was performed for all-path, 5-path, 4-path, 3-path, 2-path and 1-path Rake receivers. These plots are shown in Figures 5.74 to 5.79. In each plot the relative SNRs are normalised with respect to the highest SNR value.

Figures 5.74 to 5.79 indicate the Rake gain which can be achieved through exploitation of the inherent path diversity in a CDMA system. For urban areas, the Rake gain is quite significant in moving from a 1-path receiver to a 5-path receiver. For example, in URBAN1, the difference in relative SNRs between a 1- and 5-path receiver is about 5 dB for a 50 % CDF value. In the rural open area and supermarkets, the Rake gain is comparatively smaller when all paths are combined as opposed to only the first five paths. The measurements in the train station indicated a similar trend that was observed in the urban locations (Figure 5.79). This is mainly due to the number of multipath components that were resolved. Chan [5.17] investigated the effect of reducing the system bandwidth, which will result in a reduced number of multipath echoes. In his investigations, Chan observed that a 1-

path receiver performs almost as well as a 3-path receiver for a reduced bandwidth.

5.6.2 Short-term variability of Received Signal

Since the measurements for each experimental run were continuous, the relative SNRs on each street will give insight into how the received signal level varies with small changes in distance. This was illustrated for a Rake receiver that combines all paths, 5 paths, 4 paths, 3 paths, 2 paths and 1 path using MRC. Rather than show all the results, only two typical results are shown.

Figures 5.80 through to 5.89 show the relative SNR versus distance for the different receiver systems. These plots were obtained from one of the streets in URBAN1. The plots show that, as the number of rake branches reduces, the fading rate increases and the occurrence of deep fades (up to 35 dB) increases. Similar observations are shown in Figures 5.86 to 5.91, which were generated from an experimental run in the train station. Chan [5.17] also observed that reducing the system bandwidth results in increased variation of the SNR.

For the proposed IS-95 CDMA system, power adjustment signals are sent from the base to the mobile station every 1.25 ms [5.18]. This is the closed loop power control rate which is limited to a power adjustment of 1 dB every 1.25 ms. To determine whether this rate is adequate for say, URBAN1, it should be noted that the power delay profiles are spaced about 0.0768 m apart. If a maximum vehicle speed of 13.89 m/s (50 km/h) is assumed, then the mobile would have travelled 0.01736 m within a period of 1.25 ms. During the 0.0768 m spatial distance, about 4 power adjustment signals (i.e., 0.0768/0.01736) can be made allowing for a 4 dB change in power. The above figures reveal that this is not adequate since changes of up to 20 dB over a similar distance can be observed. It is therefore possible that, it will be difficult for power control schemes to react fast enough in multipath environments as observed by Turin [5.19].

5.6.3 Probability of Occurrence of Echoes

It is evident from section 5.6.1 that all the received multipath components will not be demodulated. It is therefore, necessary to be able to design an optimum Rake receiver based on the distribution and signal levels of the multipath components. Even though the IS-95 system will use searcher receivers to provide channel estimates, knowledge of the probability of occurrence of the echoes in different environments is required for simulations, design and implementation of Rake receivers.

The probability of occurrence of the echoes at different signal levels was therefore evaluated as explained in Chapter 4. Figures 5.92 and 5.93 show the probability of occurrence versus time-delay bins and number of taps respectively. The former illustrates the time span and corresponding probability of occurrence for different signal levels. It is clear that, even at the low signal level of -25 dB, the percentage of echoes with excess delays greater than 3 μs is very small. Figure 5.93 shows a similar plot for the number of received multipath components in the power delay profiles. For example, at -20 dB, about 50 % of the power delay profiles in this location have 10 taps. Figures 5.94 through to 5.103 illustrate similar plots from the other locations that were surveyed.

These plots can be used to give an indication of the time span that an optimum Rake receiver operating in these different environments should possess and the number of branches required. These two aspects are very important as highlighted in the previous sections.

REFERENCES

[5.1] Bajwa, A. S., 'Wideband Characterisation of UHF Mobile Radio Propagation in Urban and Suburban Areas', PhD. Thesis, Department of Electronic and Electrical Engineering, University of Birmingham, 1979.

[5.2] Lee, W.C.Y., 'Mobile Communication Design Fundamentals', Sams, 1986.

[5.3] Sousa, E.S., Jovanovic, V.M. and Daigneault, C., 'Delay Spread Measurements for the Digital Cellular Channel in Toronto', IEEE Trans. on Veh. Tech., Vol. 43, No. 4, Nov. 1994, pp837-847.

[5.4] Natarajan, N., 'Wideband Characterisation of Mobile Radio Channels at 1.8 GHz', PhD. Thesis, Department of Electrical Eng. and Electronics, University of Liverpool, 1992.

[5.5] Cox, D. C., 'Delay Doppler Characteristics of Multipath Propagation at 910 MHz in a Suburban Mobile Radio Environment', IEEE Transactions on Antennas and Propagation, Vol. AP-20, No. 5, Sept. 1972, pp625-635.

[5.6] Arowojolu, A. A., 'Microcellular Mobile Radio Measurements and Modelling', PhD. Thesis, Department of Electrical Eng. and Electronics, University of Liverpool, 1994.

[5.7] Rappaport, T. S., 'Characterisation of UHF Multipath Radio Channels in Factory Buildings', IEEE Transactions on Antennas and Propagation', Vol. 37, No. 8, Aug. 1989, pp1058-1069.

[5.8] Devasirvatham, D. M. J. and Murray, R.R., 'Time Delay Spread Measurements at 850 MHz and 1.7 GHz Inside a Metropolitan Office Building', Electronics Letters, Vol. 25, No. 3, Feb. 1989, pp194-196.

[5.9] Cox, D.C. and Leck, R.P., 'Distribution of multipath delay spread and average excess delay for 910 MHz urban mobile radio paths', IEEE Trans. on Ant. and Prop., Vol. 23, No. 2, 1975, pp. 206-213.

[5.10] Demery, D. A., 'Wideband Characterisation of UHF Mobile Radio Channels in Urban Areas', PhD. Thesis, Department of Electrical Eng. and Electronics, University of Liverpool, 1989.

[5.11] Collin, R.E., 'Field Theory of Guided Waves', McGraw-Hill, London, 1960.

[5.12] Saleh, A.A.M. and Valenzuela, R.A., 'A statistical model for indoor multipath propagation', IEEE J. Selected Area Comms., Vol. 5, No. 3, Feb. 1987, pp. 128-137.

[5.13] Alexander, S.E., 'Radio Propagation within buildings at 900 MHz', Electronics Letters, Vol. 18, No. 21, 1982. pp913-914.

[5.14] Pahlavan, K., Ganesh, R. and Hotaling, T., 'Multipath Propagation Measurements on Manufacturing Floors at 910 MHz', Electronics Letters, Vol. 25, No. 3, Feb. 1989. pp225-227.

[5.15] Bultitude, R.J.C., 'Measurement, Characterisation and Modelling of Indoor 800/900 MHz Radio Channels for Digital Communications', IEEE Communications Magazine, Vol. 25, No. 6, June 1987, pp5-12.

[5.16] Rappaport, T.D. and McGillem, C.D., 'Characterising the UHF Factory Radio Channel', Electronics Letters, Vol. 23, No. 19, Sept. 1987, pp1015-1017.

[5.17] Chan, N.L.B., 'Multipath Propagation Effects on a CDMA Cellular System', IEEE Trans. on Veh. Tech., Vol. 43, No. 4, Nov. 1994, pp849-855.

[5.18] Qualcomm Inc., 'An Overview of the Application of Code Division Multiple Access (CDMA) to Digital Cellular Systems and Personal cellular Networks', 1992.

[5.19] Turin, G.L., 'The Effects of Multipath and Fading on the Performance Direct Sequence Spread CDMA Systems',IEEE Trans. on Veh. Tech., Vol. VT-33, No. 4, Aug. 1984, pp213-219.

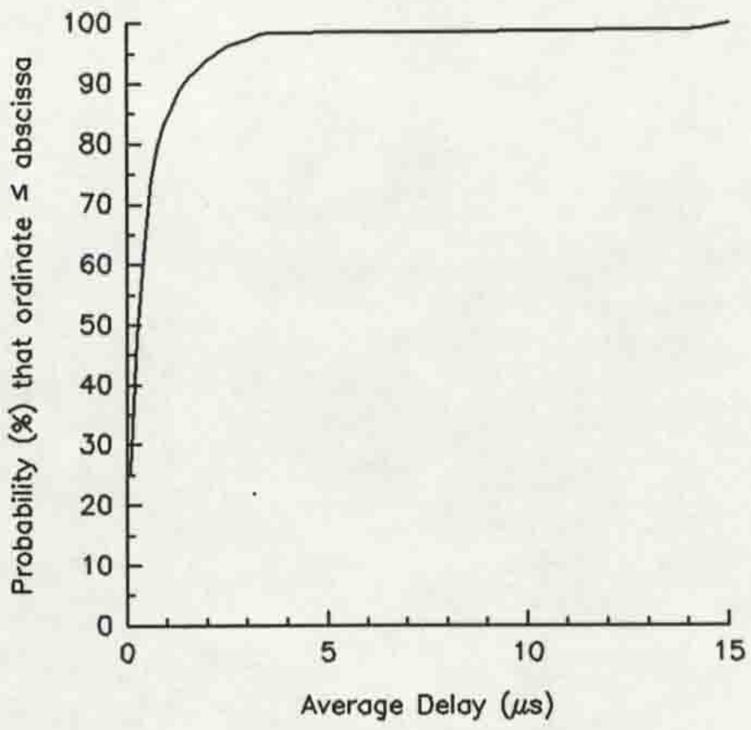

Figure 5.1 CDF of average delay for URBAN1.

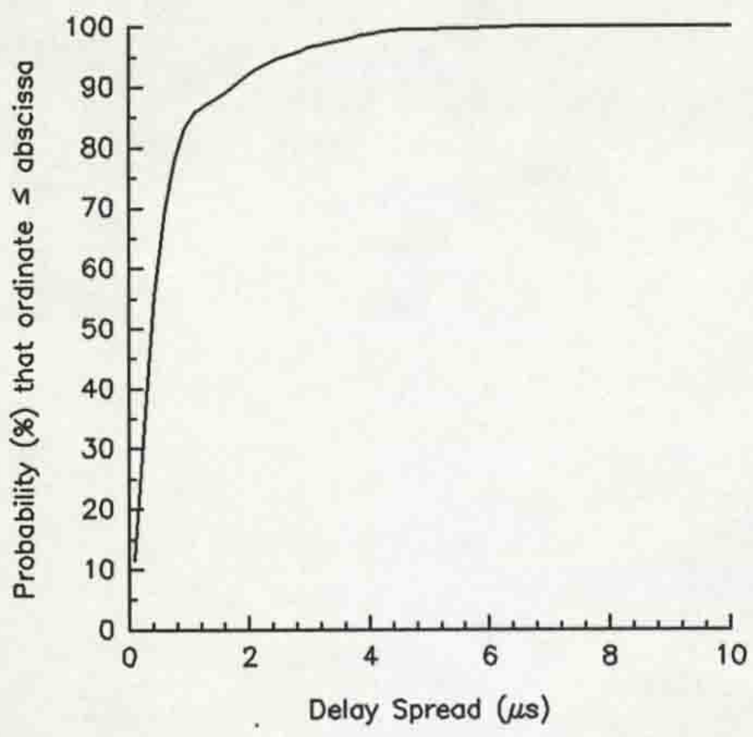

Figure 5.2 CDF of delay spread for URBAN1

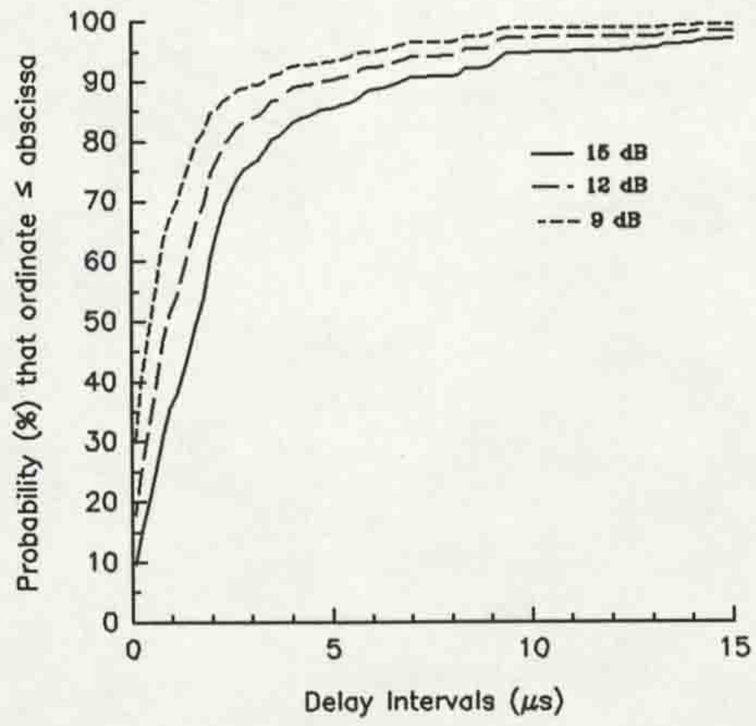

Figure 5.3 CDFs of delay intervals for URBAN1.

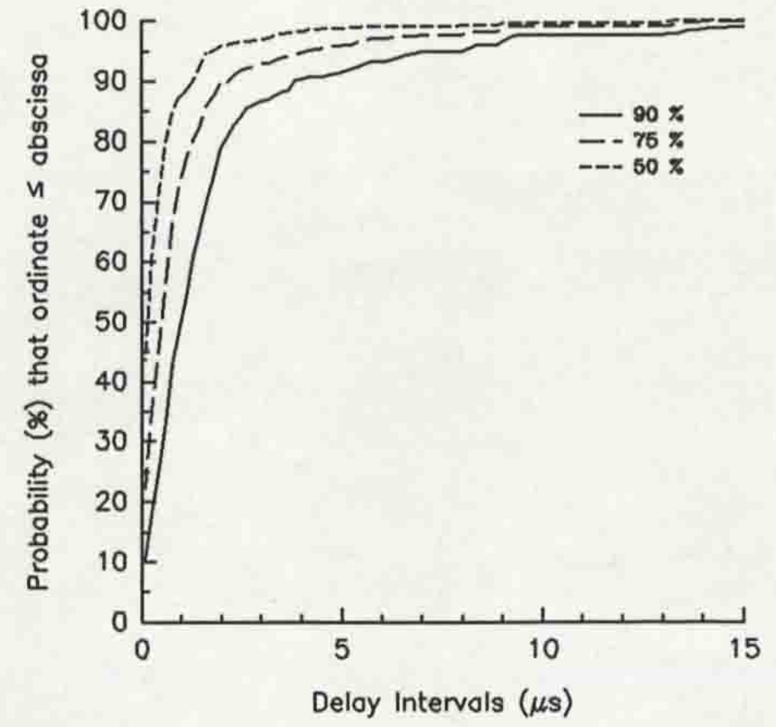

Figure 5.4 CDFs of delay windows for URBAN1.

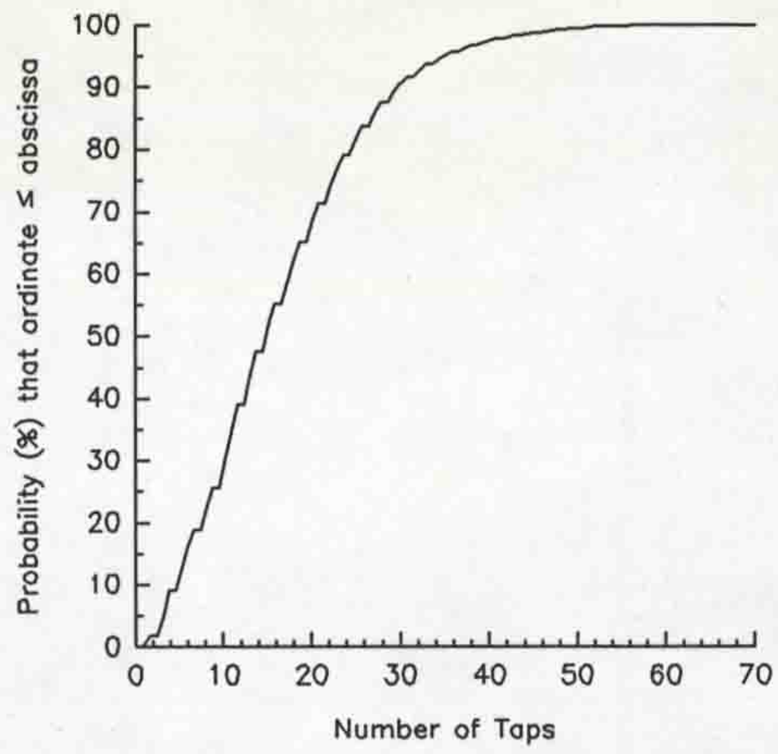

Figure 5.5 CDF of the number of taps for URBAN1.

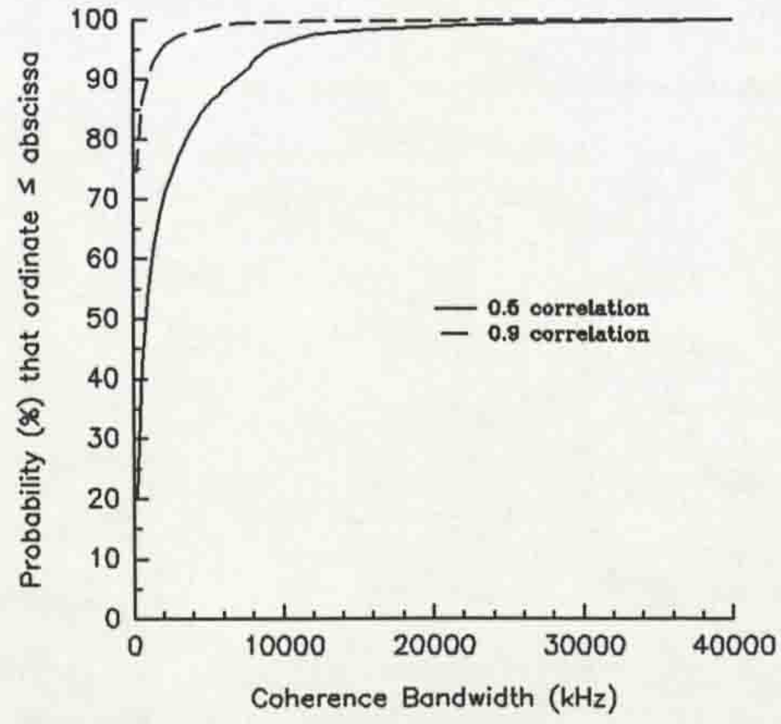

Figure 5.6 CDFs of the coherence bandwidths for URBAN1.

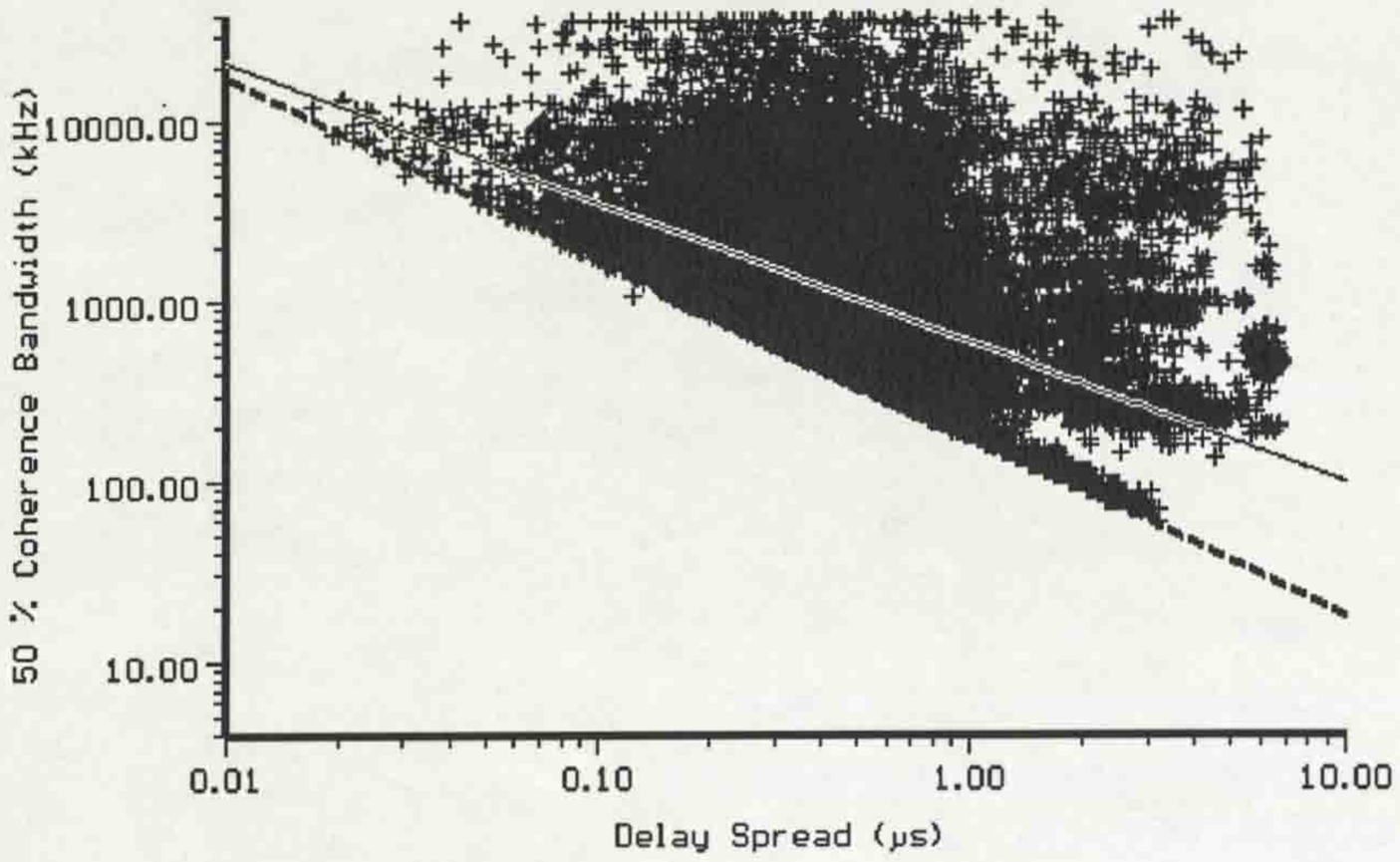

Figure 5.7 Scatter plot of coherence bandwidth at 0.5 correlation versus delay spread for URBAN1.

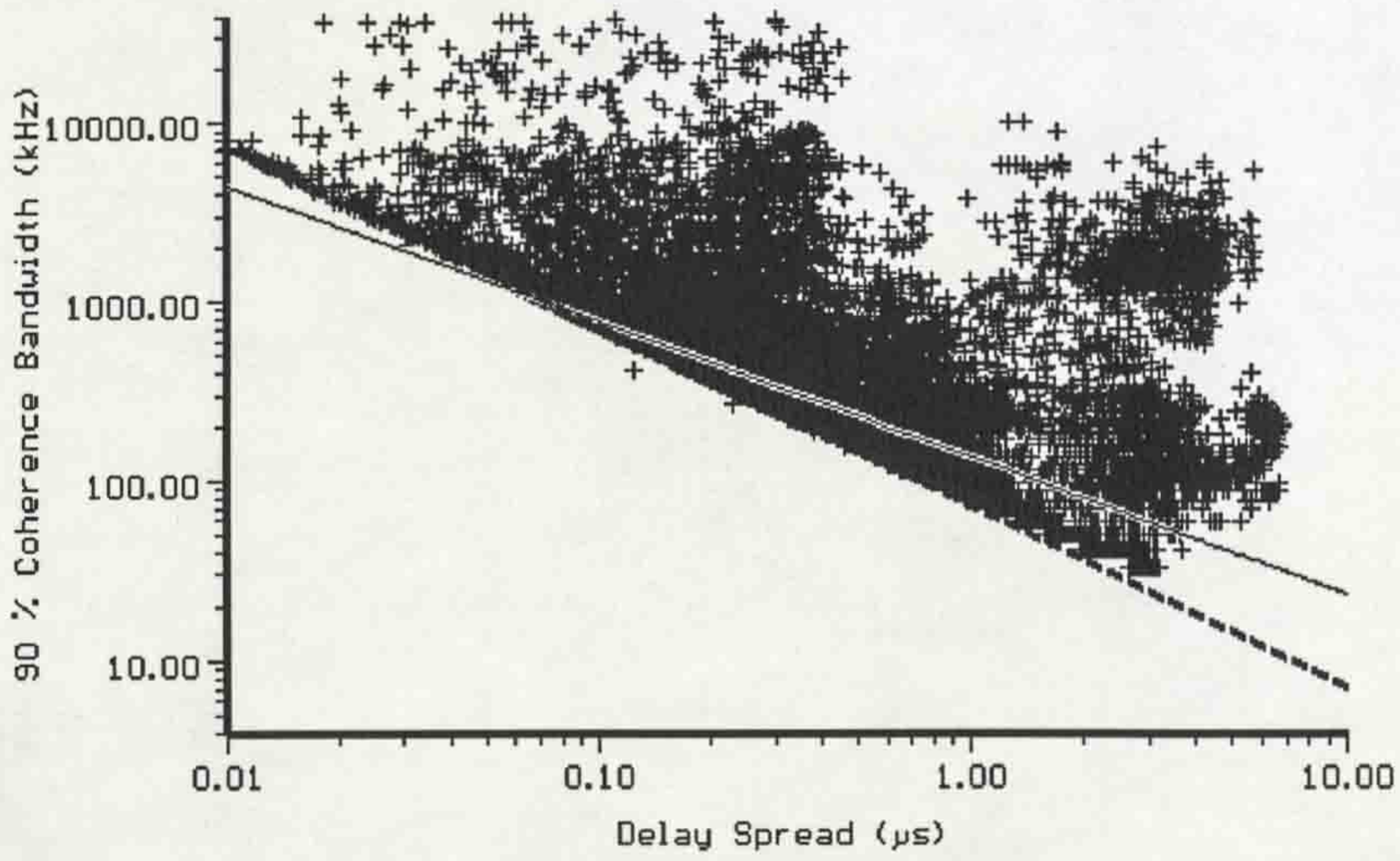

Figure 5.8 Scatter plot of coherence bandwidth at 0.9 correlation versus delay spread for URBAN1.

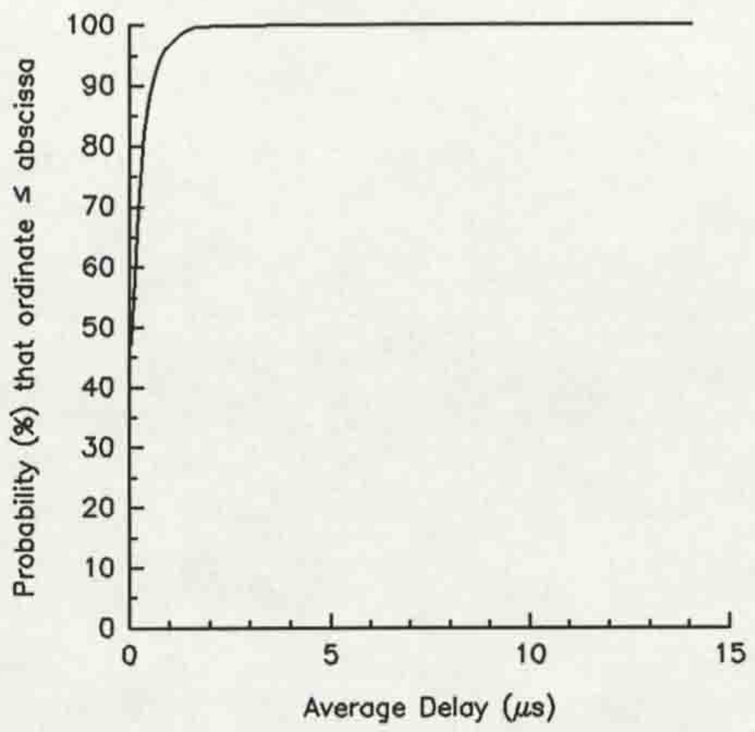

Figure 5.9 CDF of average delay for URBAN2.

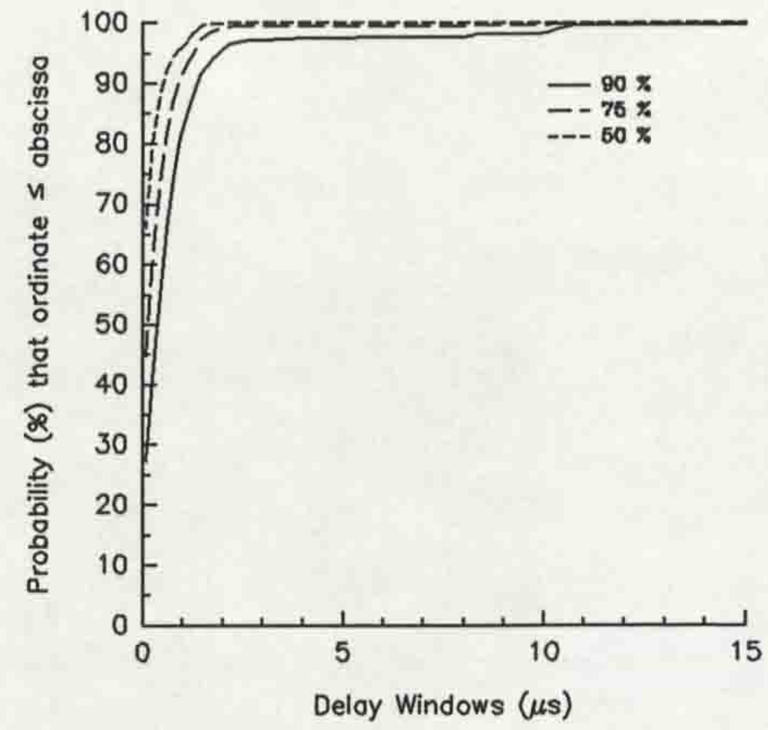

Figure 5.12 CDFs of delay windows for URBAN2.

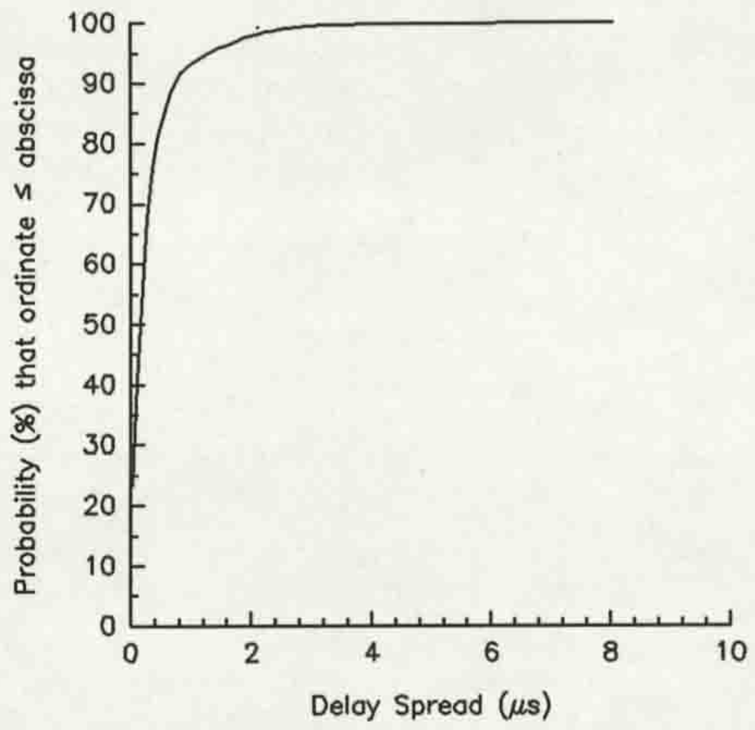

Figure 5.10 CDF of delay spread for URBAN2

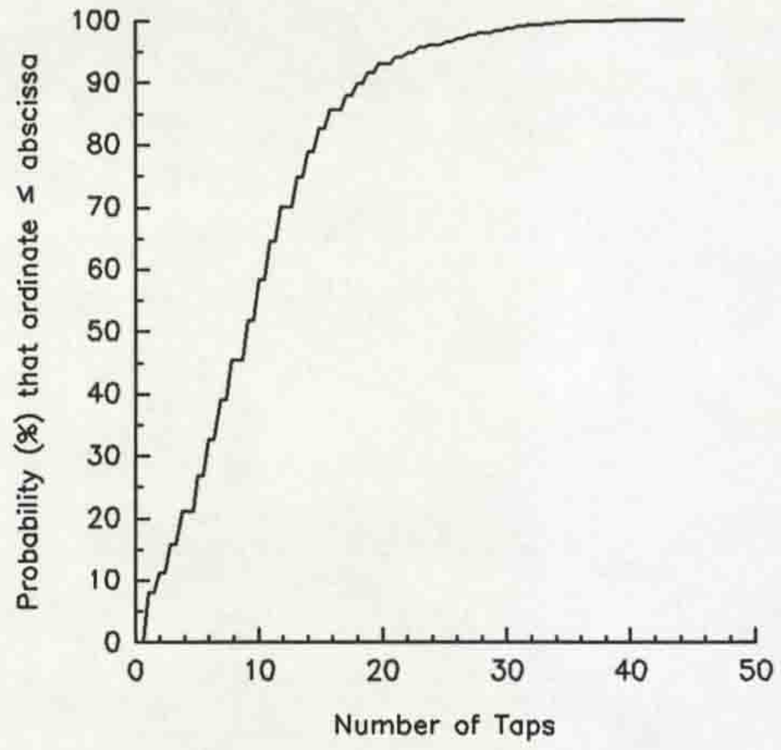

Figure 5.13 CDF of the number of taps for URBAN2.

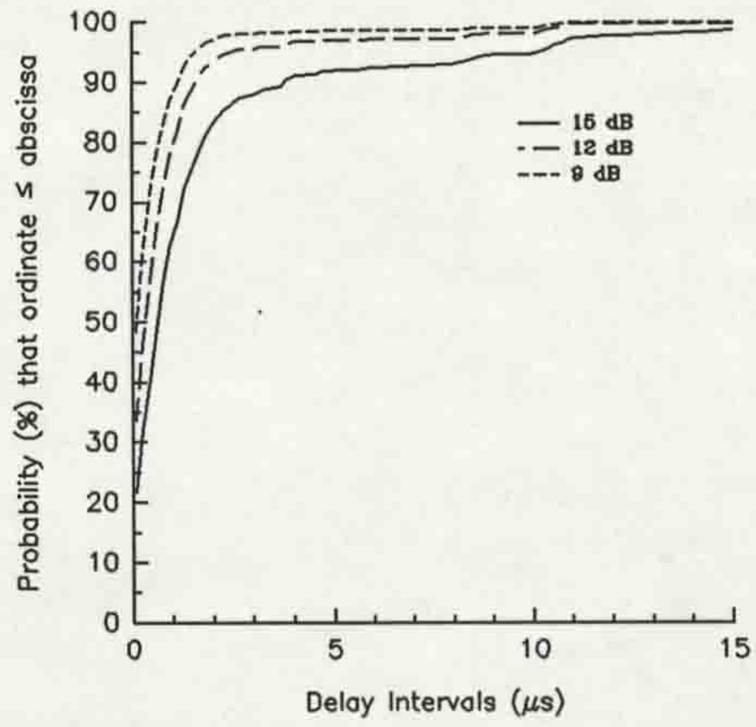

Figure 5.11 CDFs of delay intervals for URBAN2.

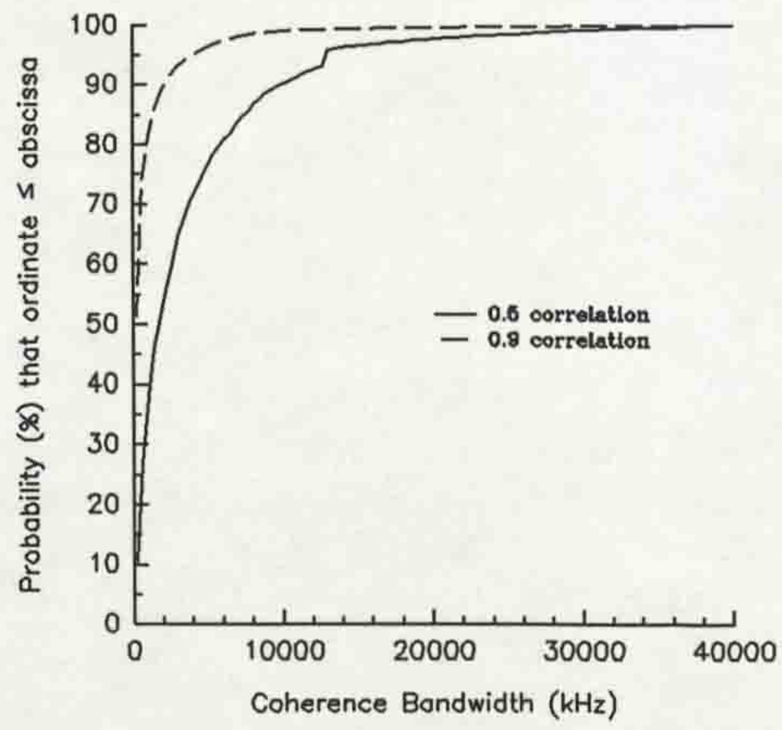

Figure 5.14 CDFs of the coherence bandwidths for URBAN2.

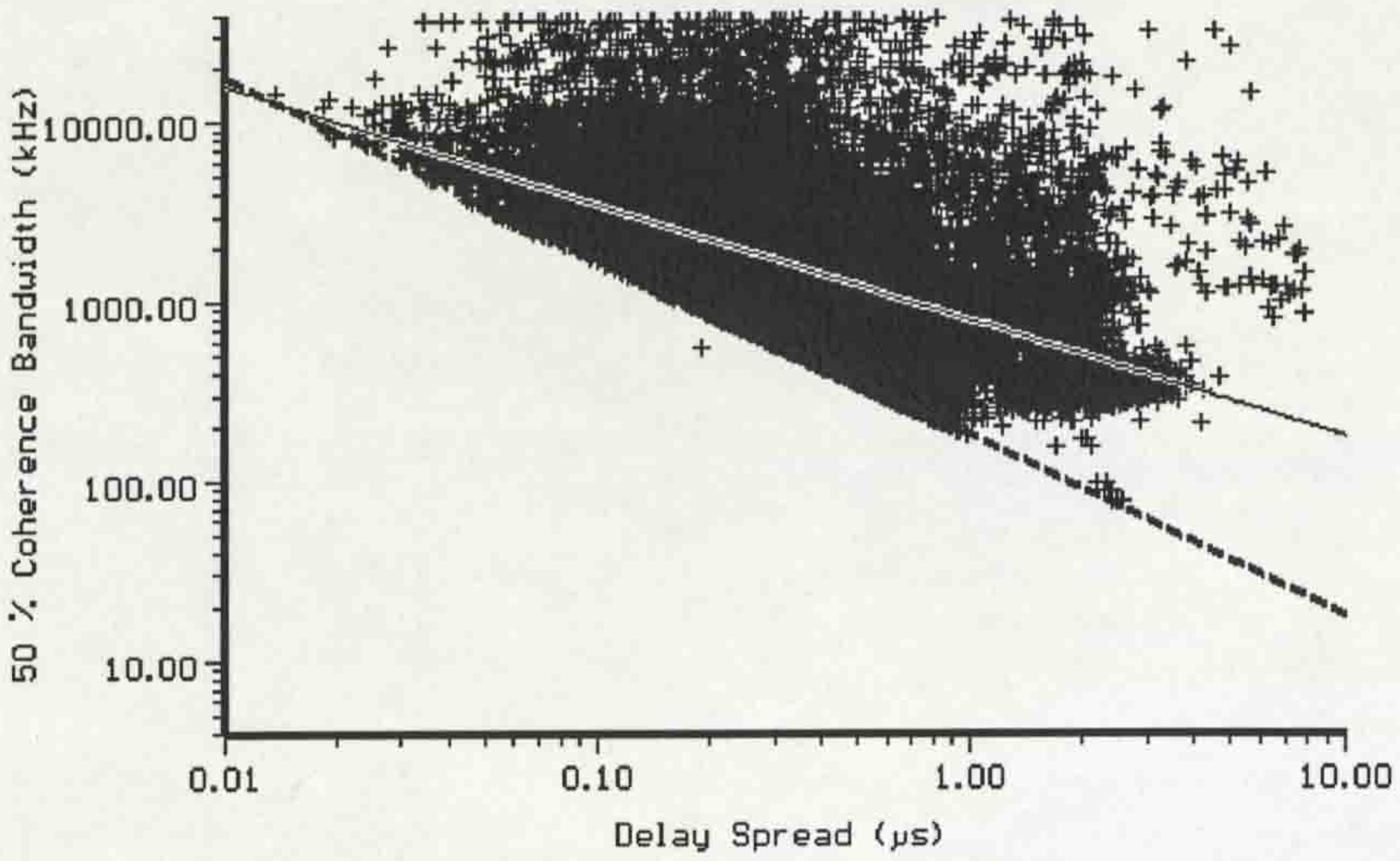

Figure 5.15 Scatter plot of coherence bandwidth at 0.5 correlation versus delay spread for URBAN2.

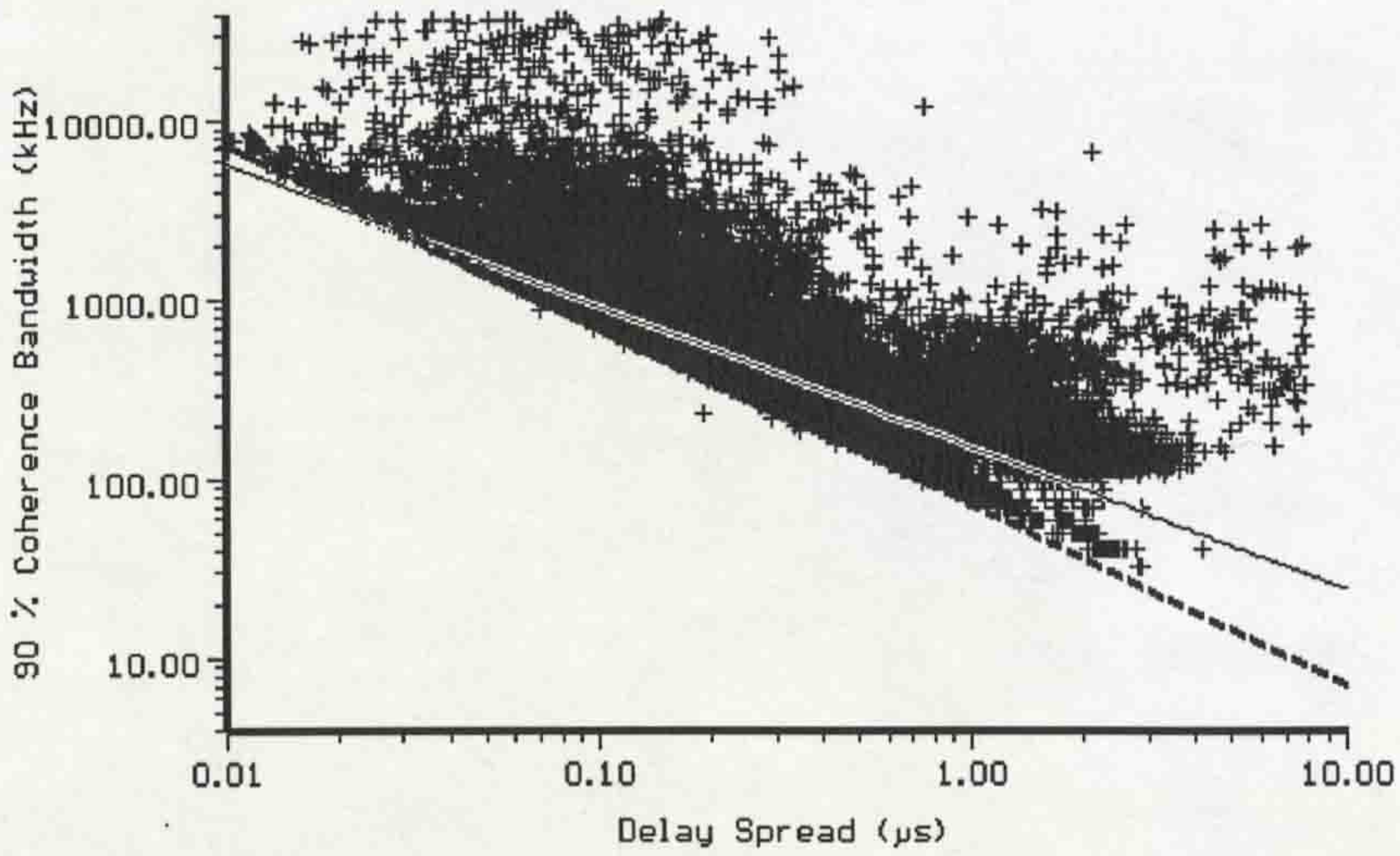

Figure 5.16 Scatter plot of coherence bandwidth at 0.9 correlation versus delay spread for URBAN2.

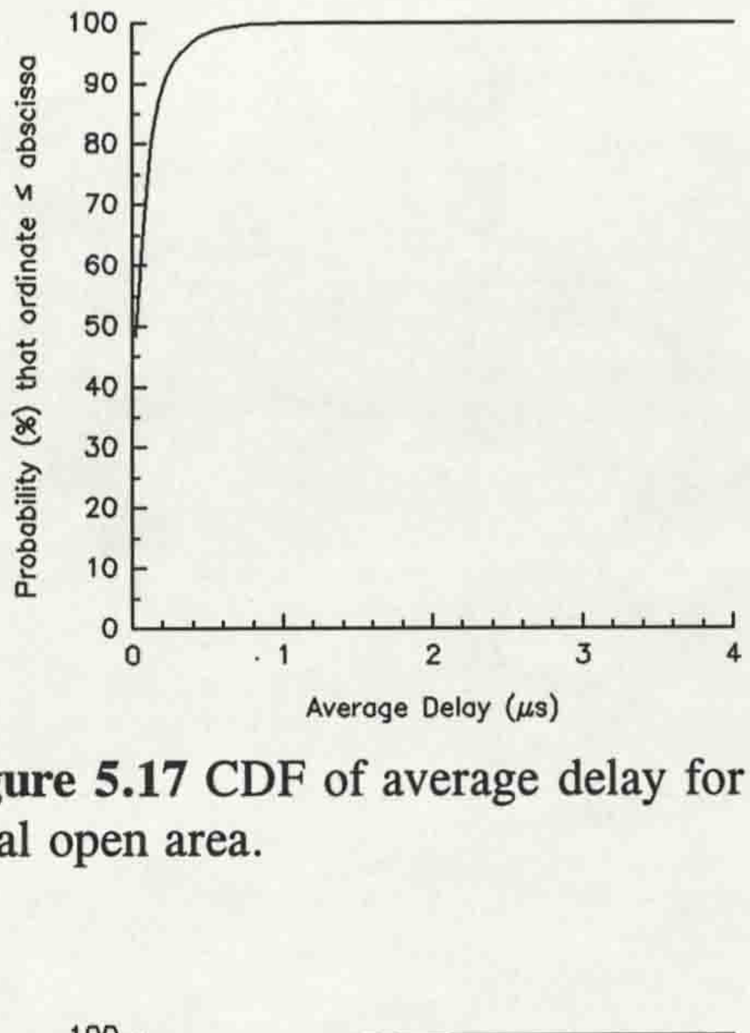

Figure 5.17 CDF of average delay for the rural open area.

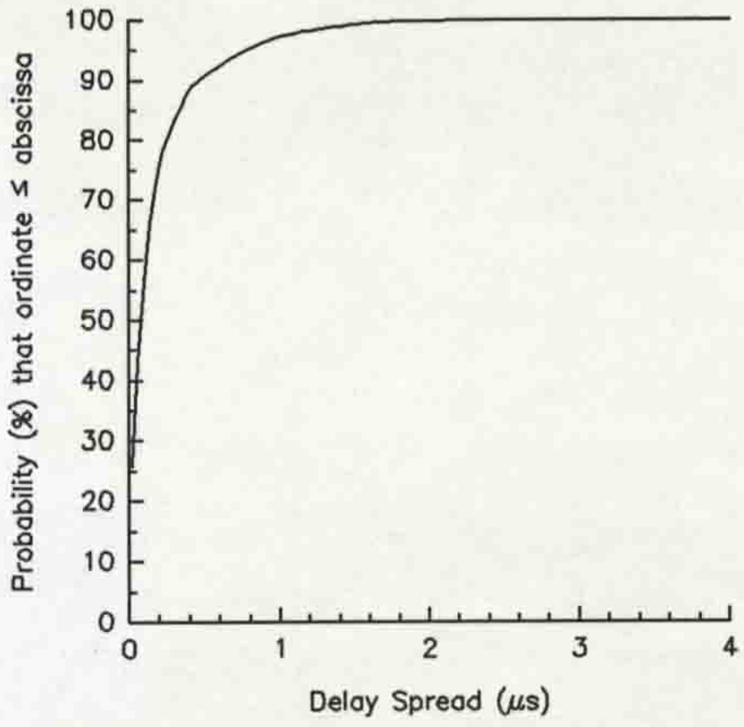

Figure 5.18 CDF of delay spread for the rural open area.

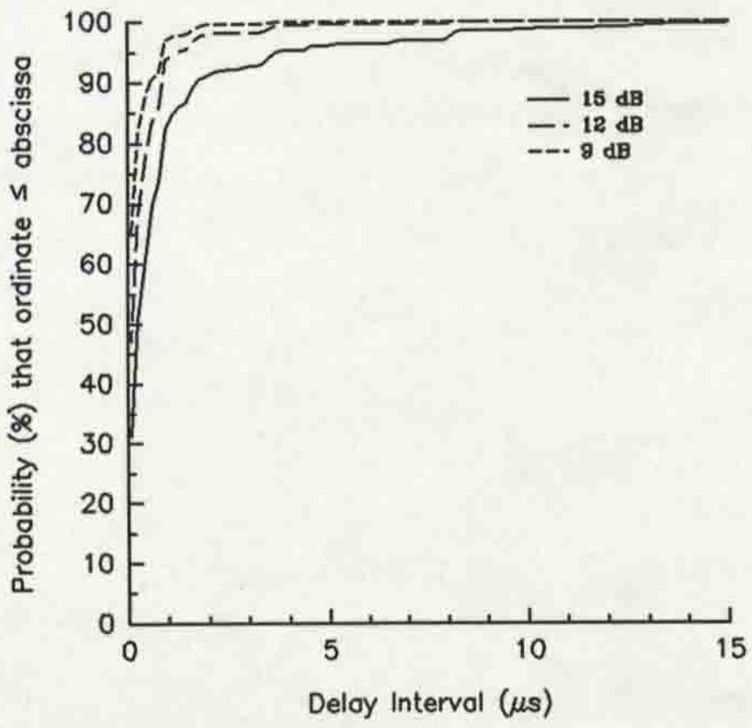

Figure 5.19 CDFs of delay intervals for the rural open area.

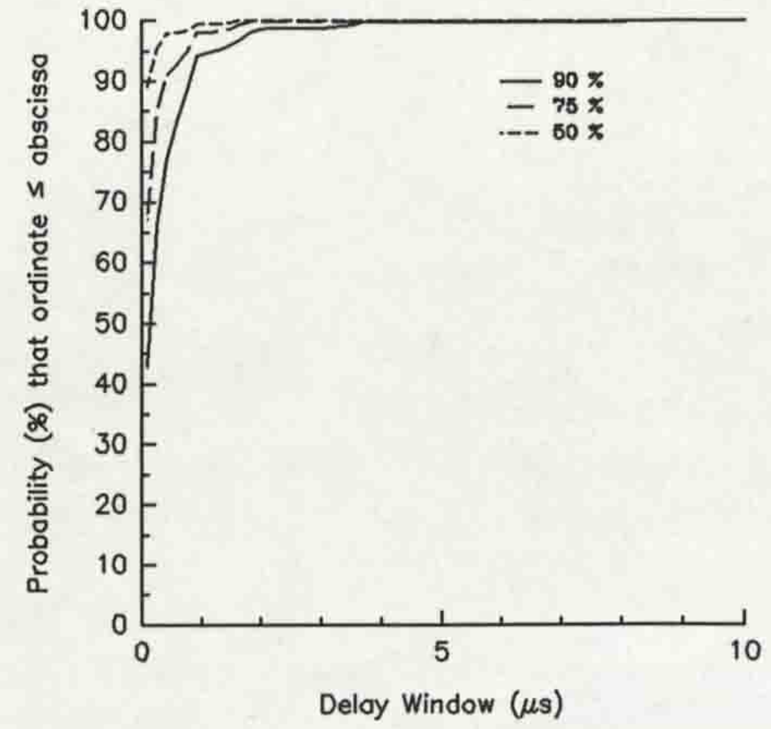

Figure 5.20 CDFs of delay windows for the rural open area.

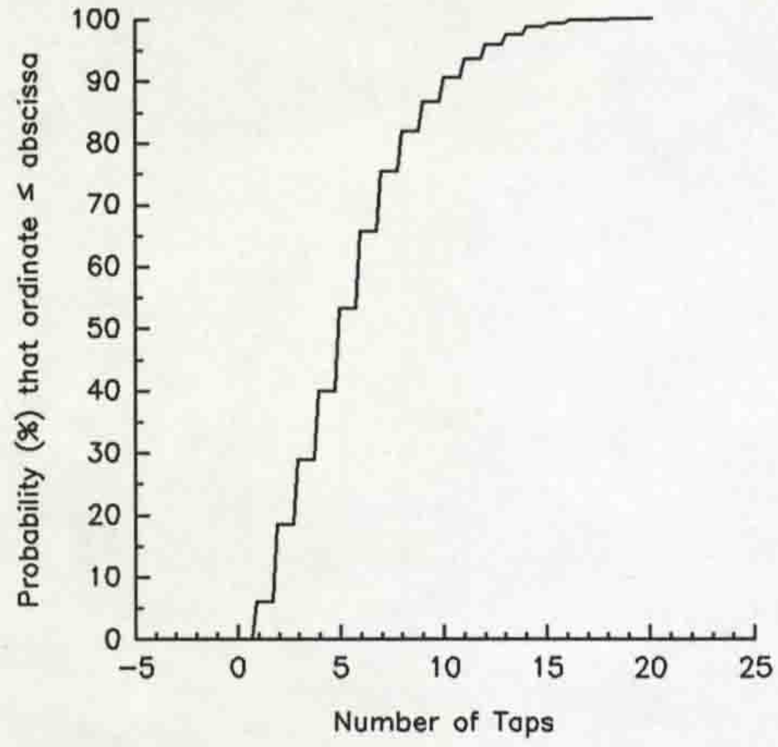

Figure 5.21 CDF of the number of taps for the rural open area.

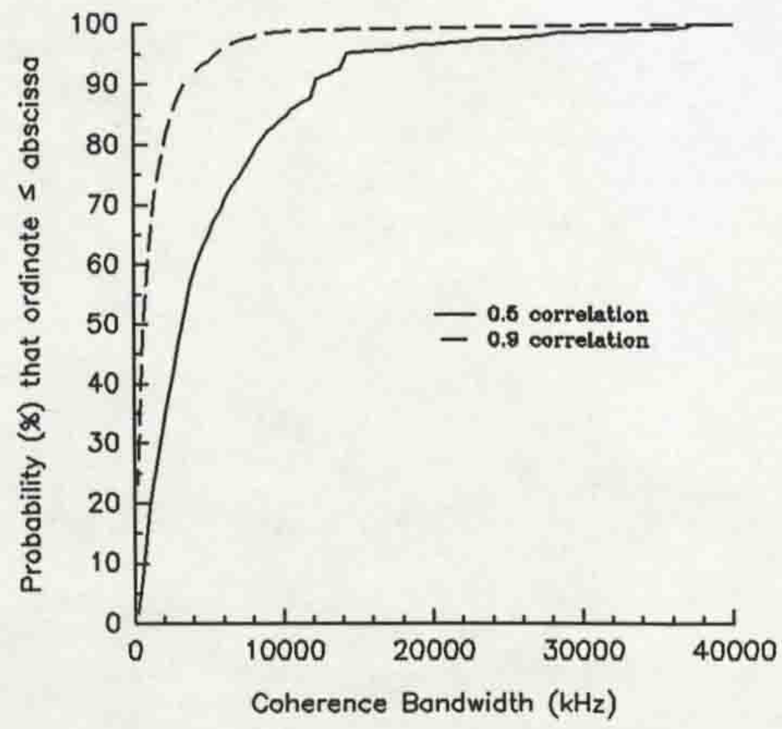

Figure 5.22 CDFs of the coherence bandwidths for the rural open area.

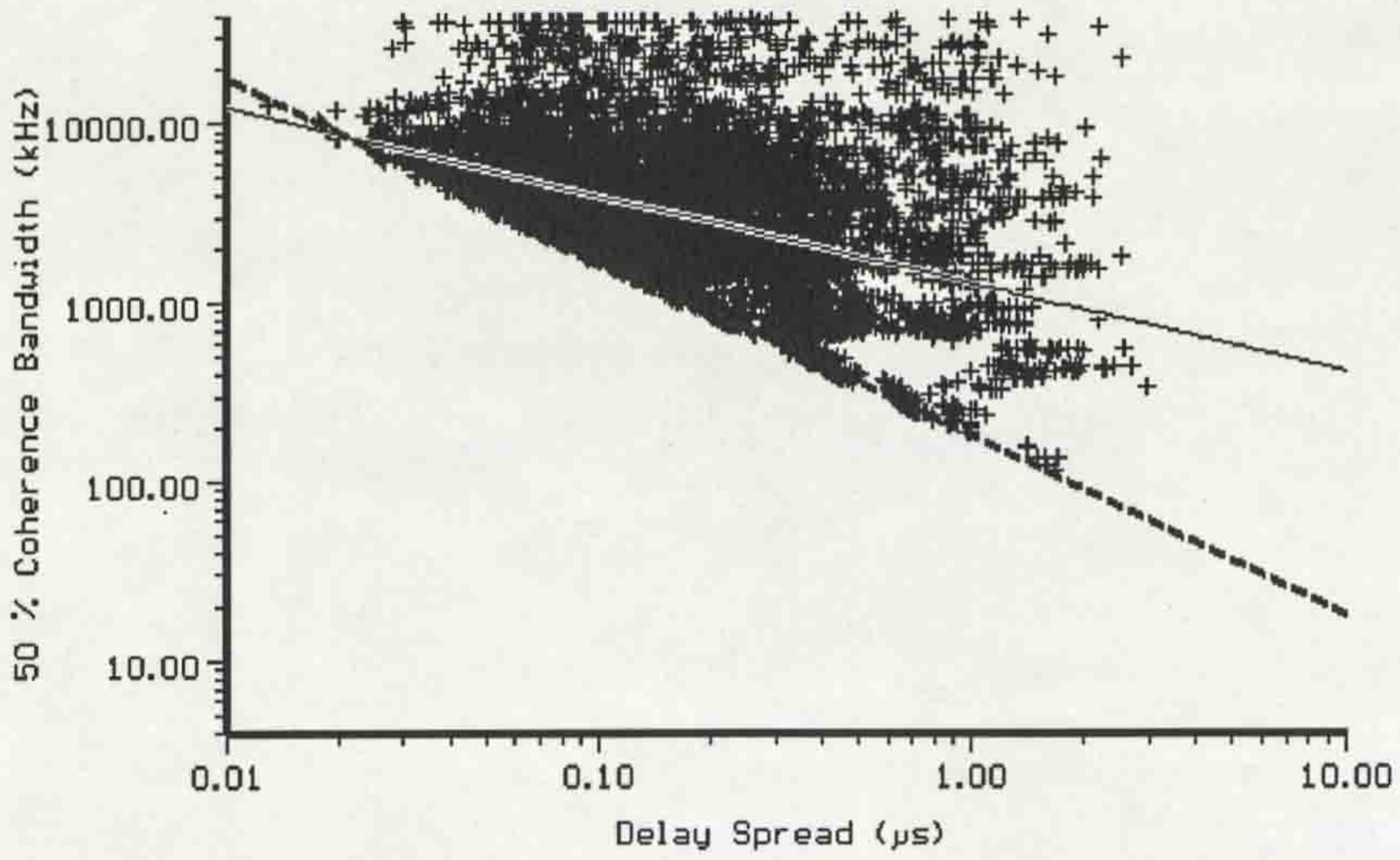

Figure 5.23 Scatter plot of coherence bandwidth at 0.5 correlation versus delay spread for the rural open area.

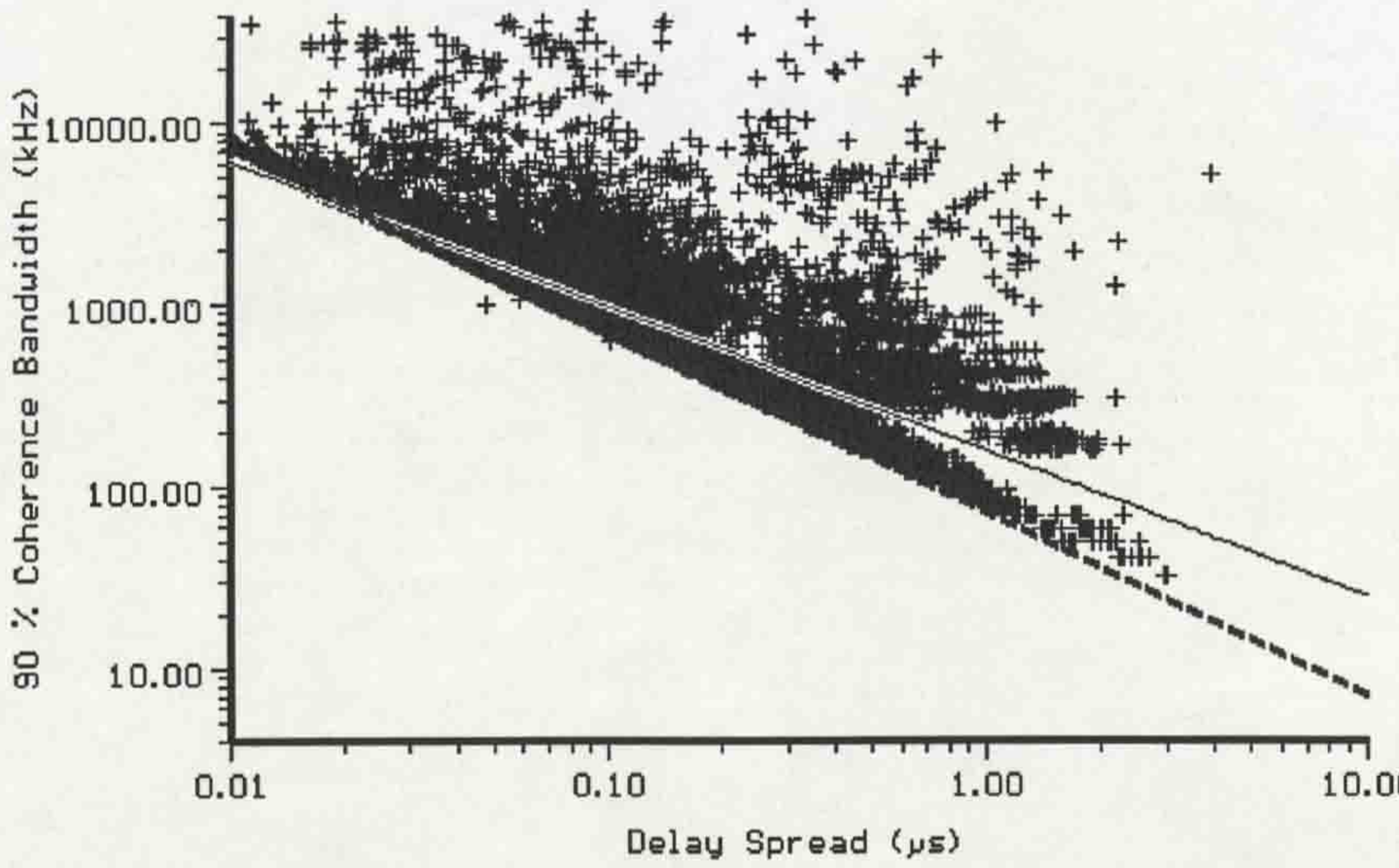

Figure 5.24 Scatter plot of coherence bandwidth at 0.9 correlation versus delay spread for the rural open area.

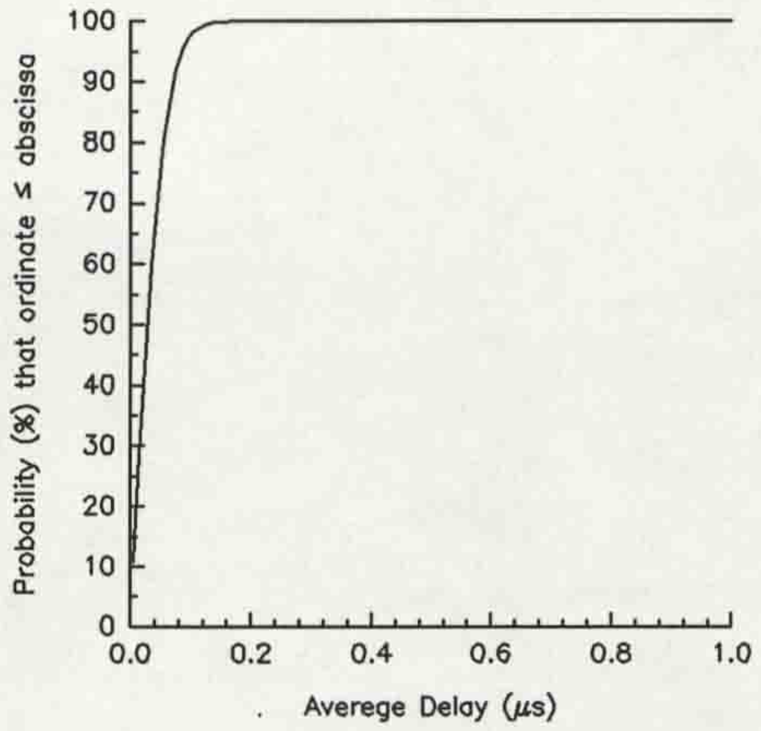

Figure 5.25 CDF of average delay for SMARKET1.

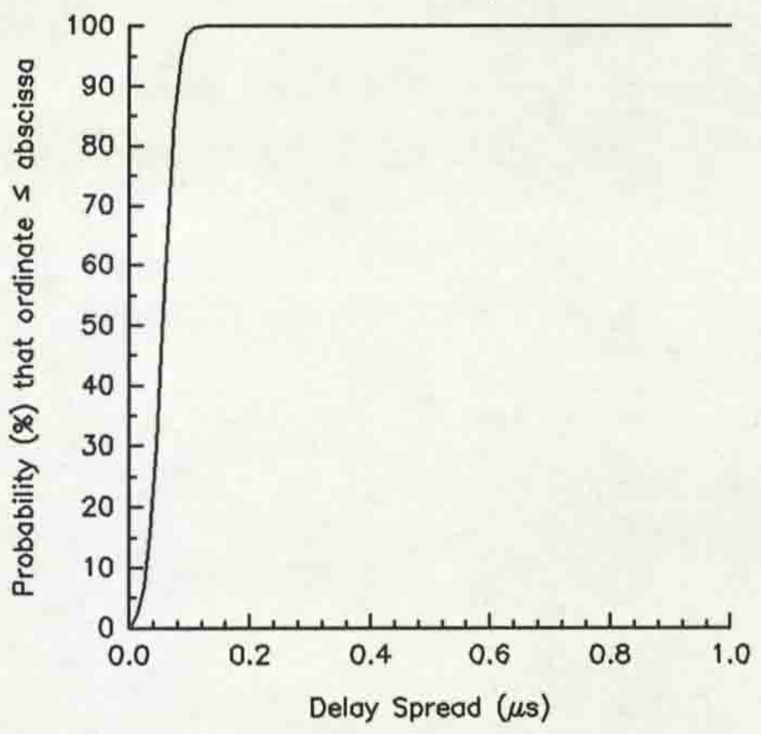

Figure 5.26 CDF of delay spread for SMARKET1.

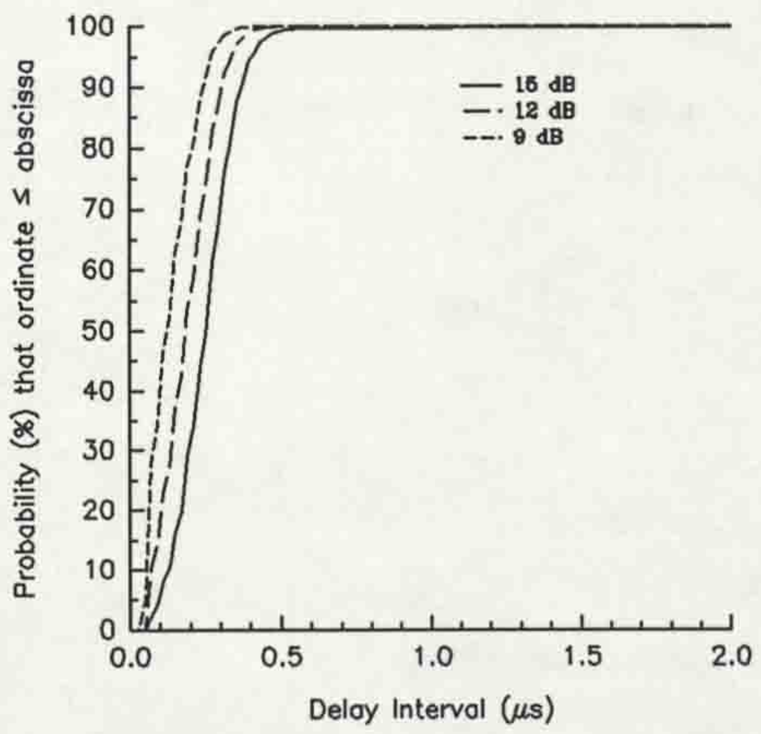

Figure 5.27 CDFs of delay intervals for SMARKET1.

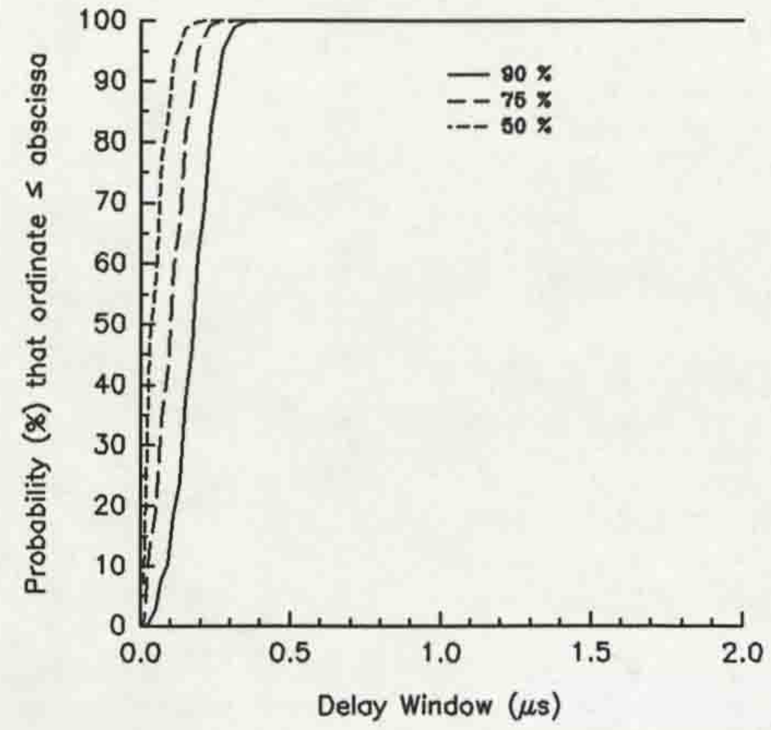

Figure 5.28 CDFs of delay windows for SMARKET1.

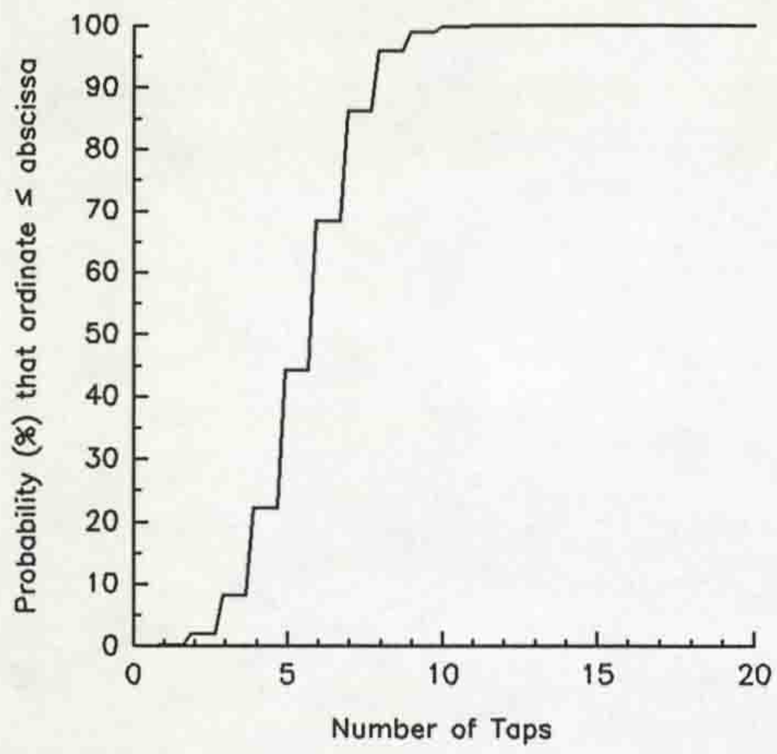

Figure 5.29 CDF of the number of taps for SMARKET1.

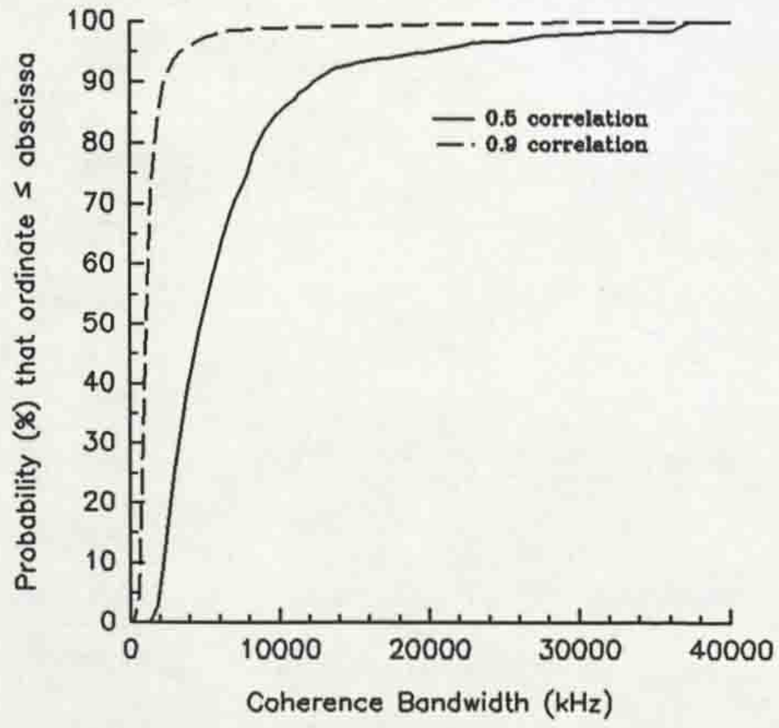

Figure 5.30 CDFs of the coherence bandwidths for SMARKET1.

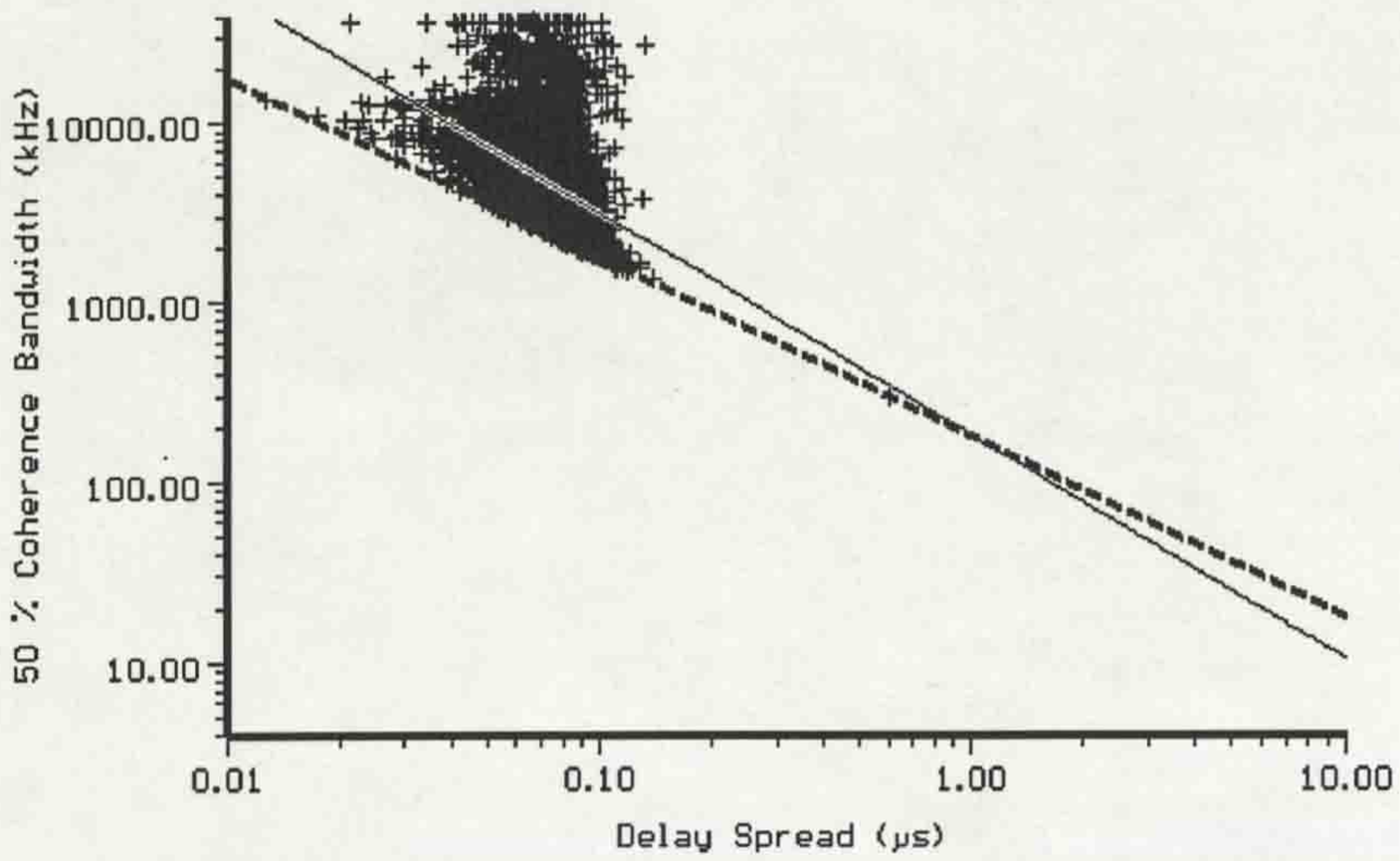

Figure 5.31 Scatter plot of coherence bandwidth at 0.5 correlation versus delay spread for SMARKET1.

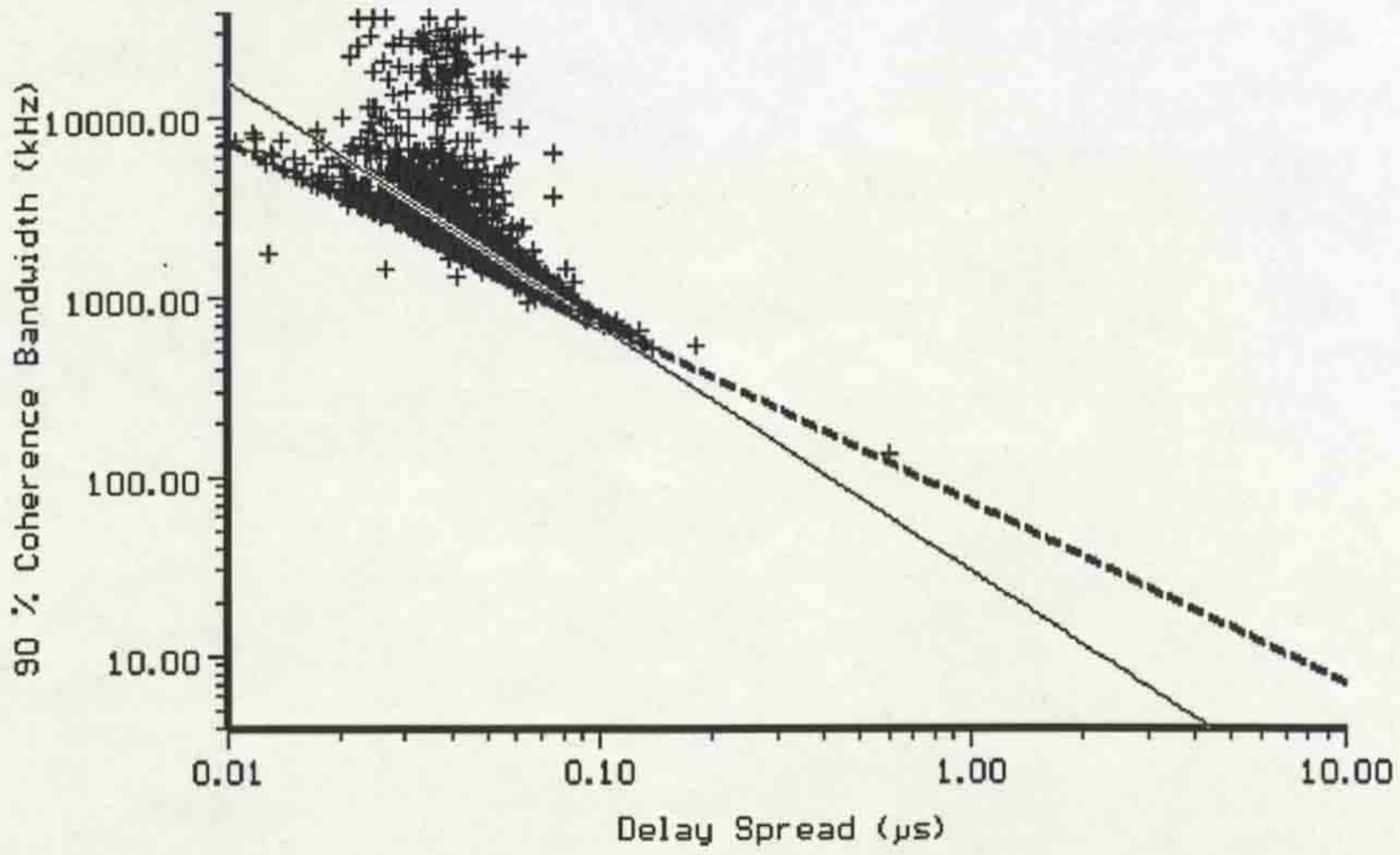

Figure 5.32 Scatter plot of coherence bandwidth at 0.9 correlation versus delay spread for SMARKET1.

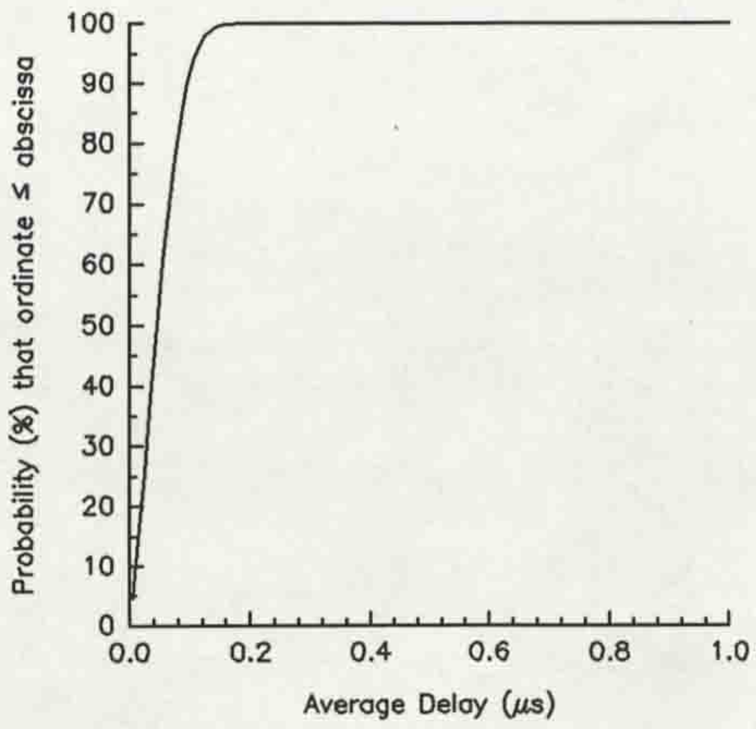

Figure 5.33 CDF of average delay for SMARKET2.

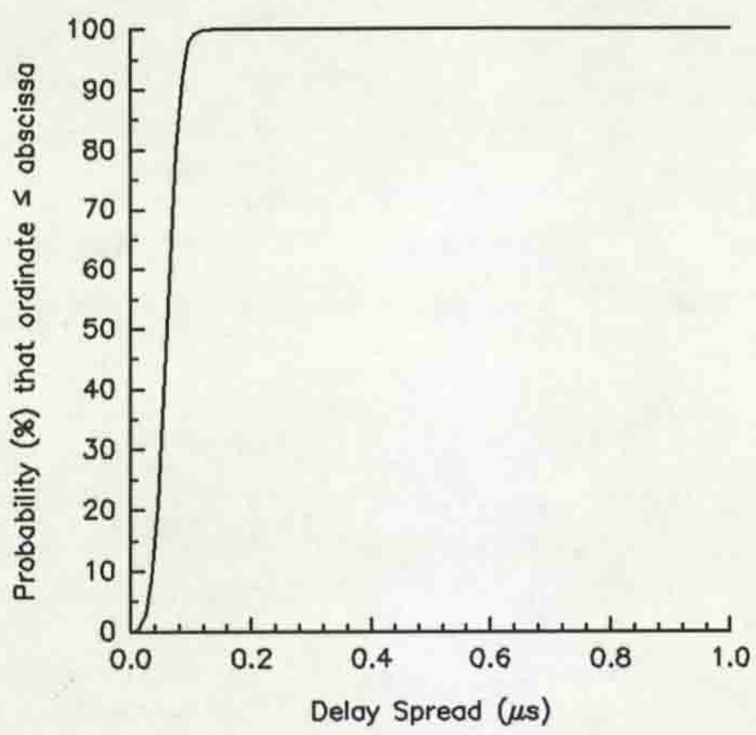

Figure 5.34 CDF of delay spread for SMARKET2.

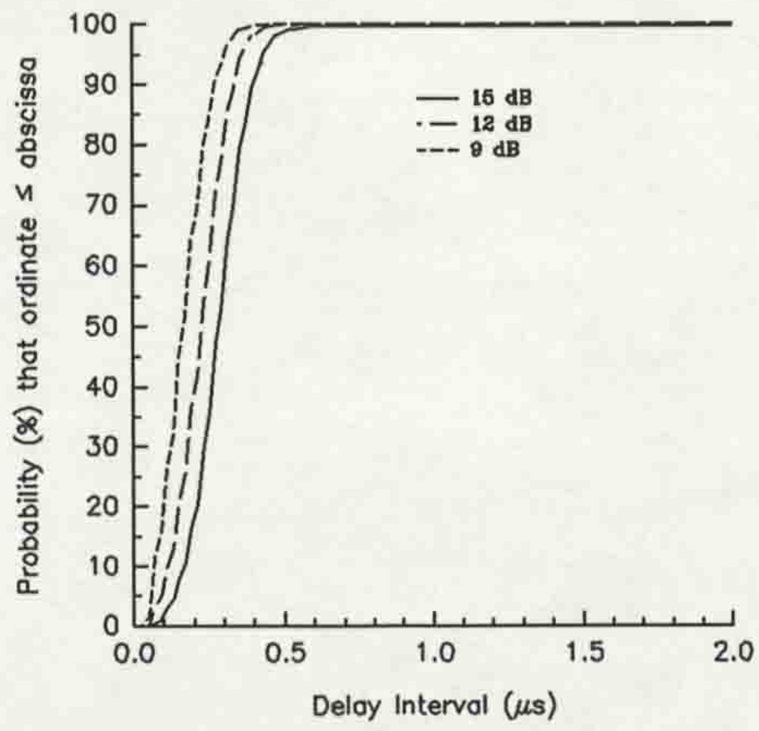

Figure 5.35 CDFs of delay intervals for SMARKET2.

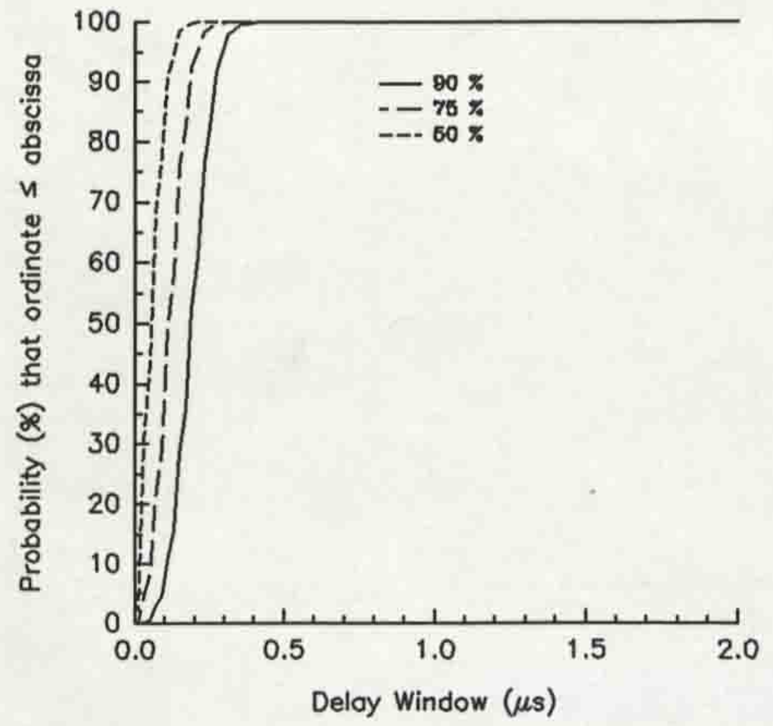

Figure 5.36 CDFs of delay windows for SMARKET2.

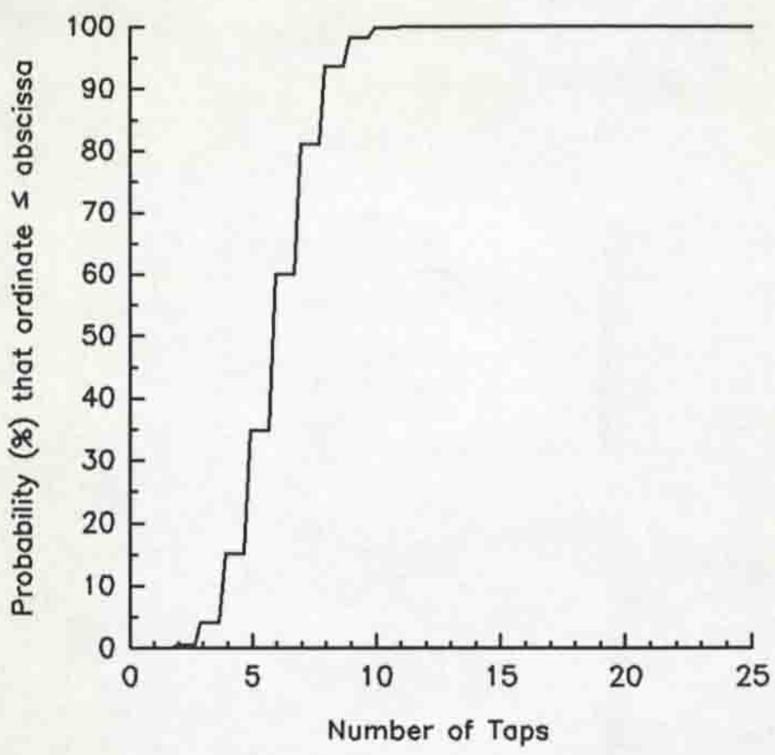

Figure 5.37 CDF of the number of taps for SMARKET2.

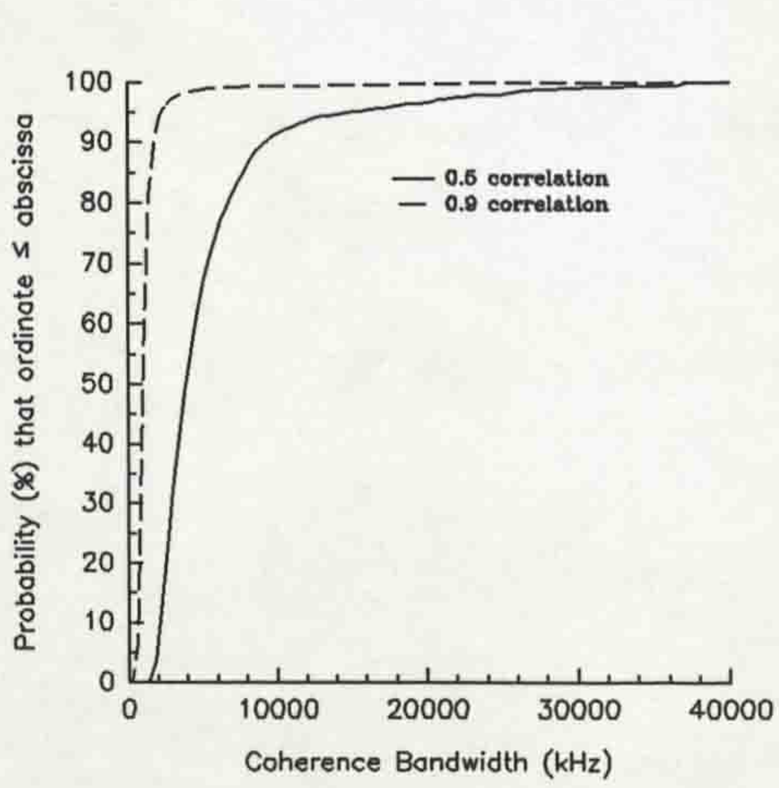

Figure 5.38 CDFs of the coherence bandwidths for SMARKET2.

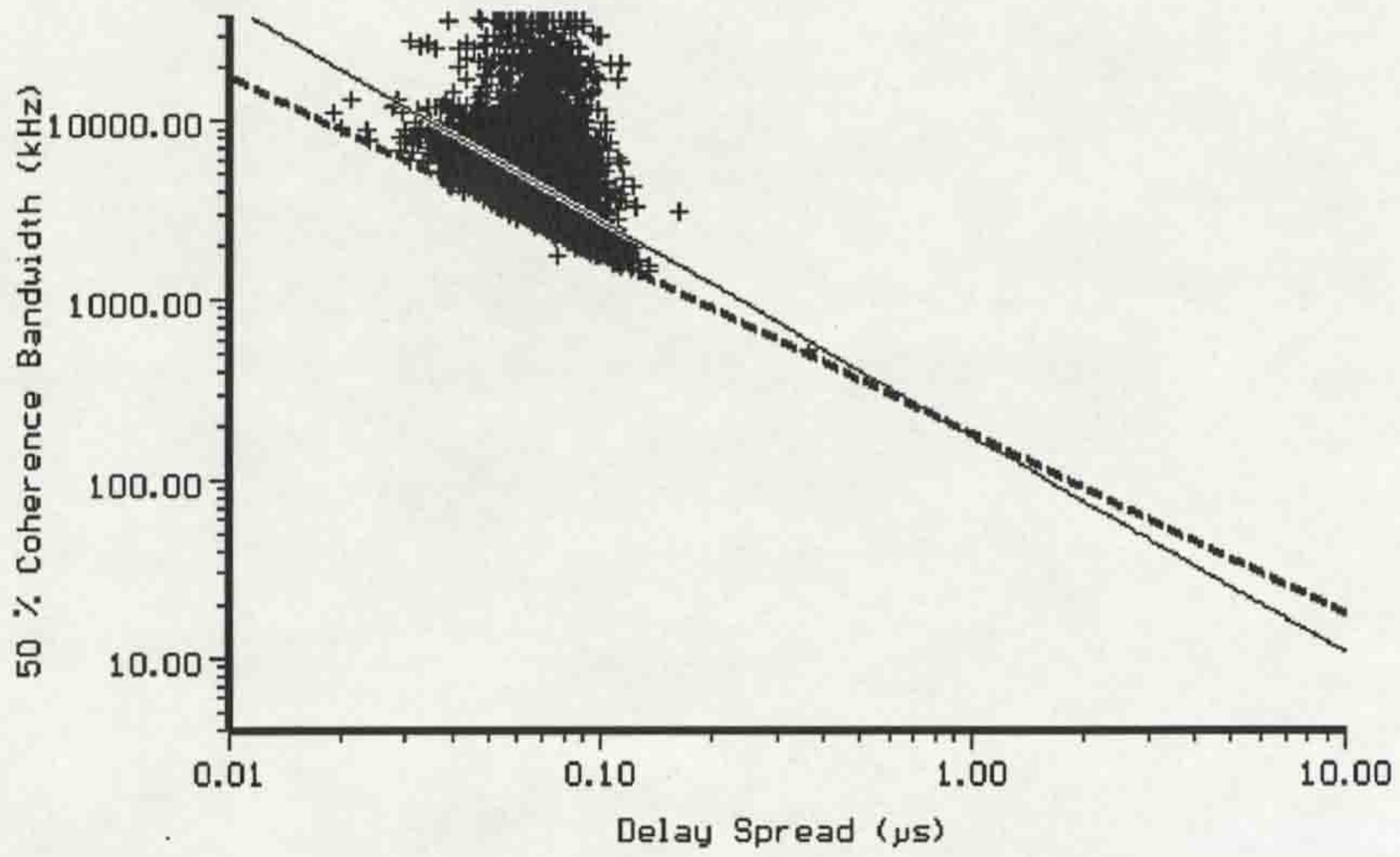

Figure 5.39 Scatter plot of coherence bandwidth at 0.5 correlation versus delay spread for SMARKET2.

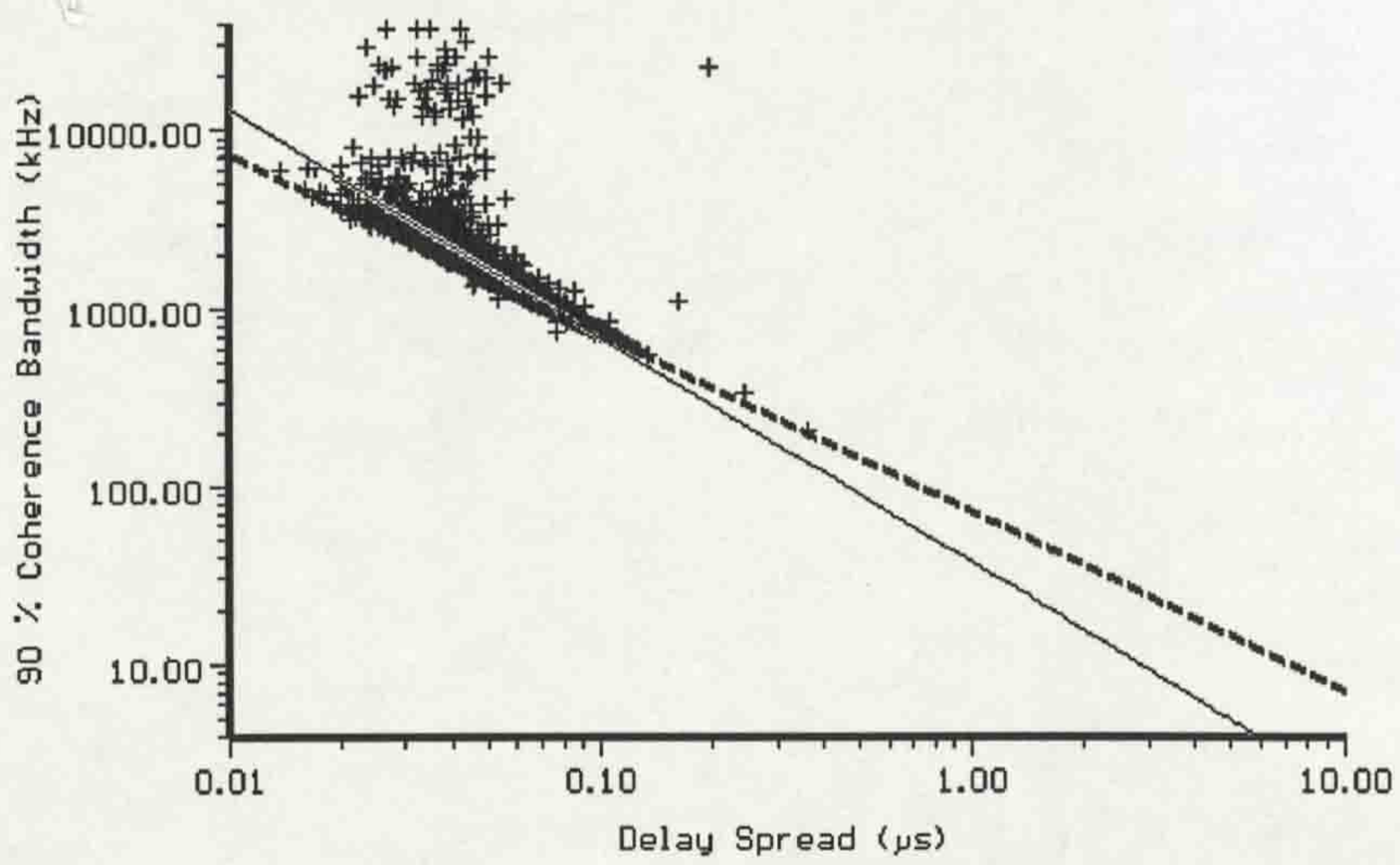

Figure 5.40 Scatter plot of coherence bandwidth at 0.9 correlation versus delay spread for SMARKET2.

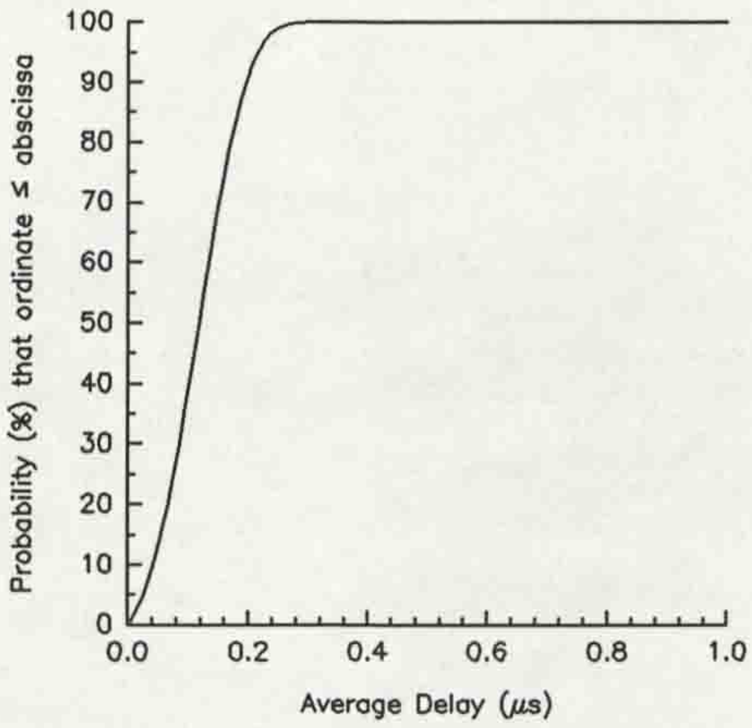

Figure 5.41 CDF of average delay for the train station.

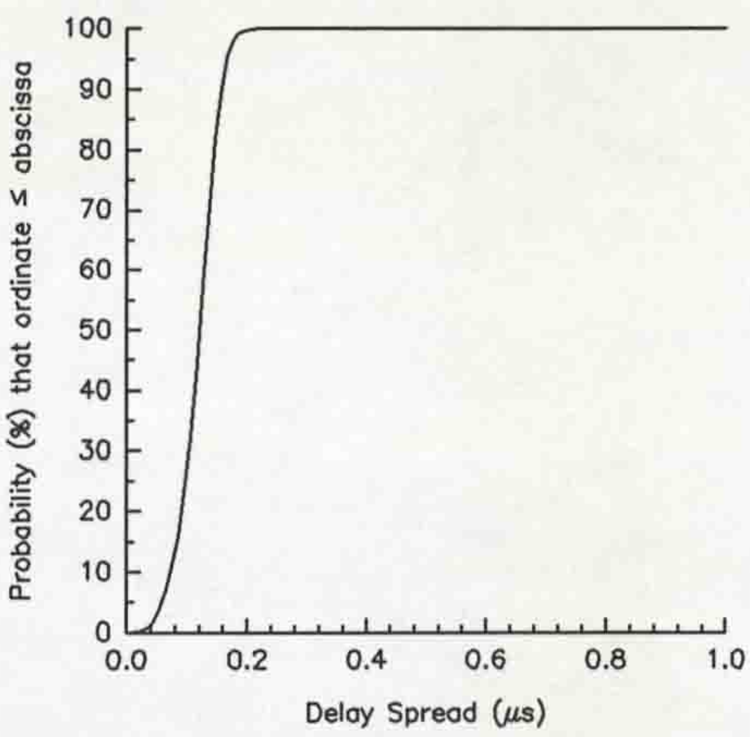

Figure 5.42 CDF of delay spread for the train station.

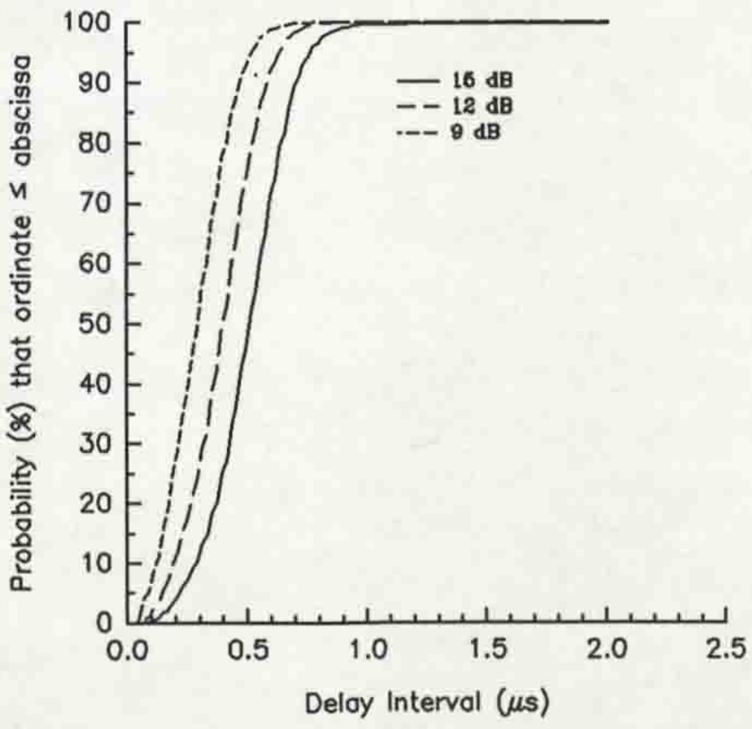

Figure 5.43 CDFs of delay intervals for the train station.

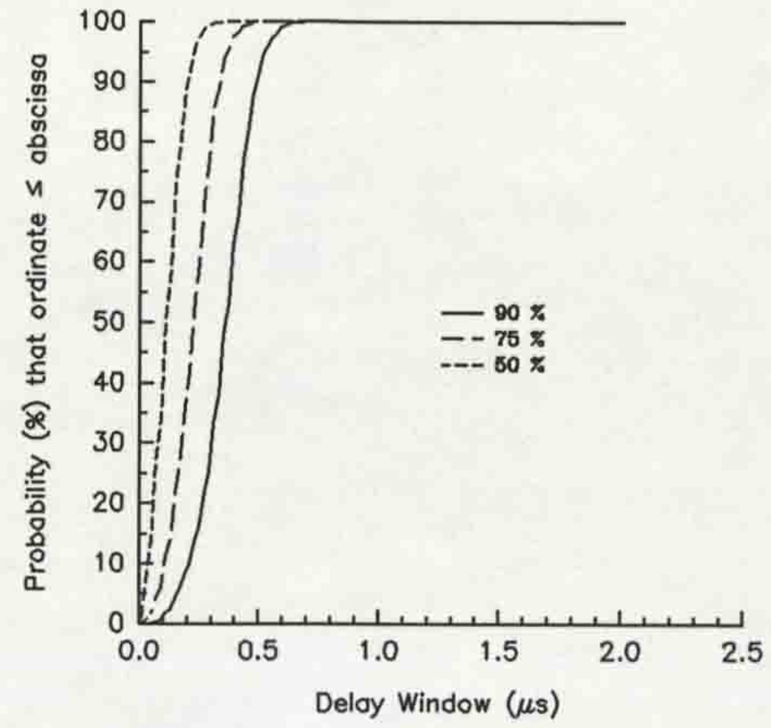

Figure 5.44 CDFs of delay windows for the train station.

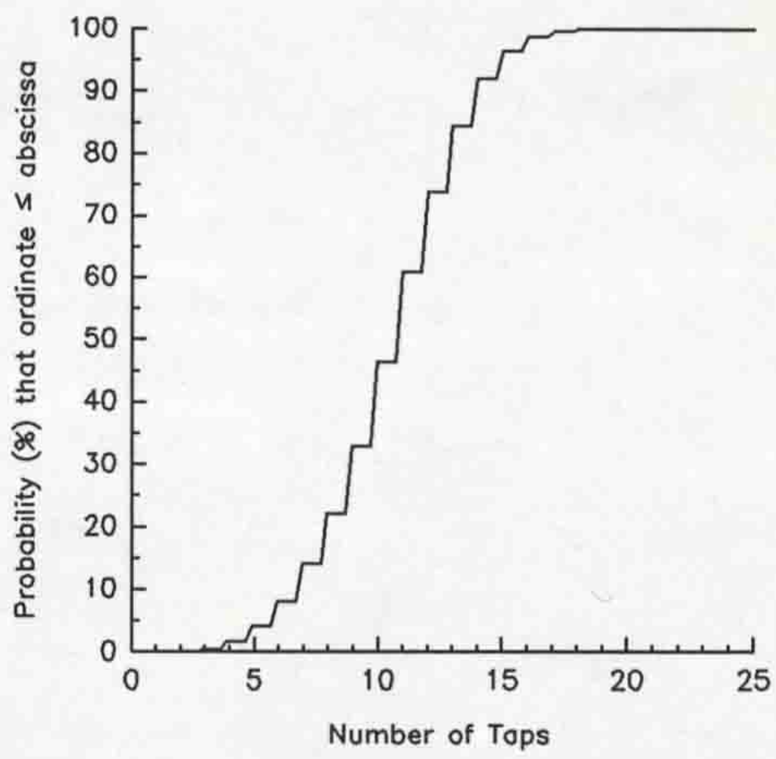

Figure 5.45 CDF of the number of taps for the train station.

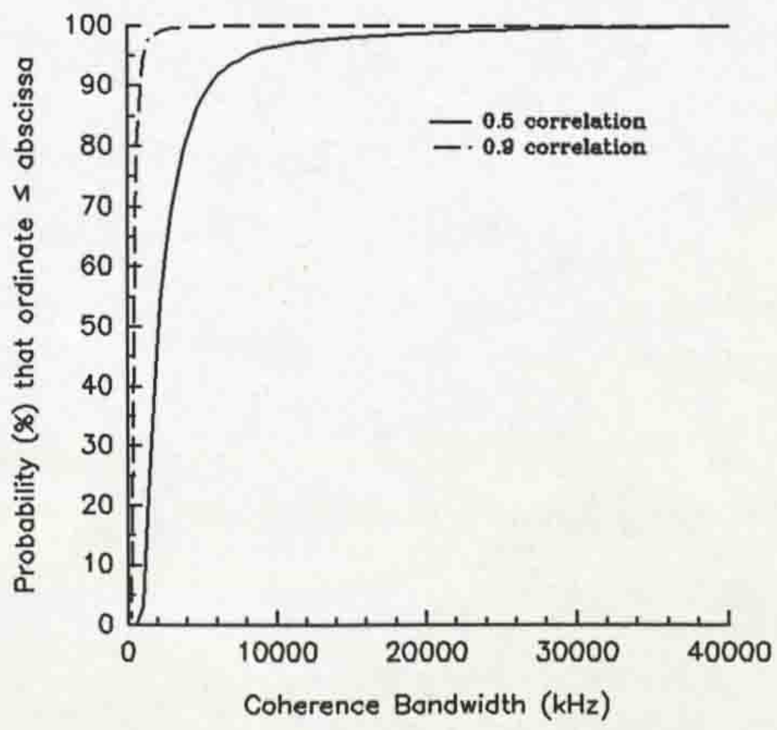

Figure 5.46 CDFs of the coherence bandwidths for the train station.

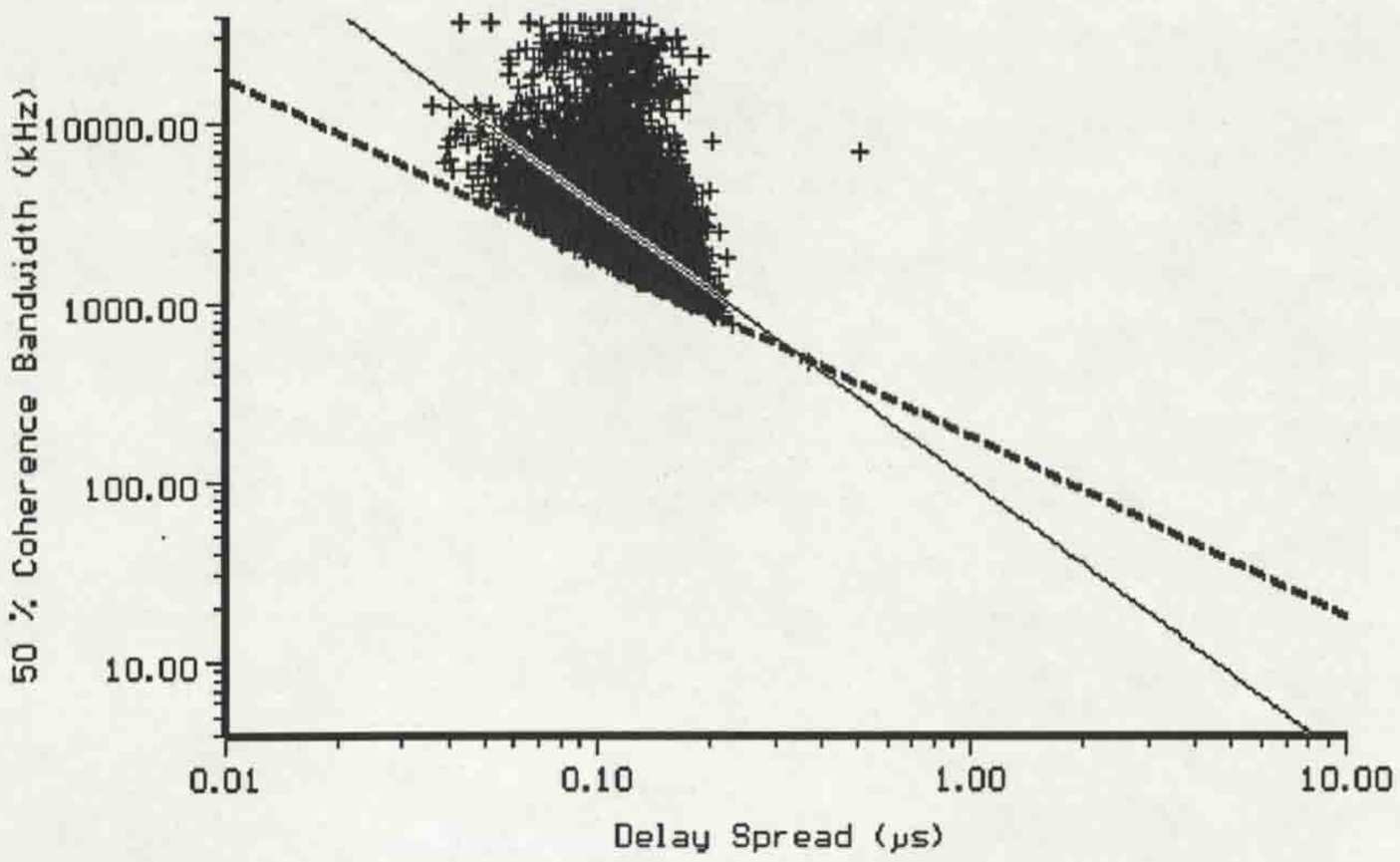

Figure 5.47 Scatter plot of coherence bandwidth at 0.5 correlation versus delay spread for the train station.

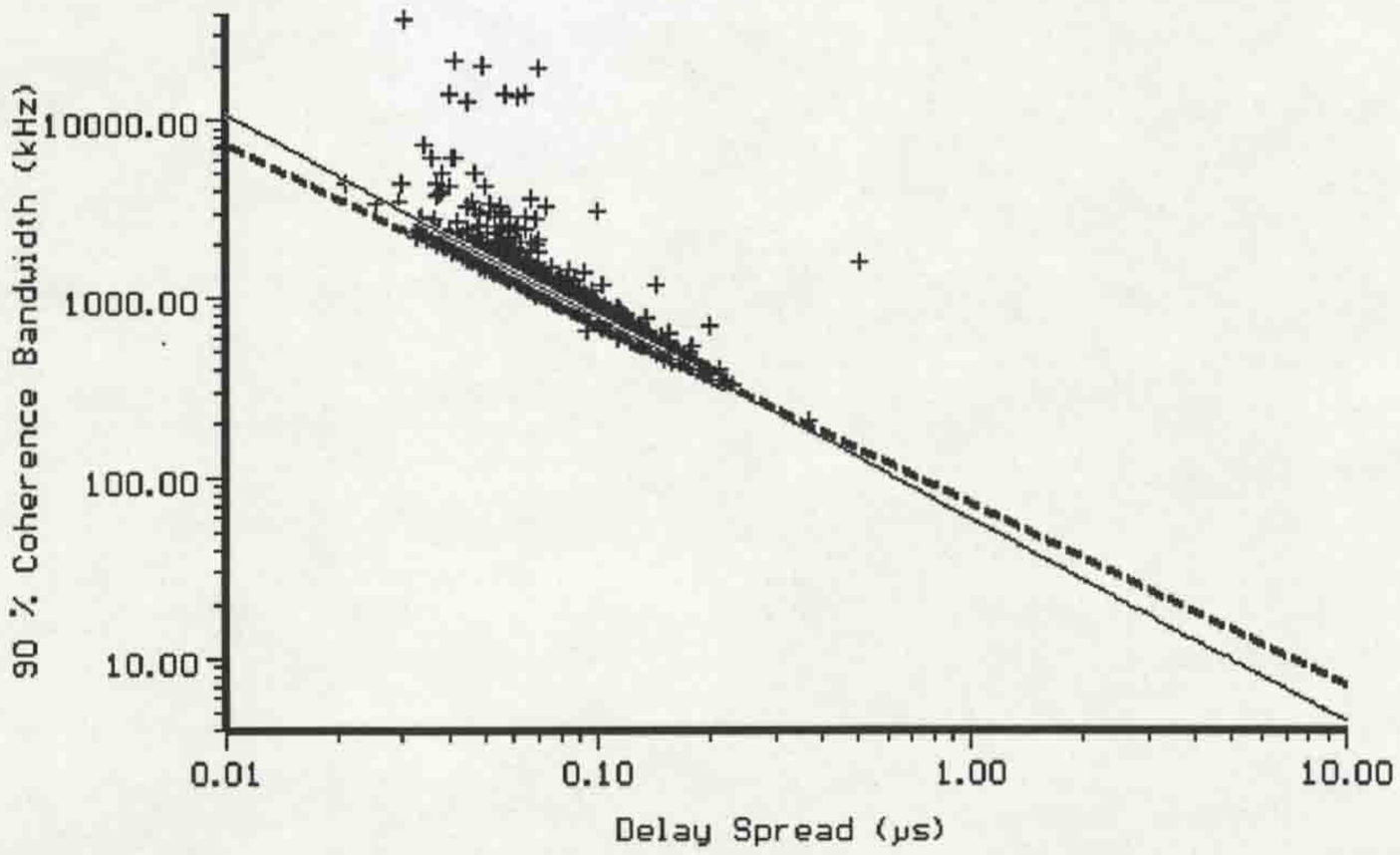

Figure 5.48 Scatter plot of coherence bandwidth at 0.9 correlation versus delay spread for the train station

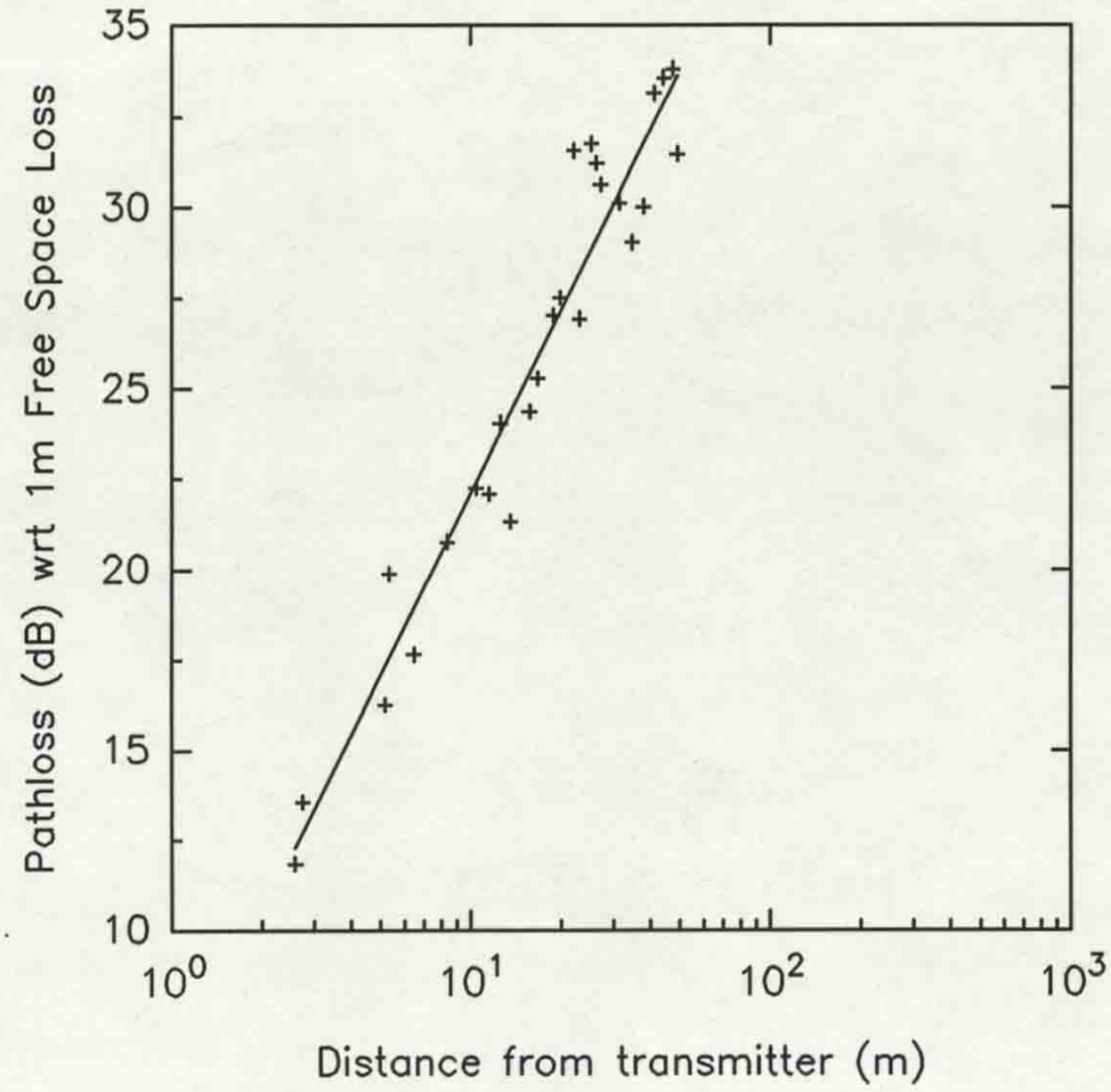

Figure 5.49 Measured pathloss versus distance in one of the main aisles (M2) in SMARKET1.

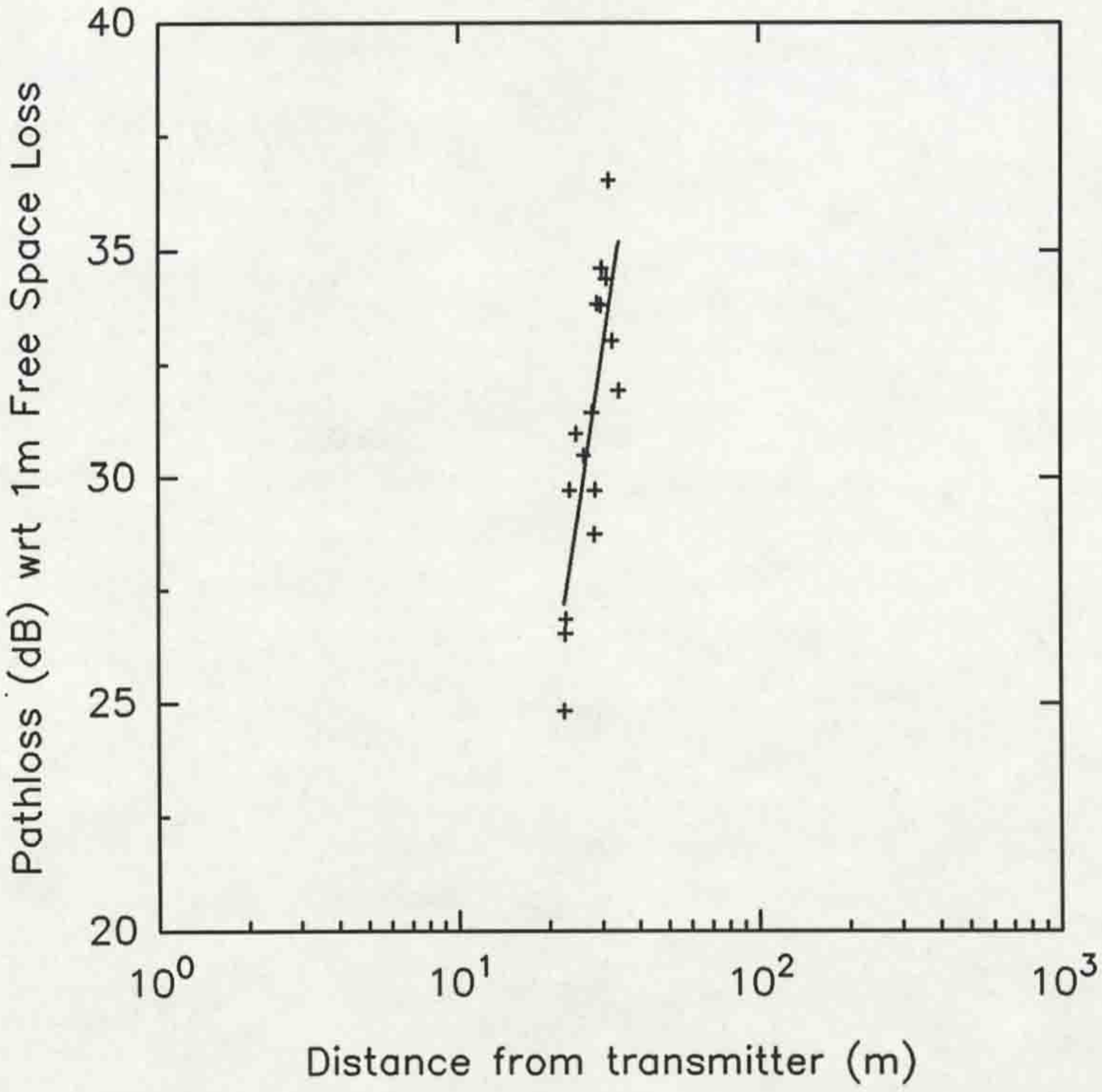

Figure 5.50 Measured pathloss versus distance for main aisle 1 (M1) in SMARKET1.

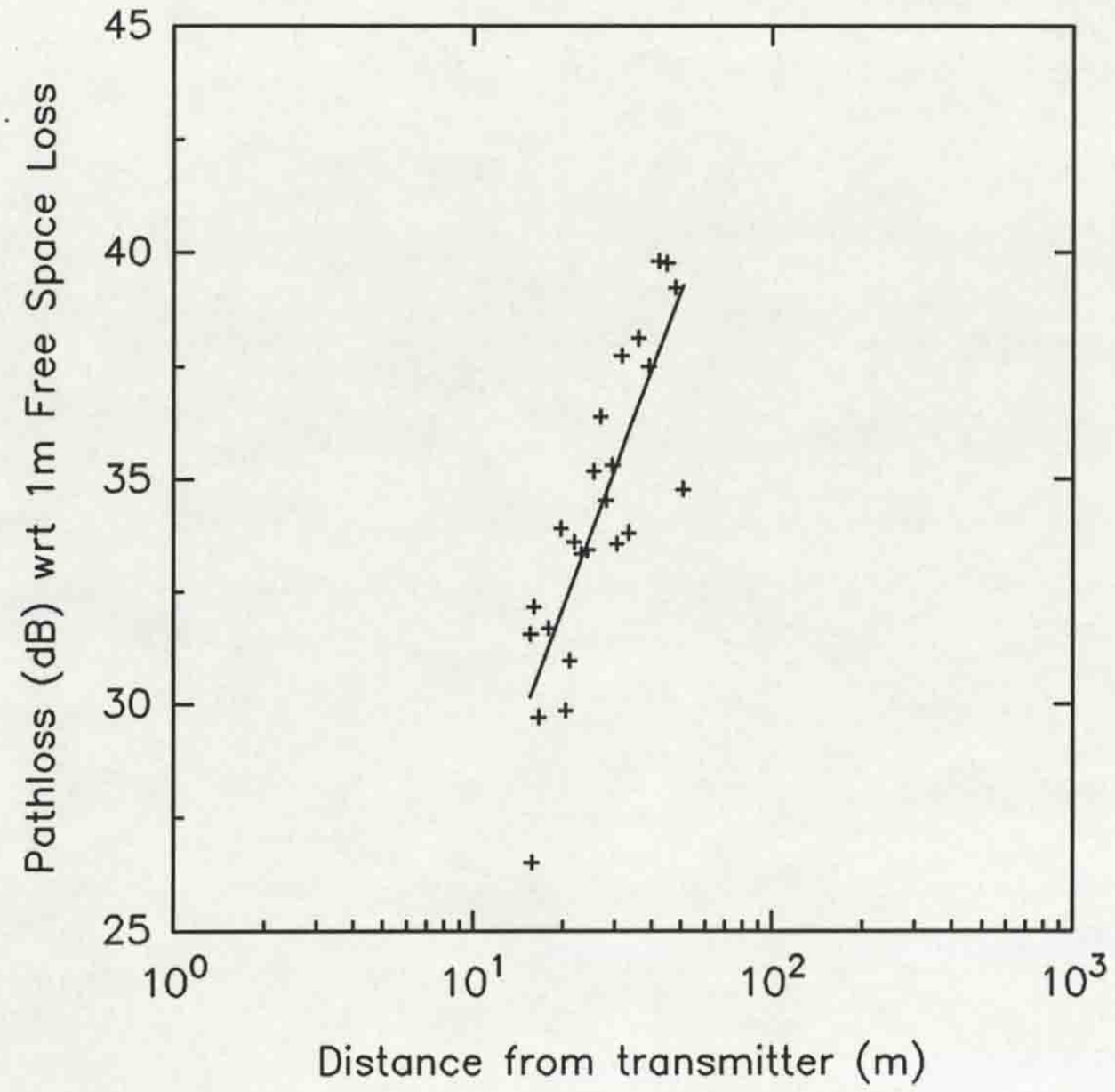

Figure 5.51 Measured pathloss versus distance for main aisle 3 (M3) in SMARKET1.

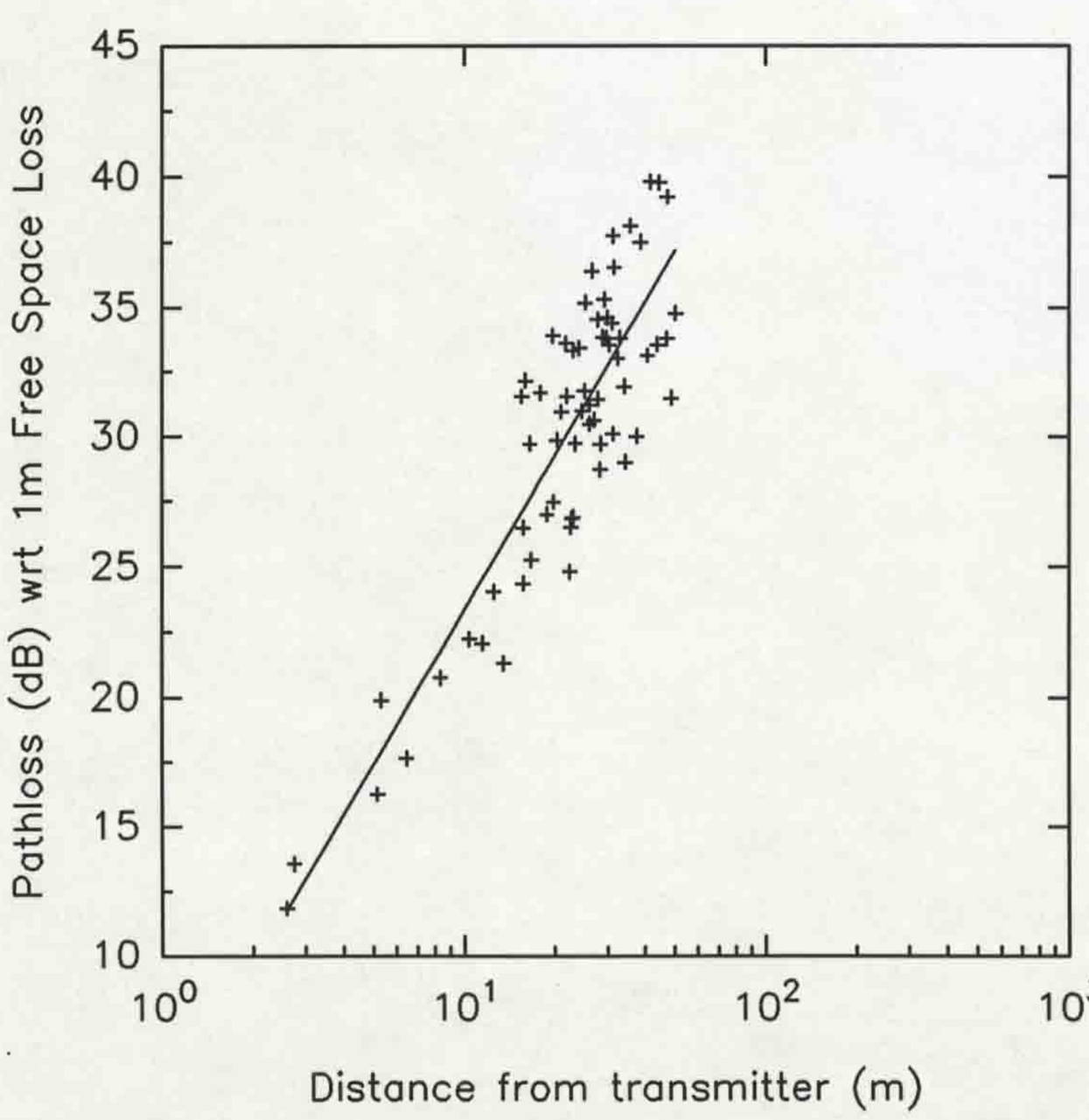

Figure 5.52 Measured pathloss versus distance for all main aisles in SMARKET1.

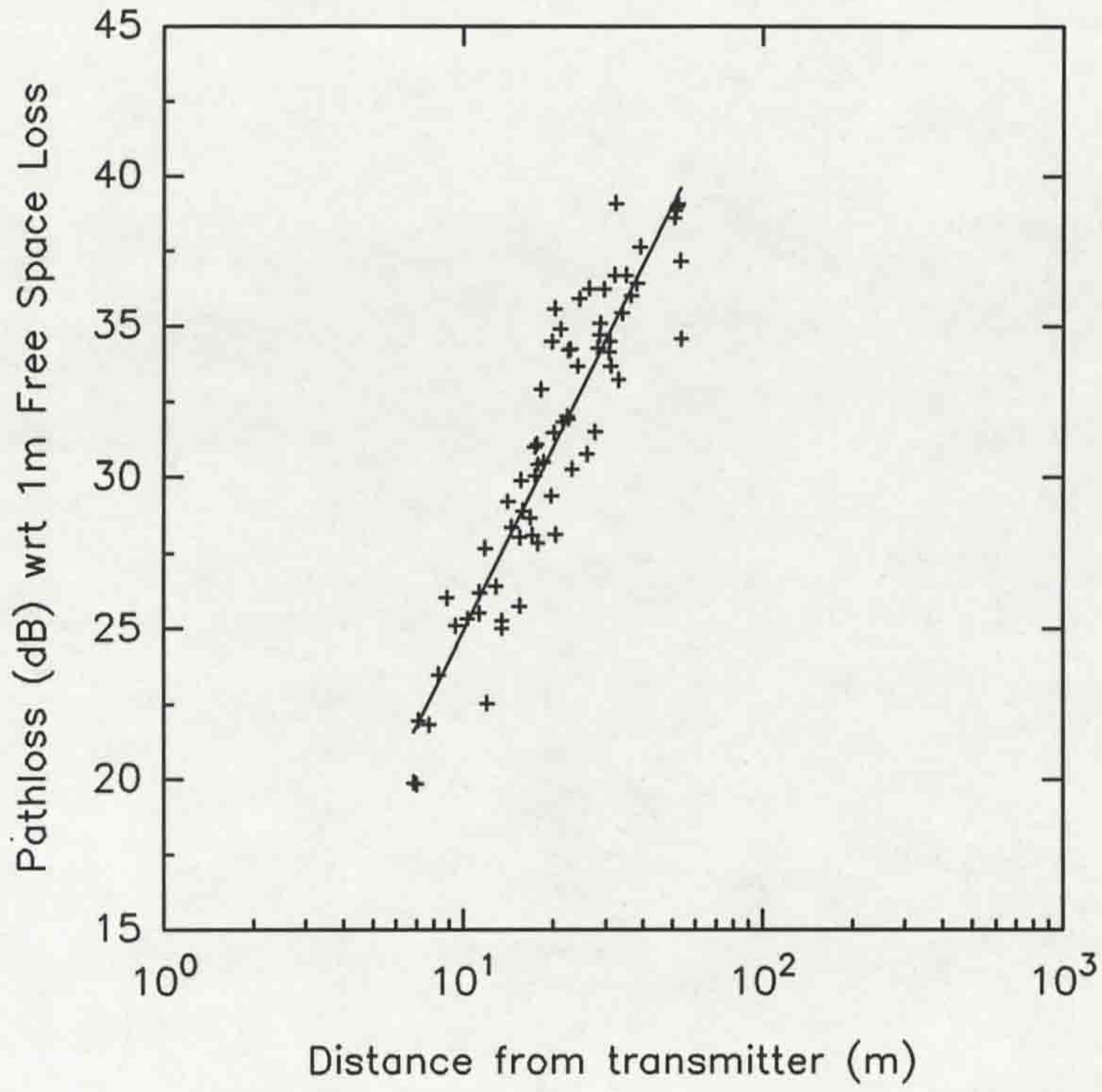

Figure 5.53. Measured pathloss versus distance for all the minor aisles in SMARKET1.

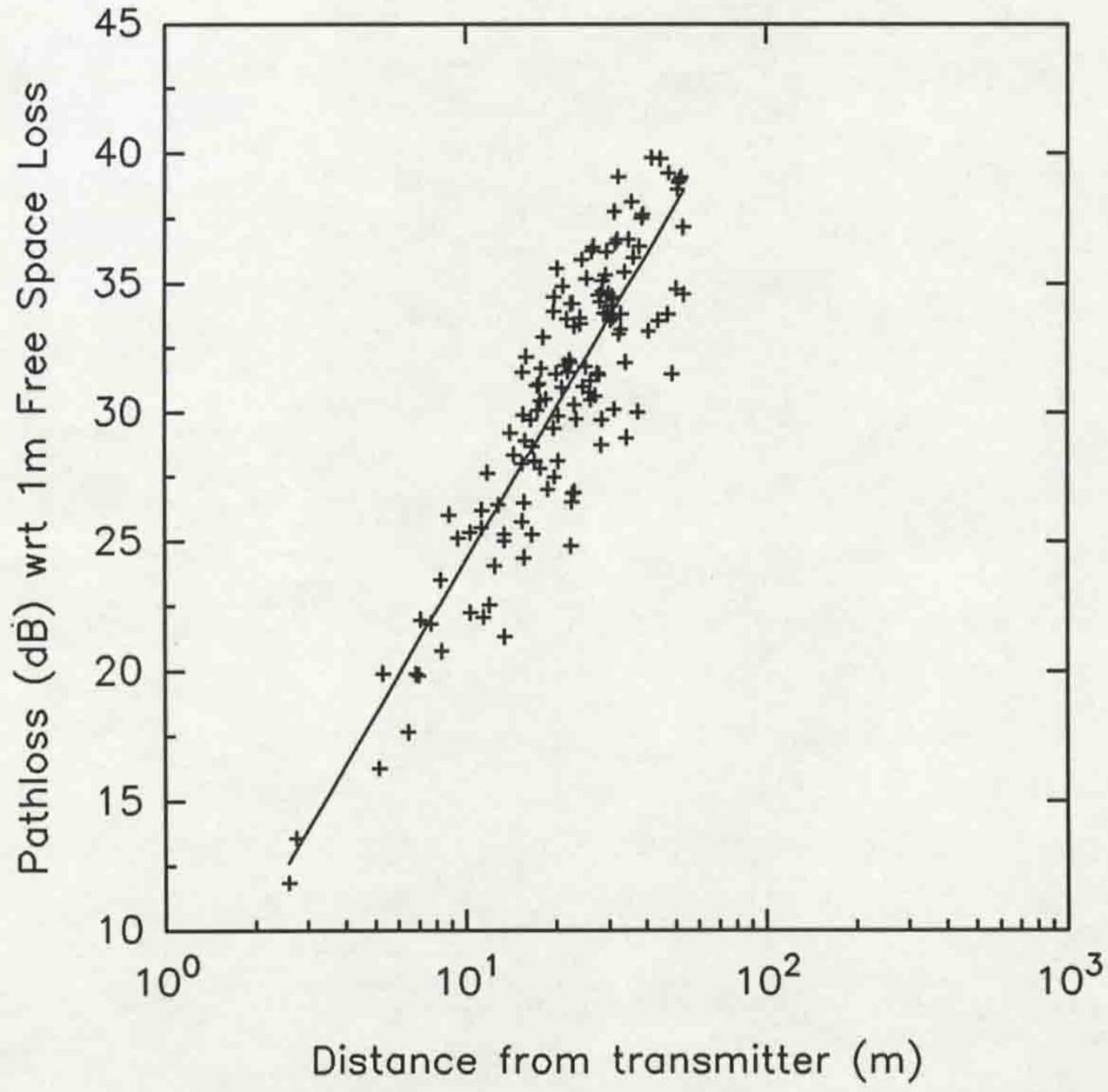

Figure 5.54 Measured pathloss versus distance for the entire supermarket (SMARKET1).

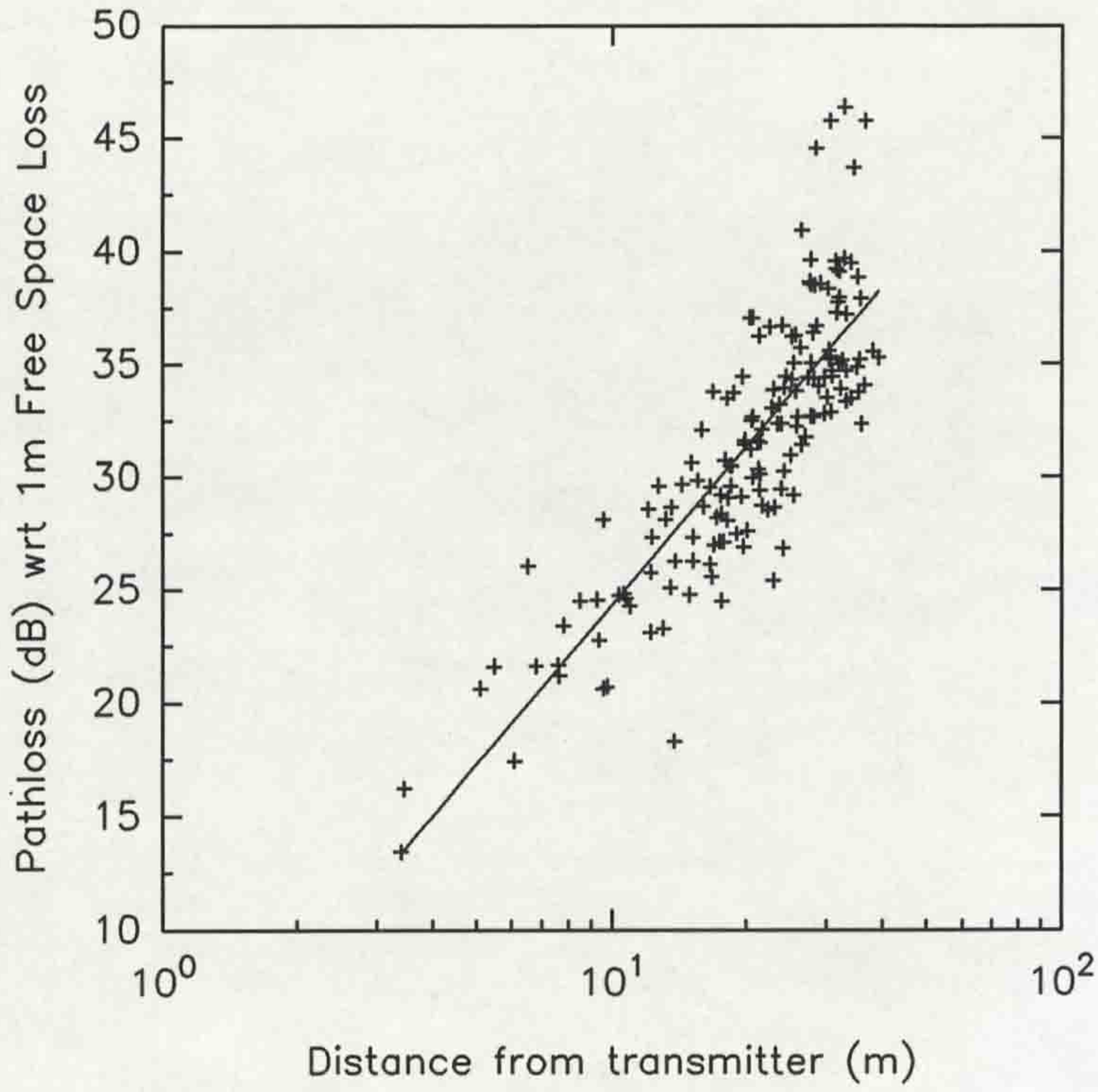

Figure 5.55 Measured pathloss versus distance for NLOS areas in SMARKET2.

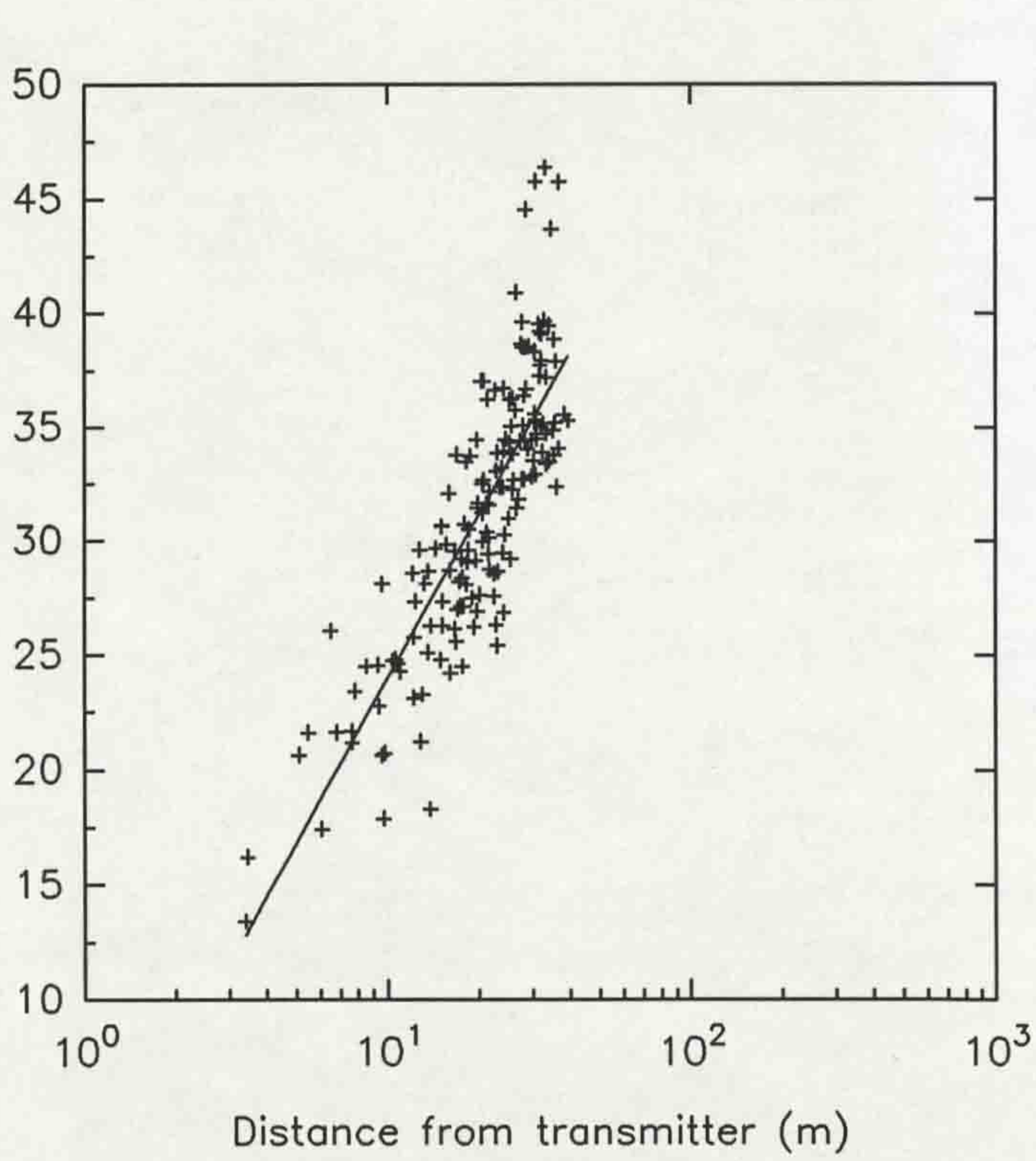

Figure 5.56 Measured pathloss versus distance for the entire superstore (SMARKET2).

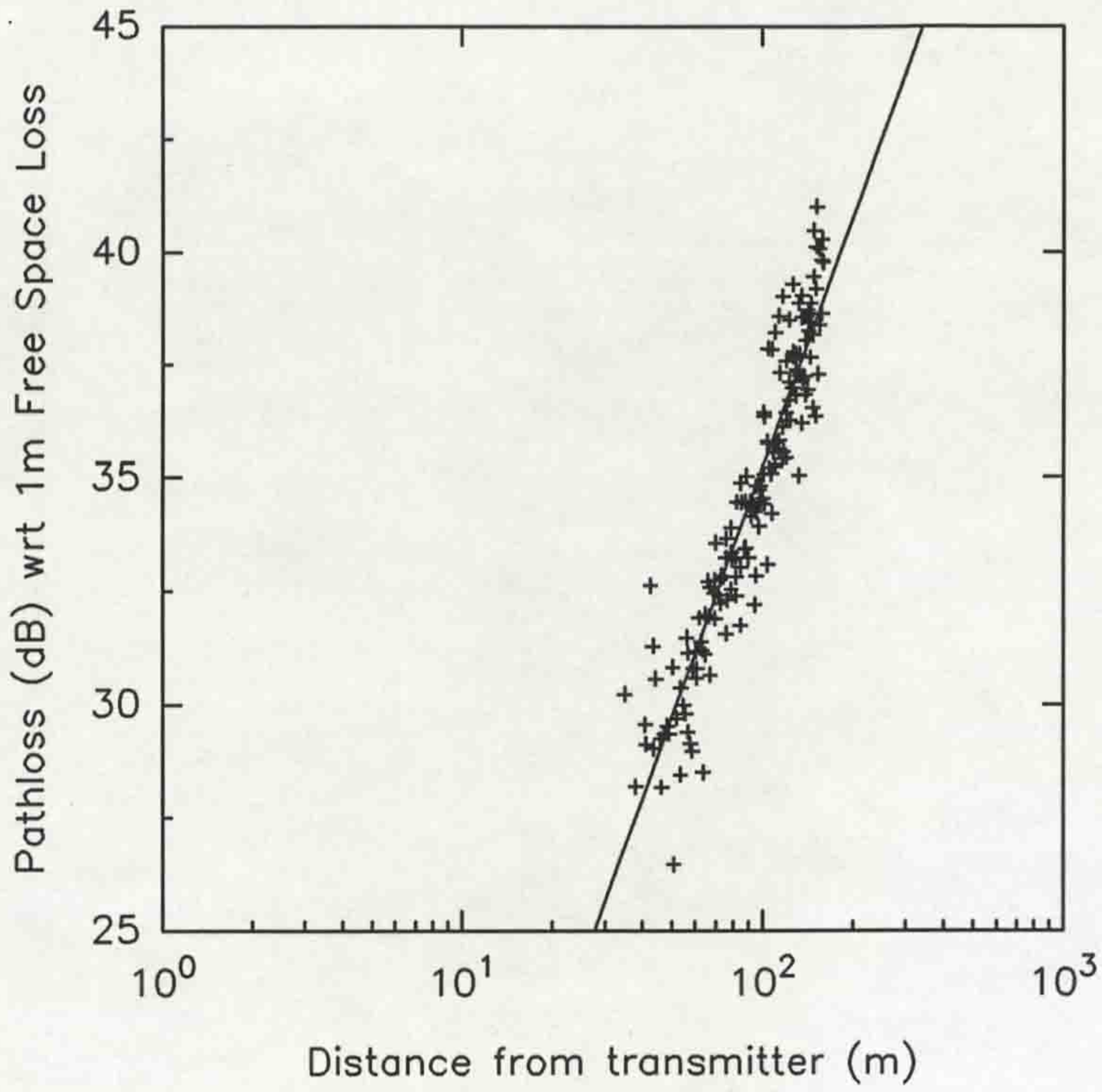

Figure 5.57 Measured pathloss versus distance for P1, P3 and P4 in the train station.

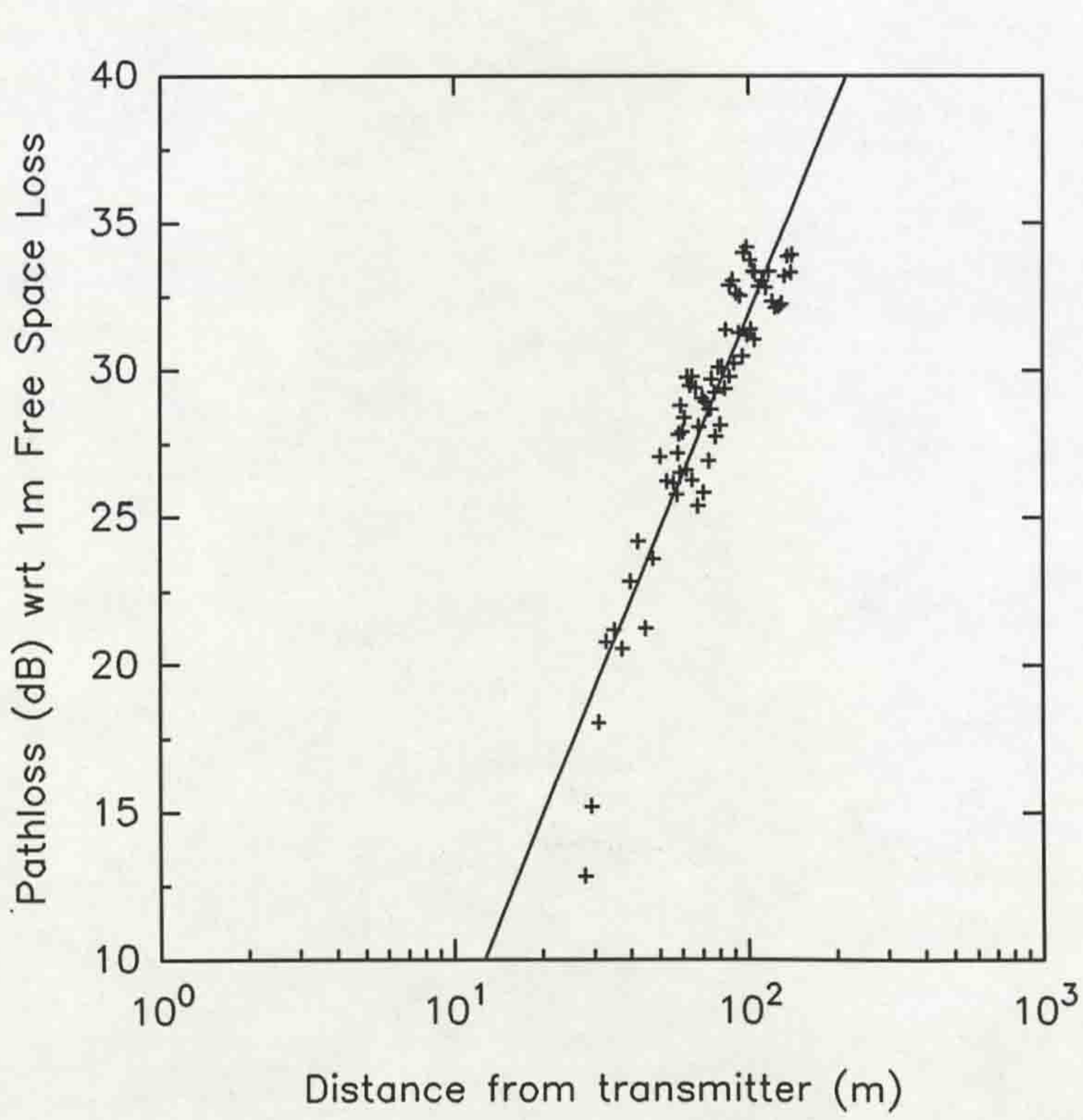

Figure 5.58 Measured pathloss versus distance for P7 and P9 in the train station.

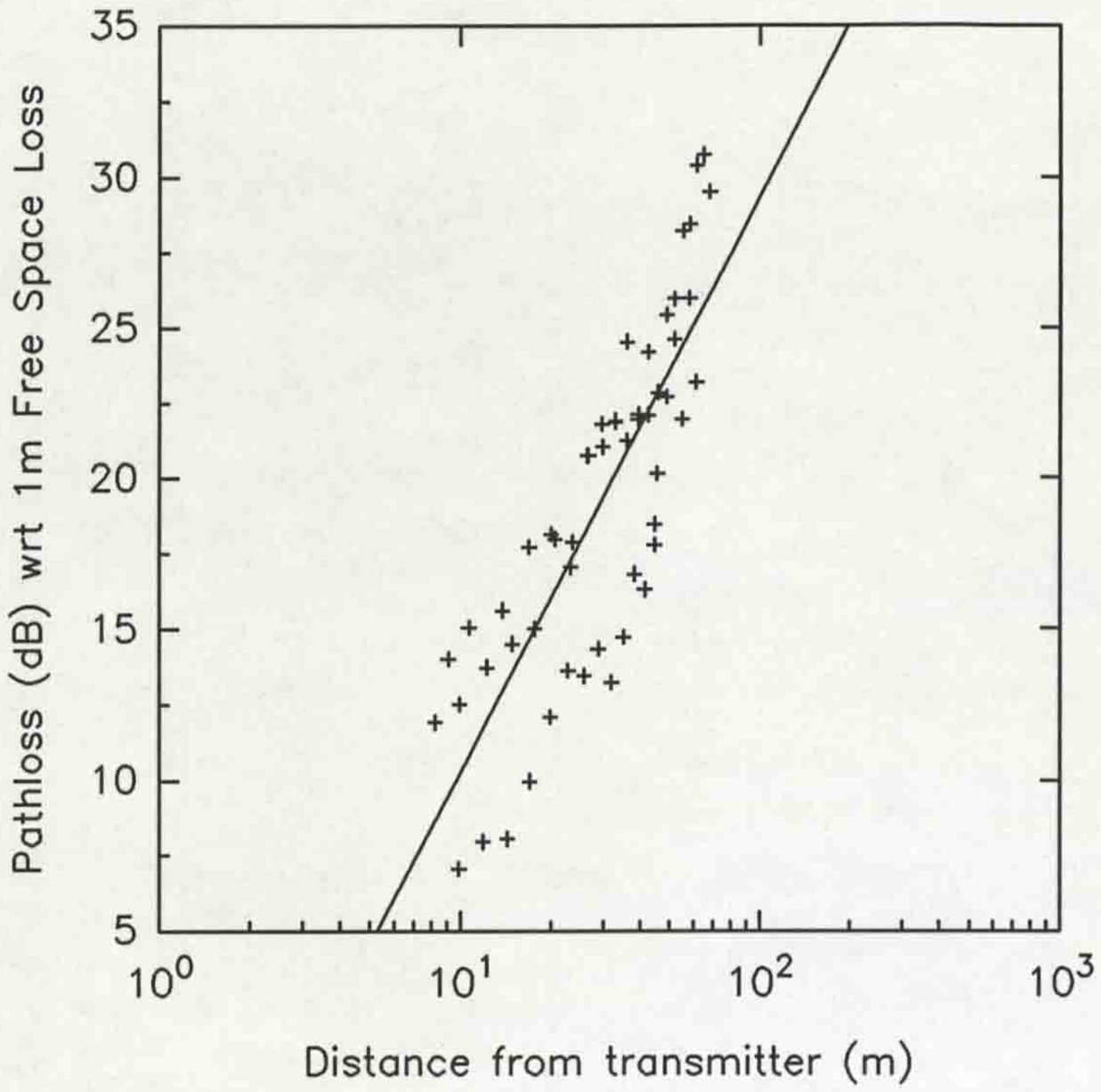

Figure 5.59 Measured pathloss versus distance for LOS areas in the train station (concourse area.

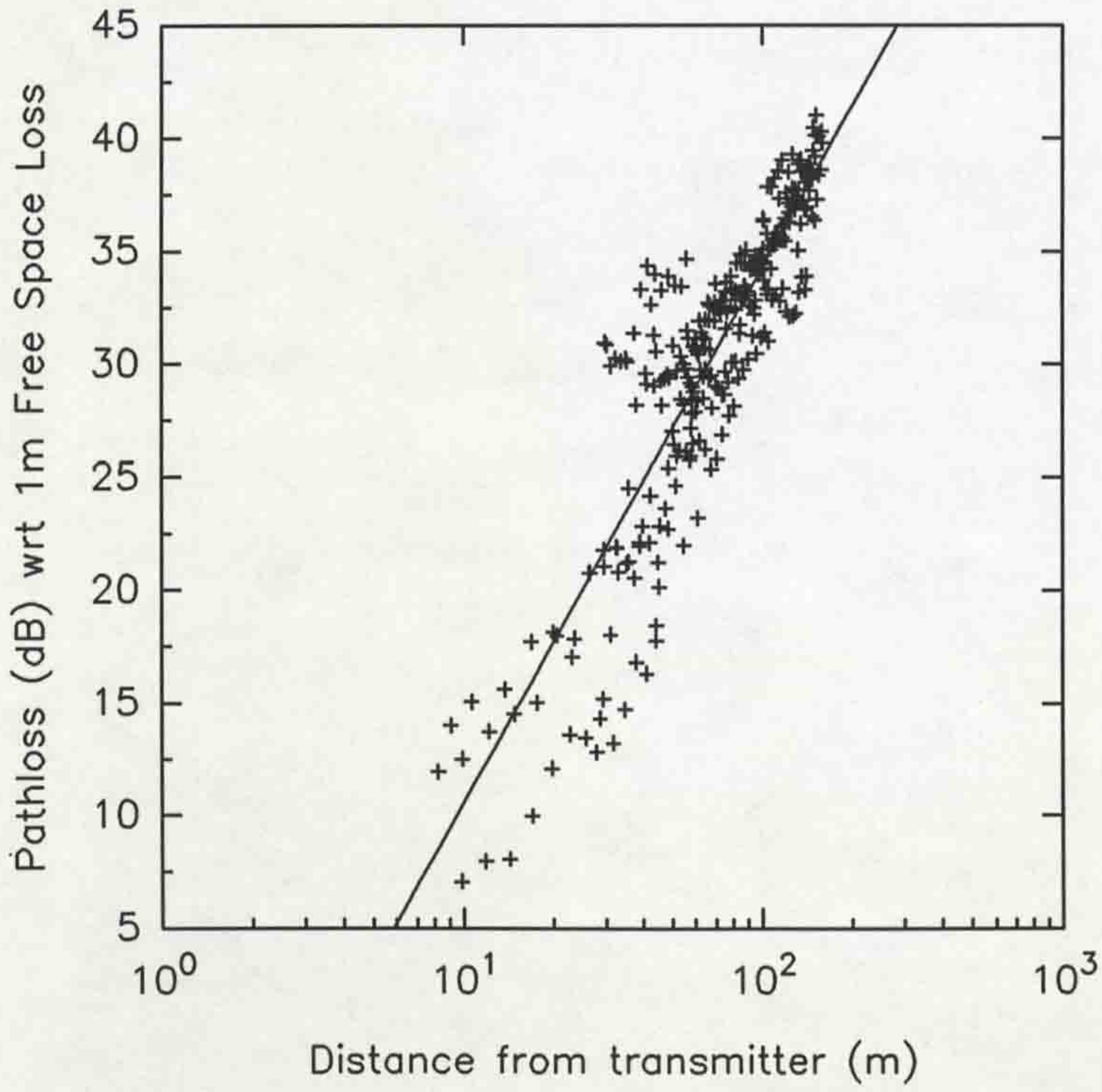

Figure 5.60 Measured pathloss versus distance for the entire train station,

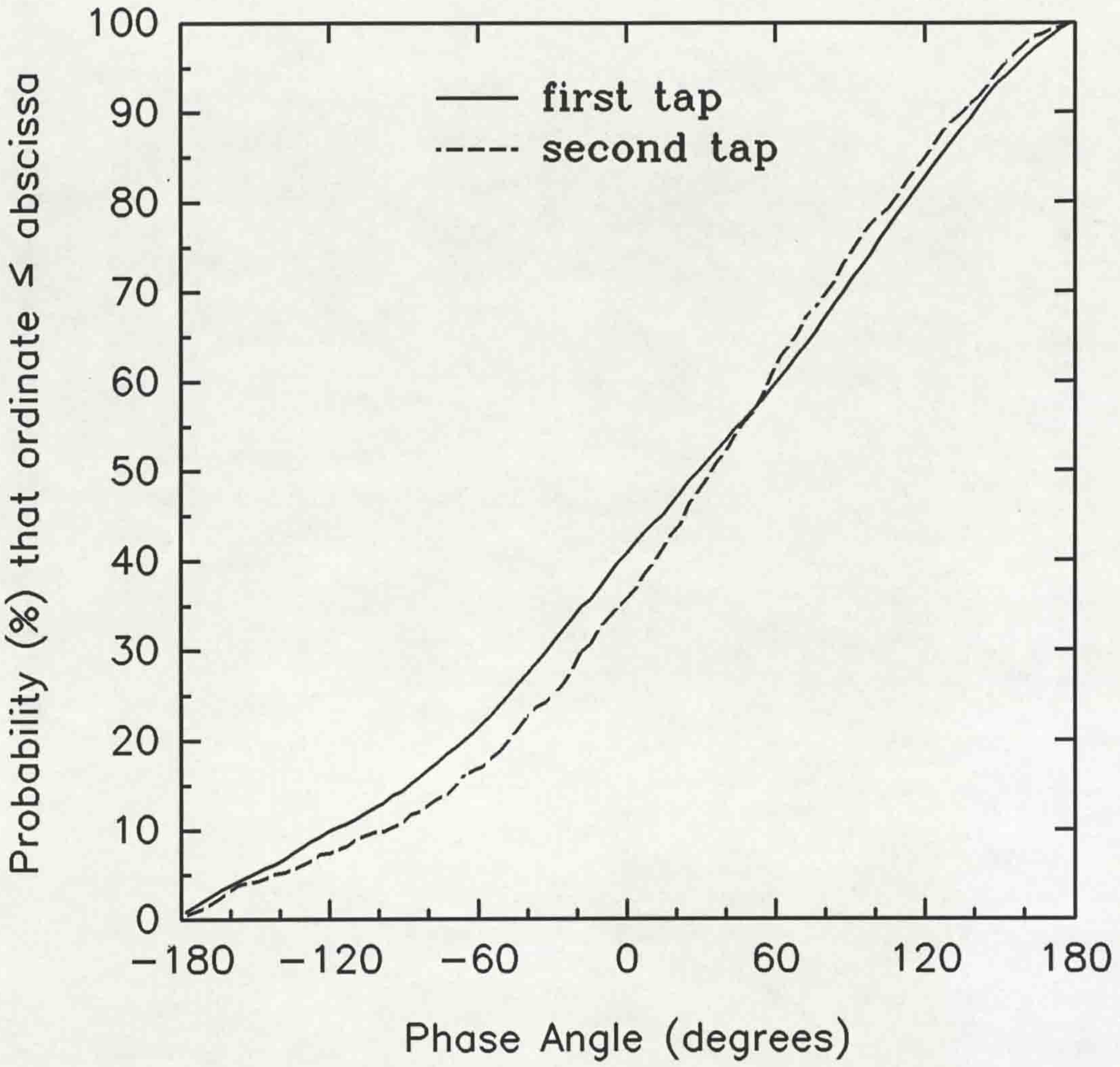

Figure 5.61 Phase distribution of the first two taps in SMARKET2.

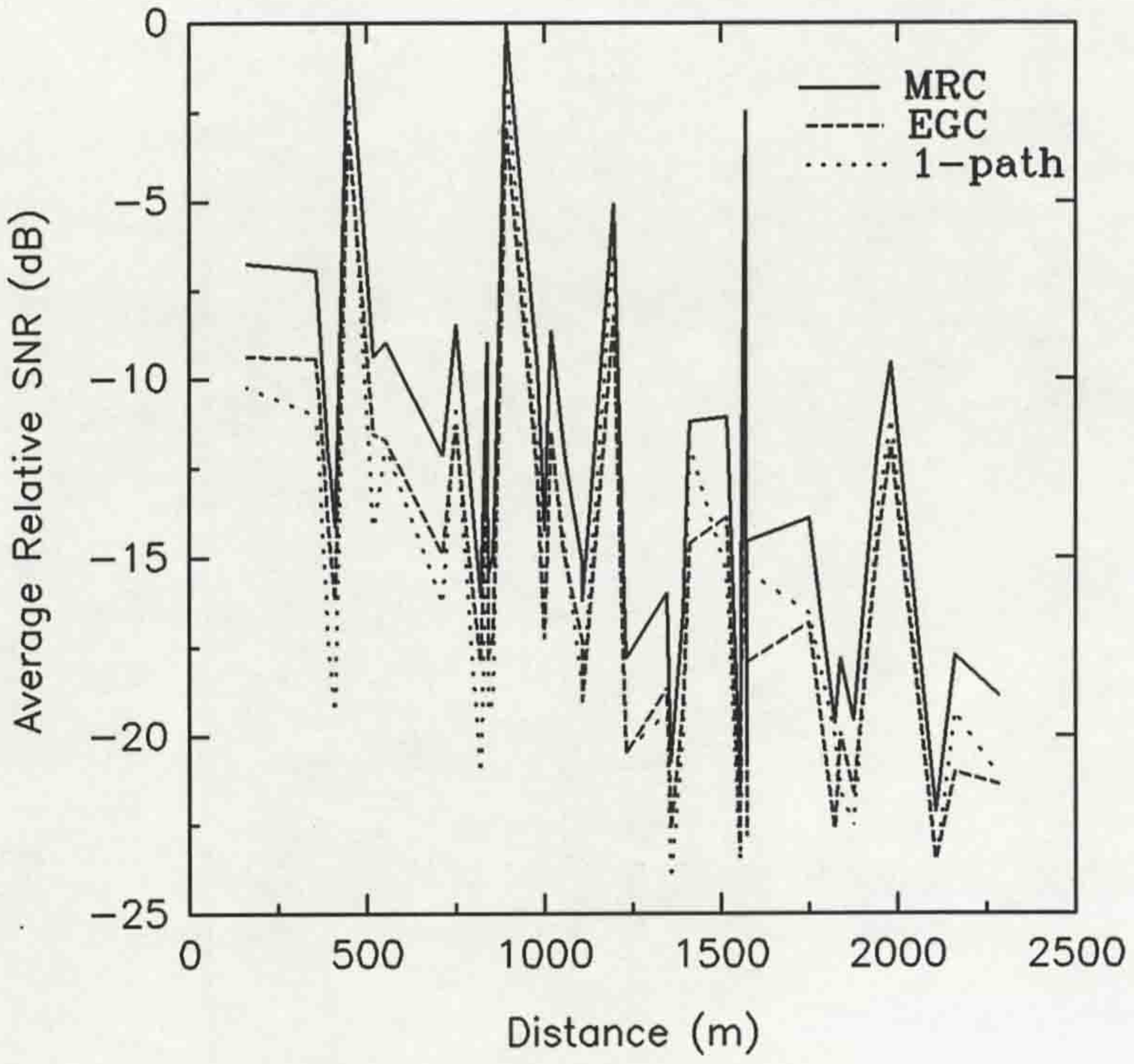

Figure 5.62 Average relative SNR versus distance for URBAN1.

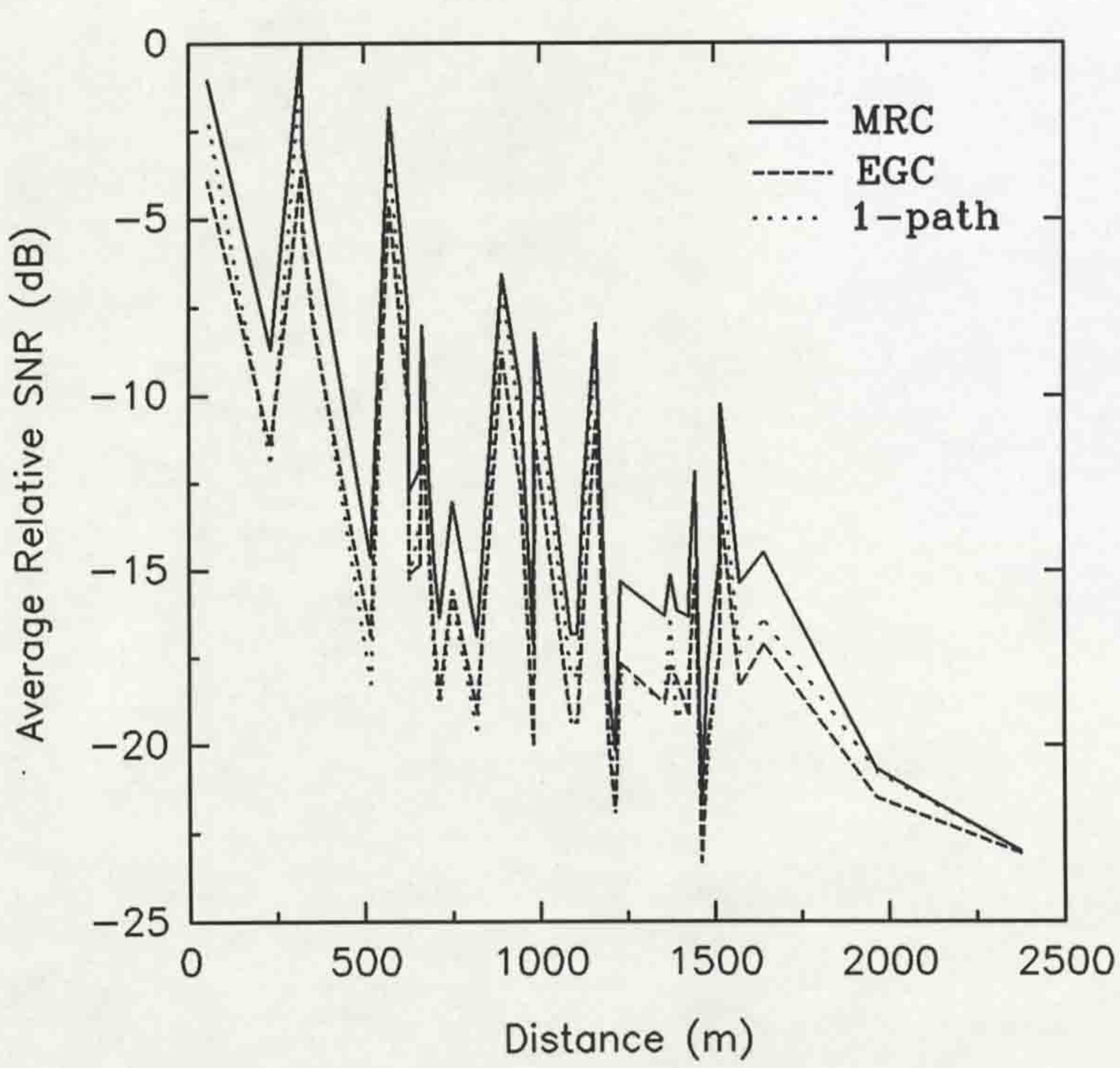

Figure 5.63 Average relative SNR versus distance for URBAN2.

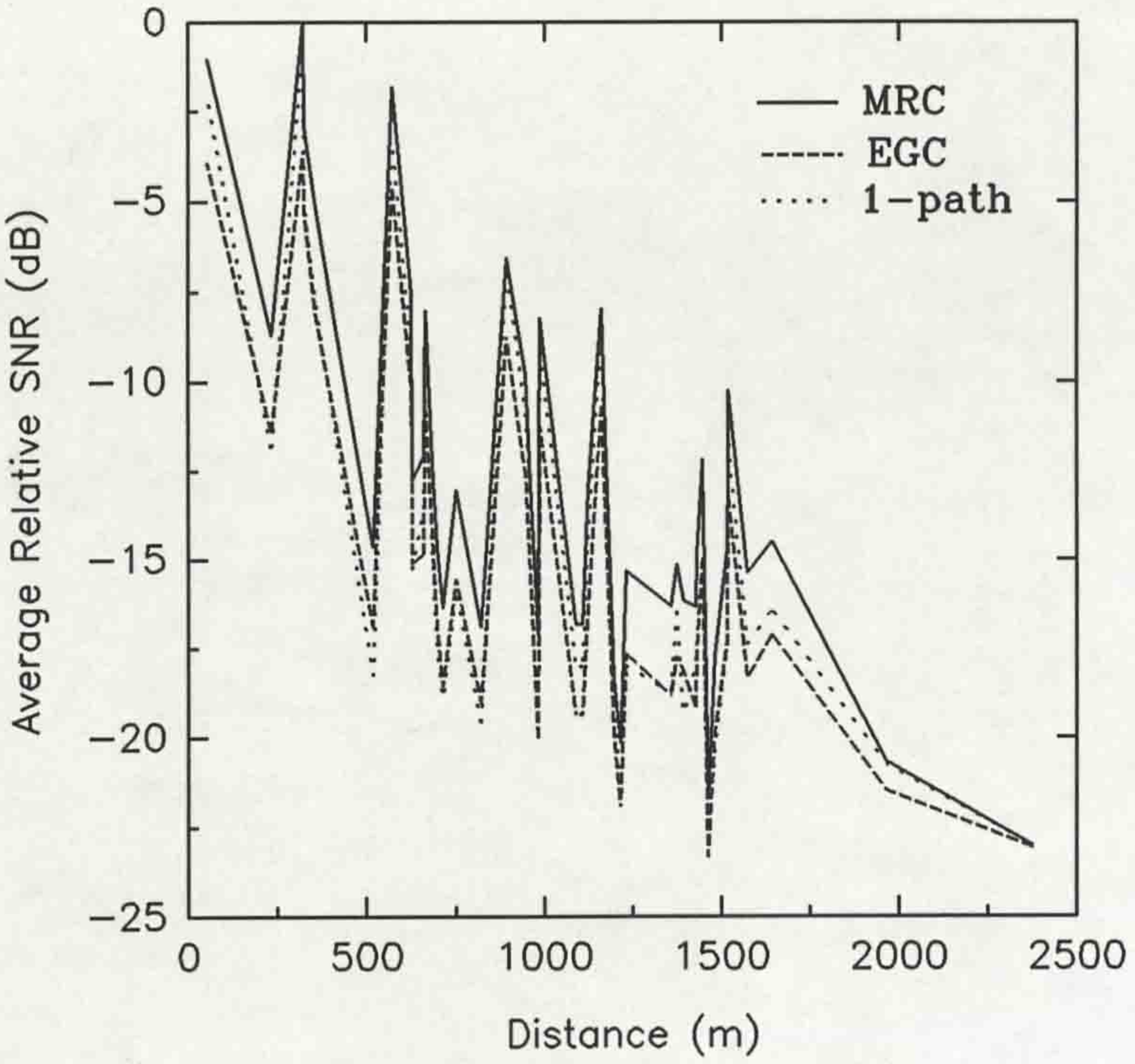

Figure 5.64 Average relative SNR versus distance for the open rural location.

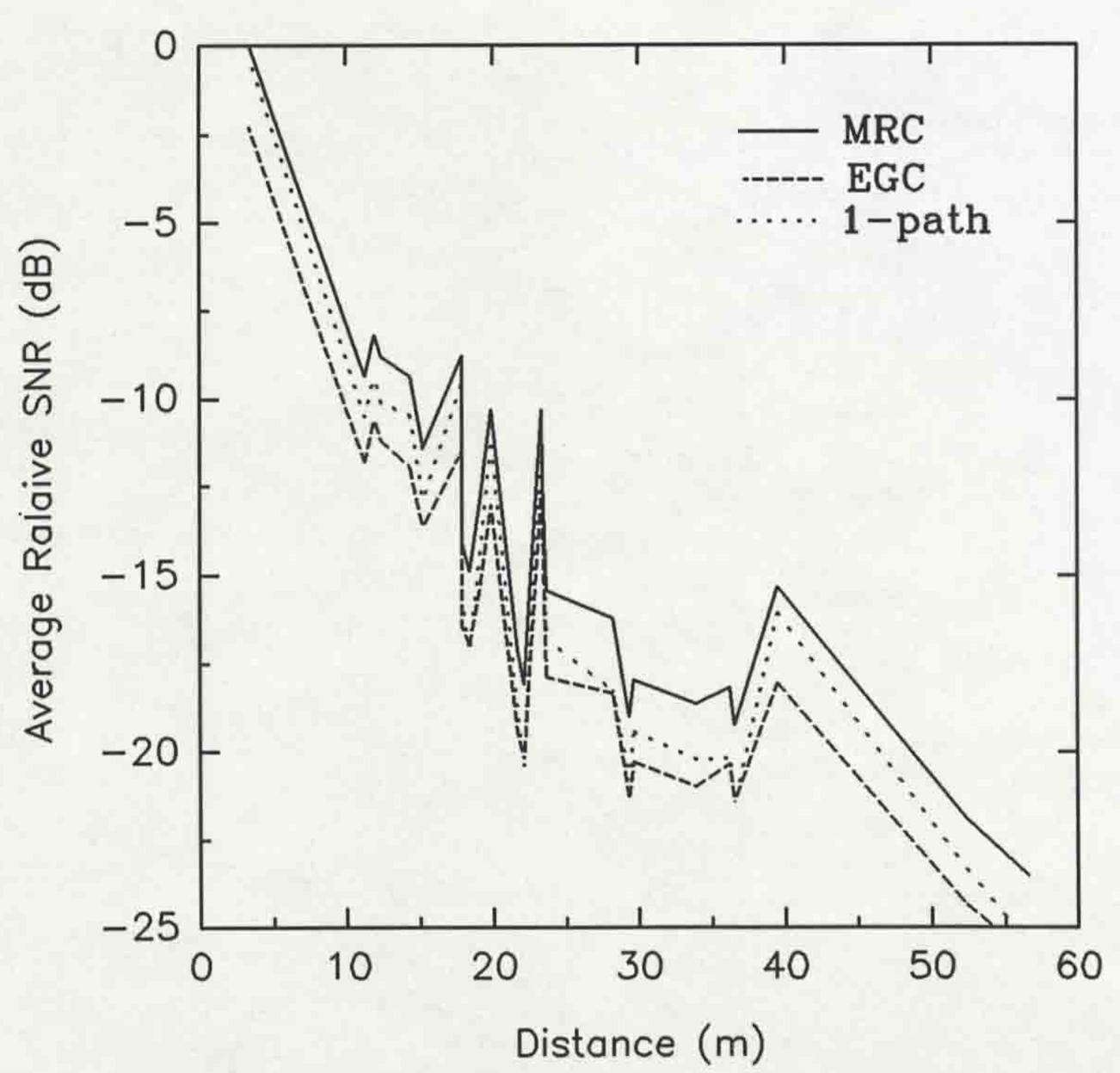

Figure 5.65 Average SNR relative versus distance for SMARKET1.

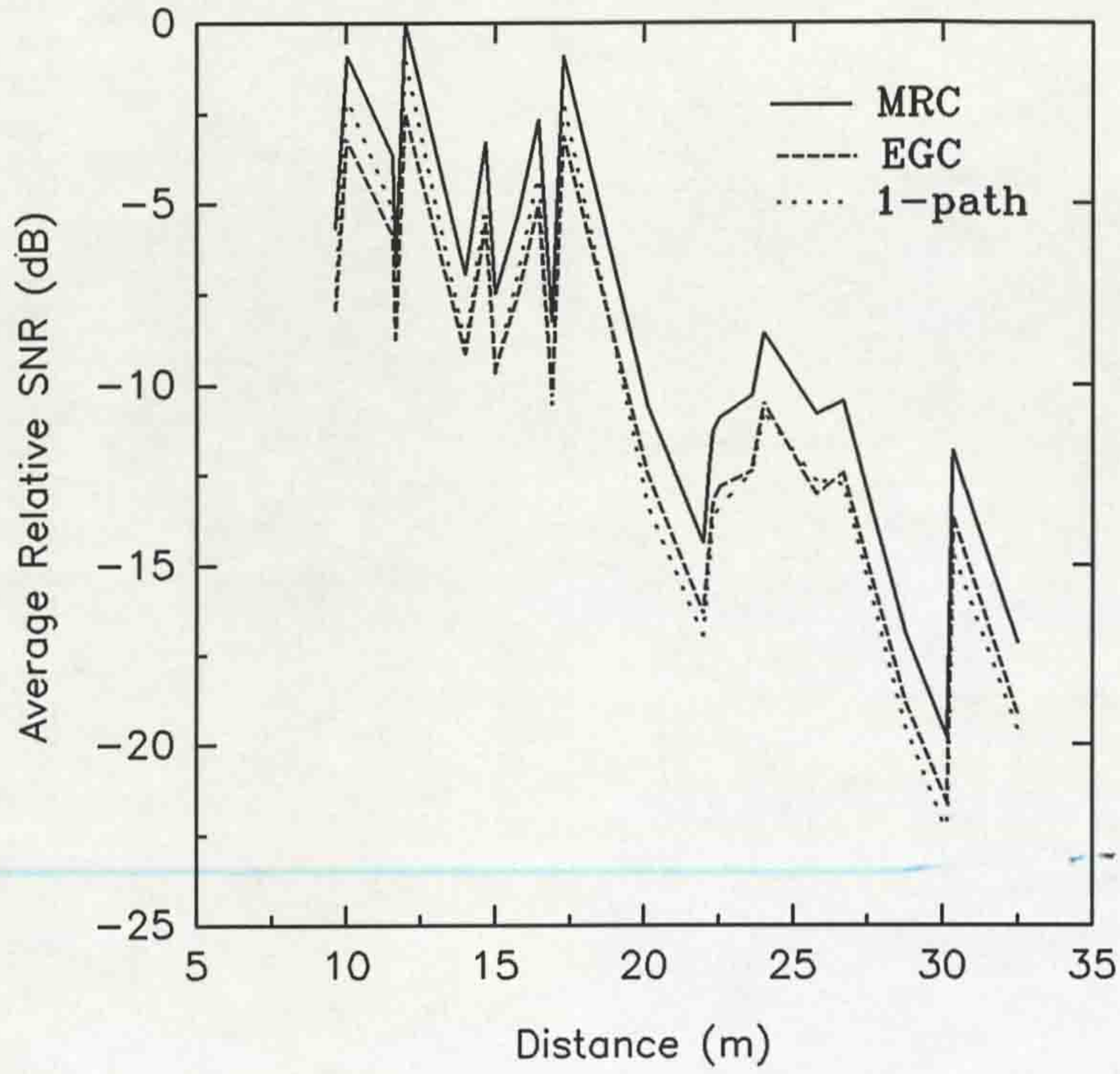

Figure 5.66 Average relative SNR versus distance for SMARKET2.

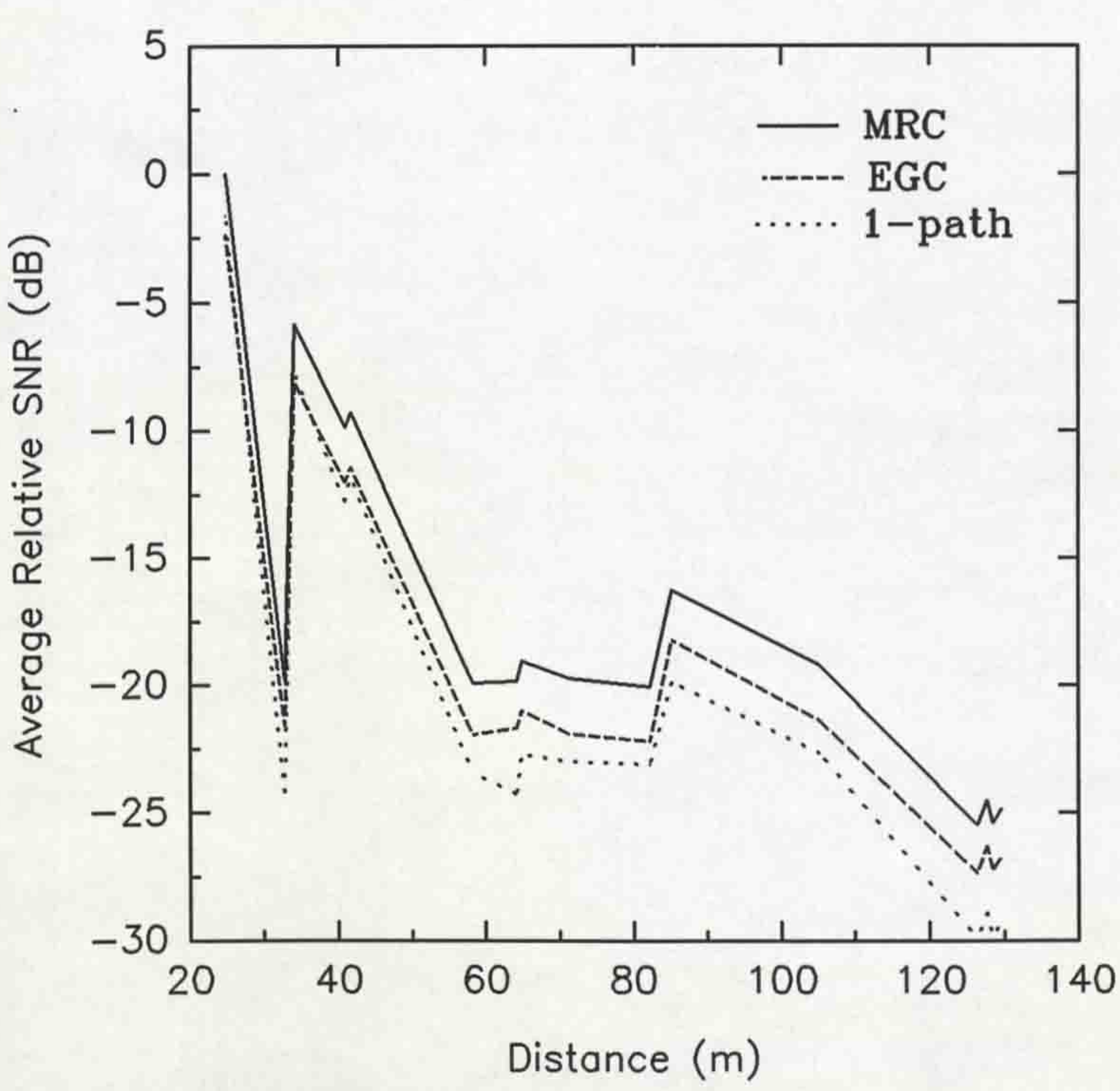

Figure 5.67 Average SNR relative versus distance for the train station.

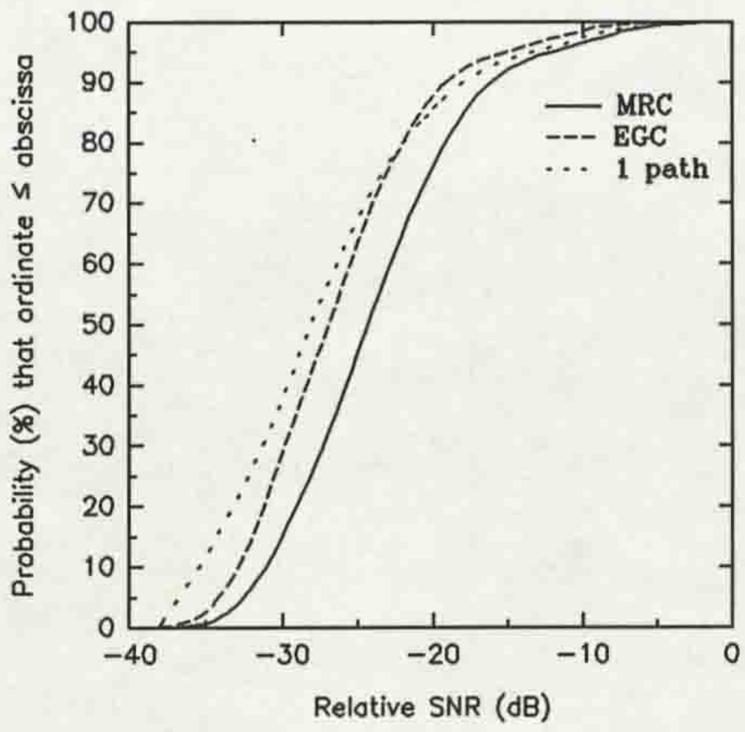

Figure 5.68 CDF of relative SNR for URBAN1.

Figure 5.69 CDF of relative SNR for URBAN2.

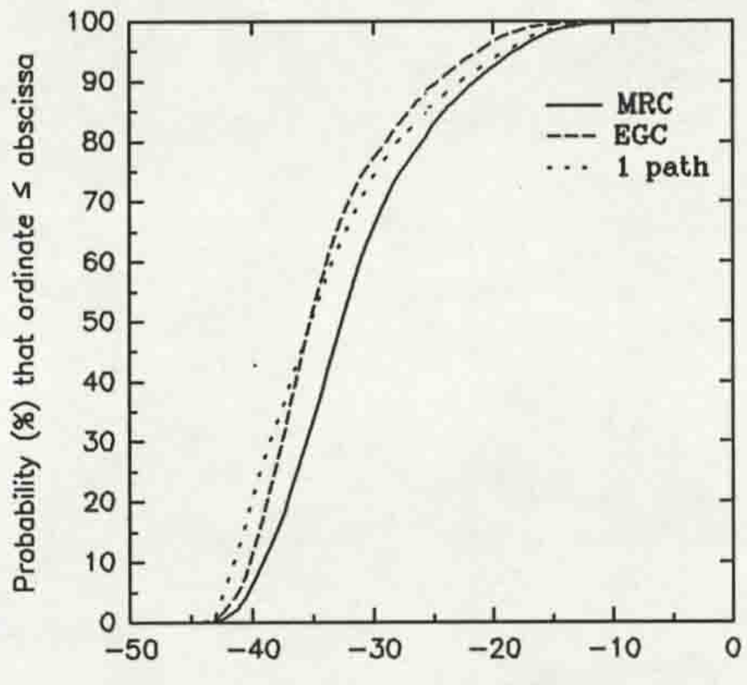

Figure 5.70 CDF of relative SNR for the rural open area.

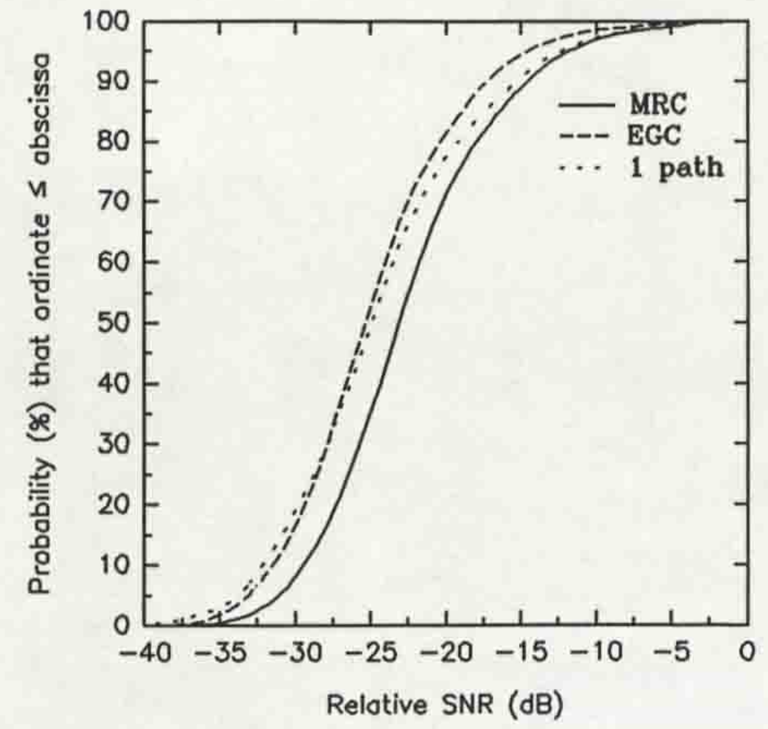

Figure 5.71 CDF of relative SNR for SMARKET1.

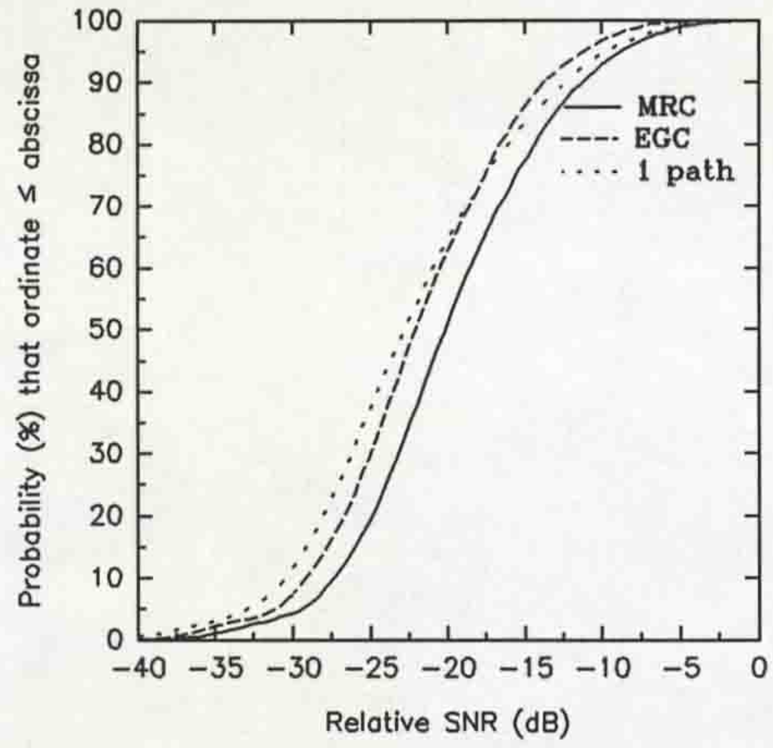

Figure 5.72 CDF of relative SNR for SMARKET2.

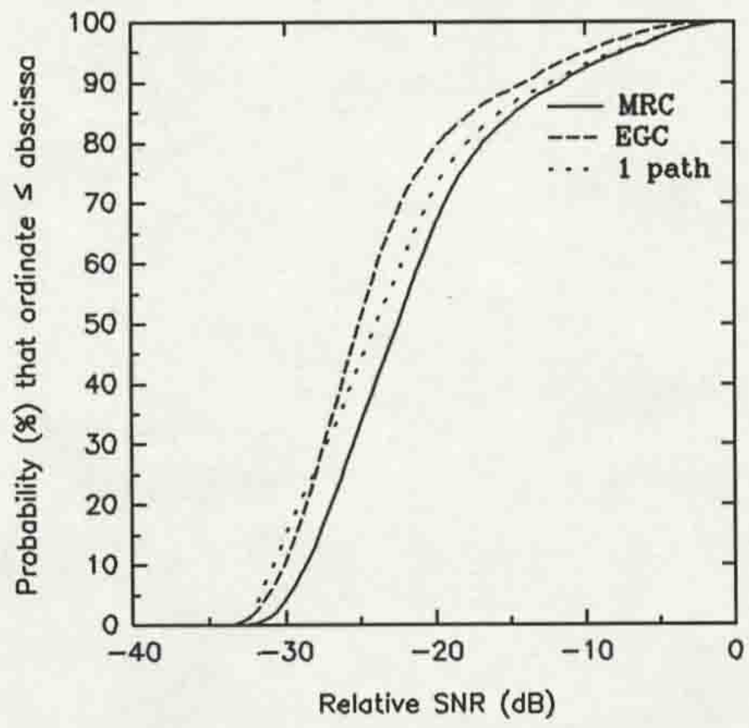

Figure 5.70 CDF of relative SNR for the rural open area.

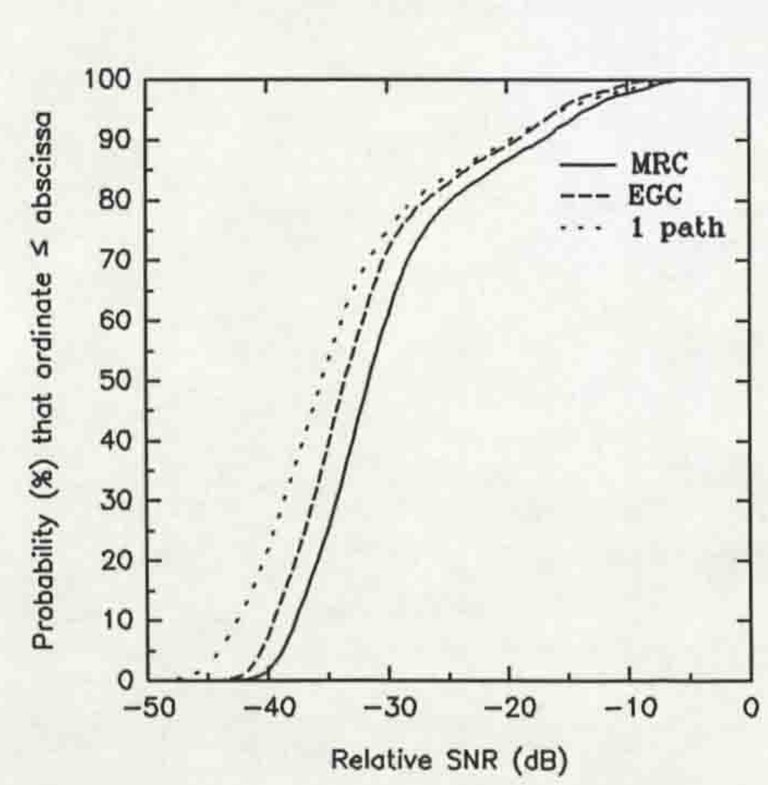

Figure 5.73 CDF of relative SNR for the train station.

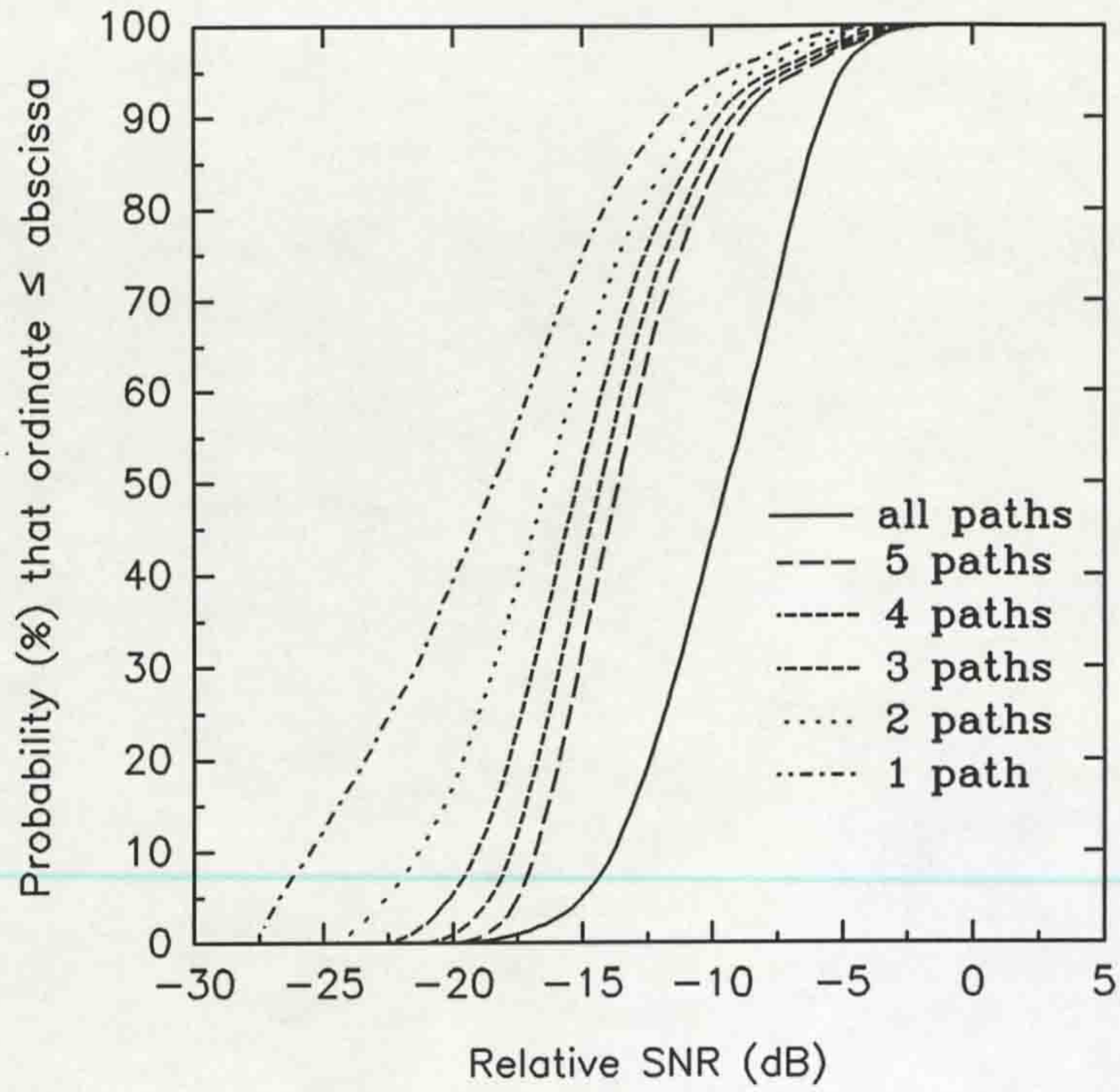

Figure 5.74 CDF of relative SNR for an L-path Rake receiver for URBAN1.

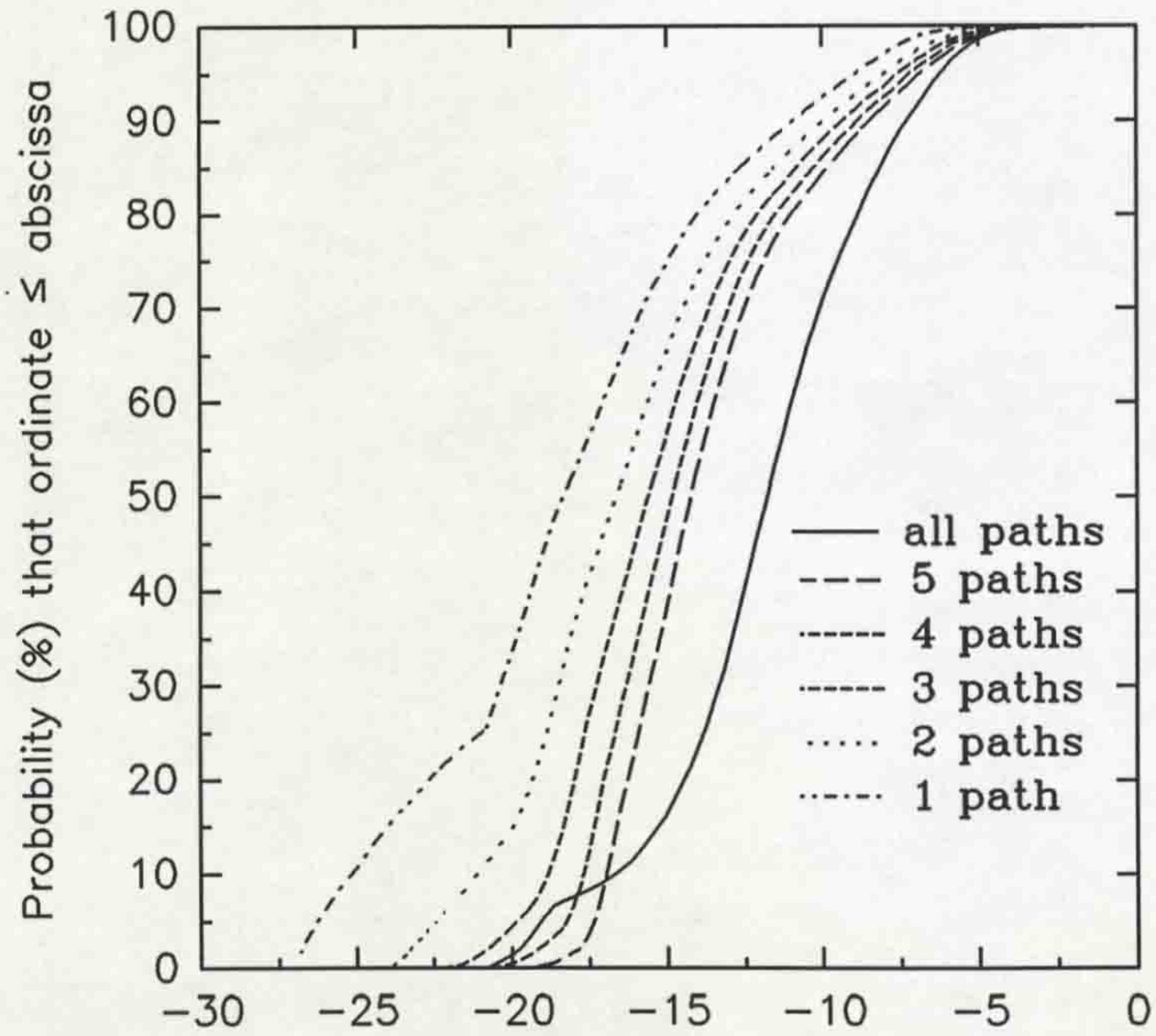

Figure 5.75 CDF of relative SNR for an L-path Rake receiver for URBAN2.

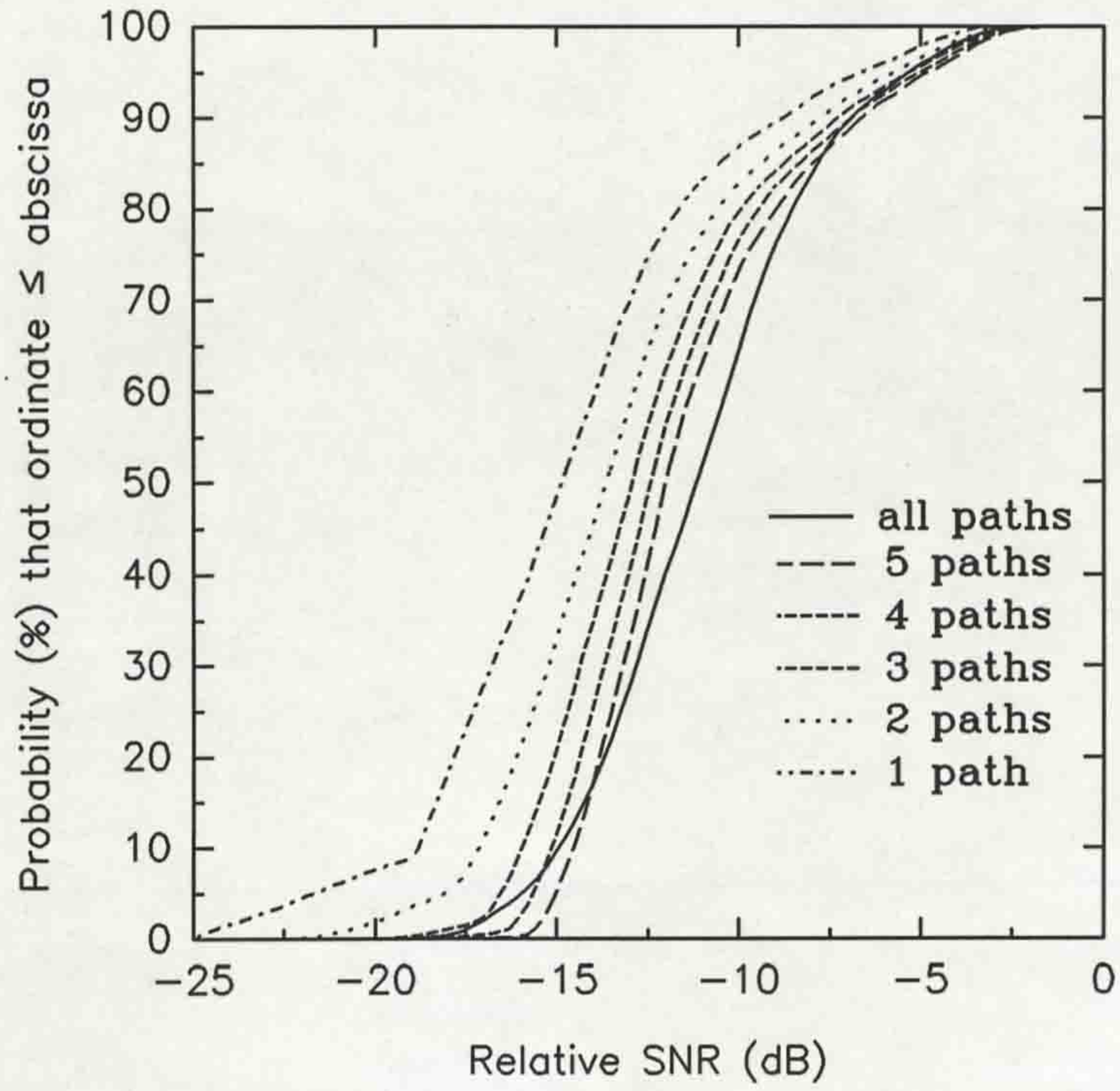

Figure 5.76 CDF of relative SNR for an L-path Rake receiver for the rural open area.

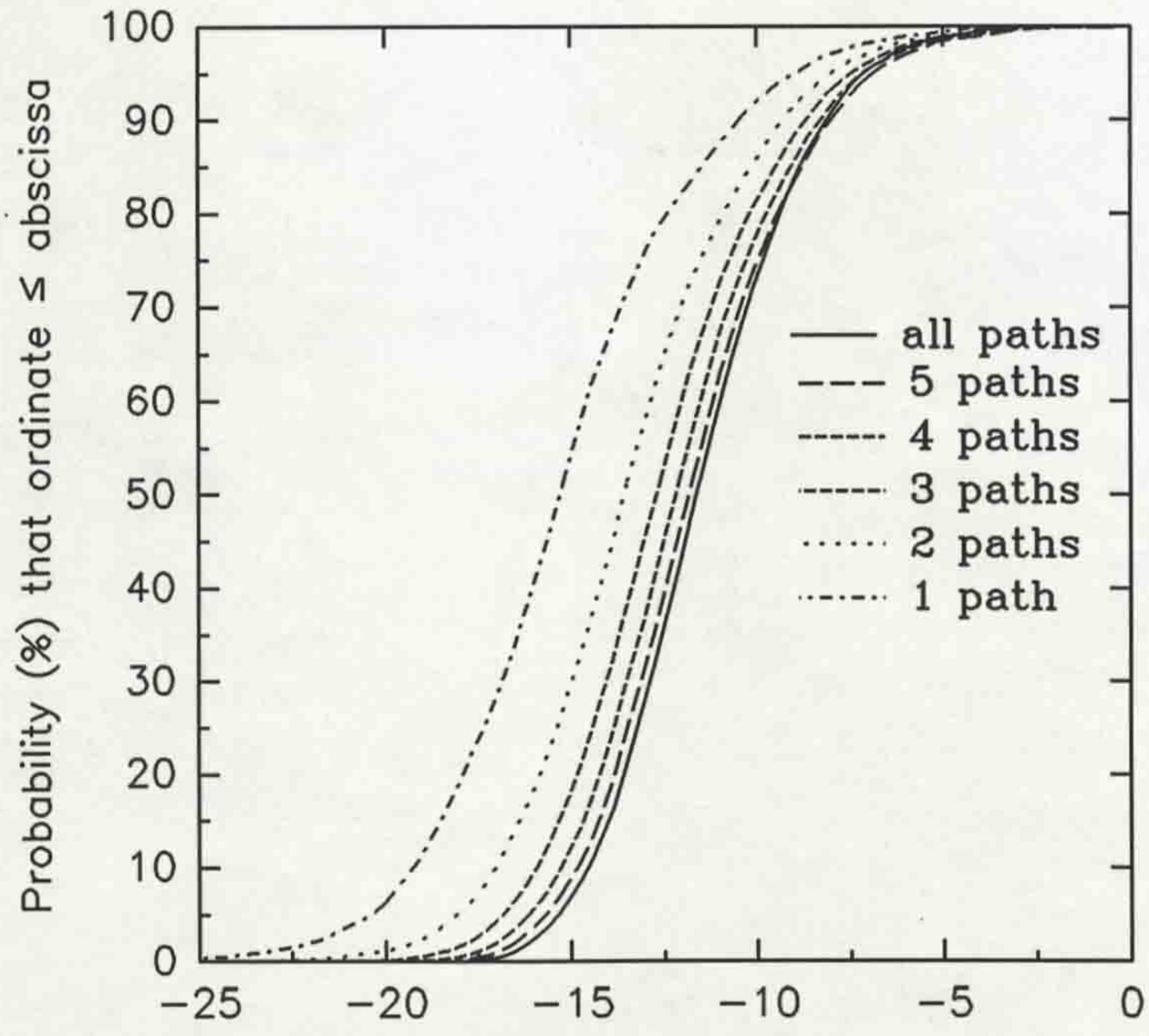

Figure 5.77 CDF of relative SNR for an L-path Rake receiver for SMARKET1.

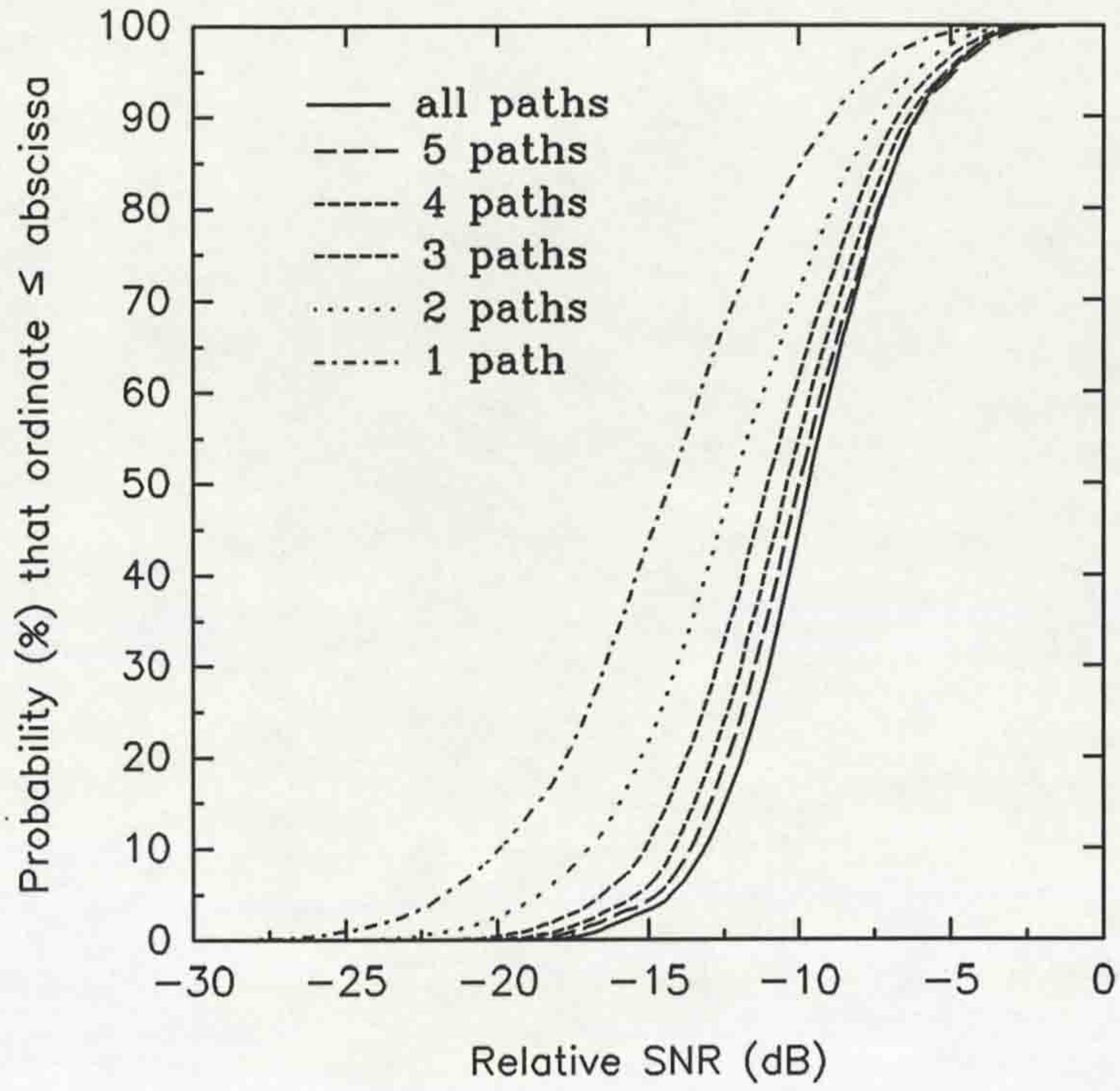

Figure 5.78 CDF of relative SNR for an L-path Rake receiver for SMARKET2.

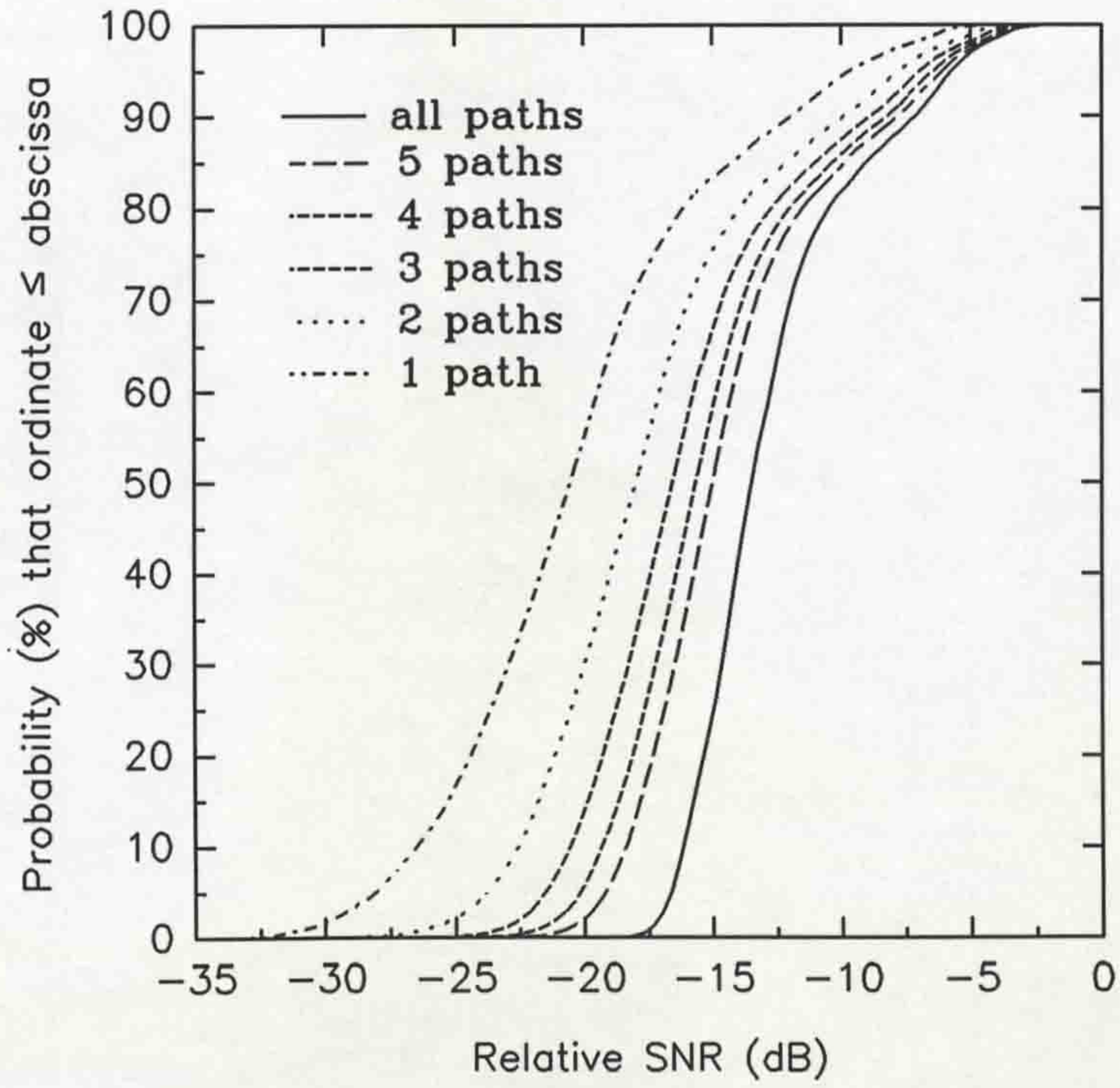

Figure 5.79 CDF of relative SNR for an L-path Rake receiver for the train station.

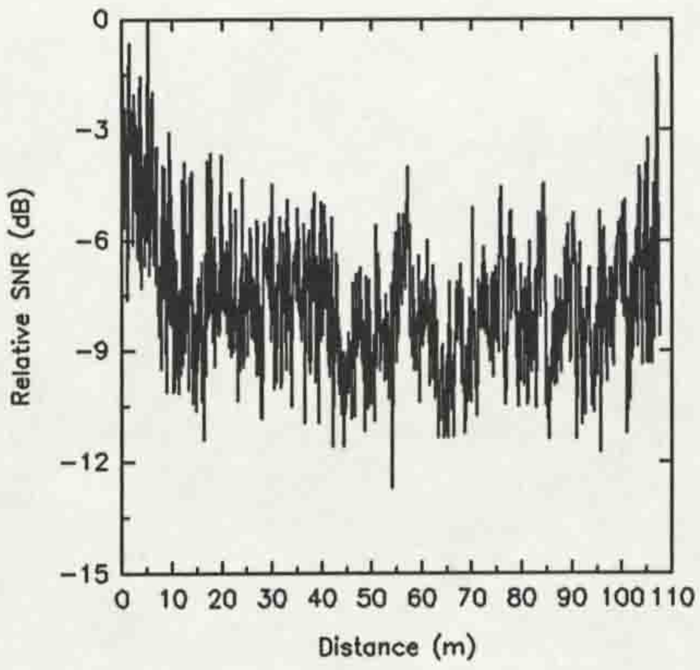

Figure 5.80 Short-term variations of relative SNR on a street in URBAN1 for an all-path Rake receiver.

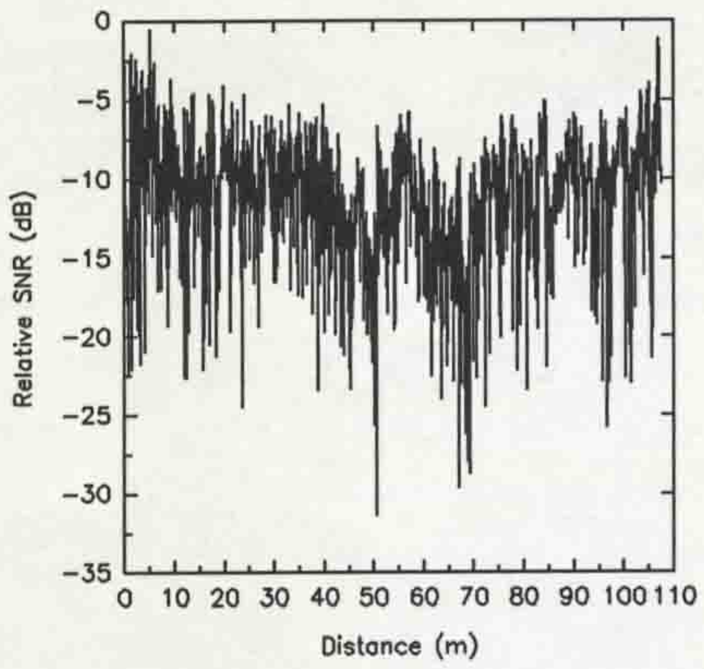

Figure 5.81 Short-term variations of relative SNR for a 5-path Rake receiver (URBAN1).

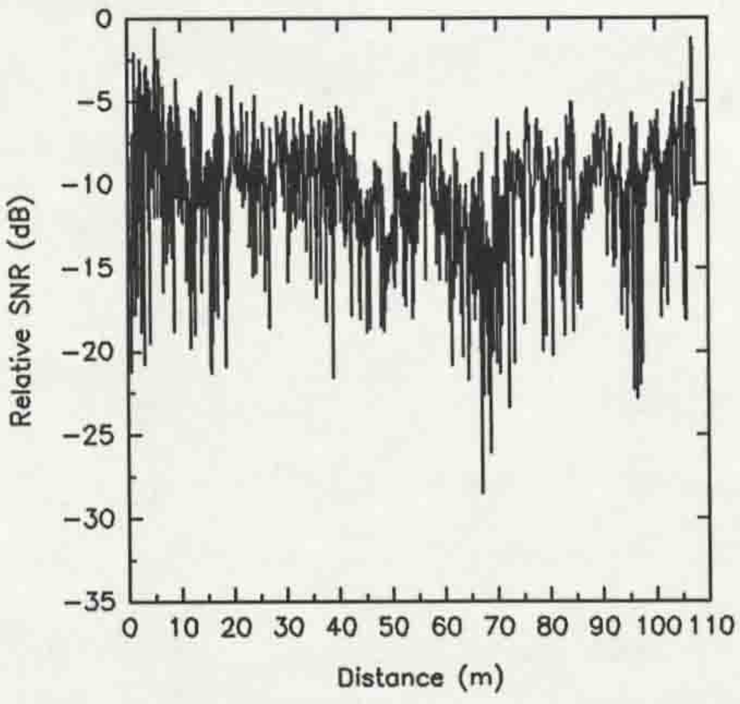

Figure 5.82 Short-term variations of relative SNR for a 4-path Rake receiver (URBAN1).

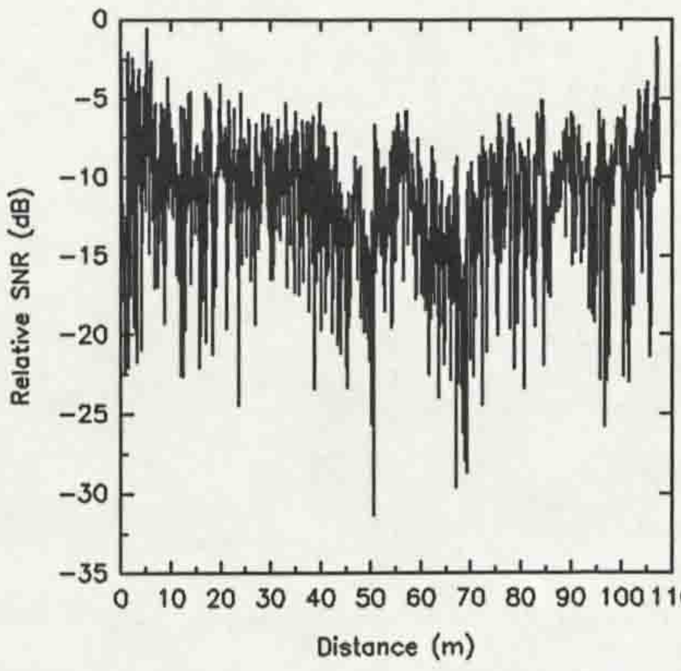

Figure 5.83 Short-term variations of relative SNR for a 3-path Rake receiver (URBAN1).

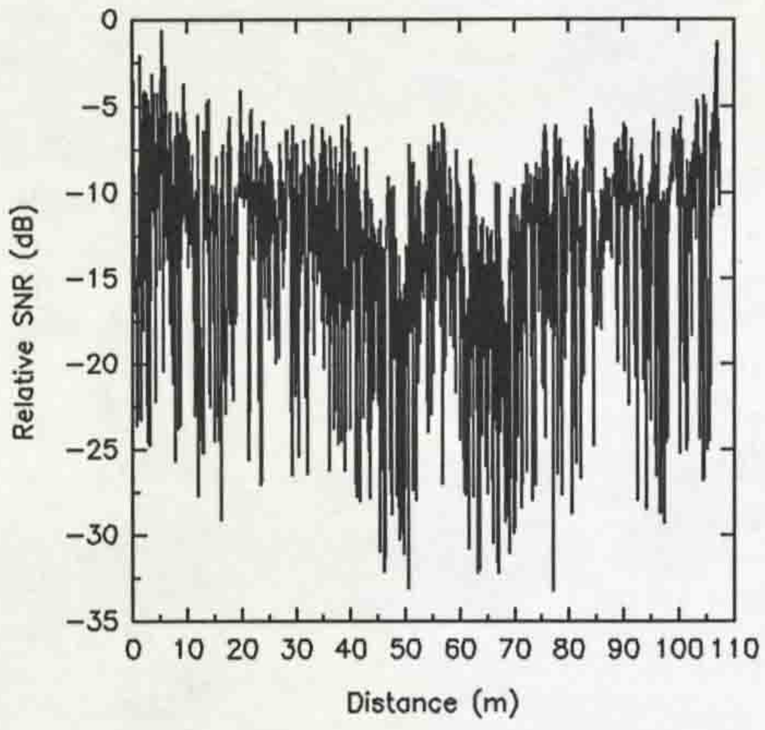

Figure 5.84 Short-term variations of relative SNR for a 2-path Rake receiver (URBAN1).

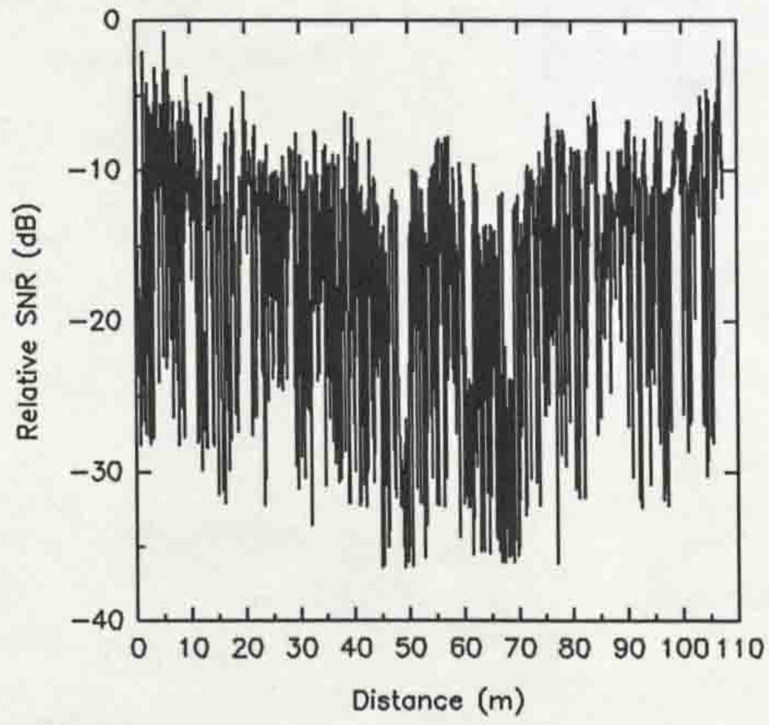

Figure 5.85 CDFs of the coherence bandwidths from URBAN1.

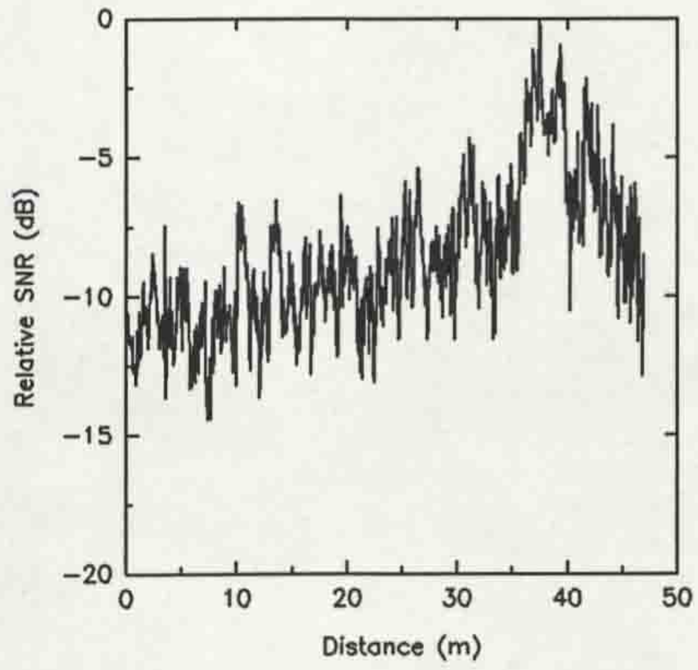

Figure 5.86 Short-term variations of relative SNR for an all-path Rake receiver on a platform in the train station.

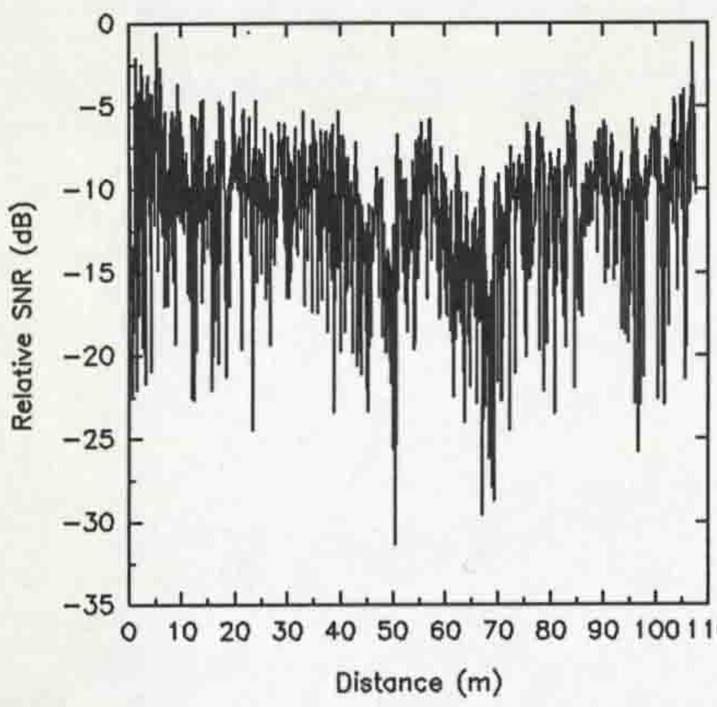

Figure 5.87 Short-term variations of relative SNR for a 5-path Rake receiver (train station).

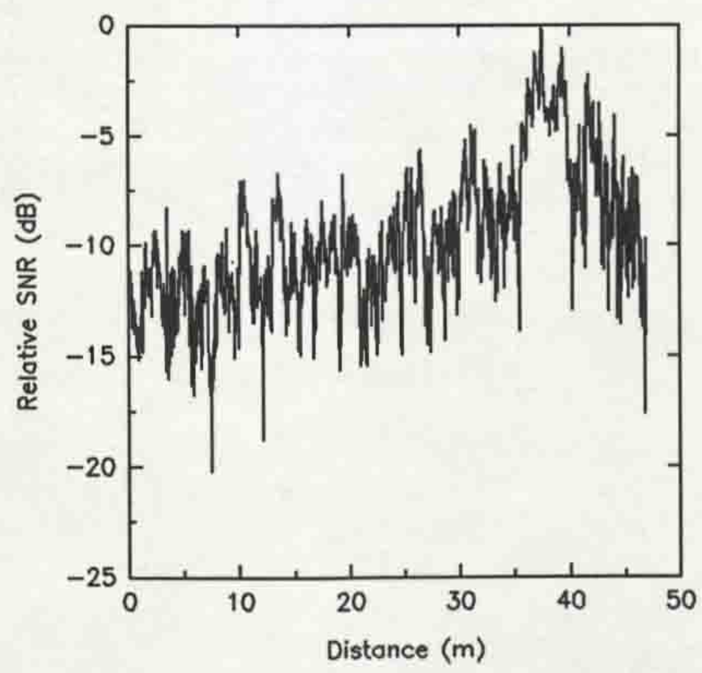

Figure 5.88 Short-term variations of relative SNR for a 4-path Rake receiver (train station).

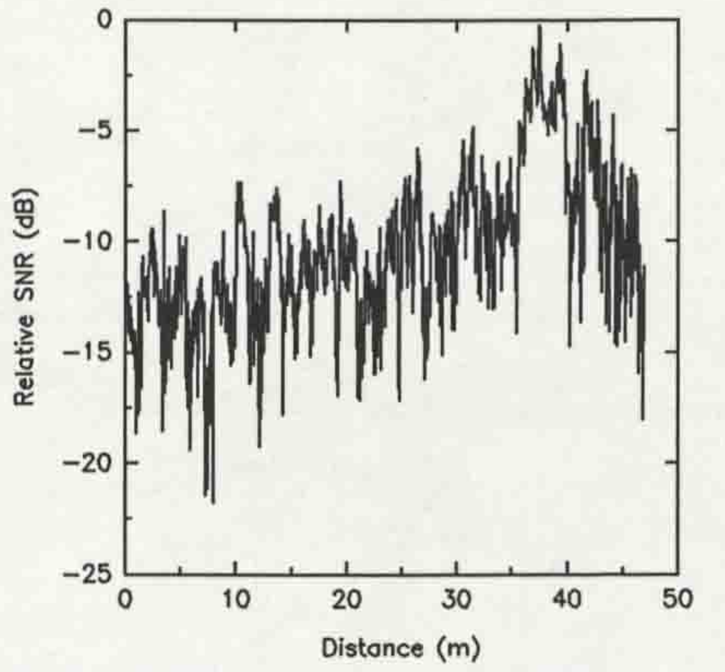

Figure 5.89 Short-term variations of relative SNR for a 3-path Rake receiver (train station).

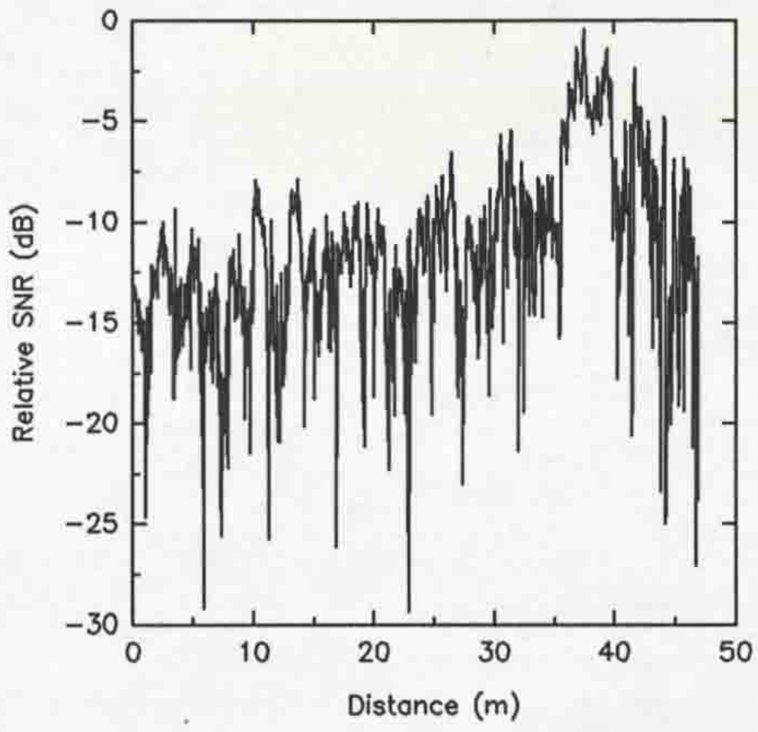

Figure 5.90 Short-term variations of relative SNR for a 2-path Rake receiver (train station).

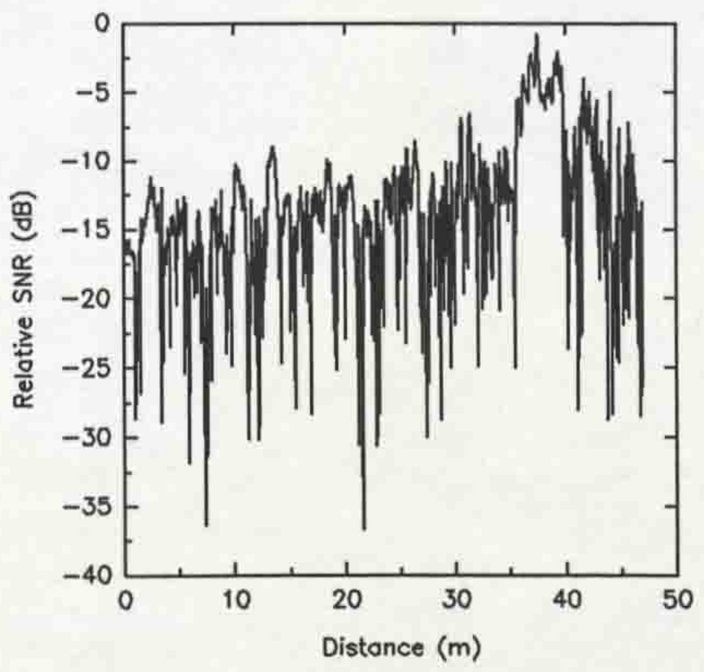

Figure 5.91 Short-term variations of relative SNR for a 1-path Rake receiver (train station).

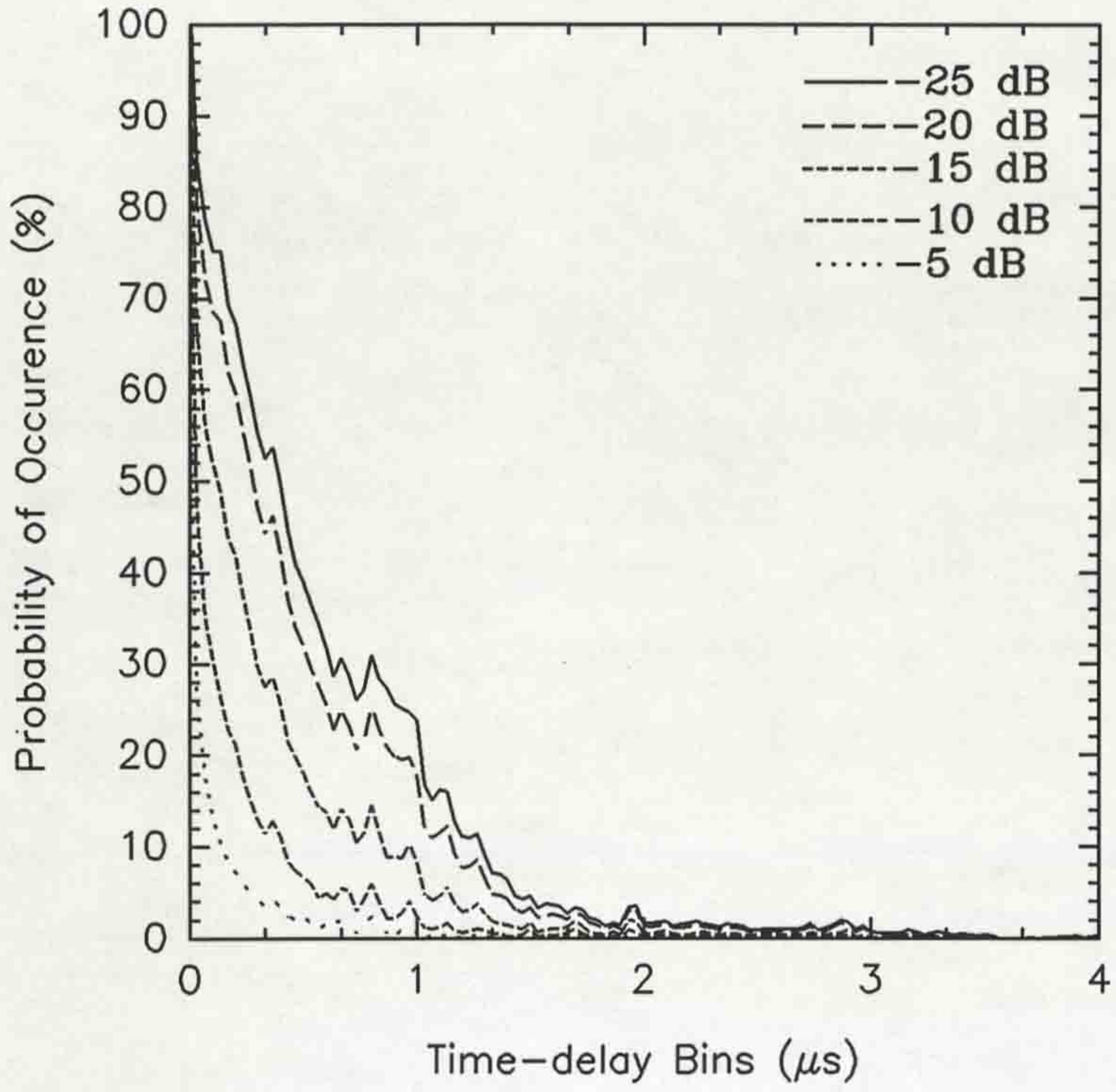

Figure 5.92 Probability of occurrence versus time-delay bins for URBAN1.

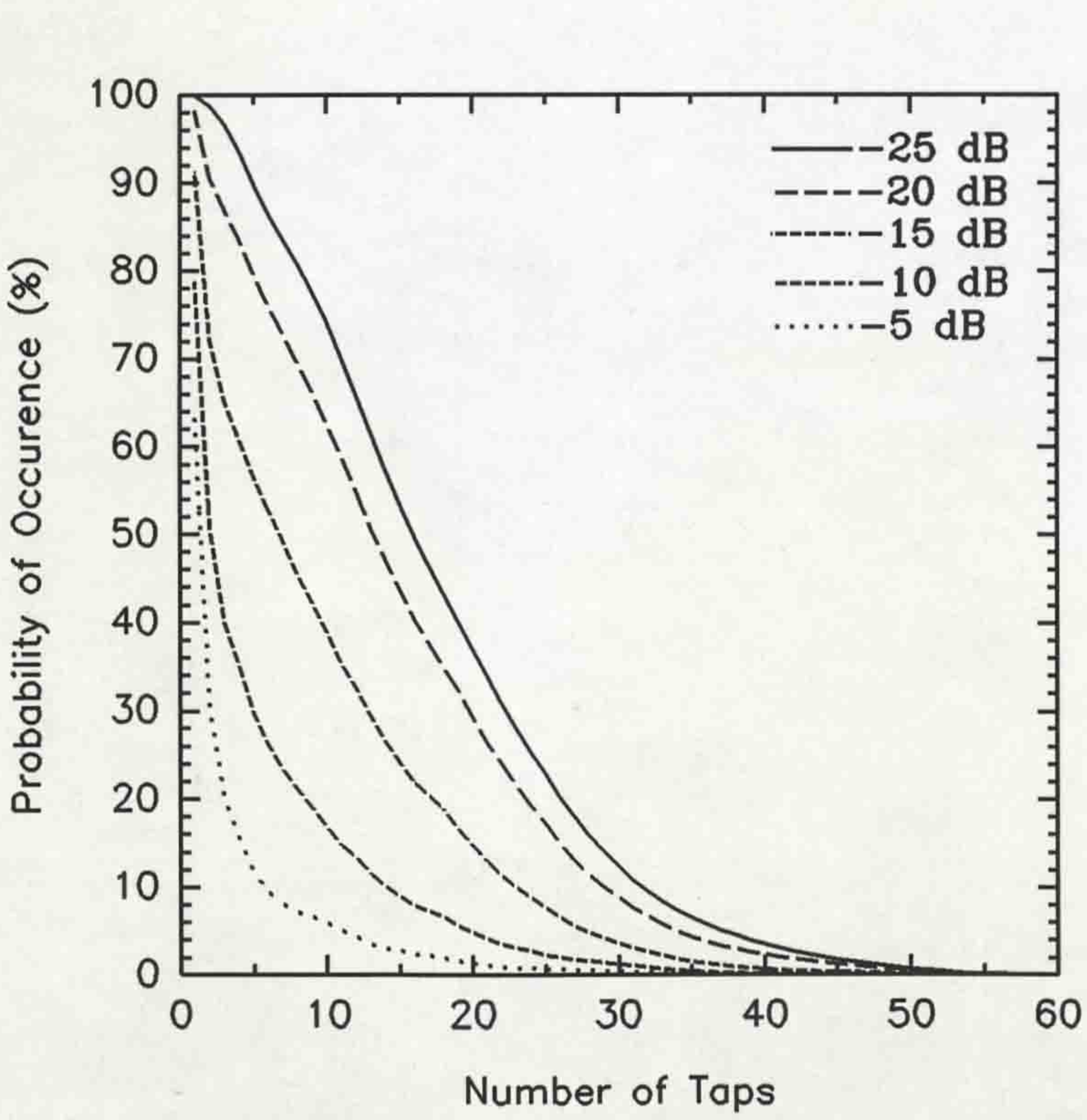

Figure 5.93 Probability of occurrence versus the number of taps for URBAN1.

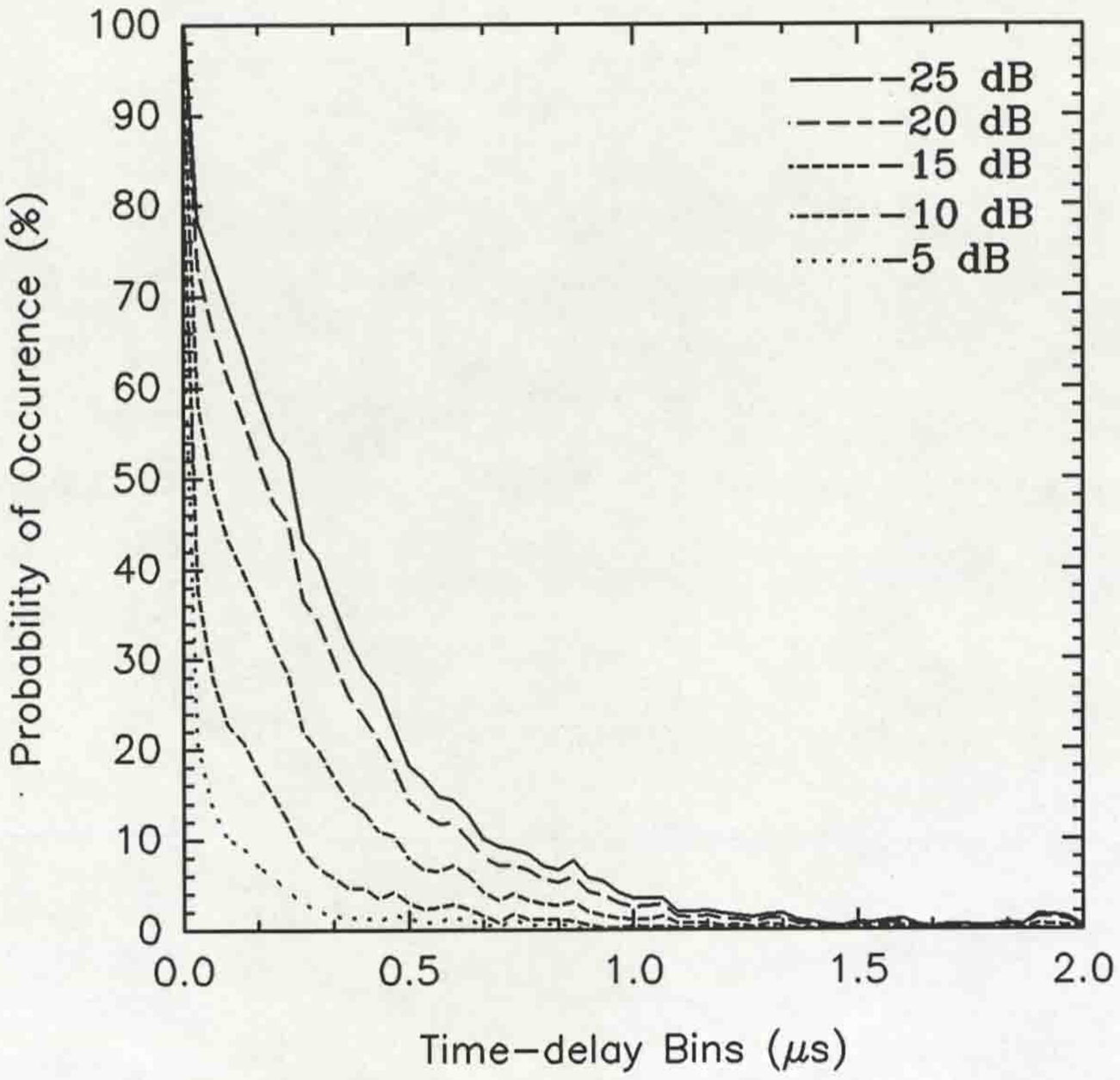

Figure 5.94 Probability of occurrence versus time-delay bins for URBAN2.

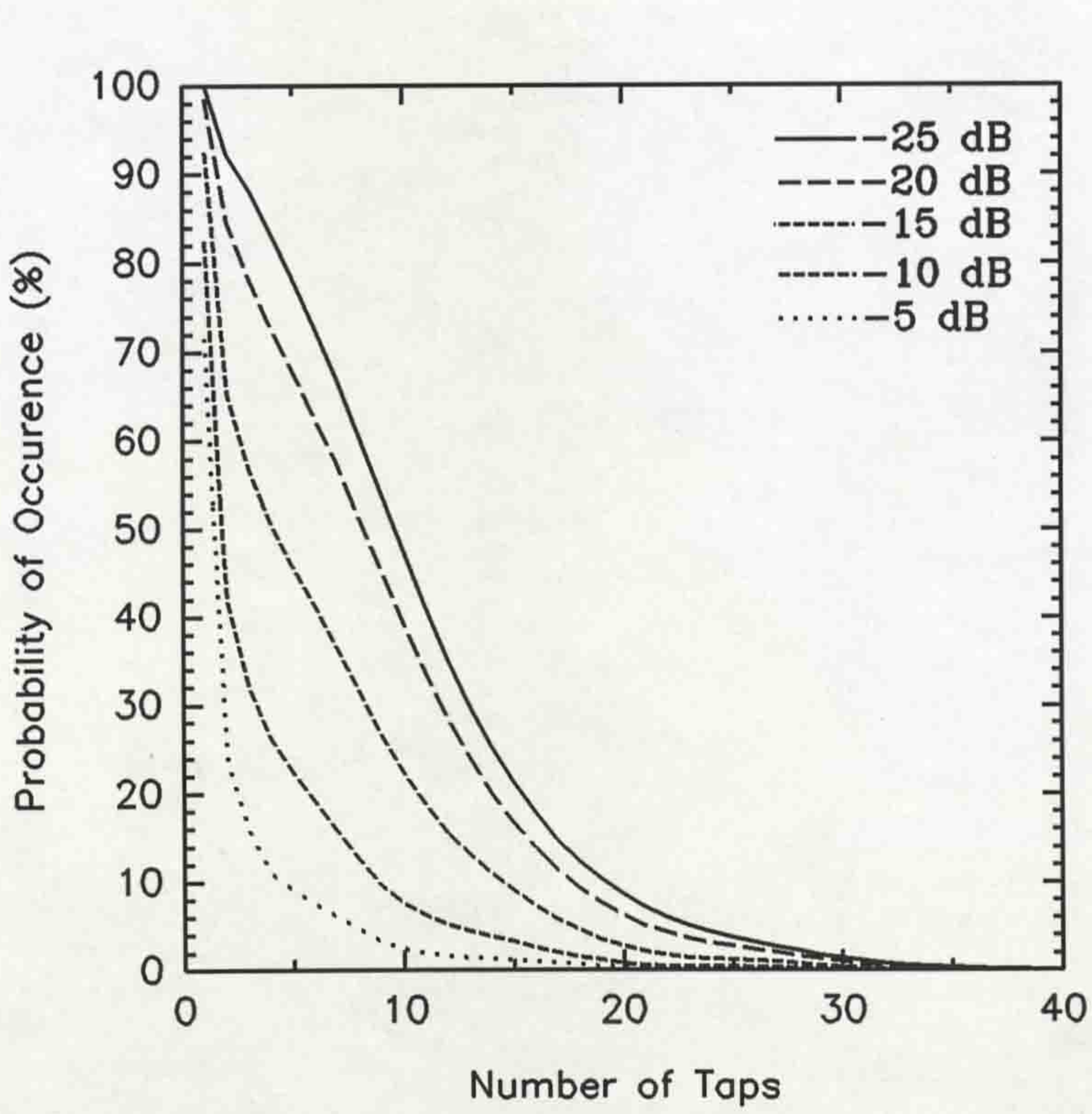

Figure 5.95 Probability of occurrence versus the number of taps for URBAN2.

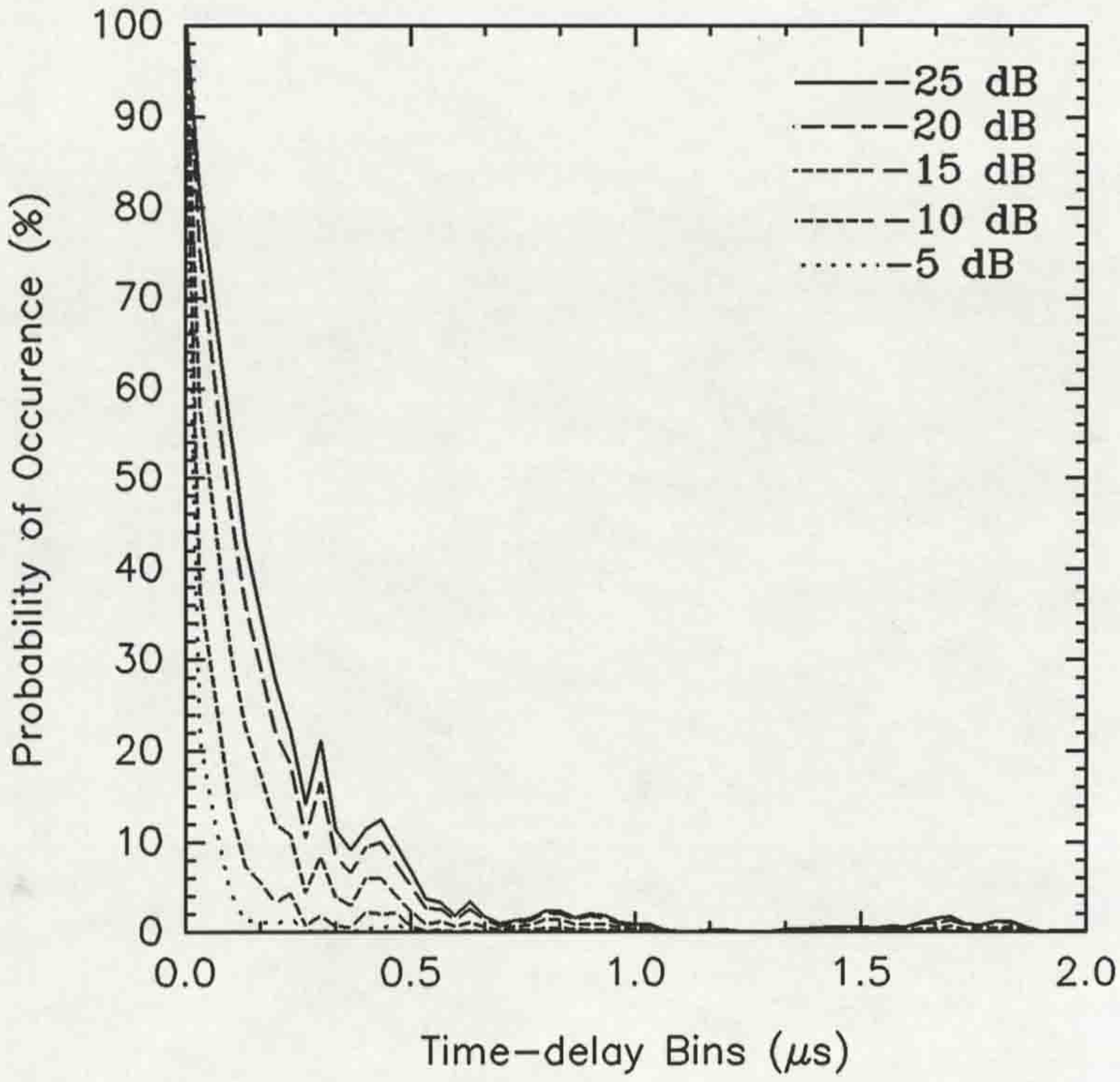

Figure 5.96 Probability of occurrence versus time-delay bins for the rural open area.

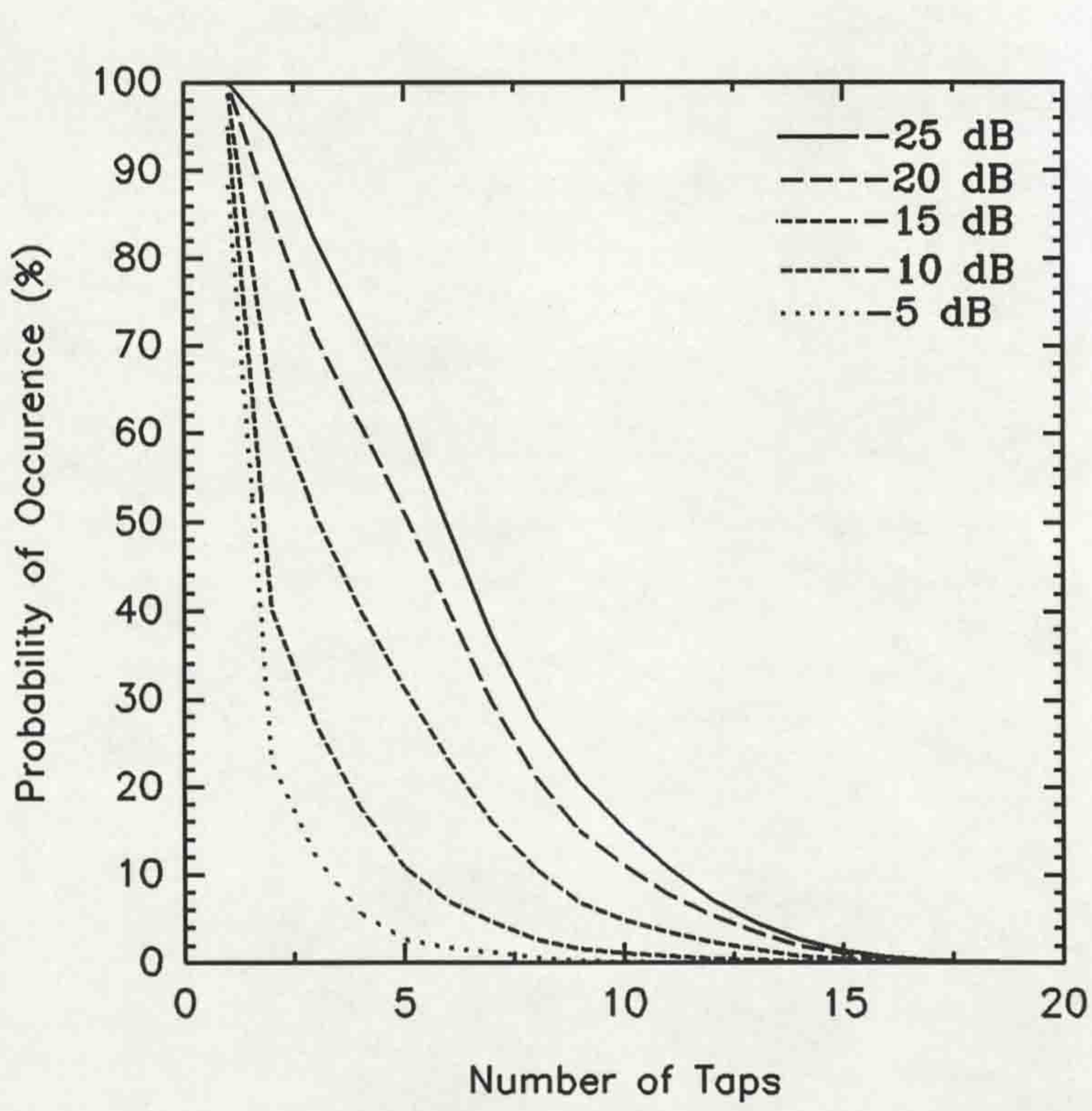

Figure 5.97 Probability of occurrence versus the number of taps for the rural open area.

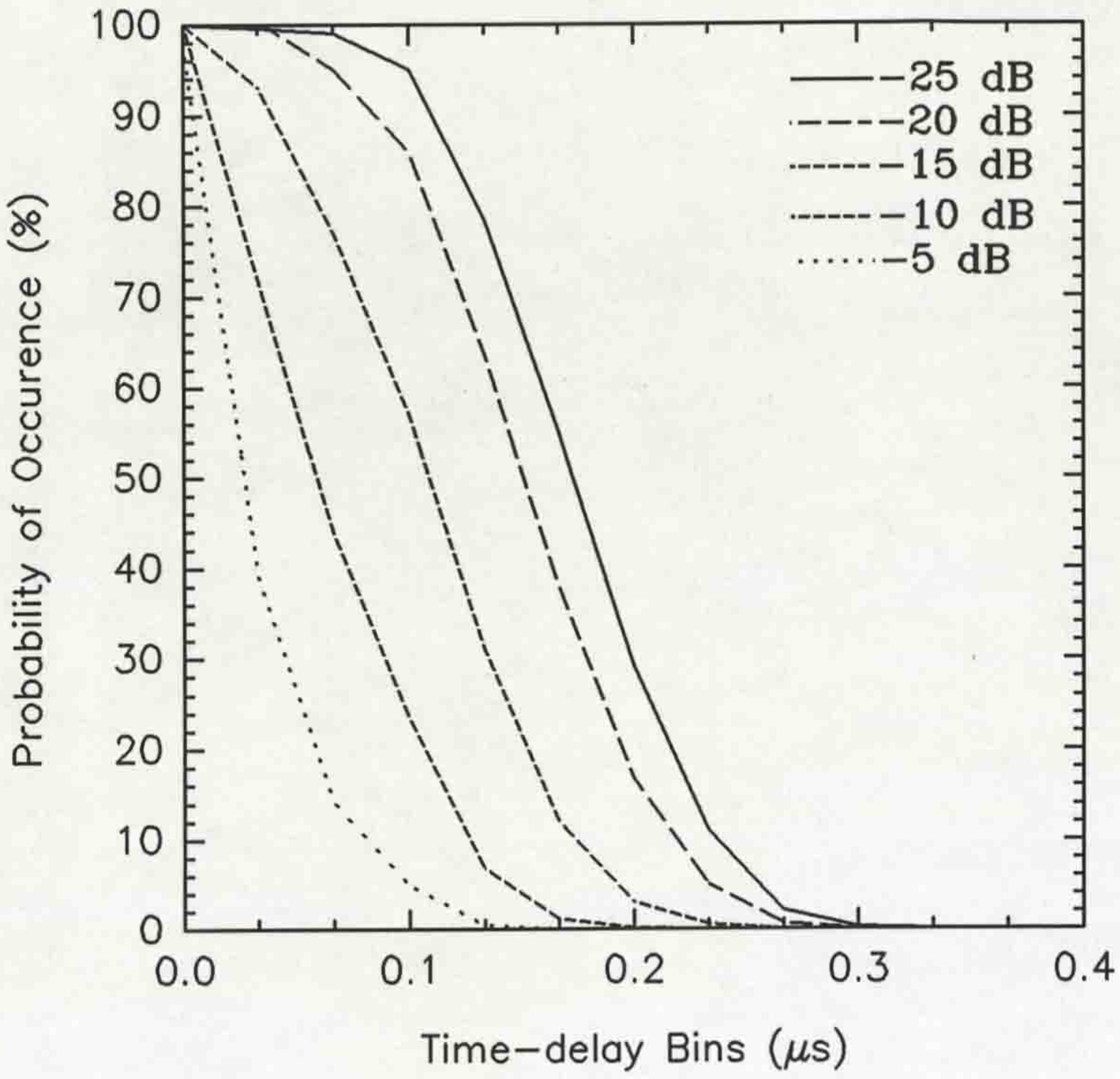

Figure 5.98 Probability of occurrence versus time-delay bins for SMARKET1.

Figure 5.99 Probability of occurrence versus the number of taps for SMARKET1.

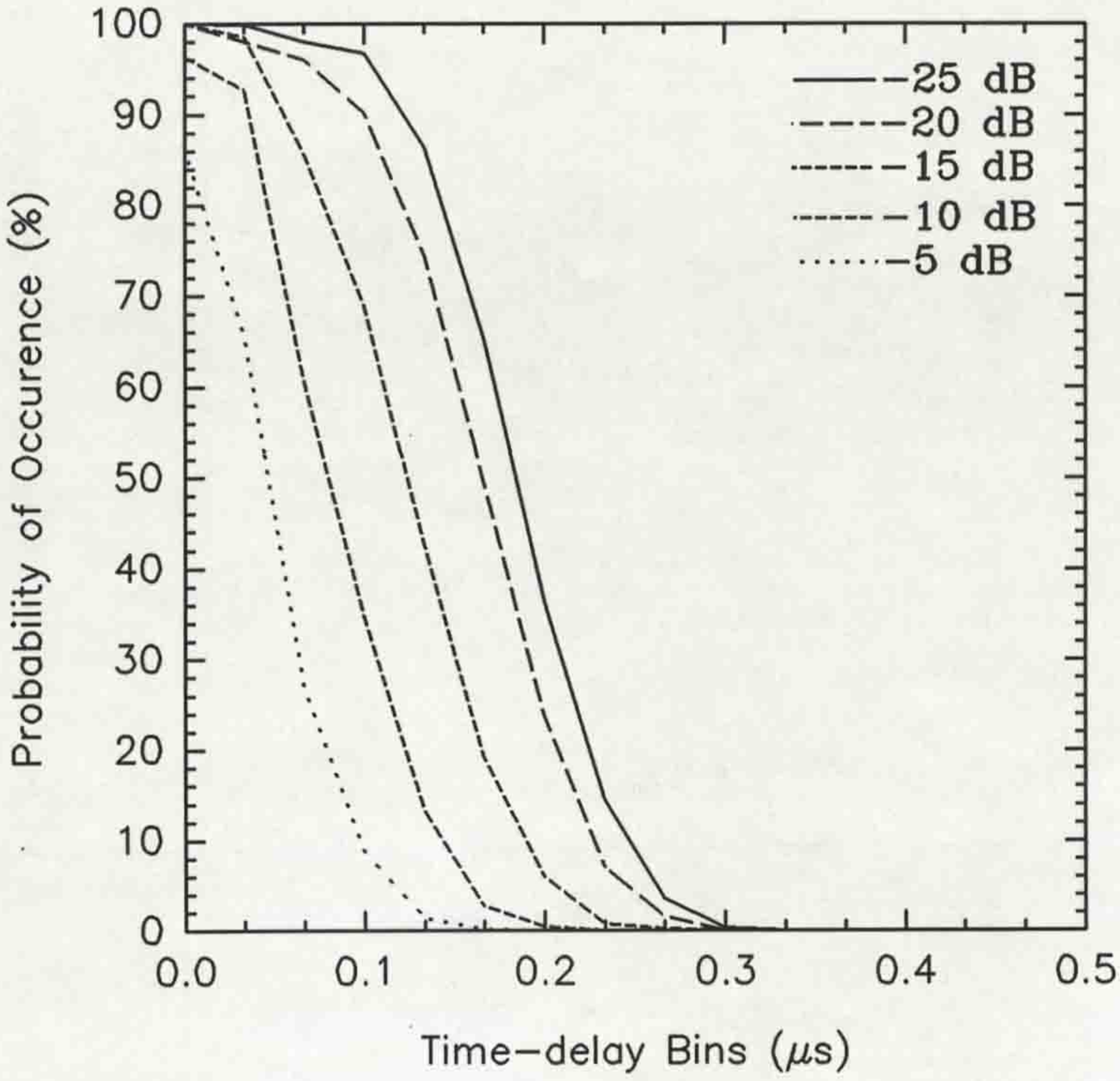

Figure 5.100 Probability of occurrence versus time-delay bins for SMARKET2.

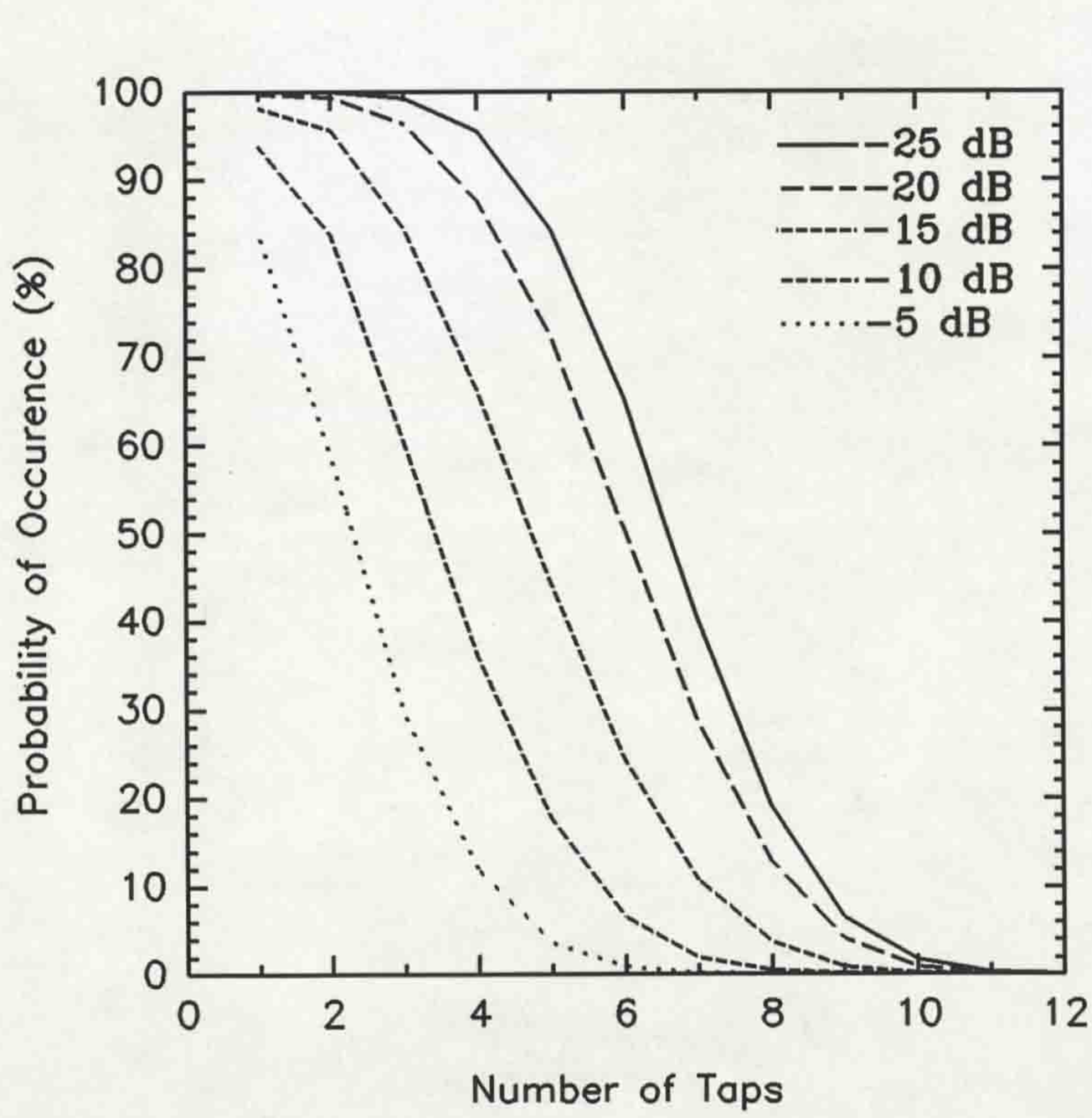

Figure 5.101 Probability of occurrence versus the number of taps for SMARKET2.

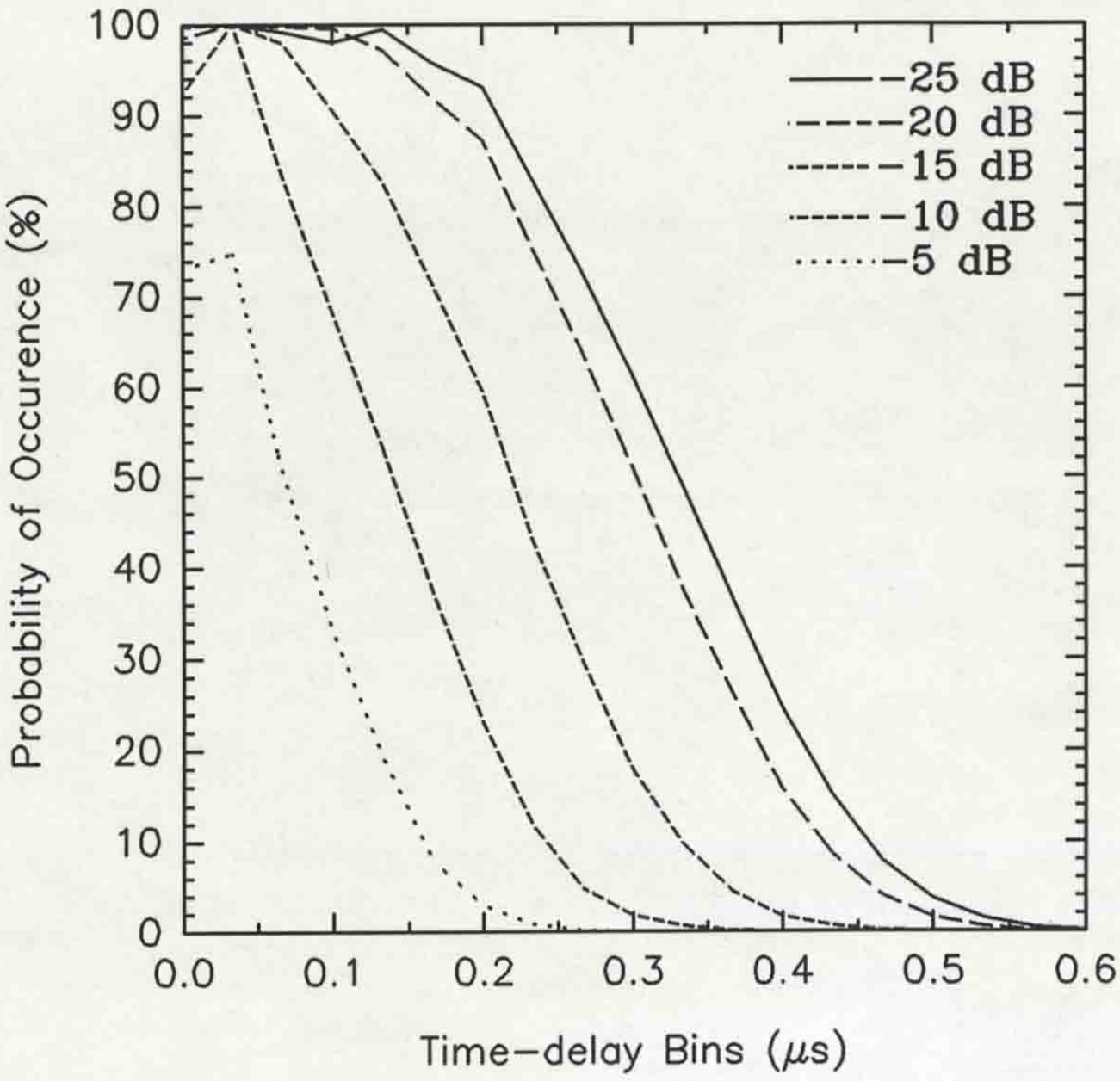

Figure 5.102 Probability of occurrence versus time-delay bins for the train station.

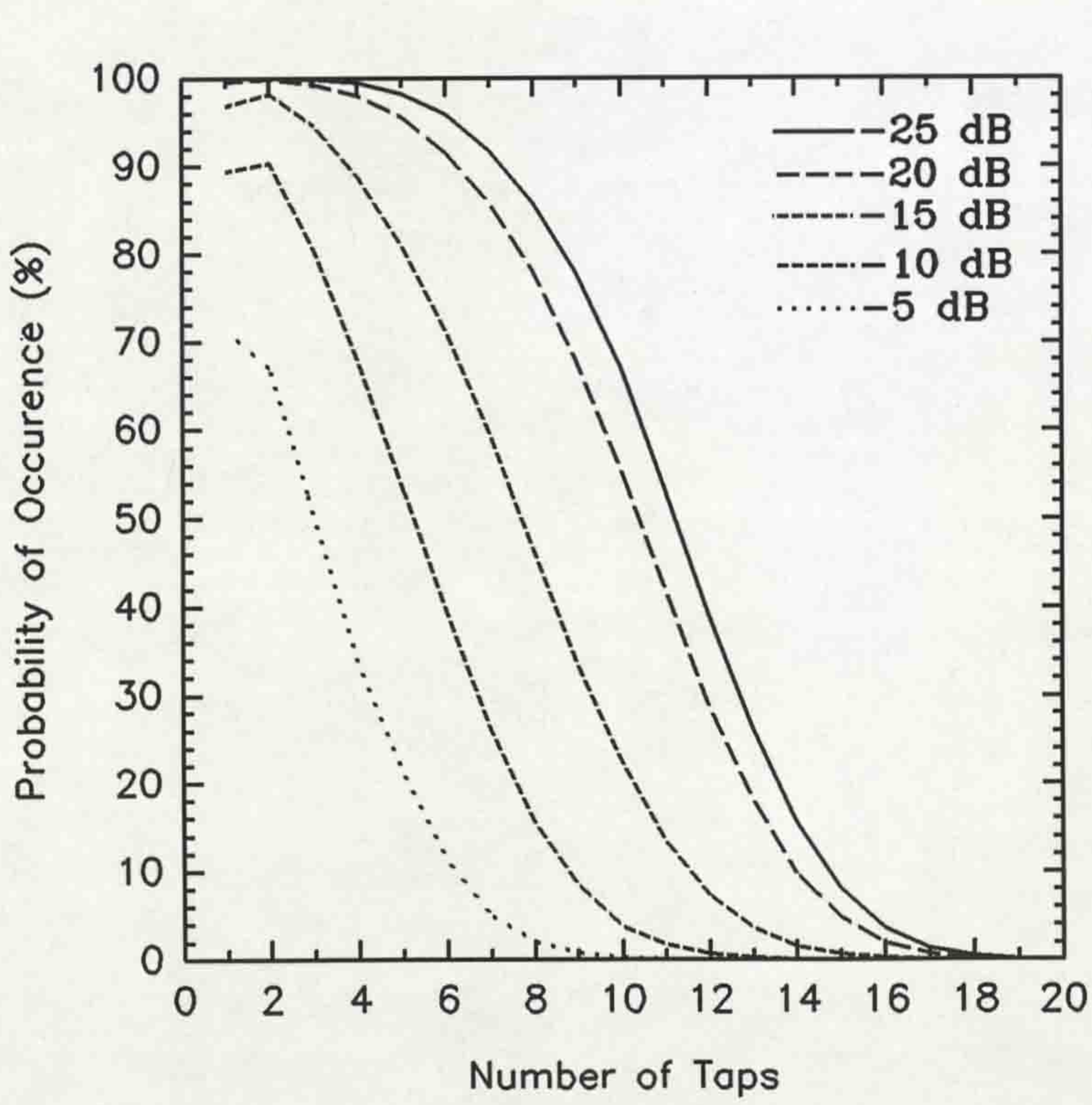

Figure 5.103 Probability of occurrence versus the number of taps for the train station.

Chapter Six

CONCLUSIONS AND FUTURE WORK

6.1 CONCLUSIONS

The need to provide mobile radio communication services to an ever increasing number of users within the limited available frequency spectrum has necessitated a transition from the first generation of narrowband analogue systems to wideband digital techniques. In the light of this, systems such as the GSM system and its derivatives were developed. Even with these sophisticated second generation systems, the advent of PCS implies that capacity will still be a problem. Today, many researchers are turning to spread spectrum techniques, which until now have been used exclusively for military purposes. At the forefront of this is Qualcomm of the U.S.A., who have proposed a second generation system based on spread spectrum techniques. This is a CDMA system, the so-called IS-95, which is envisaged to provide several advantages over the other second generation mobile radio systems. Although the properties and advantages of CDMA systems are well known in the military arena, these have not been thoroughly investigated in mobile radio systems. As a major prerequisite to the design of any system, knowledge of the propagation characteristics of the radio channel is required. This should include not only its dispersive properties, but also its fading characteristics. However, there is very limited statistical data which can be used in the design and implementation of future CDMA systems. There is therefore, a need to obtained statistical data that provides a reliable picture of the multipath propagation channel.

In the light of this, experimental investigations have been carried out in different environments. A substantial amount of wideband data was collected and analysed, the results of which have been presented in this thesis. General conclusions concerning the important aspects and observations from this study are presented in this chapter.

For any experimental investigation, the measurement system and experimental design

are very important. Having discussed the advantages and disadvantages of the various channel sounding techniques, the Swept Time-Delay Cross-Correlator (STDCC) channel sounder was found to be the optimum in the light of the requirements proposed for the experimental system. These requirements, implementation and evaluation of the experimental system were presented in Chapter 3. The overall system provided a 33.3 ns time resolution and an impulse response sounding rate of about 16 power delay profiles per second. A significant improvement in the system performance was achieved by incorporating automatic gain control (AGC) circuitry in the RF stage of the receiver. In addition, the use of coherent demodulation combined with the use of high quality frequency sources at the transmitter and receiver provided a system with a phase change of 1 cycle in 360 s. This superior stability coupled with the inclusion of the AGC circuitry permitted continuous measurements for longer spatial distances of up to 100 m, using a PC-based direct data digitisation technique. The system was then used to create a large database of complex power delay profiles from different environments, namely, urban and rural open areas, supermarkets and a train station.

To design and implement any future mobile radio system, knowledge of a realistic picture of the propagation channel is important. Hence, the experimental design was formulated to cater for this issue so as to avoid over- or under-estimating the various channel parameters. Generally, a substantial number of complex power delay profiles were collected in a random manner around each base station, with no preferences given to the nature of the power delay profiles. Hence, the results should provide true estimates of the channel descriptors.

Next, the small-scale channel descriptors, which were defined in Chapter 4, were evaluated. Due to gross non-stationarity in the propagation channel, the time dispersion results were presented in the form of cumulative distribution functions of the small-scale channel descriptors in order to show their large-scale behaviour. Generally, the measured values of the various parameters from the outdoor locations are lower than some of those which have been reported in the literature, even though

delay spread values of up to 7.87 μs were recorded. This was attributed to the manner in which previous experimental data was collected and the sparsity of the data. The performance of the GSM system was examined based on a relationship between the irreducible bit error rate (IBER) and delay spread. Based on this relationship, it was observed that the large values of delay spread will cause a significant deterioration in performance. However, the percentage of locations with these large delay spread values was found to be very small.

The time dispersion measurements for the within building experiments were generally lower than those from the outdoor locations as expected. For the supermarkets, the results were generally lower than those reported for multistorey buildings. This was attributed to the fact that, typically, supermarkets contain little or no glass sections, hence, no external multipath components which can cause the existence of late echoes were present. However, estimates of the delay spreads in these areas were in the same order of magnitude as those recorded for street-level microcells. It was also observed that, even though the two supermarkets differ in terms of their contents, layout of display shelves and building construction, the time dispersion results were similar. The maximum delay spread of 0.6 μs in SMARKET1, which was recorded in a main aisle, was therefore attributed only to the size of the building.

The measured results obtained from Lime Street Station were generally higher than those from the supermarkets, about a factor of 2 higher. It was also observed that the number of multipath components was higher, with a mean value of 10.6 compared to about 6 for the supermarkets. This was attributed to the results of the scattering effects of the crisscross pattern of metal that dominated the structural contents of this building.

By evaluating the frequency correlation functions (FCF) of the power delay profiles the coherence bandwidths at 0.5 and 0.9 correlation were obtained. Having obtained their CDFs, it was found that URBAN1 would present frequency selective effects severe enough to effect systems such as GSM, which utilise a bandwidth of 200 kHz.

It was also shown that the Qualcomm's IS-95 system will suffer a similar effect in 50% of the locations in URBAN1 if the coherence bandwidth at 0.5 correlation is taken as a measure of performance. It was also shown that, for any value of delay spread there exists a minimum value of the coherence bandwidths. These two equations were derived from the experimental data and are shown to be in agreement with previous results. This was explained by acknowledging that, in most of the previous experimental investigations, worst case power delay profiles were often sought.

Wideband pathloss was also evaluated for the within building data. Using a reference distance of 1 m and averaging over a distance of approximately 20λ, scatter plots of pathloss against distance were generated. Least square fits made to the data provided the pathloss exponent, n. Generally, the correlation between pathloss and distance was very high and n varied between 1.67 and 4.4. In some locations in SMARKET1 and the train station, n was less than 2, indicating the existence of a wave guiding effect. In SMARKET1, this was due to the long aisles which were flanked by metal display shelves. In the train station, this could have been due to the high concentration of metal that dominates the structure of the building. In SMARKET2, the aisles which were narrower and shorter were flanked by higher display shelves, with some extending to the roof. Overall, the value of n in SMARKET1 was about 2 compared to 2.4 for SMARKET2 and the train station. In addition, the microcell scenario where a sharp decrease in signal level occurs when the receiver moves from the main street into a side street was observed in the supermarkets when the receiver moves from the main aisle into a minor aisle.

The amplitude and phase of some of the echoes in different time-delay bins were briefly examined. The amplitude distributions do not fit either a Rayleigh or Rician distribution. This attested to the fact that as the resolution of the channel sounder increases, the individual echoes are resolved. The distribution of the phases showed a good approximation to a uniform distribution from $-\pi$ to π for the first two taps.

One of the main advantages of direct sequence CDMA system is the possibility of exploiting the multiple forms of diversity through the use of a Rake-type receiver. Moreover, accurate power control in a CDMA system is critical, not only for better system performance, but also for enhancing capacity. The measured data was therefore used to demonstrate the Rake gain. The Rake receiver model that was presented in Chapter 4 was utilised. In these investigations, the signal-to-noise ratio (SNR) was used as a measure of performance.

Firstly, an all-path Rake receiver that uses maximal ratio combining was compared to one that uses equal gain combining and a standard receiver that demodulates only the strongest tap. It was observed that the Rake receiver with maximal ratio combining outperformed the others. The performance of the Rake receiver with equal gain combining and the 1-path receiver were very close and in some cases the latter performs even better. By analysing the large-scale behaviour of the relative SNRs, variations of 40 dB were observed, signifying the need for power control.

For the above investigations all the received multipath echoes were demodulated. In practice, and ignoring the added complexity and cost in implementing an all-path receiver, there is a diminishing return in terms of the Rake gain as the number of branches increased. Hence, the performance of Rake receivers with varying number of branches were examined. The results showed that, even though the all-path receiver is the optimum, a gain of 5 dB could be achieved in moving from a 1-path to a 5-path receiver. This was true particularly for the urban locations. In the supermarkets, there was no significant gain in using an all-path receiver.

By examining the short-term variations of the SNR, the reaction time of the power control schemes could be estimated. It was illustrated that the control rate of the closed loop power control scheme in the IS-95 system may not be adequate. It was also observed that as the number of branches reduced, fading increases and the probability of occurrence of deep fades increases.

Finally, the probability of occurrence of the echoes was evaluated for different signal levels. It was shown how these curves can be used to aid in the design of an optimum Rake receiver.

6.2 RECOMMENDATIONS FOR FUTURE WORK

The main objective of this study has been to provide reliable wideband data which can be used in the design and implementation of future CDMA systems or indeed, any wideband system. The results and salient conclusions drawn from analysing the data have been presented. In the light of the results presented, when compared to some of the previous wideband results, it is safe to recommend that future experimental investigations should be designed in such a way that analysis of the data will provide a reliable picture of the wideband propagation channel.

Since experimental investigations are always expensive and time consuming, it is important to investigate the possibility of predicting the channel response by modelling the wideband data.

Spread spectrum systems have the capability of providing certain advantages which can not be exploited in the conventional TDMA and FDMA systems. Some of these aspects include:

i. Investigating whether there is an optimum bandwidth for spread spectrum systems. It is appropriate to investigate this issue experimentally rather than using a convolution process on data collected at a higher bandwidth.

ii. In the IS-95 system, soft handoff is one of its advantages. More information on the variations of the propagation characteristics from several transmitters to a particular receiver in a fringe area between cells is required in order to assess the performance of the soft handoff procedure.

iii. Power control is a key issue in direct sequence spread spectrum systems. More investigation on the required reaction time of power

control algorithms is required, since the power control strategy affects both the system performance and the capacity.

Appendix

LIST OF PUBLICATIONS

[1] Nche, C., Turkmani, A.M.D. and Arowojolu, A.A., 'Channel Sounder for PCN Networks', IEE Colloquium on High Bit Rate UHF/SHF Channel Sounders - Technology and Measurement, Digest No. 1993/233, Dec. 1993.

[2] Nche, C., Lewis, D.G. and Turkmani, A.M.D., 'Wideband Characterisation of Mobile Radio Channels at 1.8 GHz', IEEE 44th Vehicular Technology Conference, Vol 3, June 1994, pp1775-1779.

[3] Nche, C., Parsons, J.D. and Turkmani, A.M.D., 'Indoor and Outdoor Time Dispersion Measurements at 1.8 GHz', IEE 9th Intl. Conf. on Antennas Propagation, ICAP95, IEE Conf. Publication No. 407, Vol. 2, April 1995, pp13-17.

CHANNEL SOUNDER FOR PCN NETWORKS

[1]C. Nche, A.M.D. Turkmani and A.A. Arowojolu.

1. Introduction

The research in wideband transmissions dates as far back as 1950 [1], with a substantial amount of literature already available to the public domain. The published work, although valuable, has focused mainly on a basic understanding of the mobile radio channel and an evaluation of the disruptive effects of this channel on the performance of wideband transmissions. Most previous researches have been undertaken with a view of promoting certain techniques and basic ideas for a possible future wideband radio system. Nowadays, these aspects are changing since at least three wideband mobile radio systems are well defined and one of which (GSM) is already operational in Europe. The other two are expected to be fully operational in Europe in the near future, namely DCS1800 (PCN) and DECT. Hence, wideband systems are now a reality and different operators are currently seeking systems which can be used in the field not only to characterise the radio channel but also to evaluate and/or predict the performance. For example, the GSM system which is now operational may have problems in certain areas because of coverage, interference or time dispersion. In this situation the operators would require a well-designed, portable and reliable system which can identify the problem in the field, so that a solution can be sought. Identifying a time dispersion problem is not easy since it necessitates measuring the channel characteristic in the "trouble" area and then determining the expected system performance under the measured channel condition. The need here, therefore, is for a system which can measure not only the time dispersion (i.e. channel sounder) but also to predict the system performance in the field. This paper describes a portable wideband channel sounding system which is easy to use in the field and is capable of satisfying the above requirements.

2. A review of wideband channel sounding

Wideband channel sounding provides a practical means of measuring the time-dispersive characteristics of the mobile radio channel. A number of sounding techniques are now well established which give results in time or frequency domain. The choice of the sounder depends on the parameters to be measured and its intended application.

2.1. Pulse sounding techniques

When an impulse is used to excite the mobile radio propagation channel, the received signal represents the convolution of the sounding pulse with the channel impulse response. In order to observe the time-varying behaviour of the channel, periodic pulse sounding must be used. The pulse repetition period must be sufficient to allow observation of the time-varying response of the individual echo paths, whilst also being long enough to ensure that all multipath echoes have decayed between successive impulses. Channel sounding employing this method, therefore amounts to measuring the channel impulse response, and explicitly show the time-delay multipath characteristics. If coherent detection of the inphase and

---

[1] The University of Liverpool, Dept. of Electrical Engineering and Electronics, P.O. Box 147, L69 3BX, U.K.

quadrature components of the pulse is employed, the Doppler shifts associated with each time delay can be extracted and hence the angle of arrival can be obtained.

The above method has been utilised extensively by several researchers [1-3]. The simplicity of constructing a sounder of this sort is of great advantage. However, there are certain disadvantages associated with it. The main limitation of this technique is the peak power requirement necessary for the detection of weak echoes. Additionally the interference to other users will limit the required transmitter power in the already congested radio spectrum.

2.2. Pulse compression techniques

This technique is accomplished by transmitting a code sequence with a noise-like character. In the receiver, the code sequence is compressed into a narrow pulse by either convolution (matched filtering) or correlation detection. The output of such a system gives the impulse response of the channel since the code sequence has noise-like characteristics.

The main difference between convolution and correlation detections is that, the output of the former is a real-time measure of the impulse response, whereas the output of the latter is a measure of the impulse response at a certain time delay. The two techniques can be made equivalent by using an infinitesimal bank of correlators which produce samples of the impulse response for all time delays. However, it is possible to utilise only one correlation stage in the receiver by varying the relative delay between the codes. This can be achieved by discretely stepping the code through each of its phases or offsetting the clock frequencies of the codes, thus enabling the relative delay between them to vary linearly with time.

In practice, pulse compression is achieved either by correlating the received signal with a replica of the transmitted signal or by applying the received IF signal to the input of a filter matched to the transmitted code sequence. The code sequence used must be deterministic and should possess noise-like characteristics. A maximal length pseudo random binary sequence (m-sequence or PRBS) is often used because of its excellent periodic autocorrelation function.

The convolution technique was used by Bajwa [5], in which an experimental surface acoustic wave (SAW) device was employed to achieve the match filtering. The bandwidth of the IF stage is the clock rate of the m-sequence (12.75 MHz), hence a reduction was required before recording onto an FM instrumentation tape. The main disadvantages of this method is the inability to accurately reduce the IF bandwidth and the practical implementation of the SAW devices.

In contrast, the correlation detection technique has been widely utilised [5-7]. Cox [5] first used this in a mobile radio environment, but a significant improvement was made by Demery [6] by removing the IF stage and directly modulating the RF carrier with a 127 bit PRBS. This resulted in an IF bandwidth reduction from twice the clock frequency to twice the slip rate (4 kHz).

2.3. Frequency domain sounding

Wideband channel measurements in the frequency domain permits the study of the frequency selectivity of this channel directly. This can be achieved by the spaced tone method in which two adequately spaced carriers are transmitted. The main limitation of this method is the fact that the mobile needs to be stationary before data can be recorded, hence the Doppler shifts cannot be extracted from the measurements. Alternatively, a frequency hopping technique can be deployed, but this requires a lot of computation to obtain the time-domain parameters. This limitations also apply to swept frequency continuous wave (Chirp) sounders which also require fast switching synthesizers.

3. The University of Liverpool channel sounder

In this section a detailed description of the wideband channel sounder currently available at the University of Liverpool will be given. It uses the swept time-delay cross-correlation (STDCC) sounding technique. The block diagram of the sounder is shown in Figure 1.

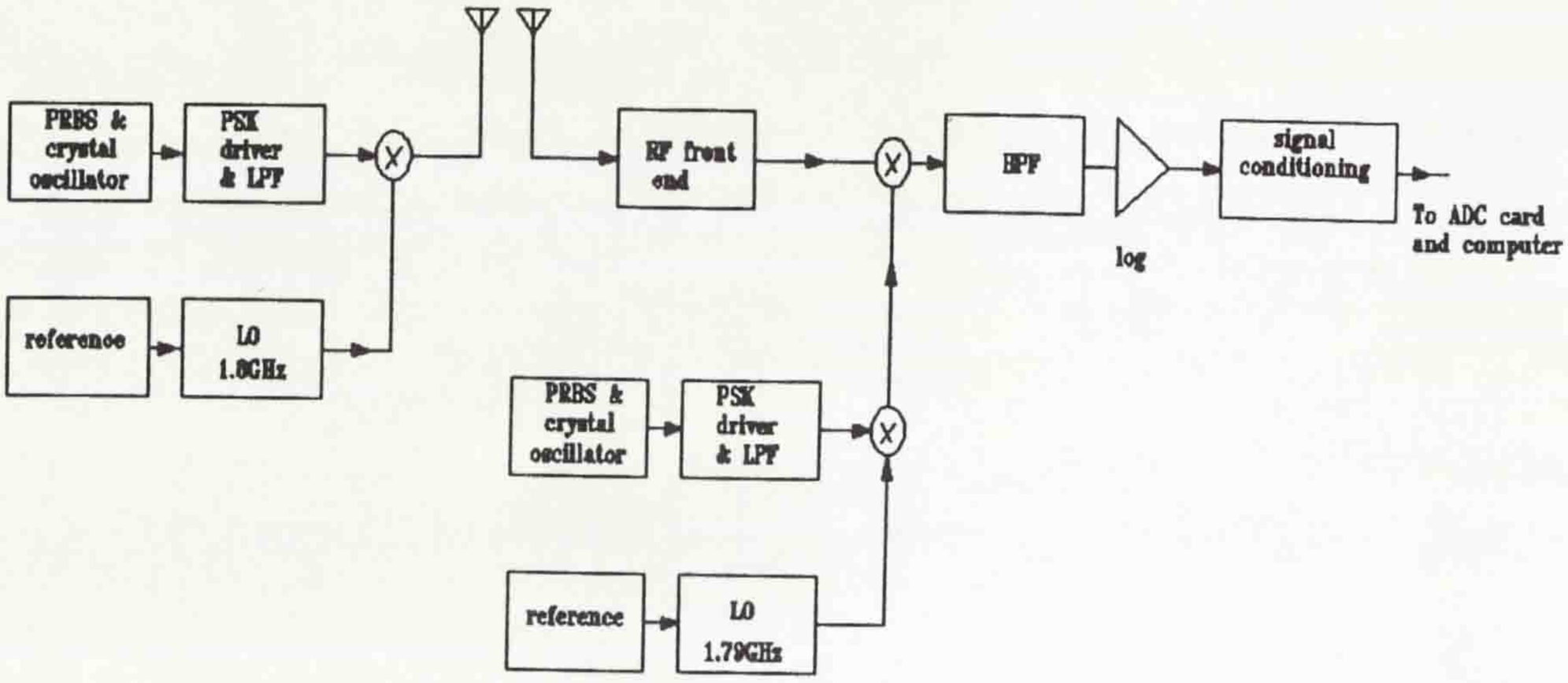

Figure 1 Block diagram of the transmitter and receiver of the STDCC sounder.

A 511-bit PRBS clocked at 30 MHz is fed to the input of a PSK driver, the output of which is subsequently filtered using a 30 MHz, 3dB bandwidth low pass filter. The output of the filter is used to phase-reversal modulate a 1.8 GHz carrier which is locked to a highly stable frequency standard. The low pass filter takes out the unwanted sidelobes which can cause severe interference to other users. This therefore, eliminates the need for any RF filtering before transmission. The spectrum of the transmitted signal is shown in Figure 2.

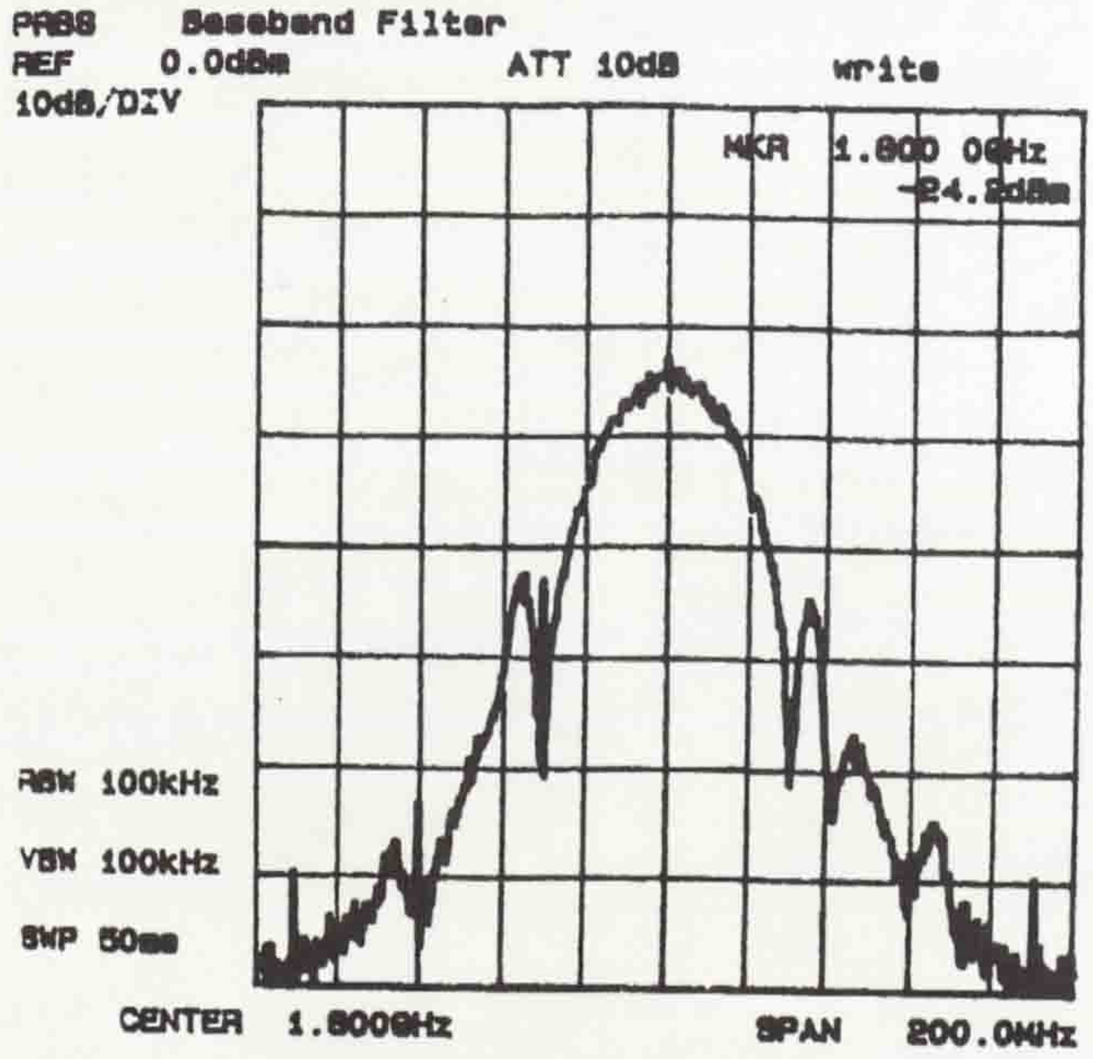

Figure 2 Typical transmitted spectrum.

The receiver is made up of four distinctive sections: the RF front end, the regenerated offset modulated PRBS, the IF/envelope detection and data acquisition/analysis sections. The RF front end consists of low-noise wideband amplifiers, a 60 MHz RF bandpass filter, a wideband attenuator and a mixer. Translation to an IF of 10 MHz is effected by mixing with a 1.79 GHz local oscillator locked to a high stability frequency standard, which has been phase-reversal modulated by the locally generated m-sequence identical to that of the transmitter but clocked at a slower rate (29.992 MHz). The IF signal is passed through a 10 MHz crystal bandpass filter and a logarithmic amplifier performs the envelope detection. The resulting output is suitably conditioned and passed to an 8-bit analog to digital converter which is interfaced to a laptop or personal computer via the printer port. A typical power delay profile from the system is shown in Figure 3.

The main features of the STDCC channel sounder are summarised in the table below.

Characteristic	**Typical Value**	**Comment**
Clock Rate	30 MHz	This gives a time delay resolution of 33ns or 10m spatial resolution.
Maximum measurable excess delay	17.03μs	This is given by the product of the PRBS length (511) and the time delay resolution.
Slip rate	8 kHz	This gives a bandwidth reduction factor of 3750 and a sounding rate of about 16 profiles per second
Dynamic range (obtained from back-to-back measurement	30dB	The measured difference between the height of the main echo and the spurious floor level.
Frequency stability	2 x 10^{-10}/day	Both transmitter and receiver are locked to highly stable 10 MHz frequency references.
Single sideband phase noise power spectral density of signal sources	-80dBc in a 1Hz bandwidth at a carrier offset of 10kHz	-

4. Data acquisition and analysis

In all the previous systems the method of acquiring the data precluded the implementation of any on-line processing. For example Young and Lacy [1] used a 16mm camera and Natarajan [7] used an analogue FM instrumentation tape. This latter approach requires digitisation before any processing is carried out, hence, the systems which used this method were often bulky and processing could not be carried out in the field. The former technique is even more limiting in that it makes post-processing even more difficult. All the above limitations have been successfully addressed in the current University of Liverpool's channel sounder.

The output of the channel sounder is interfaced to a laptop or personal computer via an 8-bit analogue to digital converter (ADC). The ADC plugs into the printer port of the computer and a pull-down menu-driven software package takes control of the sampling and

data processing. The sampling rate of the ADC is controlled by the computer and this can be set to up to 45 kHz. The acquired data is stored on the hard disk of the computer which can also be viewed on-line. The software allows printing of the result file and the power delay profiles as well as allowing flicking through the individual profiles on-line.

After acquisition of data, the start of profile is manually located before the software can allow any further processing. The small scale parameters that can be evaluated as recommended by CCIR are : average delay, delay spread, delay window (90, 75 and 50%) and delay interval (15, 12 and 9dB). For each data file these parameters are calculated and stored in a result file, an example of which is shown in Figure 4. In all the calculations only profiles which satisfy the CCIR requirement of 15dB and 3dB margin of the peak to spurae are used, hence, those profiles which do not meet this requirement are discarded as shown in Figure 4. The result file also shows the total number of profiles, the total number of 'good' profiles, the means of the delay spread and average delay, and the total number of taps per profile. The predicted irreducible bit error rate (IBER) for a GSM-based system is also calculated based on an in-house simulation of the GSM system. This is given by [8]

$$IBER = 0.1945x(\frac{s}{T})^{1.8878}$$

where s is the mean value of the delay spread and T is the bit period which is equal to 3.7μs for the GSM system.

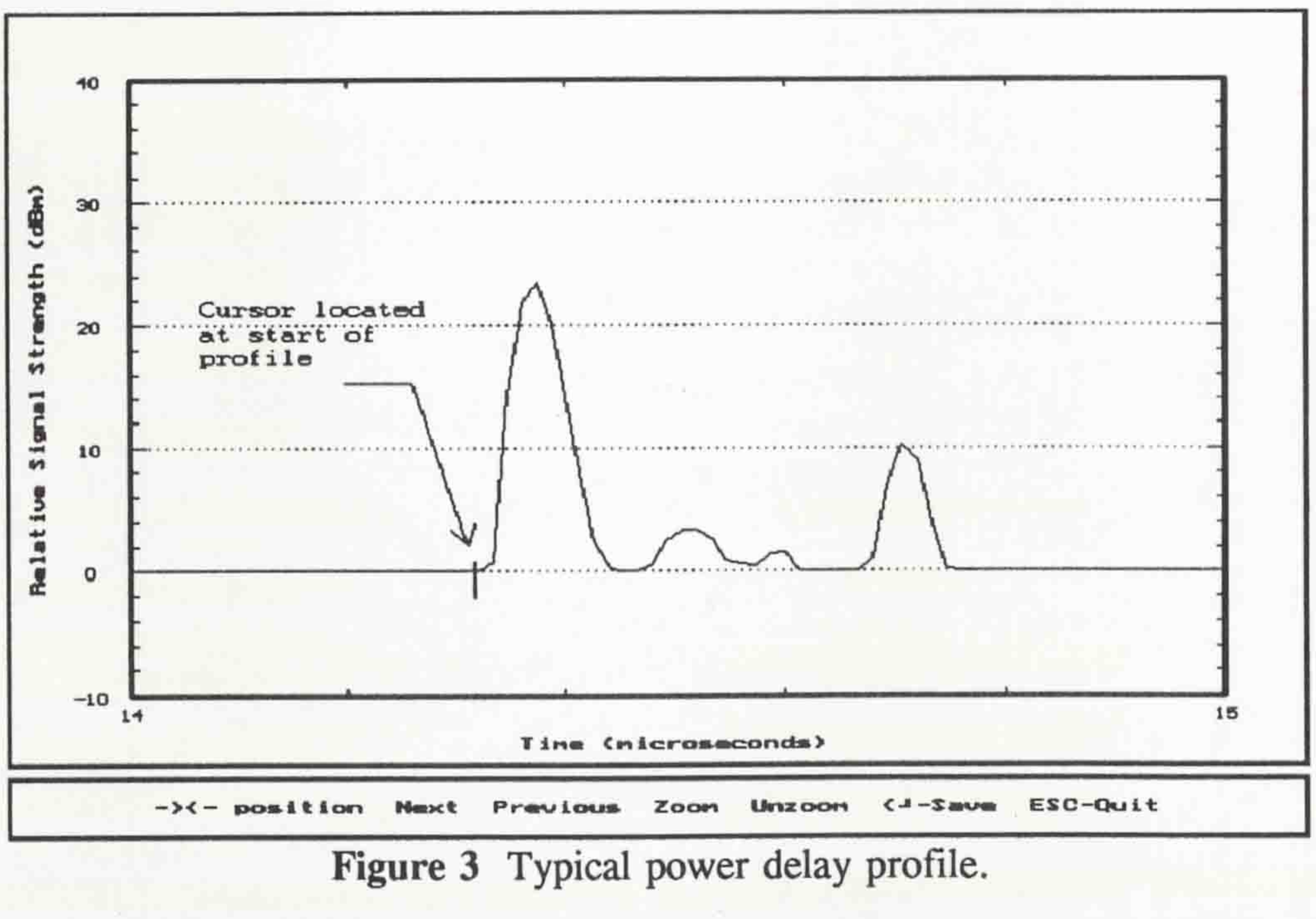

Figure 3 Typical power delay profile.

5. Further improvements

The dynamic range of STDCC sounders is often limited and therefore, a manual attenuator in the RF chain is often used. This requires previewing the measurement site before data acquisition and precludes continuous measurements. Because of this limitation (30dB dynamic range), an automatic gain control (AGC) system has been incorporated within the RF front end of the system. This AGC will suitably place the dynamic range window of the system such that continuous measurements can be obtained. The AGC signal can also be

recorded in order to obtain the absolute signal levels of individual echoes.

The phase angles which are required to determine the frequency selectivity of the channel can also be obtained from the system by coherently demodulating the IF signal to get the inphase and quadrature components. Computations to obtain the phase are handled by the software.

```
Profile Average Delay    Delay   Intervals      Delay  Windows        Taps
Number  Delay   Spread   15dB    12dB   9dB     90%    75%    50%     (Peaks)
100     0.019   0.038    0.173   0.160  0.160   0.120  0.107  0.027     2
101     0.051   0.047    0.200   0.173  0.173   0.133  0.120  0.080     4
102     0.013   0.031    0.173   0.120  0.107   0.120  0.080  0.027     4
103     0.018   0.044    0.227   0.187  0.107   0.147  0.067  0.040     5
Profile 104 does not satisfy the CCIR requirement.
105     0.047   0.053    0.200   0.173  0.173   0.133  0.120  0.093     2
Profile 106 does not satisfy the CCIR requirement.
107     0.051   0.039    0.187   0.173  0.147   0.133  0.107  0.080     2
108     0.006   0.025    0.000   0.000  0.067   0.000  0.027  0.027     4
109     0.016   0.034    0.173   0.147  0.147   0.120  0.093  0.027     3
110     0.006   0.047    0.067   0.067  0.067   0.053  0.027  0.027     4
111     0.006   0.041    0.093   0.067  0.053   0.067  0.027  0.027     4
112     0.003   0.031    0.000   0.000  0.067   0.040  0.040  0.013     4
Number of profiles identified = 112
Number of good profiles = 100
Mean of Delay spread = 0.037μs
Mean of Average delay = 0.028μs
Predicted IBER for GSM system(270kb/s) = 3.24e-05
```

Figure 4 Typical result file.

6. Conclusion

A properly designed, versatile and portable channel sounder and performance evaluator has been presented. This system with its user-friendly, menu-driven software package can easily be adapted to predict the performance of any wideband system by changing some of the parameters in the software. The system has been comprehensively tested in-house and in the field. With the receiver running off a 12V, 3A supply, the ADC plugs into the printer port of a laptop computer, the system can be used at anytime anywhere!

References

1) Young W. R. and Lacy, L. Y., "Echoes in transmission at 450 megacycles from land-to-car radio units", Proc. IRE, March 1950, Vol. 38, pp255-258.
2) Turin, G. L., Clapp, F. D., Johnston, T. L., Fine, S. B. and Lavry, D., "A statistical model of urban multipath propagation", IEEE Trans. Veh. Technol., Feb. 1972, Vol. VT-21, No. 1, pp 1-9.
3) Van Rees, J., "Measurements of the wideband radio channel characteristics for rural, residential and suburban areas", IEEE Trans. Veh. Technol., Feb. 1987, Vol. VT-36, No. 1, pp2-6.
4) Bajwa, A. J., Wideband characterisation of UHF mobile radio propagation in urban and suburban areas", PhD Thesis, Department of Electronic and Electrical Engineering, The University of Birmingham, 1979.
5) Cox, D. C., "Delay Doppler characteristics of multipath propagation at 910MHz in a suburban mobile radio environment", IEEE Trans. Antennas Propagat., Sept. 1972, Vol. AP-20, No. 5, pp625-635.
6) Demery, D. A., "Wideband characterisation of UHF mobile radio channels in urban areas", PhD Thesis, Dept. of Electrical Eng. and Electronics, The University of Liverpool, 1989.
7) Natarajan, N., "Wideband characterisation of mobile radio channels at 1.8 GHz", PhD Thesis, Dept. of Electrical Eng. and Electronics, The University of Liverpool, 1992.
8) Chaaban R. M., "Performance evaluation of a TDMA digital mobile radio system", PhD Thesis, Dept. of Electrical Eng. and Electronics, The University of Liverpool, 1993.

Wideband Characterisation of Mobile Radio Channels at 1.8GHz

C. Nche, D. G. Lewis and A.M.D. Turkmani*

Department of Electrical Engineering and Electronics,
The University of Liverpool, P.O. Box 147, Liverpool L69 3BX, U.K.

* Now with Mobile Systems International,
Floor 12, 1 Harbour Exchange Square, London E14 9GE, U.K.

Abstract: **This paper describes the results of an experimental investigation into wideband channel characterisation at 1.8GHz. The experiments were undertaken in the City of Liverpool using a swept time-delay cross-correlation (STDCC) channel sounder. This was used to measure the complex impulse response of the channel. The inclusion of an automatic gain control in the RF stage allowed continuous measurements for up to 200m. The results show smaller values for the time domain descriptors and only fades of about 1.5dB in the frequency domain.**

I. Introduction

The demand for mobile radio services has risen dramatically over the past five years with the result that the radio spectrum below 1GHz is now severely congested. The most probable solution to the problem is to utilise the spectrum around the 1-2GHz band and the 60GHz band. In the U.K., the frequency band 1800-1880MHz will be used for personal communications networks (DCS1800). In the USA a corresponding frequency band at 1900MHz will be used for personal communications systems (PCS1900). One of the problems in using these bands is the fact that not enough propagation data concerning the channel characteristics is available. Most wideband propagation studies have been conducted at frequencies below 1GHz. The measurements have utilised different designs of channel sounders with varying complexities and capabilities to measure the impulse response of the channel. Most of these previous measurements have concentrated on the measurement of the power delay profile [1], i.e, excluding the path phases. Because of the limitation in dynamic range of wideband channel sounders, the measurements have been conducted along short and specific areas of streets.

The objective of this paper is to present wideband propagation measurements at 1.8GHz for a dense-urban area. In the measurements, the envelope of the complex bandpass impulse response of the wideband propagation channel is measured using a Swept Time-Delay Cross-Correlator (STDCC) channel sounder, with a time delay resolution of 33ns, a maximum measurable excess delay of 17μs and a 60MHz channel characterisation bandwidth capability. The STDCC sounder used in the measurements has an automatic gain control, and yields the complex power delay profiles (i.e amplitude and phase). The use of automatic gain control in the RF stage allowed continuous measurements over longer distances, up to 200m. This sounder was used to measure the small-scale characteristics of the channel in the City of Liverpool. The results are presented in the form of cumulative distribution functions for the time domain parameters. The availability of the phase information facilitated the study of the frequency selective fading over a 10MHz bandwidth.

These measurements are part of the first phase of an experimental investigation of wideband channels in various environments including: urban, residential, hilly areas and wideband propagation into and within buildings (train stations and supermarkets). These investigations are useful in connection with future TDMA and CDMA (direct sequence and frequency hopping) mobile radio systems.

II. Measurement system

The measuring system is based on the pulse compression technique. In the transmitter a 511-bit m-sequence clocked at a frequency of 30MHz is used to phase reversal modulate a 1.8GHz carrier [2]. In the receiver the RF signal is translated to an IF of 10MHz by a 1.79GHz carrier that has been phase reversal modulated by a locally generated m-sequence clocked at a slower rate. Using a hybrid power splitter, the IF output is split into two cophasal signals. One of these outputs is used to obtain the envelope of the impulse response through the use of a logarithmic

amplifier and the other goes into an I and Q demodulator. The video output of the logarithmic amplifier was suitably conditioned in order to provide the AGC control signal. It also enabled visual inspection of the power delay profiles and for checking the integrity of the I and Q outputs, since the video output is approximately given by

$$video\ output = \sqrt{I^2 + Q^2} \qquad (1)$$

The I and Q outputs are low-pass filtered to obtain the inphase and quadrature components of the power delay profile, from which the phases of the individual echoes are computed. This was done using the relationship

$$P_e = \tan^{-1}\left(\frac{I_e}{Q_e}\right) \qquad (2)$$

where P_e is the phase of the echo, and I_e and Q_e are the magnitudes of the inphase and quadrature components respectively.

A programmable attenuator was included in the RF front end of the receiver. The setting of the attenuation was controlled by a digital circuit whose control signal was derived from the level of the power delay profile. To prevent this attenuator (AGC) from continuously switching, a window was suitably set within which the attenuator should not change. Outside this window the attenuation increases or decreases depending on the level of the power delay profile. This enabled the collation of data continuously for longer distances and without previewing the measurement site.

The time resolution of the STDCC sounder is 33ns corresponding to a spacial resolution of 10m. The maximum measurable excess delay is 17.03μs. The system offered a dynamic range of 30 dB. These values were verified by connecting the system back-to-back. A detailed description of the system is presented in [2].

The bandwidth compression (time scaling) which is inherent in the STDCC sounder, places a limitation on the maximum speed of the car if the Doppler shift information is to be resolved. The scaling factor for the system is 3750, giving a maximum speed of 1.3m/s [3]. To enable the mobile vehicle to travel at the required speed, a speed indicator was installed to make sure that the vehicle was moving at the required speed.

In order to obtain the impulse response of the channel, it is necessary to use stable frequency references in both the transmitter and the receiver. Rubidium standard oscillators were therefore used at the receiver and transmitter. This provided a stable reference and hence the variation of the phase due to the system was minimal.

III. Experimental procedures.

The transmitter was set up on the roof of the Electrical Engineering building in the precinct of the University of Liverpool. This is six storeys high and it is one of many high rise buildings in the vicinity. The experiments were carried out around the building in 8 different streets. Most of these streets have buildings up to 9 storeys high and are within 800m of the transmitter location. The experiments are intended for microcells with a cell radius of about 1km for PCN services.

The output of the transmitter was connected to a 2.5W broadband power amplifier before connection to a wideband discone antenna via a low loss cable. In the mobile vehicle, another wideband discone antenna was coupled to the receiver via a low loss cable. The outputs of the receiver were then connected to a 12-bit ADC card installed in the computer for digitization and storage.

IV. Data collection and analysis.

Four outputs were obtained from the receiver, i.e, the video output, the AGC level, and the I and Q outputs. These were connected to a 16 channel I/O card installed in the computer. The card was controlled by a purpose written software package. The sampling rate used was 20KHz which corresponds to a real time sampling rate of 75MHz. These four outputs were sampled simultaneously, the samples being stored in the extended memory of the computer. When the experimental run was over, the samples were transferred to the hard disk for permanent storage and analysis.

The analysis was carried out only after the start of the profile had been manually located. Only profiles which satisfied the CCIR requirement of 15 dB and 3 dB margin of peak to spurii were used, and hence those profiles which did not meet this condition were discarded. The phase was calculated from the I and Q outputs using equation 2 and the recording of the AGC output enabled the absolute signal levels of individual echoes to be calculated. The time domain parameters evaluated were: the average delay, delay spread, delay intervals (15dB, 12dB

and 9dB) and delay intervals (90%, 75%, and 50%) [3]. The cumulative distribution functions of these parameters were evaluated in order to show the large-scale variation of these parameters. The number of echo paths (taps) per profile were also determined and the CDF was evaluated. Figures 1 - 5 show the CDFs of these parameters.

The predicted irreducible bit error rate (IBER) for a GSM-based system was also calculated based on an in-house simulation of the GSM system [4]. This is given by

$$IBER = 0.1945X(\frac{s}{T})^{1.8878} \qquad (3)$$

where s is the mean value of the delay spread and T is the bit period which is equal to 3.7μs for the GSM system.

The phases of the individual echo paths for each profile were extracted and a CDF of the phases of the first echoes was obtained and plotted on a normal paper (Figure 6). To determine the frequency selectivity of the channel, assume that a profile with N echoes is received and that a CW signal at a frequency of w_c was transmitted. The output of the system in terms of the inphase and quadrature components is given by

$$I_{wc} = \sum_{i=1}^{N} P_i \cos(\theta_i - w_c \Delta\tau_i) \qquad (4)$$

$$Q_{wc} = \sum_{i=1}^{N} P_i \sin(\theta_i - w_c \Delta t_i) \qquad (5)$$

where P_i is the level of the ith path, Θ_i is its phase and $\Delta\tau_i$ is its relative time. Thus the amplitude can be computed. The frequency can then be varied over a specified range to show the frequency selective fading. This was done for a bandwidth of 10MHz centred on 1.8GHz in 100KHz steps for two profiles on two different streets. Figures 7 and 8 show the power delay profile and frequency selectivity over a 10MHz bandwidth for Brownlow Hill for the first profiles. Figures 9 and 10 show similar plots for West Derby Street which has smaller values of average delay and delay spread.

V. Results and Discussions

In general the maximum value of delay spread was obtained on Brownlow Hill (0.82μs). This can be attributed to the many high rise buildings along the street. The maximum value of the average delay was obtained on Crown street (1.02μs), with sparse high rise buildings. The mean value of the delay spread is 0.23μs. This gives an IBER of 1.1 x 10^{-3}. These relatively small values indicate that the multipath situation arises mainly from local scatterers in the vicinity of the mobile.

Table I shows the 50% and 90% cumulative values for the time domain parameters. The values compared to the results published in [1] are relatively smaller in magnitude. This may be due to the fact that the selected locations were relatively closer to the transmitter as it will be for a microcell. The general trend is therefore that the 90% and 50% cumulative values are lower. It can also be noted that 90% of the profiles had 10 taps and 50% had 5 taps. The high number of taps may be due to the sparsity of high rise buildings close to the streets. Figure 6 shows the CDF of the phases of the first echoes plotted on a normal paper. This shows a great deviation from the normal distribution.

Figures 8 and 10 indicate very little frequency selective fading for the profiles analyzed. The profile in Figure 8 has 12 taps all within a 1.33μs interval from the first echo. Figure 10 shows a similar plot in which the forth profile is shown. This profile has 3 taps all within a 0.64μs interval. These small values of time delay will give very high values of the coherence bandwidth and hence fading will be minimal. It can be noted that as the time in which all the echoes arrive is increased, there is more variation in the waveforms.

VI. Conclusion.

Results of an experimental investigation of the wideband channel have been presented. The results show smaller values of the time domain descriptors compared to those in the literature [1], and very little frequency selective fading over a 10MHz bandwidth. This indicates that a PCN microcell will be able to operate in this area without being affected by frequency selectivity and delay spread. The distribution of the phases of the first echoes do not follow a normal distribution.

References.

[1] Natarajan, N., "Wideband characterisation of mobile radio channels at 1.8GHz", PhD thesis, Dept. of Electrical Engineering and Electronics, The

University of Liverpool, 1992.

[2] Nche C.,Turkmani, A.M.D. and Arowojolu ,A. A., "Channel Sounder for PCN Networks", IEE Colloquium, Dec. 1993.

[3] Parsons J. D., "The Mobile Radio Propagation Channel", Pentech Press, London 1992.

[4] Chaaban R. M., "Performance Evaluation of a TDMA digital mobile radio system", PhD thesis, Dept. of Electrical Eng. and Electronics, the University of Liverpool, 1993.

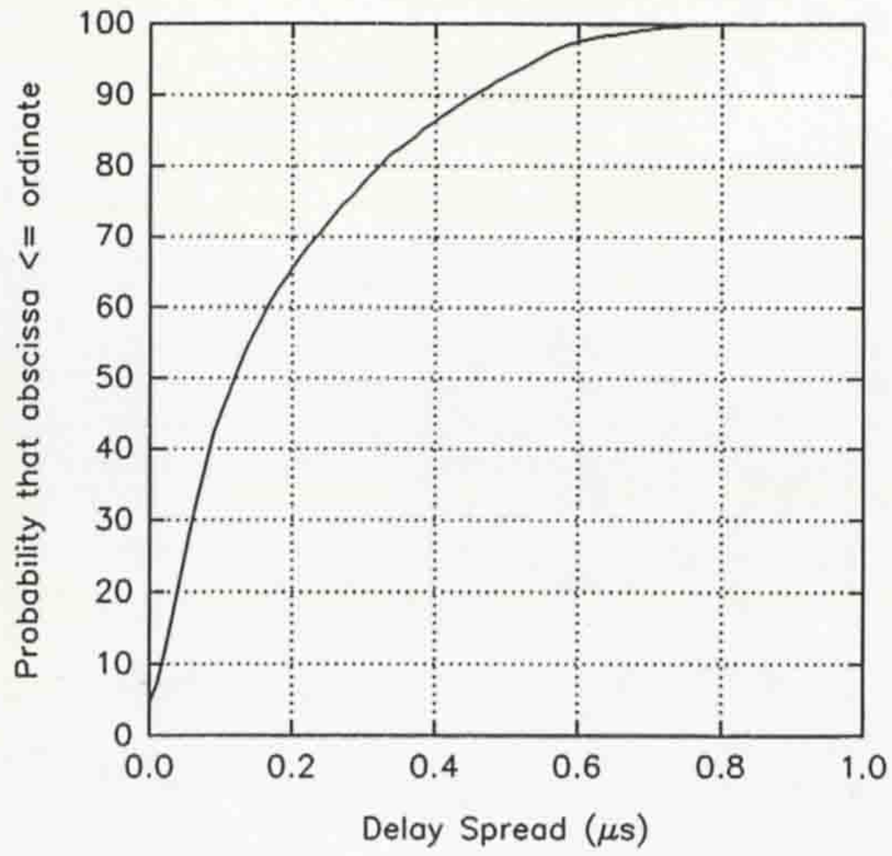

Figure 2. CDF of the delay spread.

Table 1. 90% and 50% cumulative values.

Parameter	50%	90%
Average delay	0.04μs	0.44μs
Delay spread	0.12μs	0.45μs
15 dB delay interval	0.36μs	1.67μs
12 dB delay interval	0.17μs	1.37μs
9 dB delay interval	0.08μs	1.17μs
90% delay window	0.20μs	1.29μs
75% delay window	0.08μs	0.97μs
50% delay window	0.03μs	0.40μs
number of taps per profile	5.15	10.17
Echo phase of the first taps	33.72°	153.6°

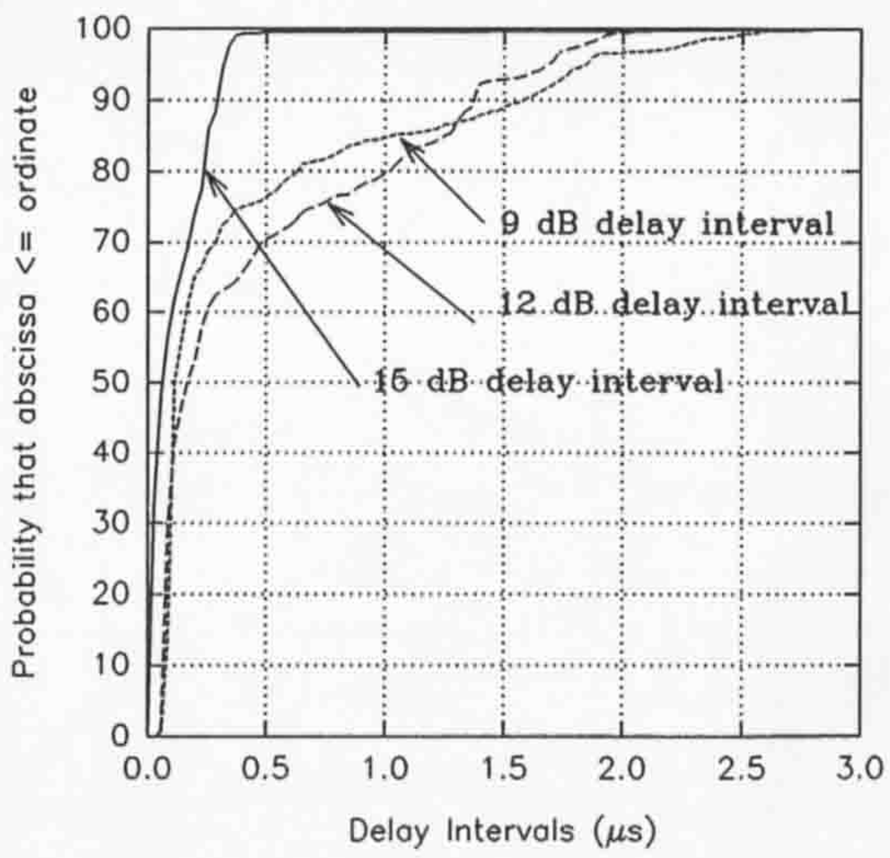

Figure 3. CDFs of delay intervals.

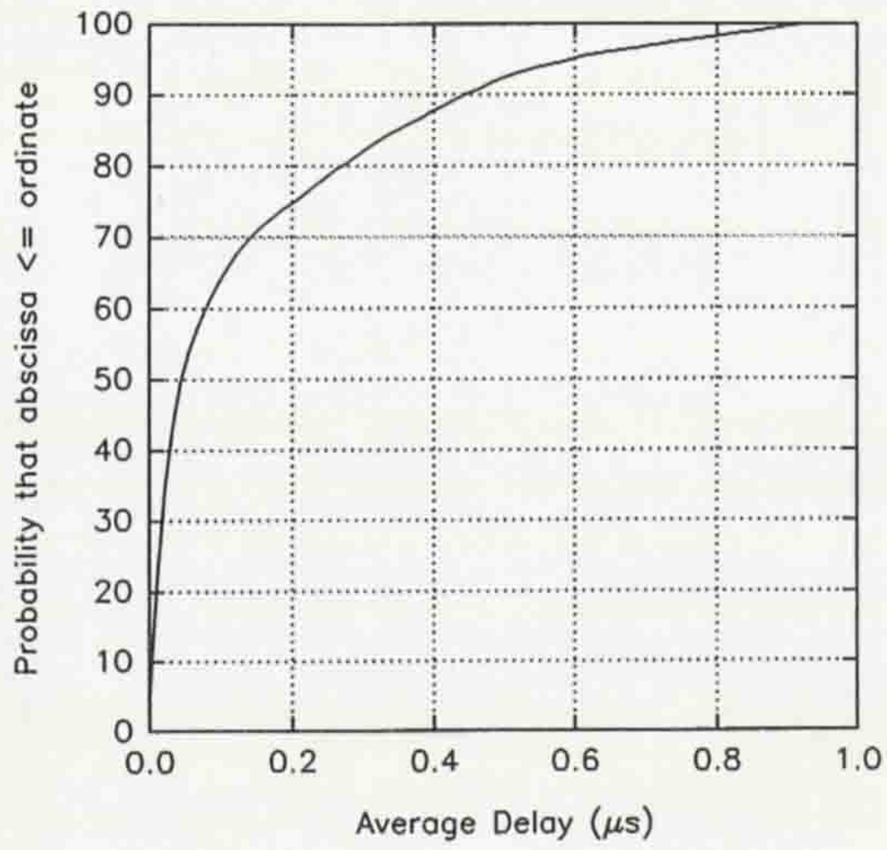

Figure 1. CDF of the average delay.

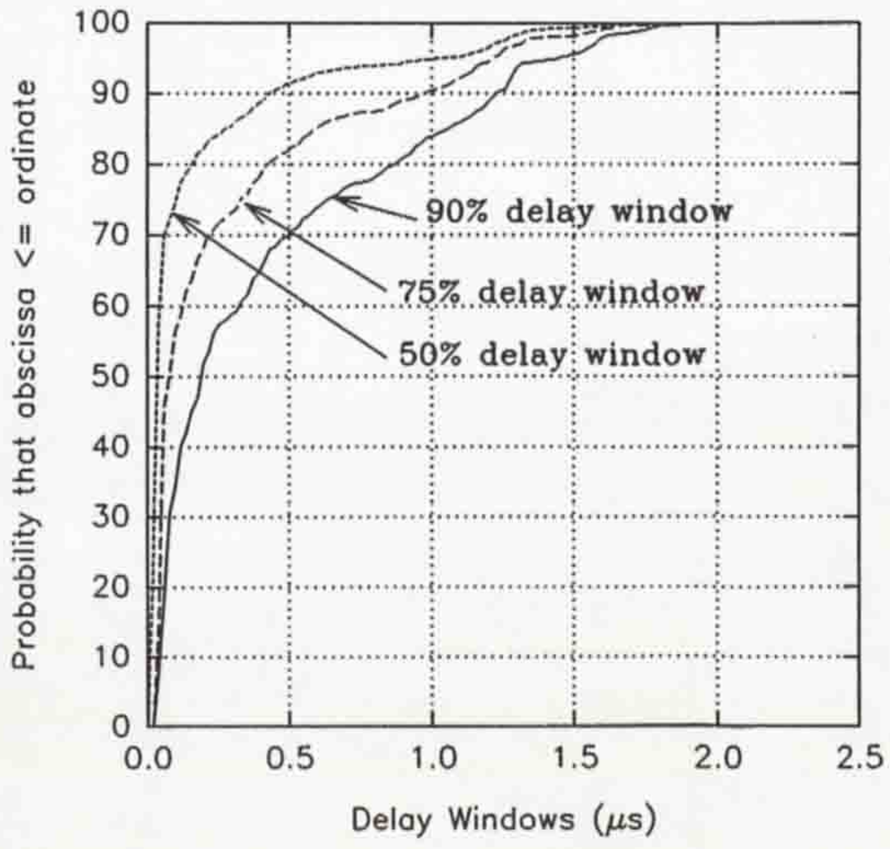

Figure 4. CDFs of delay windows.

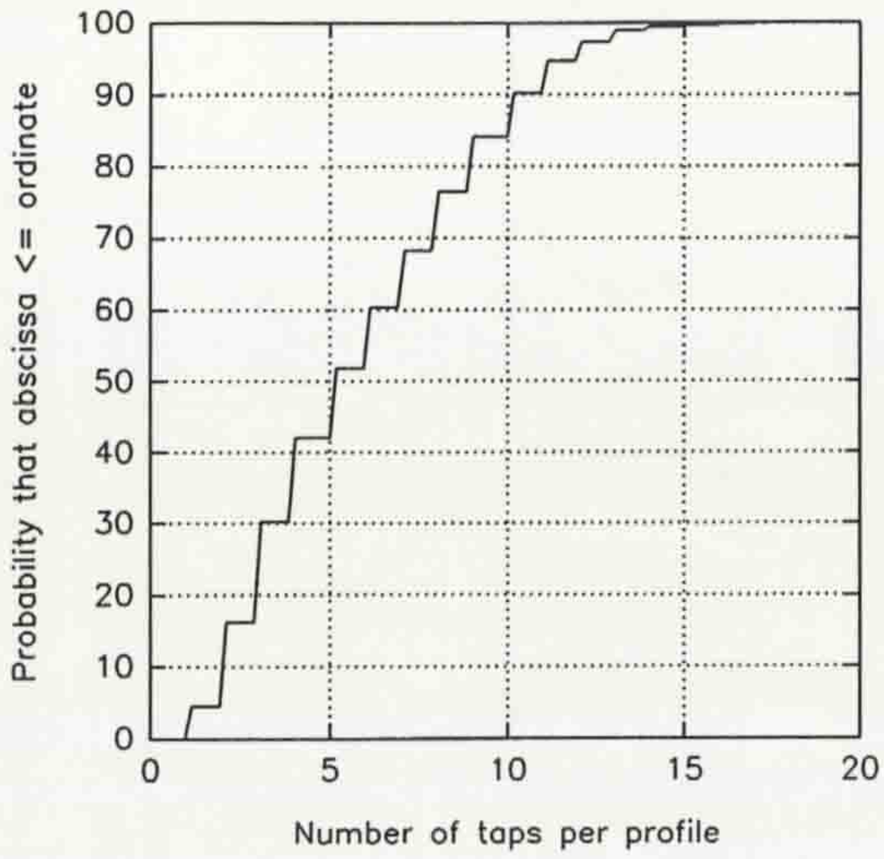

Figure 5. CDF of the number of taps.

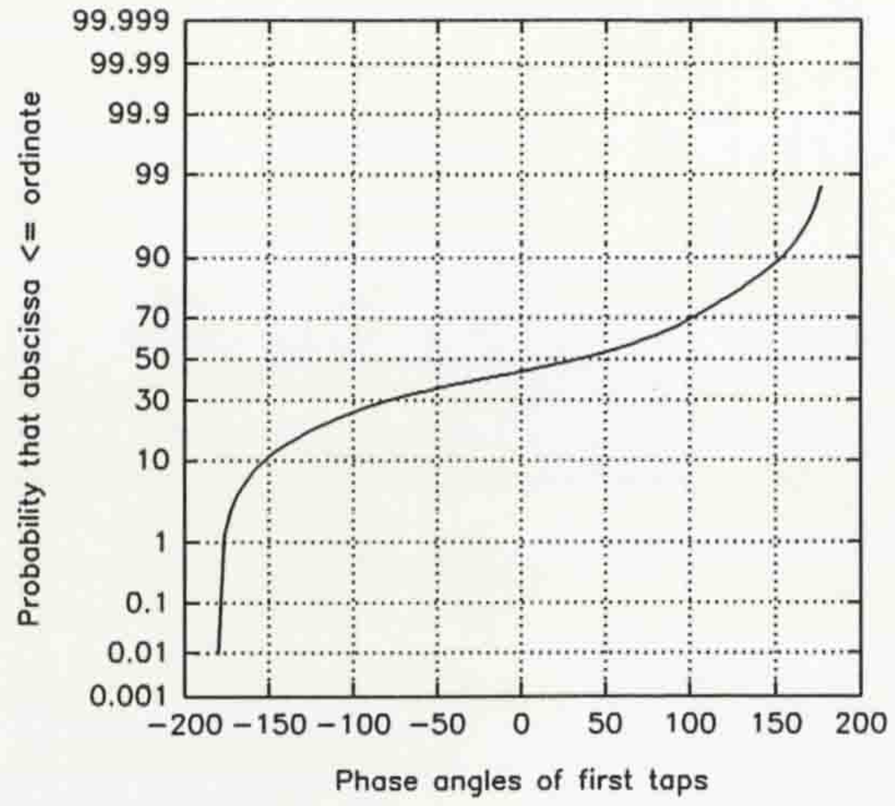

Figure 6. CDF of the phases of the first echoes.

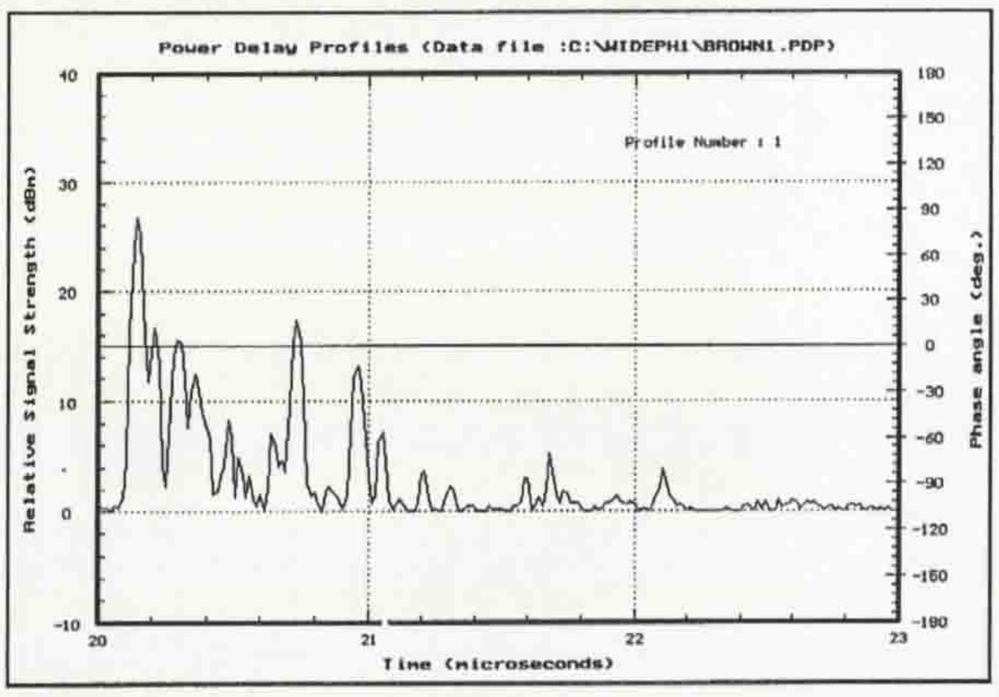

Figure 7. Power delay profile for Brownlow Hill.

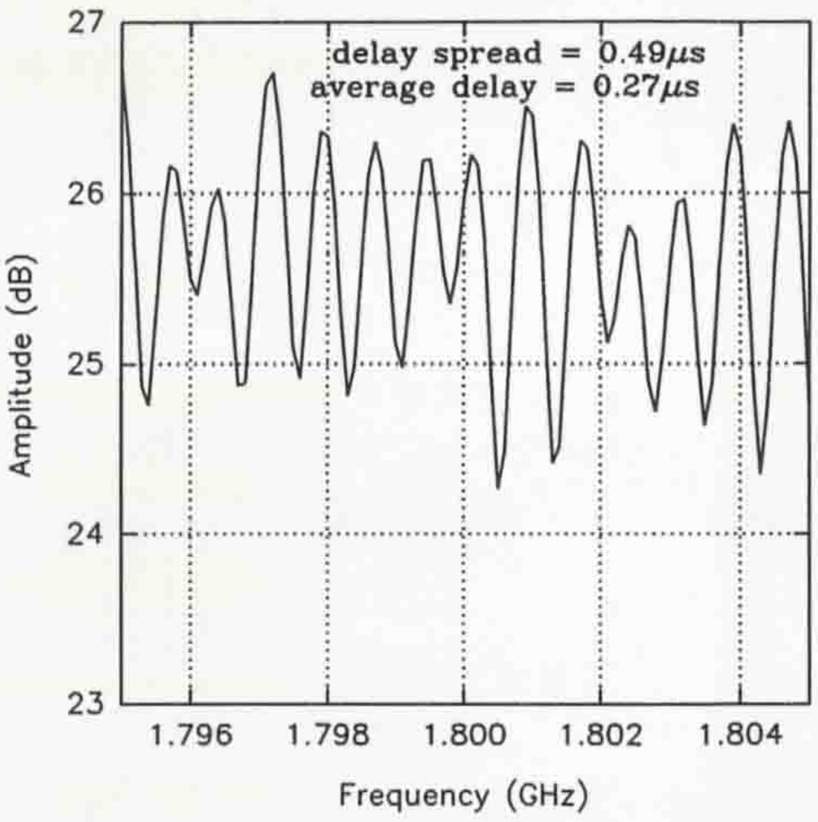

Figure 8. Frequency selectivity for Brownlow Hill.

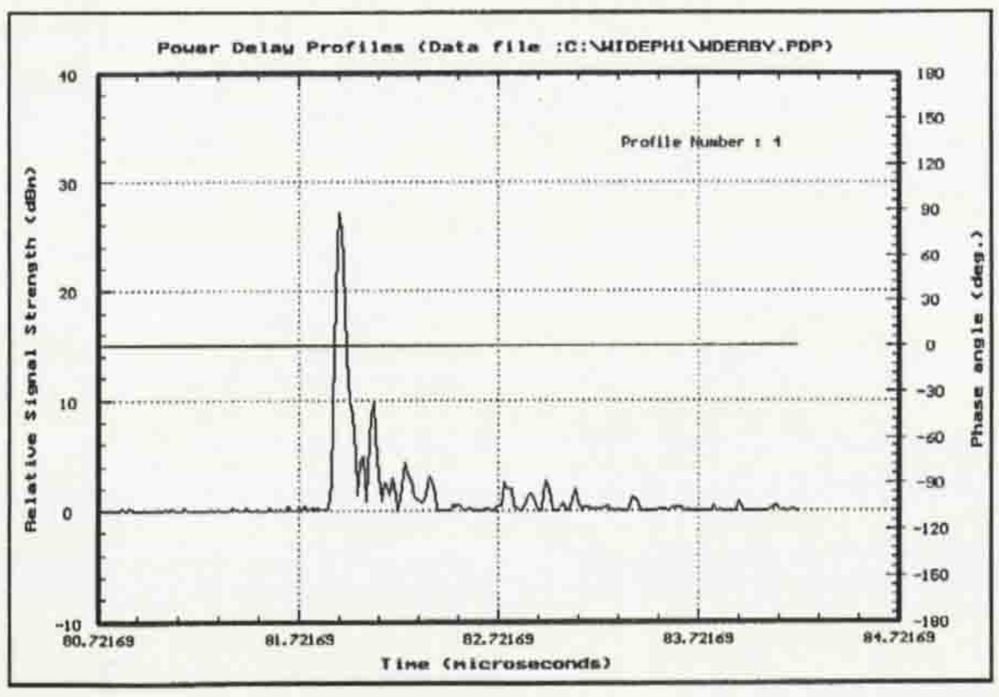

Figure 9. Power delay profile for West Derby Street.

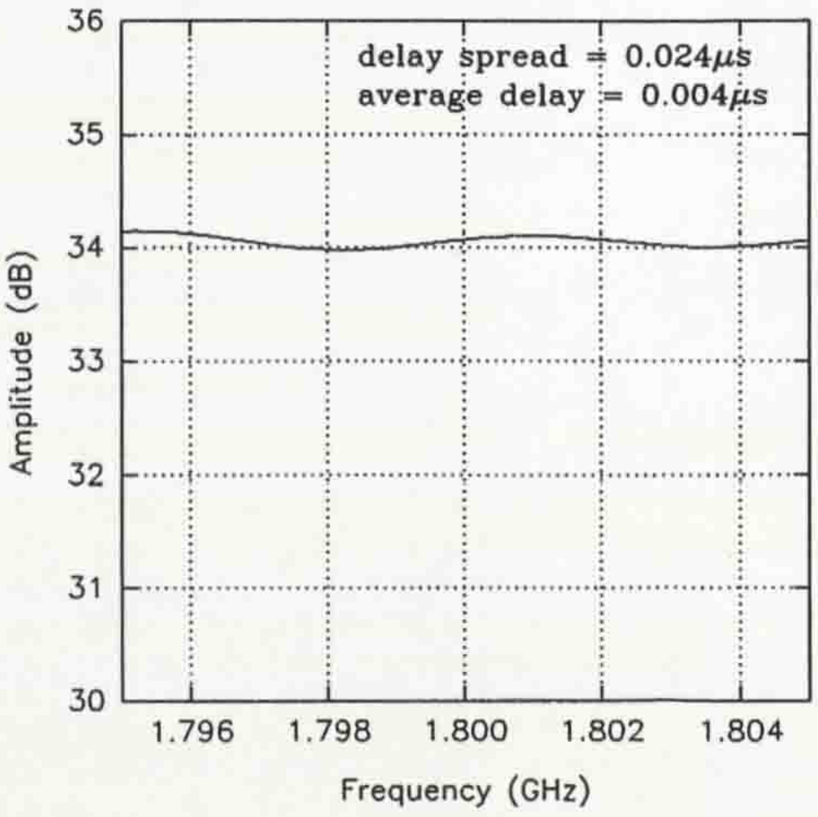

Figure 10. Frequency selectivity for West Derby Street

INDOOR AND OUTDOOR TIME DISPERSION MEASUREMENTS AT 1.8 GHz

C. Nche, J.D. Parsons and A.M.D. Turkmani*

Department of Electrical Engineering and Electronics,
The University of Liverpool, P.O. Box 147, Liverpool L69 3BX, U.K.
* Mobile Systems International,
Floor 12, 1 Harbour Exchange Square, London E14 9GE, U.K.

ABSTRACT: The results of time dispersion measurements in and around the City of Liverpool at 1.8 GHz are presented in this paper. Measurements were conducted in three different locations: urban, open area with residential houses and a modern superstore. A swept time-delay cross-correlation (STDCC) channel sounder with 33 ns resolution was employed to measure the complex bandpass impulse response of the channel. The complete system provided a phase change of 1 cycle in 360s. This superior stability coupled with the inclusion of an automatic gain control circuitry in the RF stage allowed continuous measurements for longer distances (130m), the only limitation being the amount of extended memory in the PC. The system was used to create a large database of power delay profiles from each area.

I INTRODUCTION

Personal Communications Systems (PCS) have recently been introduced in the U.K. These systems will utilise wideband time division multiple access (TDMA) techniques which imply that frequency selective fading will be inherent in the propagation channel. The launching of the GSM 900 MHz system, the DCS1800 system and the possible introduction of future code division multiple access systems (CDMA), produces a need to comprehensively characterise the wideband channel in all possible environments. Most of the previous measurements undertaken in this frequency band have concentrated on areas from selected main streets around the experimental base site, where only the power delay profile was measured. The number of power delay profiles used in the analysis of these surveys was therefore small. Furthermore, any operational system will be expected to provide service in all locations from main streets to side streets and within buildings (including shopping malls, railway stations, etc.), therefore measurements geared towards these systems must account for all these situations. System engineers will require necessary statistics of the channel including the phase statistics which until now, have been generally assumed to be uniformly distributed.

To achieve these aims, a wideband channel sounder based on the swept time-delay cross-correlation (STDCC) technique was used to measure the complex impulse response of the channel. The system has a time resolution of 33 ns and a maximum measurable excess delay of 17.01μs. The system utilises automatic gain control (AGC) circuitry in the RF stage of the receiver. This permits the observation of the spatial variation of the complex power delay profile, which was not possible in most of the past measurements as AGC was not employed. The analysis of the phase is not included in this paper.

The measurements were undertaken in an urban area, an open area with residential houses and a modern superstore. Results are presented in the form of cumulative distribution functions (CDF) of the time and frequency domain parameters.

II EXPERIMENTAL DESIGN

A limited number of results from time dispersion measurements in outdoor as well as indoor environments have been published [1-3]. Most of the outdoor measurements were based on selected short portions of main streets around the experimental base site, hence, the data was too sparse to derive reliable echo statistics. It was therefore necessary to design outdoor experiments which will cover all possible streets irrespective of their widths or orientations. We also sought to perform measurements in a random manner rather than search for what is deemed to be the worse case power delay profiles and to perform the measurements in longer stretches of streets.

Microcell structures for coverage and capacity enhancement into buildings such as shopping malls, railway stations, etc., where large numbers of people congregate necessitates wideband studies in these locations. Measurements were therefore conducted in a modern superstore. Again, it was deemed necessary to cover most of the floor of the superstore.

A. The Measurement Apparatus

The wideband channel sounder used is based on the swept time delay cross-correlation (STDCC) technique [4], a detailed description of which is presented in [5]. In the transmitter a 30 MHz 511-bit PRBS is used to phase reversal modulate a 1.8 GHz RF carrier that is

locked to a highly stable Rubidium frequency standard. The receiver's front end translates the received signal to an IF of 10 MHz with a 1.79 GHz local oscillator (LO) which has been phase reversal modulated by an identical locally generated PRBS clocked at a slightly slower rate. The LO is also locked to an identical Rubidium frequency standard. The IF signal was bandpass filtered before splitting into two cophasal signals. One of these is used to obtain the envelope of the impulse response by utilising a logarithmic amplifier with an 80 dB dynamic range and the other undergoes quadrature demodulation. The latter therefore provided a means of acquiring the phases of the resolvable echoes. The use of high quality LOs with good phase noise characteristics together with the high stability of the frequency standards provided a system with a phase change of 360° in 360s. This is superior to Cox [6] and Demery [7] who had 360° phase changes in 10s and 30s respectively.

The AGC was implemented using a programmable RF attenuator in the front end of the receiver. Suitable conditioning of the video output provided the AGC control signal. Thus, the high stability of the system together with the AGC enabled the collation of power delay profiles for longer distances and without previewing the measurement site.

The system has a time resolution of 33 ns (a spatial resolution of 10m). It provides an impulse response sounding rate of 16 profiles per second, a maximum measurable excess delay of 17.01μs and dynamic range of 30 dB. The addition of the AGC in the RF front end of the receiver allowed optimum positioning of this limited dynamic range window and hence permitted the recording of the short and long term as well as the distance dependent variations of the power delay profiles.

The antennas used in the transmitter and receiver were both laboratory-constructed wideband vertically polarised discones. These have an omni directional azimuthal radiation pattern and a VSWR of 1:1.25 over the 1700-1900MHz frequency band.

Data logging was achieved through the use of a personal computer which housed a 16 channel I/O commercial data acquisition card. Four outputs were recorded from the receiver; namely, the video output, AGC signal, I and Q outputs. The video output was also used for visual inspection of the power delay profiles during the course of any experiment to ensure that the recorded profiles had a high enough signal strength. This is important since the CCIR [8] recommendations are followed during the analysis. The data acquisition software package also allows on-line viewing of the recorded power delay profiles. The sampling rate used was 20 kHz which corresponds to a real time sampling rate of 75 MHz. This is equivalent to oversampling the time delay bin of 33 ns by a factor of 5. A typical power delay obtained from the system is shown in Figure 1.

B. Description of measurement sites and experimental procedures

Time dispersion measurements were conducted in three locations; namely, urban area, open area with some residential houses and a modern superstore. A brief description of the each follows.

Location I: Urban area. The transmitter was coupled to a linear power amplifier giving an average power of 7W. This was placed on the roof of a 10 storey building in Liverpool City centre. This building is significantly taller than the surrounding buildings. The streets in the city centre are flanked on both sides by buildings which are at least four storeys high, with the occasional building having a height in excess of 7 storeys. South east of the transmitter, about 0.6km away, is the River Mersey which is about 1.2km wide. There are buildings across the river which can significantly affect the propagation characteristics in this area. The receiver system was housed in a mobile and measurements were conducted on a random selection of streets (radial, tangential, etc.) up to 4km away.

Location II: Open area with residential houses. The transmitter was coupled to a linear power amplifier giving an average power of 7W. This was placed on the roof of a 3 storey building in the outskirts of Liverpool. In the immediate vicinity of the transmitter, there are mainly open fields and woods with relatively small winding roads. Some residential houses were located south east of the transmitter and about 750m away. Small farm houses were dotted around the open areas. With the receiver system housed in a mobile, measurements were conducted on street portions up to 2km away. Again, the streets were chosen in a random manner.

Location III: Superstore. The transmitter was coupled to a linear power amplifier giving an average power of 0.6W. The transmitting discone antenna was placed in the centre of the superstore, 2m above ground level. This was located such that the antenna cleared all obstructions, which were mainly metal display shelves 1.8m high. This superstore is of a typical modern design with three main aisles running the length. Minor aisles flanked on both sides by metal shelves run across these main aisles. The main aisle on the left is wider as it contains checkout desks. Concrete metal truss works supports a corrugated steel roof. In this case the receiver system was mounted on a trolley with the receiving antenna mounted 1.7m above ground level. Measurements were conducted at random on the main

locked to a highly stable Rubidium frequency standard. The receiver's front end translates the received signal to an IF of 10 MHz with a 1.79 GHz local oscillator (LO) which has been phase reversal modulated by an identical locally generated PRBS clocked at a slightly slower rate. The LO is also locked to an identical Rubidium frequency standard. The IF signal was bandpass filtered before splitting into two cophasal signals. One of these is used to obtain the envelope of the impulse response by utilising a logarithmic amplifier with an 80 dB dynamic range and the other undergoes quadrature demodulation. The latter therefore provided a means of acquiring the phases of the resolvable echoes. The use of high quality LOs with good phase noise characteristics together with the high stability of the frequency standards provided a system with a phase change of 360° in 360s. This is superior to Cox [6] and Demery [7] who had 360° phase changes in 10s and 30s respectively.

The AGC was implemented using a programmable RF attenuator in the front end of the receiver. Suitable conditioning of the video output provided the AGC control signal. Thus, the high stability of the system together with the AGC enabled the collation of power delay profiles for longer distances and without previewing the measurement site.

The system has a time resolution of 33 ns (a spatial resolution of 10m). It provides an impulse response sounding rate of 16 profiles per second, a maximum measurable excess delay of 17.01μs and dynamic range of 30 dB. The addition of the AGC in the RF front end of the receiver allowed optimum positioning of this limited dynamic range window and hence permitted the recording of the short and long term as well as the distance dependent variations of the power delay profiles.

The antennas used in the transmitter and receiver were both laboratory-constructed wideband vertically polarised discones. These have an omni directional azimuthal radiation pattern and a VSWR of 1:1.25 over the 1700-1900MHz frequency band.

Data logging was achieved through the use of a personal computer which housed a 16 channel I/O commercial data acquisition card. Four outputs were recorded from the receiver; namely, the video output, AGC signal, I and Q outputs. The video output was also used for visual inspection of the power delay profiles during the course of any experiment to ensure that the recorded profiles had a high enough signal strength. This is important since the CCIR [8] recommendations are followed during the analysis. The data acquisition software package also allows on-line viewing of the recorded power delay profiles. The sampling rate used was 20 kHz which corresponds to a real time sampling rate of 75 MHz. This is equivalent to oversampling the time delay bin of 33 ns by a factor of 5. A typical power delay obtained from the system is shown in Figure 1.

B. Description of measurement sites and experimental procedures

Time dispersion measurements were conducted in three locations; namely, urban area, open area with some residential houses and a modern superstore. A brief description of the each follows.

Location I: Urban area. The transmitter was coupled to a linear power amplifier giving an average power of 7W. This was placed on the roof of a 10 storey building in Liverpool City centre. This building is significantly taller than the surrounding buildings. The streets in the city centre are flanked on both sides by buildings which are at least four storeys high, with the occasional building having a height in excess of 7 storeys. South east of the transmitter, about 0.6km away, is the River Mersey which is about 1.2km wide. There are buildings across the river which can significantly affect the propagation characteristics in this area. The receiver system was housed in a mobile and measurements were conducted on a random selection of streets (radial, tangential, etc.) up to 4km away.

Location II: Open area with residential houses. The transmitter was coupled to a linear power amplifier giving an average power of 7W. This was placed on the roof of a 3 storey building in the outskirts of Liverpool. In the immediate vicinity of the transmitter, there are mainly open fields and woods with relatively small winding roads. Some residential houses were located south east of the transmitter and about 750m away. Small farm houses were dotted around the open areas. With the receiver system housed in a mobile, measurements were conducted on street portions up to 2km away. Again, the streets were chosen in a random manner.

Location III: Superstore. The transmitter was coupled to a linear power amplifier giving an average power of 0.6W. The transmitting discone antenna was placed in the centre of the superstore, 2m above ground level. This was located such that the antenna cleared all obstructions, which were mainly metal display shelves 1.8m high. This superstore is of a typical modern design with three main aisles running the length. Minor aisles flanked on both sides by metal shelves run across these main aisles. The main aisle on the left is wider as it contains checkout desks. Concrete metal truss works supports a corrugated steel roof. In this case the receiver system was mounted on a trolley with the receiving antenna mounted 1.7m above ground level. Measurements were conducted at random on the main

aisles as well as the minor aisles at random.

III DATA ANALYSIS AND RESULTS

Figure 1 shows a power delay profile for which each time delay bin (33ns) is represented by 5 samples. It is therefore necessary to determine the magnitudes and time delays of the resolvable echo paths in each bin for use in the analysis. These will be the peaks in the power delay profiles and hence, a peak identification algorithm was included in the analysis. This can be regarded as more accurate compared to other studies [7] which did not employ any oversampling of the data.

The effects of noise and spurious signals in the system can be very significant since the analysis of the power delay profiles is based on the identification of the peaks. The CCIR recommendation of 15 dB peak to spurii and a 3 dB noise margin was therefore imposed [8]. Furthermore, the AGC signal indicates where the programmable attenuator switched during the course of any experiment. Hence, all profiles which satisfy the CCIR recommendations and do not contain an AGC switch were deemed as 'good' profiles. Figure 2 shows the normalised profile of Figure 1 which has undergone the peak identification process and the CCIR recommendations.

For each 'good' profile, the average delay (D), delay spread (S), delay intervals at 15 dB, 12 dB and 9 dB (I_{15}, I_{12} and I_9) and delay windows at 90%, 75% and 50% (W_{90}, W_{75} and W_{50}) were evaluated. Also, the number of echoes (NE) for each profile was determined so as to obtain the distribution. This is necessary since a knowledge of the distribution of the number of multipath echoes will aid in the development of wideband simulators.

The frequency correlation function (FCF) was computed by evaluating the Fourier transform of the power delay profile. Although resolution is directly related to the PRBS clock rate in the time domain, it is related to the pulse repetition frequency in the frequency domain. This will provide a resolution of 58.7 kHz. In order to improve the frequency resolution, the power delay profiles were extended to 8192 samples per profile [9]. This improved the frequency resolution from 58.7 kHz to 3.7 kHz. The coherence bandwidths at 0.5 and 0.9 correlation (B_{90} and B_{50}) were then computed. Figure 3 shows a worst case power delay profile from location I and Figure 4 is its FCF.

A CDF for each of these parameters was obtained in order to show its large scale variations. Tables I-III show the 50% and 90% cumulative values for the above parameters. These also show their mean values, standard deviation (SD) and the maximum values.

A. Location I: Urban area. A total of 48834 'good' profiles were used to obtain the results listed in Table I. For delay spread, a mean and standard deviation of $0.72\mu s$ and $0.83\mu s$ respectively were obtained. These are slightly lower than those obtained by Bajwa [2] in Birmingham (mean = $1.44\mu s$, standard deviation = $0.52\mu s$) at a carrier frequency of 436 MHz. Natarajan [3] presented his results at 1.8 GHz in the form of 50% and 90% CDF values only. The 90% CDF values are similar to those obtained in this study, however, the 50% CDF values are about a factor of 2 higher ($0.7\mu s$). The mean value of delay spread (0.72 μs) is the same as that of [10] ($0.73\mu s$). The differences in some of these figures can be attributed to the measurement environment, the total number of power delay profiles and the nature of collecting the data. In this study, a substantial number of power delay profiles were obtained from random locations around the base site with no preferences given to the nature of the power delay profiles. The maximum delay spread of $6.8\mu s$ was obtained along a street close to the River Mersey. This implies that some multipath echoes were received from across the river.

The results for the coherence bandwidth at 0.9 and 0.5 correlation reveal minimum values of 32.2kHz and 59.5 kHz respectively. Cox [6] reported minimum values of 20 kHz and 55 kHz respectively. Therefore, wideband systems will be affected by frequency selective fading in some locations. If the coherence bandwidth at 0.9 correlation is to be taken as a figure of merit to predict system performance, then the 50% CDF value of 202.2 kHz suggests that Qualcom's proposed CDMA system will be affected in 50% of the locations in this area. The large values of standard deviation implies a lot of variability in the FCFs of the power delay profiles.

Location II: Open area with residential houses. The results which were obtained from a total of 21974 'good' power delay profiles are shown in Table II. It can be seen that a maximum delay spread of $3.9\mu s$ was obtained. This might have been due to distant reflectors in the small neighbouring town near the base site. However, a mean value of $0.2\mu s$ shows that time dispersion will not be a significant problem in areas akin to this. Again a mean of delay spread of $0.2\mu s$ in this study is lower than that of Bajwa ($1.04\mu s$) in suburban Birmingham.

The minimum values of the coherence bandwidth at 0.5 and 0.9 correlation are 32.04 and 114.4kHz respectively.

Location III: Superstore. Table III shows the results which were obtained from 10654 'good' profiles that were collected in the modern superstore. In general the values for the different time and frequency domain parameters calculated are relatively smaller than those

in locations I and II. However, these values are higher than those reported in the literature [9]. The median of the delay spread is 0.06 μs in this study as compared to 0.028 μs in [11]. It can also be observed that up to 20 multipath echoes were received. Hence, it could be concluded that multiple reflections due to metal shelves is common in supermarkets, and time dispersion will therefore be more severe than in multistorey buildings.

IV CONCLUSION

The results of time dispersion measurements in three different scenarios have been presented. Analysis of the results indicate that a large number of power delay profiles are required in order to evaluate the statistics required by system designers. This is very important because a biassed method of data collection will mean that values of the required parameters may be higher. The results also indicate that time dispersion is more severe in supermarkets than in a multistorey buildings.

ACKNOWLEDGEMENT

The authors would like to thank the ESPRC for funding this project and Mr. J. G. Davies for the invaluable help in the collection of the data. The help and support of Mr. D. G. Lewis is also greatly appreciated.

REFERENCES

[1] Cox, D.C. and Leck, R.P., 1975, "Distribution of multipath delay spread and average excess delay for 910 MHz urban mobile radio paths", IEEE Trans. Ant. Propagat., Vol. ap-23 pp206-213.

[2] Bajwa, A.S. and Parsons, J.D., 1985, "Large area characterisation of UHF multipath propagation and its relevance to the performance bounds of mobile radio systems", IEE Proc., Vol. 132 Pt. F No. 2 pp99-106.

[3] Natarajan, N., 1992, "Wideband characterisation of mobile radio channels at 1.8 GHz", Ph.D thesis, The University of Liverpool.

[4] Turkmani, A.M.D., Demery, D.A. and Parsons, J.D., 1991, "Measurement and modelling of wideband mobile radio channels at 900 MHz", IEE Proc. Pt. I, Vol. 138, No. 5, pp447-457.

[5] Nche, C., Turkmani A.M.D., and Arowojolu, A.A., 1993, "Channel sounders for PCN networks", IEE Colloquium.

[6] Cox, D.C., 1972, "Delay-Doppler characteristics of multipath propagation at 910 MHz in suburban mobile radio environment", IEEE Trans. Ant. Propagat., Vol. AP-10, pp625-635.

[7] Demery, D.A., 1989, "Wideband characterisation of UHF mobile radio channels in urban areas", Ph.D thesis, The University of Liverpool.

[8] CCIR Report 567-3 (MOD F), 1990, "Propagation data and prediction methods for terrestrial land mobile service using the frequency range 30 MHz to 3 GHz", CCIR XVIIth Plenary Assembly, Düsseldorf.

[9] Parsons, J.D., Demery, D.A. and Turkmani, A.M.D., 1991, "Sounding techniques for wideband mobile radio channels: a review", IEE Proc. Part I, Vol. 138, No. 5, pp437-446.

[10] Sousa, E.S., Jovanović, V.M. and Daigneault, C., 1994, "Delay spread measurements for the digital cellular channel in Toronto", IEEE Trans. Veh. Tech., Vol. 43,No. 4. pp837-847.

[11] Bultitude J.C, Mahmoud S.A. and Sullivan, W.A., 1989, "A comparison of indoor radio propagation at 910 MHz and 1.75 GHz", IEEE Journ. Sel. Areas in Coms.,Vol.7,No.1. pp20-30.

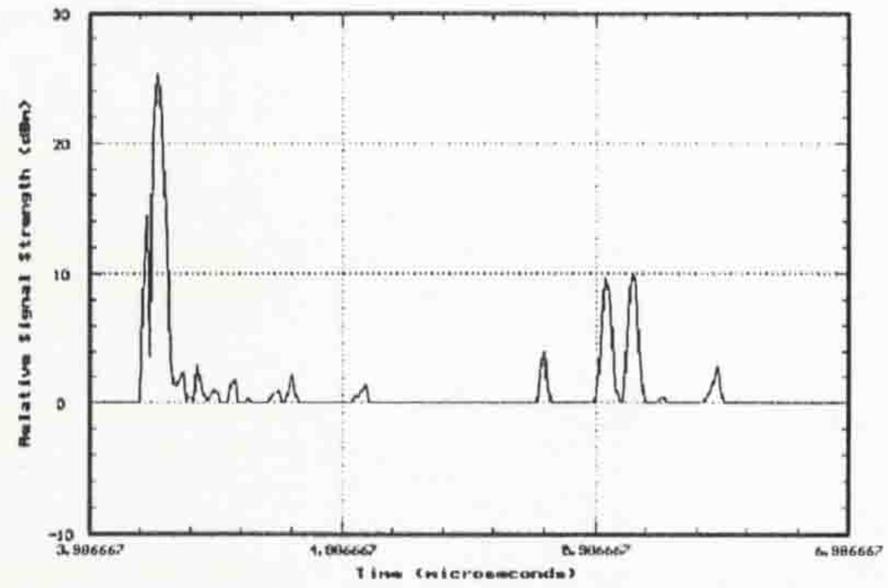

Figure 1. Typical power delay profile as recorded by the system from location II.

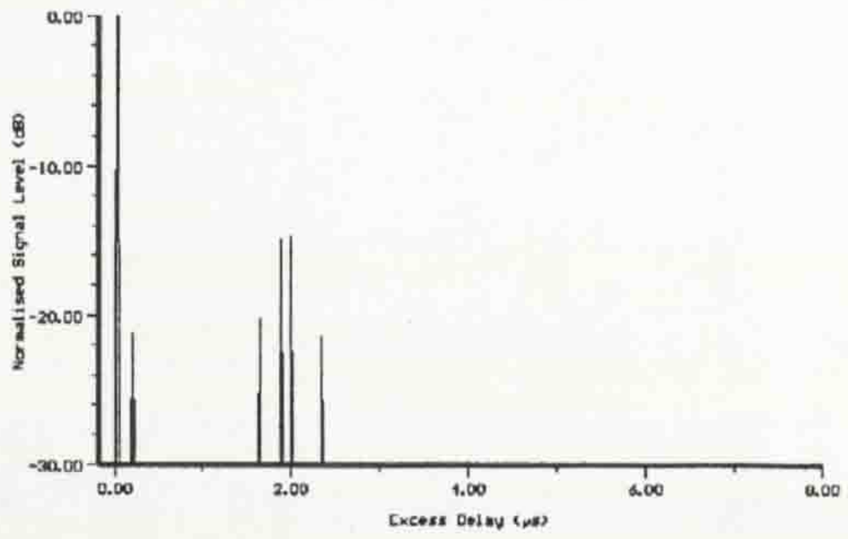

Figure 2. Normalised power delay profile of Figure 1, after the peak identification process.

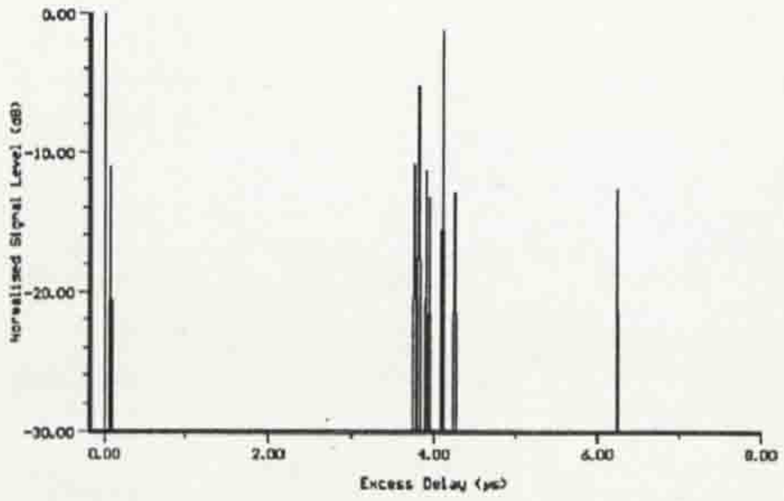

Figure 3. Normalised worst case power delay profile from location I.

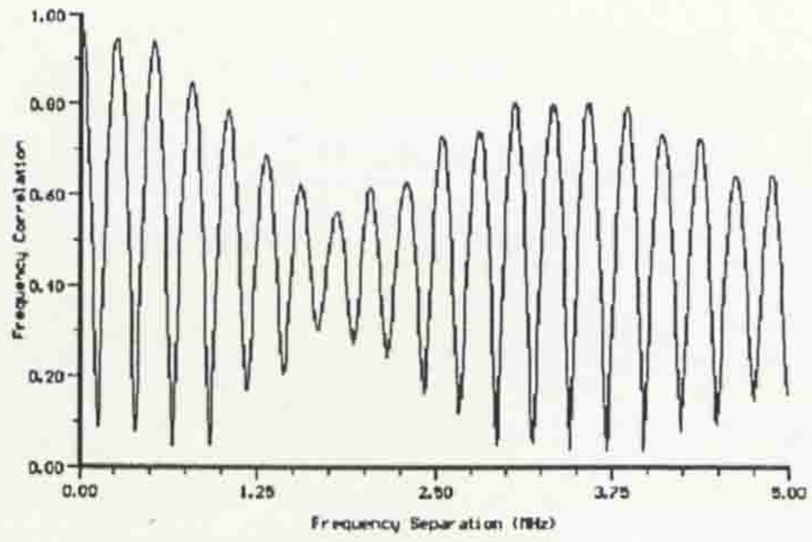

Figure 4. FCF of the power delay profile of Figure 2.

Table I. Transmitter mounted on the roof of Silkhouse Court. 48834 'good' profiles were employed for the calculations.

Parameter	D µs	S µs	I_{15} µs	I_{12} µs	I_9 µs	W_{90} µs	W_{75} µs	W_{50} µs	NE	B_{50} kHz	B_{90} kHz
50% CDF value	0.29	0.43	1.65	0.92	0.47	1.01	0.5	0.16	15	1008.1	202.2
90% CDF value	1.51	1.79	6.76	4.9	3.34	3.93	2.24	1.34	30	7006.2	1182.9
Mean	0.8	0.72	2.60	1.87	1.29	1.79	1.08	0.57	18	1497.8	461.6
SD	1.88	0.83	3.28	2.72	2.16	2.51	1.78	1.21	10	3240.5	1448.9
Maximum	15.3	6.8	16.3	16.3	16.2	16.3	15.6	14.3	69	37495.4	37495.4

Table II. Transmitter mounted on the roof of Bridgefield Forum. 21974 'good' profiles were employed for the calculations.

Parameter	D µs	S µs	I_{15} µs	I_{12} µs	I_9 µs	W_{90} µs	W_{75} µs	W_{50} µs	NE	B_{50} kHz	B_{90} kHz
50% CDF value	0.03	0.08	0.26	0.11	---	0.14	---	---	5	3465.5	830.1
90% CDF value	0.21	0.47	1.75	0.86	0.53	0.8	0.39	0.09	10	12282.5	3592.1
Mean	0.1	0.2	0.9	0.41	0.24	0.4	0.2	0.09	6	1890.0	995.6
SD	0.14	0.29	1.85	0.72	0.41	0.6	0.32	0.17	3	4256.7	2197.1
Maximum	4.35	3.94	16.4	15.8	8.1	11.4	8.1	3.7	20	37495.4	37477.1

Table III. Transmitter mounted in a modern superstore. 10654 'good' profiles were employed for the calculations.

Parameter	D µs	S µs	I_{15} µs	I_{12} µs	I_9 µs	W_{90} µs	W_{75} µs	W_{50} µs	NE	B_{50} kHz	B_{90} kHz
50% CDF value	0.03	0.06	0.18	0.19	0.12	0.18	0.1	0.04	6	4802.3	1092.1
90% CDF value	0.07	0.08	0.34	0.31	0.24	0.26	0.18	0.1	8	12322.7	2336.7
Mean	0.04	0.06	0.29	0.2	0.15	0.19	0.12	0.06	6	3324.0	1576.3
SD	0.03	0.02	0.58	0.09	0.08	0.07	0.06	0.04	2	5293.7	2180.8
Maximum	0.84	0.6	16.3	1.5	1.5	1.5	1.4	1.3	20	37458.8	37431.3